NTNU – Trondheim
Norwegian University of
Science and Technology

Economic Optimization of Shale Wells

Kirill Karadzhov

Petroleum Engineering
Submission date: June 2015
Supervisor: Curtis Hays Whitson, IPT

Norwegian University of Science and Technology
Department of Petroleum Engineering and Applied Geophysics

Abstract

The worldwide interest in development of unconventional resources resulted into significant changes in the energy market within the last decade. Successful shale revolution in the US opened global perspectives for extensive oil and gas production from shales and pushed technological progress forward. Hundreds of private companies proved that development of shale reserves can be economically attractive; therefore, other countries became interested in their unconventional resources as well. China, Argentina, Russia started focusing on shale oil and gas reservoirs, but their industry is still in infancy stage. Along with limited experience in shale development, they faced several significant hydrocarbon price falls within the last seven years making shale project's economy questionable. Thus, the significance of the balanced project economy through optimized well design came to the front stage.

This thesis deals with economic optimization of shale wells. Under economic optimization we understand the condition when the well reached optimal economic performance based on selected financial metrics. For the project, net present value, discounted profitability index and internal rate of return are chosen as metrics of interest. We believe that short-term economic performance is more crucial rather than a long-term one; therefore, the simulations are limited by five years' time frame. We also study different available cost and revenue models to select the most suitable for this thesis.

For sensitivity analysis we selected a variety of reservoir and completion parameters which have a significant influence on the economic performance of shale wells. No specific well or shale play were chosen for the project. Therefore, our main objective is to provide trends and magnitudes of change of economic performance for different parameters of reservoir-well system.

Substantially, the project covers economic performance of a shale well for three different in-situ fluids (dry gas, gas condensate and oil) with up to nine different sensitivity parameter. In addition, we quantified the effect of gas desorption process and oil and gas price change, and addressed optimal well spacing on 1×2 mi section on total economic performance of the shale project. The achieved results are handy when initial first-order economic evaluation of the project is required and allows to better understand the outcomes when selecting the optimal shale well design.

THIS PAGE INTENTIONALLY LEFT BLANK

Acknowledgements

I would like to express a sincere gratitude to my supervisor, Professor Curtis H. Whitson, for the experience and professional knowledge he shared during my studies at NTNU. His advices and high professional standards had a great impact on me and this work and I am thankful for the thesis topic we agreed on which covered my personal interest in both engineering and economic subjects.

I am grateful to Aleksander Juell, a Chief Technology Officer at Petrostreamz AS and a developer of Shale Well Optimizer for Pipe-It. Aleksander provided great support to me while working with the Template and helped to resolve many technical challenges. In addition, his comments and expertise in shales significantly contributed in my understanding of unconventional reservoirs.

I would like to acknowledge Dave Reese for his consultancy on shale well economics. His comments and ideas helped to get a better insight on financial side of shale play development.

Special thanks to Petrostramz's team who were always around during working on the thesis and made the writing routine more easy-going. Also, I would like to acknowledge Petrostreamz AS and Coats Engineering Inc. for provided Pipe-It and SENSOR licenses.

I address the deepest gratitude to my parents, Marina and Ivan, who never stop believing in me. Their personal and financial support made it possible to move to Norway, continue my education at NTNU and travel around the world. Their encouragement through my life cannot be overestimated. I dedicate this work to them.

I am happy to express my warmest thanks to Aitor Almaraz, David Lemon, Jens Hedegaard and Alexander Galazin for sharing hundreds of incredible life moments during the last two years. Having you as friends made my studying in Trondheim unique, unforgettable and feeling like at home.

Finally, I am also thankful for every person who directly or indirectly contributed to my studying here in Norway.

THIS PAGE INTENTIONALLY LEFT BLANK

Table of Contents

List of Figures

List of Tables

THIS PAGE INTENTIONALLY LEFT BLANK

Abbreviations and Acronyms

Bcf	=	Billion (10^9) of standard cubic feet
Btu	=	British thermal units
Capex	=	Capital expenditures, USD
DPI	=	Discounted Profitability Index, %
EOS	=	Equation-of-States
GOR	=	Producing Gas-Oil Ratio, scf/bbl
IRR	=	Internal Rate of Return, %
NPV	=	Net Present Value, USD
OGR	=	Producing Oil-Gas Ratio, STB/MMscf
Opex	=	Operational expenditures, USD
PI	=	Linear-flow, infinite-acting productivity index, √md-ft
PO	=	Payout time, years

THIS PAGE INTENTIONALLY LEFT BLANK

Chapter 1

Introduction

Steady increase of world energy consumption requires extensive use of all energy resources to fulfill global economic growth. Comparing with 2015, world energy demand will grow by about 40% until 2040. Fossil fuels will remain a main contributor to the total energy basket accounting about 80% of the total demand, while renewables and nuclear power will cover remaining 20%. (**Fig. 1.1**). Among fossil fuels, natural gas and liquids (mostly crude oil and its products) will cover more than 65%. High share of oil and gas in the future energy basket requires increasing in hydrocarbons production globally through involvement of difficult reservoirs located offshore and development of unconventional resources. Of course, special attention is paid towards recent success in development of shale oil and gas.

The shale revolution started in the US about 10–15 years ago unlocked the potential of shale oil and gas development. From the net importer the US transformed into self-sufficient produced of hydrocarbons. **Figs. 1.2–1.3** show total oil and gas daily production rates for major shale plays in the US between 2000 and 2015. For instance, until 2007 the average production was less than 0.5 million bbl/day of oil and about 4 billion scf/day of gas. Today, the shale oil production is almost ten times higher with 4.6 million bbl/day. Likewise, the shale gas production reached 40 billion scf/day with about eight-fold increase. Certainly, the success in shale development in the US boosted interest around shale reserves worldwide and soon will lead to important changes on oil and gas markets.

U.S. Energy Information Administration reports that total shale oil and gas reserves around the world are about 345 billion bbl of oil and 7,201 trillion scf of wet natural gas ("Technically Recoverable Shale Oil and Shale Gas Resources…", 2013). That yields that shale resources account about 10% of total oil reserves and 32% of total natural gas reserves. Russia, the US, China and Argentina are among top countries by recoverable shale oil reserves. In terms of shale gas, China solely accounts about 15% of global reserves. The world is in abundant with shale resources, but current development outside the US is still in infantry phase. For example, in Canada and Argentina shale oil production reached just 0.4 and 0.02 million bbl/d respectively. Shale gas production in China reached 0.25 billion scf/day which is less than 1% of US daily production ("Shale gas and tight oil are commercially produced in just four countries", 2015). Therefore, there is a significant future potential for shale development in several countries around the world.

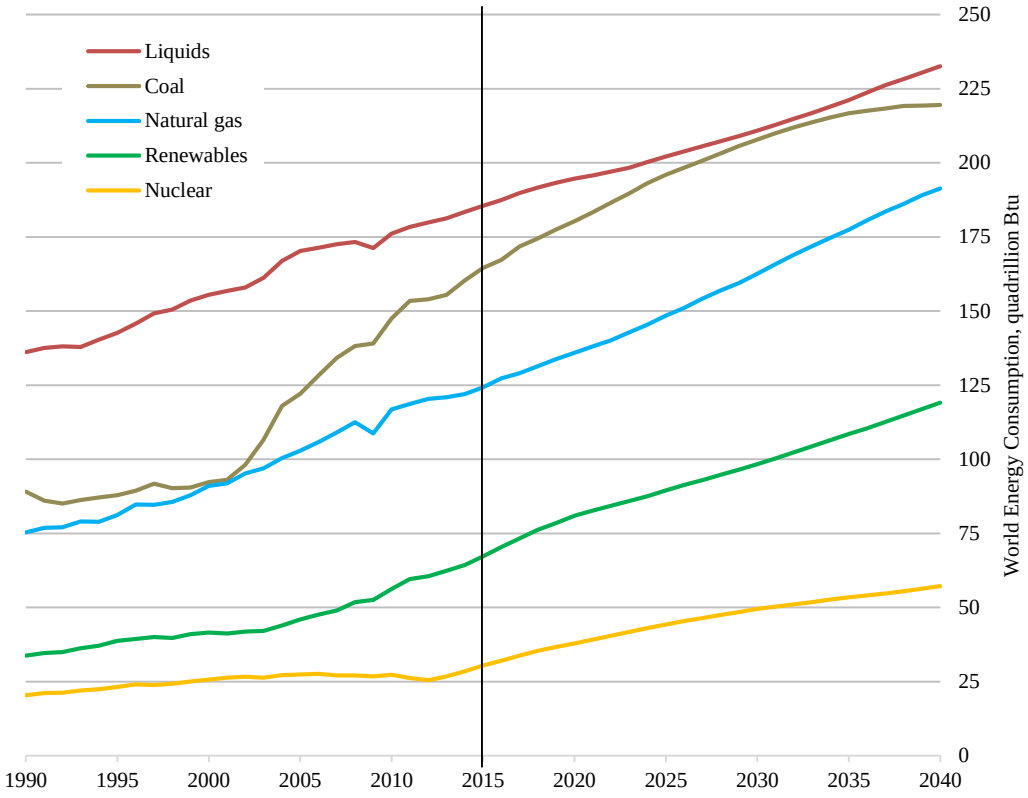

Fig. 1.1 – World energy consumption by fuel type. Source: U.S. Energy Information Administration

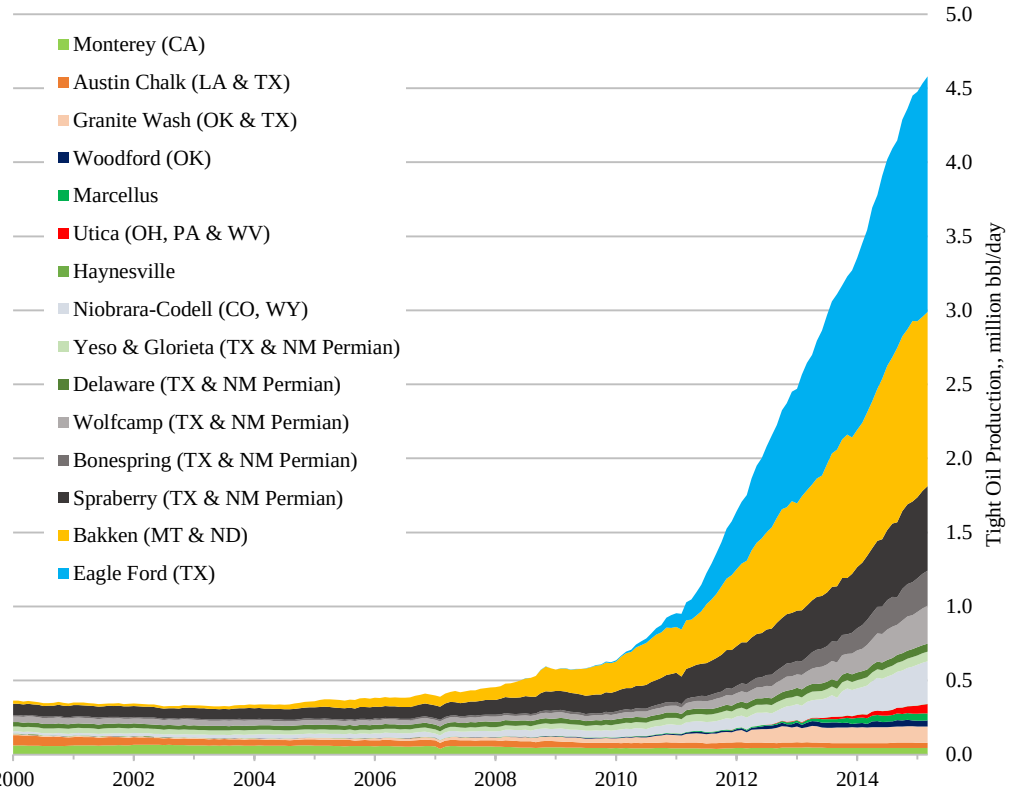

Fig. 1.2 – US tight oil production for selected plays.Source: U.S. Energy Information Administration

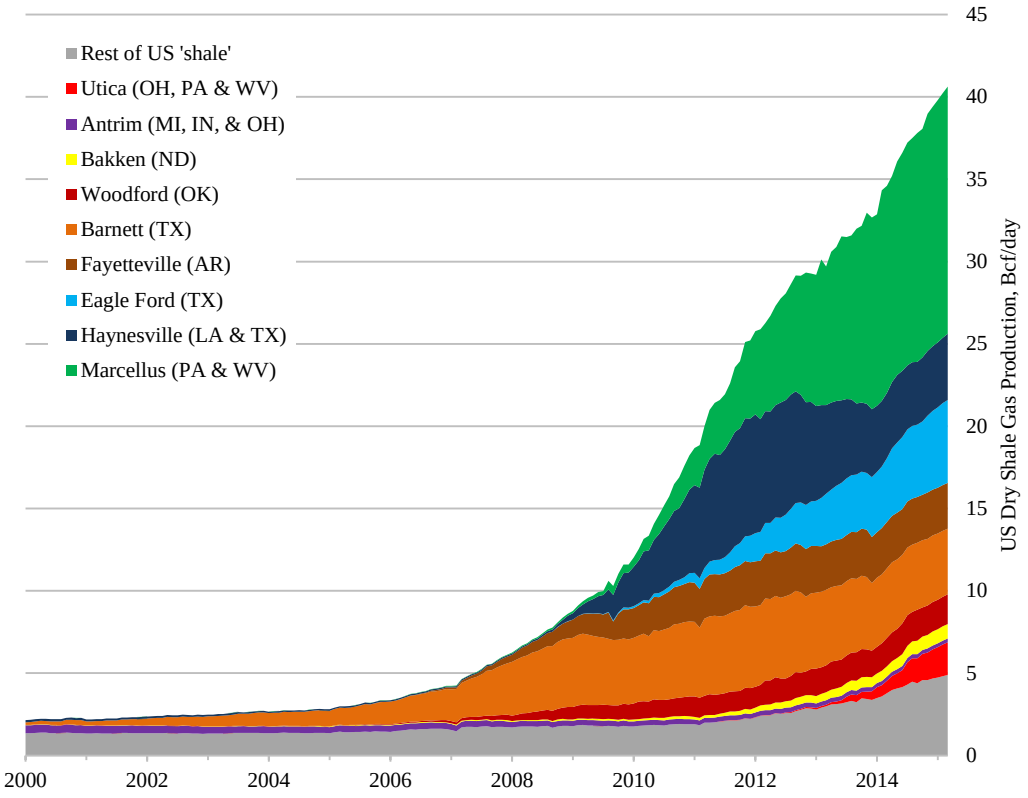

Fig. 1.3 – US dry gas production for selected shale plays. Source: U.S. Energy Information Administration

Future development of the shales will rely on balance between prices on hydrocarbons in the development region and cost of drilling and completion of horizontal wells, transportation of oil and gas and further treatment and distribution. While the prices for hydrocarbons are experiencing a downfall movement, a closer attention should be paid on the well design optimization. Since the actual costs for shale development outside of the US could be much higher due to limited number of active players on the market, the proper balance between projected production and anticipated costs in a single well scale is vital for economic attractiveness of future shale developments.

1.1 Objectives and methodology

The necessity of careful economic optimization of shale wells cannot be overestimated. While industry acquired sufficient experience in simulation and prediction of future production, it is still lack of motivation for accurate cost estimation of shale wells. Partially, the reason was in high prices on oil and gas when one will be sure to pay back their investments after a year or two. Nowadays, if you want to succeed in shale development, especially in the new regions, it is necessary to perform a comprehensive economic optimization.

This fact motivated us to prepare a comprehensive economic optimization of a single shale well covering a wide range of reservoir and completion parameters. The objective of the thesis is to analyze the effect of different parameters on the economic performance of the well based on selected financial metrics. We believe that the work will be useful at the stage of initial economic assessment of their project to understand the risks while company is lacking of accurate historic

production information. The primary idea is not to provide a specific numbers in terms of cash flow or investment efficiency, but rather show the trends and magnitude of changes of economic performance when reservoir properties or completion design are different.

Methodology is based on classic sensitivity analysis with three different in-situ fluids. While most of the cases deal with one variable, some sensitivities are meant to keep specific parameters as a constant value requiring change of two or three variables at a time. We believe that selected sensitivities cover the range of the most important parameters and provide comprehensive guidelines when estimating an economic performance of the well.

1.2 Thesis structure

The thesis consist of nine chapters and three appendixes. Chapter 1 gives a brief introduction to the importance y of the work, thesis' objectives and methodology. Chapter 2 includes technical background about shale reservoirs, horizontal well completion with hydraulic fracturing and fracture models used in numerical simulations. It also deals with economic background related to oil and natural gas prices and includes a review on available cost models for shale wells and different economic metrics. Chapter 3 gives initial model setup and sensitivity analysis description. Chapters 4–6 deal with detailed results description for dry gas, gas condensate and oil cases with different sensitivity analysis. Chapter 7 includes addition sensitivities regarding gas desorption effect for dry gas simulation and a sensitivity on change of oil and gas prices and Capex. It also include analysis of optimal well spacing in a section of 1×2 mi. Chapter 8 aggregates thesis' conclusions and Chapter 9 gives recommendations and further work discussions. In addition, there are three Appendixes in the work: (A) Units conversion; (B) Fluid composition and Equation-of-State description and (C) SENSOR input file example for gas condensate simulation case.

Chapter 2

Theoretical Background

2.1 Technical Background

2.1.1 Shale Rocks and Shale Plays

Shales refer to fine-grained sedimentary rocks usually formed as a mix of clays and quartz minerals. Compositionally, shale rocks belong to mudstones with several differences. Shales are finely laminated and fissile along the laminations. Fine lamination means that the rock is formed by compaction of thin layers, while fissile property represents easy split of the rock along the lamination ("Geologic Glossary", 2015; "Shale", 2015). The more strict classification of shales is given by Jackson and Bates (1997) who defined shales as laminated rocks containing more than 67% of clay-sized materials.

Apart from clays and quartz, shales can include other clay-size particles (for example, chert, carbonates or iron oxide minerals) and organic remains of flora and fauna. The color of shale rocks depends on the mineral composition accumulated in shallow water or low-energy depositional environments and changes between yellow, red, brown, grey and black. ("Shale Oil and Gas", 2015; "Shale", 2015). Black or grey color of shales indicates high total organic content within the rocks. Together with sufficiently high pressure, correct temperature range and oxygen-deficient environment, the black shales are excellent candidates to transform organic content into oil and gas.

Shale plays refer to formations with similar geological properties containing significant amount of hydrocarbons within specific geographical area ("Shale", 2015). Significant amount means that future exploration and development of the shale play is economically profitable based on today's technologies and commodities prices. Depends on the presented in-situ fluid in the reservoir, the plays are generally divided into oil, gas and liquid-rich shale plays.

Unlike conventional reservoirs, shales often appear to be both a source rock and a reservoir for the hydrocarbons. Formed oil and gas are trapped inside the porous media and cannot migrate out of the rock due to excellent sealing properties of shales. Natural low permeability caused by high concentration of clays makes shales not only the excellent cap rock for the hydrocarbons, but also

create challenges for effective flow within the formation during the production period. **Fig. 2.1** shows typical range for permeability in shale, tight and conventional formations. While the permeability of conventional reservoirs usually ranges between 10–100 md and up to 1 darcy for a highly permeable reservoirs, the typical range for shale reservoirs may go down to 10–1,000 nd (0.00001–0.001 md). Therefore, shale reservoirs require the increase of active drainage area around the wellbore using advanced completion and stimulation techniques.

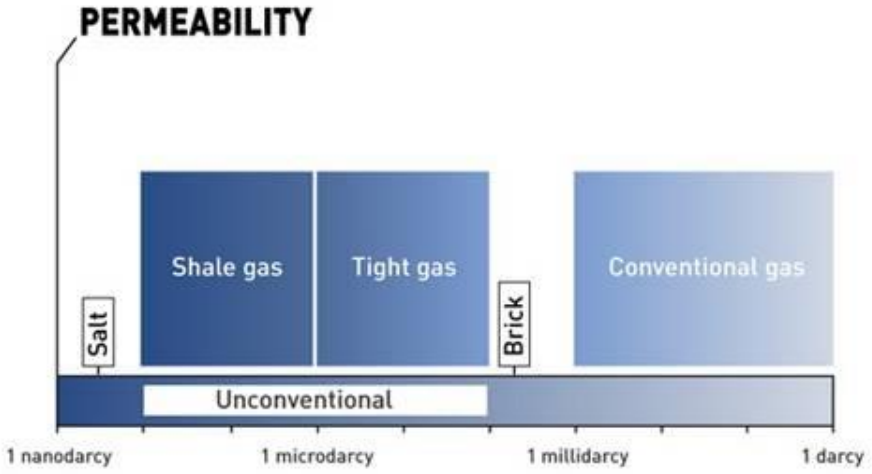

Fig. 2.1 – Typical range of permeability for different formation types. Source: Total S.A.

2.1.2 Horizontal Drilling and Hydraulic Fracturing

The combination of using horizontal wells together with hydraulic fracturing became an industrial standard in development of shale reserves. While horizontal drilling aims to increase the active drainage area by drilling the well parallel to the top of the reservoir, hydraulic fracturing increases the near-wellbore permeability allowing oil and gas flow easier from the reservoir into the well. Both technologies are crucial to achieve favorable economics in shale wells and have been widely commercialized over the last years.

Horizontal drilling is the technique of penetrating the reservoir parallel to the top of the formation with a deviation angle close to 80–90°. The technology is known in the US since 1940s; however it was not popular in the industry until 1989 when the horizontal drilling drastically increased production in highly fractured Austin Chalk reservoir (Pendleton, 1991). This success re-focused companies on further development of horizontal drilling and led to economical re-assessment of many low-marginal or non-economical projects. The share of horizontal completion among total number of wells has significantly grown within the last 20 years. For example, in 1991 in the US only 9% of the rigs were allocated for horizontal drilling, while today more than 75% of the rigs are used for it ("Rig Count", 2015). Based on the total number of land wells in the US, about 28,000 wells were completed horizontally during the last year. Average drilling time for all types of well was about 18 days per well in 2014 (**Fig. 2.2**).

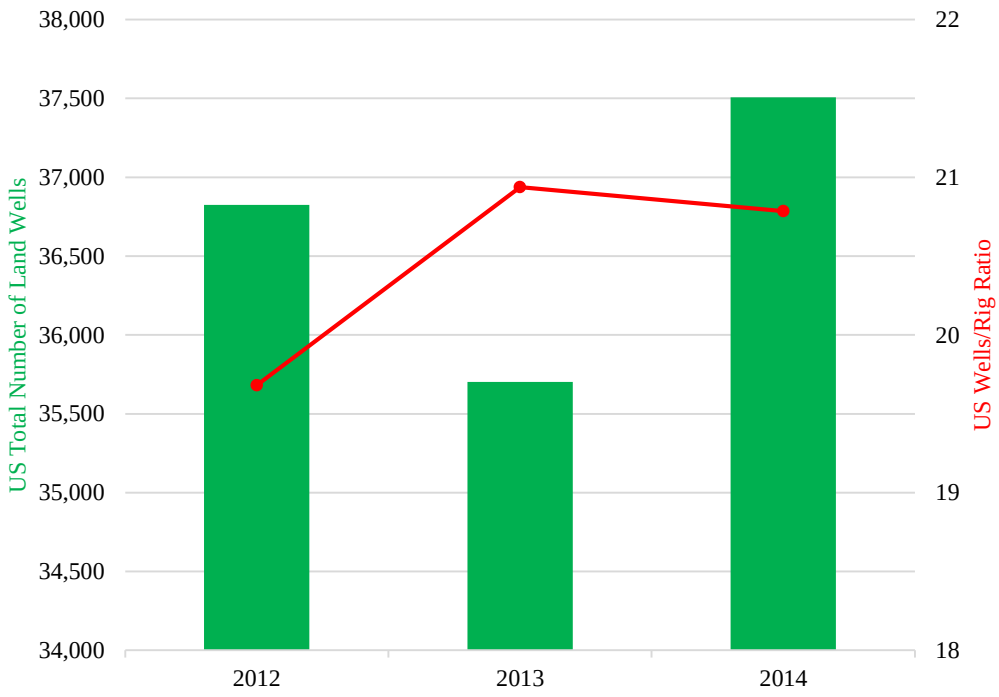

Fig. 2.2 – Total number of drilled wells and Wells/Rig ratio in the US. Source: Baker Hughes Inc.

Horizontal wells are costly comparing with traditional vertical wells; however the improved drainage area is a key factor for economic development of shales. For example, assuming the area of 640 acre (1 mi^2), the reservoir can be developed either by 16 vertical wells (well spacing of 40 acre) or just 4 horizontal wells (well spacing of 160 acre). Having initial costs for vertical and horizontal wells case relatively equal, the production in case of using horizontal wells could be higher by 20%, positively reinforcing project's economy (Caputo, 2011). Important to remember that each development plan for shale reservoirs has to be evaluated carefully and individually; however, in general, horizontal wells proved to be an effective solution in increasing shale reservoir performance, especially when combined with hydraulic fracturing.

Hydraulic fracturing (or commonly known as fracking) is a process of inducing fracture network in the formation around the wellbore to stimulate hydrocarbons' flow and achieve higher production profile from the well ("The Process of Hydraulic Fracturing", 2015). The stimulation is done by pumping a mix of water, sand and/or proppant and other chemicals down to the formation under high pressure. When the increased pressure inside of the well overcomes formations' fracturing pressure, the fracture creating process starts. After the required size of the fracture is achieved, pressure is released. Sand and proppant fill the volume of the fracture to prevent its collapsing. The result of the stimulation is an increased permeability of near-wellbore region and higher cumulative production from the reservoir. Hydraulic fracturing is done in both vertical and horizontal wells and applicable for any type of the reservoir, but became crucial in development of shale plays.

Fig. 2.3 – Top view on hydraulic fracturing process. Source: SodaHead

To increase the economic effect from the treatment, the well is fractured several times along the wellbore. The total number of fractured intervals can vary significantly between 10–100 stages and purely dictated by economic calculations ("Hydraulic Fracturing 101", 2015). **Fig. 2.3** show the top view of hydraulic fracturing process in a well. In general, when the incremental costs overcome the incremental revenues from creating a new fracture stage, the optimum number of fracs is achieved. During the stimulation, the process is commonly controlled by the number of gauges at the surface equipment together with a micro-seismic monitoring from the offset wells ("Understanding Hydraulic Fracturing", 2015). The seismic data allow estimating the direction and size of the induced fractures, while gauges and real-time pressure data help to optimize the treatment's duration. However, often the actual fracture parameters deflect from pre-calculated due to the differences in rock properties and overall efficiency of the treatment. This parameters' difference may significantly influence on the economy of the project and cannot be precisely estimated until first production data is available and history matching of the well is done.

Therefore, the selection of treatment design can be a challenging task, especially when fracturing complex and heterogeneous reservoirs. Additional questions arise when selecting the fracture model for well performance simulation. It could be useful to observe the performance of previously done stimulations in offset wells located in the same area to quantify the possible difference between pre-calculated and actual fracturing parameters and estimate overall treatment efficiency.

2.1.3 Simulation Fracture Models

Production forecast depends on not only completion and treatment design, but also on the assumption about the general shape of the fracture network induced. Different physical assumptions behind the models causing difference in models' performance; therefore selection of the fracture model is an important issue. **Figs. 2.4–2.6** represent three different simulations models: (1) planar fracture model, (2) fracture network model and (3) dual-porosity model.

Planar fracture model (or bi-wing fracture model) is one of the commonly used models for numerical simulations. The fracture represented by a group of cells extended perpendicularly from the wellbore on a distance specified as a fracture half-length (Fig. 2.4). Physical parameters of the fracture (for example, fracture width and conductivity) are used to estimate the effective fracture permeability. Together with increased porosity, fracture works as a conveyer for the fluid from the reservoir to the wellbore.

Fracture network model represents another approach in fractures' simulation. Each frac is represented by number of interconnected channels with the predefined total fracture area (Fig. 2.5). The channels' spacing is defined by the size and number of blocks in between. The channels are gridded symmetrically providing accelerated drainage of the blocks inside the network. All the channels have the same porosity and effective permeability. Both planar and network fracture models can be compared if the total fracturing area is kept identical.

Dual-porosity model consist of three regions each representing different fracture density created after the treatment (Fig. 2.6). Region 1 is a dual porosity region representing the volume of the reservoir with the highest fracture density and connected with the perforation point. Region 2 is a dual porosity region which defines the volume with the lower fracture density representing the surroundings of the main stimulation area. Region 3 represents single porosity region which have not been affected by stimulation job at all. The flow between the regions is defined so that fluid from Region 3 can only flow into Region 2, but not into Region 1. Subsequently, Region 1 is only connected with Region 2. Fractures in dual porosity model are not introduced explicitly as it is done in planar or network models.

In addition, instead of simulation of the whole well, the significant reduction in simulation time can be achieved when the performance of one fracture is multiplied by two (to cover both sides of the wellbore) and also by the total number of the fractures. This approach can be applied for any fracture model. However, it is only feasible under the assumption of fractures' identity along the wellbore and complete homogeneity of the reservoir.

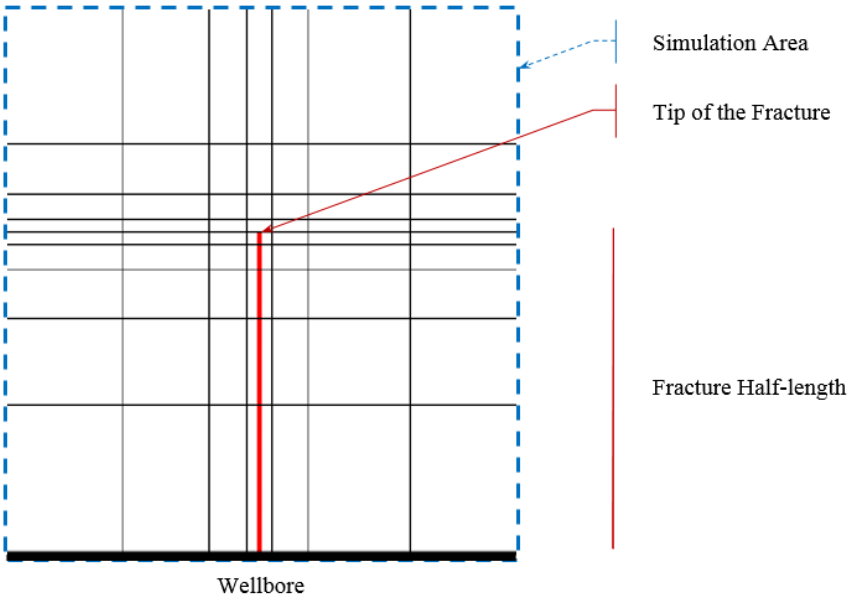

Fig. 2.4 – Planar fracture model. Adopted from: "Pipe-It Manual"

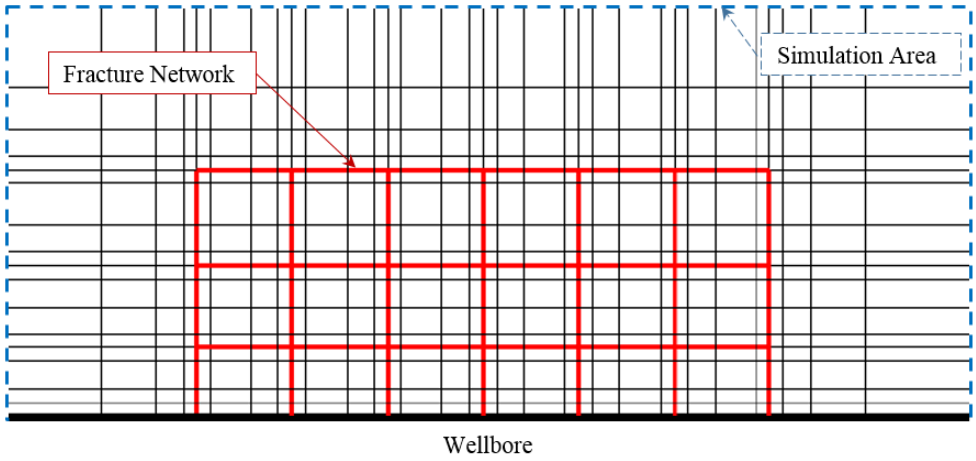

Fig. 2.5 – Fracture network model. Adopted from: "Pipe-It Manual"

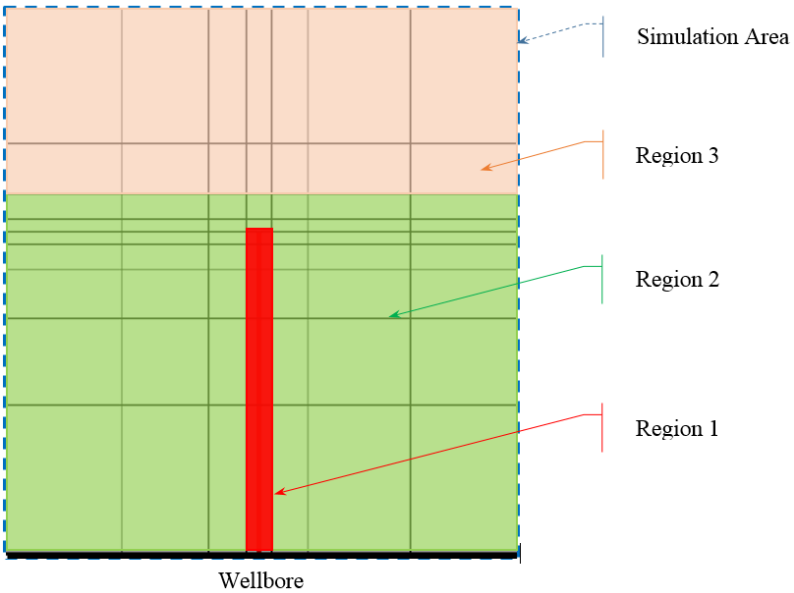

Fig. 2.6 – Dual porosity model. Adopted from: "Pipe-It Manual"

2.2 Economic Background

2.2.1 General Economics of Shale Well

Shale well economics can be split into two parts: (1) expense part, including capital and operational expenditures (usually referred as Capex and Opex), royalties and payments of interest rate on the raised funds, depreciation of the equipment, purchase of land rights, transportation of oil and gas and water disposal; and (2) profit part, which depends on the volumes of produced hydrocarbons and the price on commodities in the market. When the price of hydrocarbons are stable or production rates are sufficiently high, company cash flows are secured. The problem arises when the profit part shrinks disproportionately faster than expense part due to production decline or rapid change in oil and gas prices.

Costs associated with development of shale reservoirs are usually much higher comparing with conventional reservoirs onshore. Coupling it with a rapid production decline within the first year, the economy of shale wells may become very sensitive to the market fluctuations and ineffective cost control (Nobakht et al., 2013; Gonzales and Callard, 2011; "The Dangerous Economics of Shale Oil", 2014). Additional problem may occur with excessive liquid drop-out in liquid-rich shale reservoirs. Lowering bottomhole pressure (BHP) below the saturation pressure will result in oil condensing from the gas. With very low mobility ratio (due to low relative permeability), oil will be trapped at the rock surface without possibility for later extraction (Juell and Whitson, 2013). This would reduce the economic value of the well and making pre-planned project cash flow difficult to achieve.

Another specific aspect of working with shale projects associated with constant need of investments to continue drilling of new wells. Many small players are lack of money to cover total drilling expenditures by themselves; therefore, they borrow funds from the investors on the return basis. Debt investment is seemed to be a common way to raise funds at the beginning of shale revolution, meaning that the bank gives the money without taking part in the company's operations. Another approach is when banks are investing into assets of the company, sharing the development risks and reducing the cost of capital for a company. The second option is commonly used nowadays and may influence on lowering the break-even price of shale developments.

In either way, the company usually will not get all the money at a time; at first it needs to prove the project potential by drilling few wells and observe production rates and production decline curves. If the production correlates with the expectations supporting the investment decision, the project will get the rest of the funds. However, if drilling fails or actual Capex and Opex grow significantly, the economy of the project could shrink considerably. Therefore, shale players have to focus not only on the production optimization of the well, but pay close attention of the market economic, look for appropriate cost models and combine different economic metrics for project evaluation.

2.2.2 Crude Oil and Natural Gas Prices

The project's economy is highly dependent on both production estimation and oil and gas prices forecast. Even with accumulated experience in forecasting production profile using numerical models of the reservoirs, there is still a huge uncertainty in prediction of hydrocarbon prices. The main challenge associated with price forecasting is the vast amount of global variables influencing the price change. Markets are very sensitive on fluctuations in hydrocarbon production across the world, economic situation of major consumers of crude oil and natural gas, total hydrocarbon storage capacity, local conflicts and wars, involvement of unconventional resources into development and many other factors.

The historical data of BRENT oil and Henry Hub natural gas prices are shown in **Fig. 2.7**. Before the shale revolution in the US and World Economic Crisis which happened in early 2008, the prices for oil and gas showed significant steady grow. Then, just in a 12 months, the oil price sinks from 140 USD/bbl down to 50 USD/bbl losing more than 60% of the original price! The same trend observed for natural gas with 65% change in the price. Since that, the price of natural gas fluctuates around the same low level due to significant increase in the shale gas production in the US. The low gas price made the economy of the shale gas projects questionable, switching companies' attention towards shale oil plays. Together with the stabilization of oil prices between 2009 and 2014, the share of rigs used for drilling oil wells grew significantly from 26 to 80% (**Fig. 2.8)**.

The forecast of oil and gas prices is constantly updated based on the available information about global production, consumption, storage capacities and periodically reviewed by companies, inversing banks and energy agencies. Of course, there is no assurance in the accuracy of the prognoses; especially taking into account that the methodologies to estimate the future prices are different and often proprietary. However, the project's economy should be based on the realistic scenario and preferably by using price's forecast consensus.

The forecast for BRENT oil for 2015 ranges between 50 and 85 USD/bbl with a consensus at 65 USD/bbl (**Fig. 2.9**). The market expects stabilization of oil prices in short-to-medium term associated with general balancing of global oil demand and supply as the actual production will be reduced on high-cost shale plays in the US. At the same time, oil inventories are at the highest level in the United States, showing on the one hand the possible strategy of investment funds to buy oil now with a positive future outlook on the prices and, on the other hand demonstrating low underlying demand for crude oil ("Oil Prices Fall Amid Record Inventories", 2015). In addition, current financing cuts in exploration programs may result in shortage of production capabilities in the next 5–7 years if the low prices stay for significantly longer period.

Henry Hub natural gas prices are forecasted between 2.8 and 4.5 USD/Mscf with a consensus at 3.5 USD/Mscf (**Fig. 2.10**). The price keeps staying at the low level since mid-2008 and there is no downside expectations. Gas prices are close to the minimum sustainable level and the pressure of the low prices have already pushed companies seeking a bankruptcy protection ("Quicksilver Resources Files Bankruptcy as Gas Price Drops", 2015). This trend may force banks to review the risks of funding small companies and slow down not only development of shale gas, but shale oil projects as well.

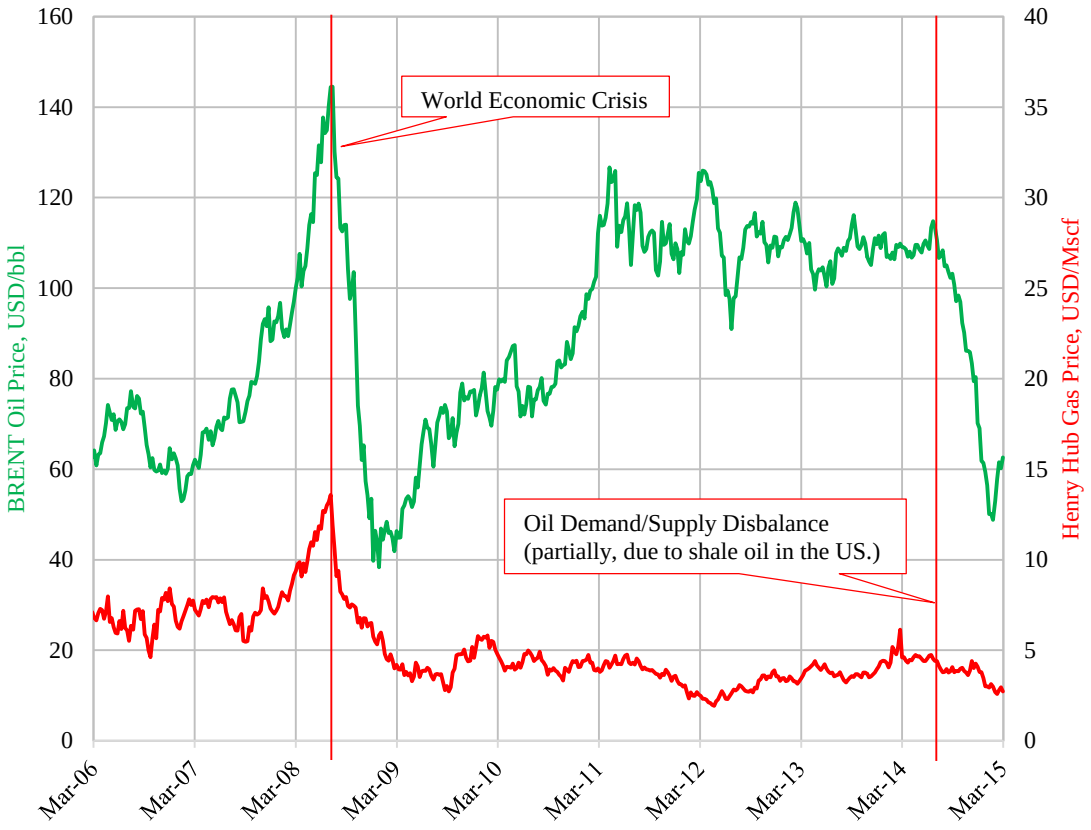

Fig. 2.7 – BRENT oil and Henry Hub gas prices history. Source: Bloomberg Professional Service

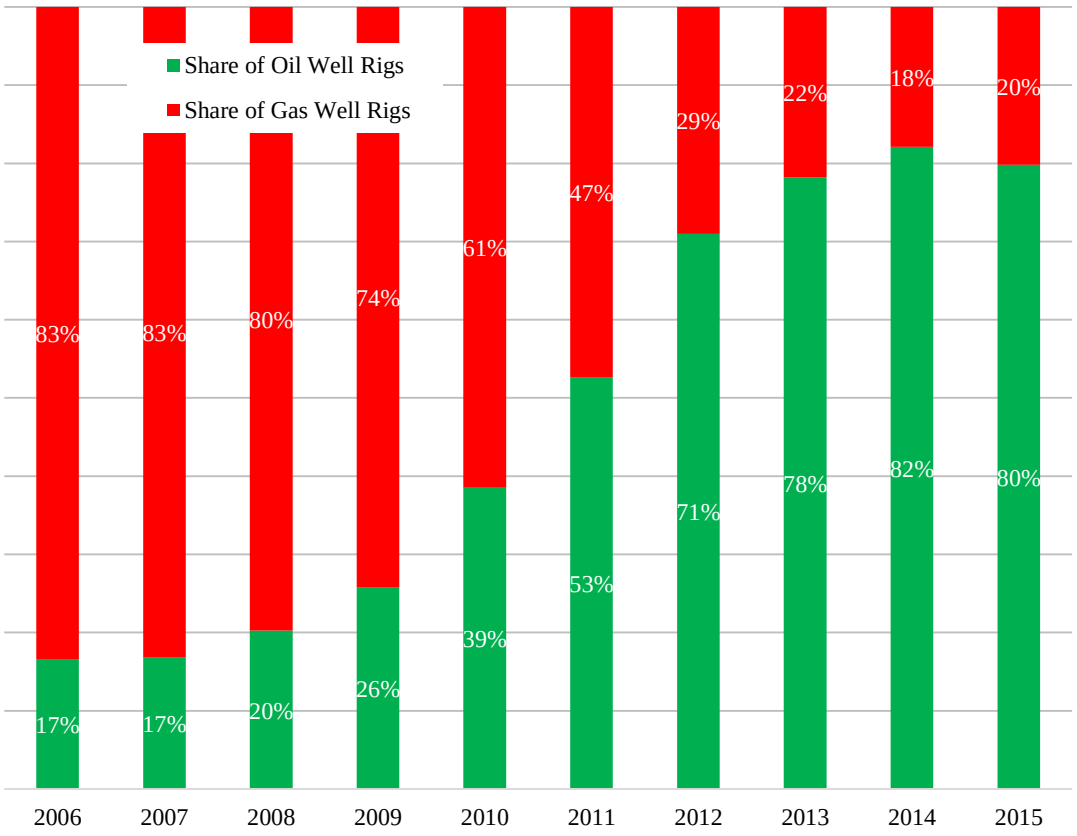

Fig. 2.8 – Shares of oil and gas rigs in the US. Source: Baker Hughes Inc.

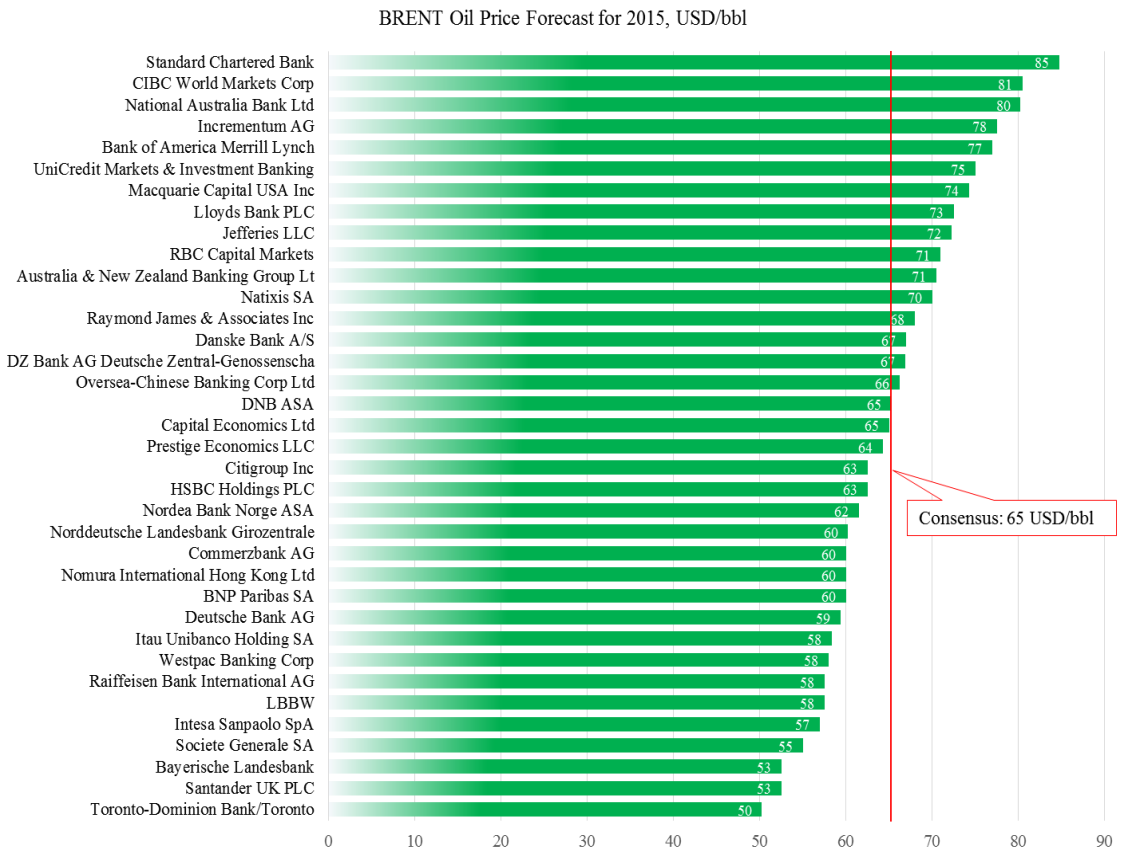

Fig. 2.9 – BRENT oil price forecast and consensus for 2015. Source: Bloomberg Professional Service

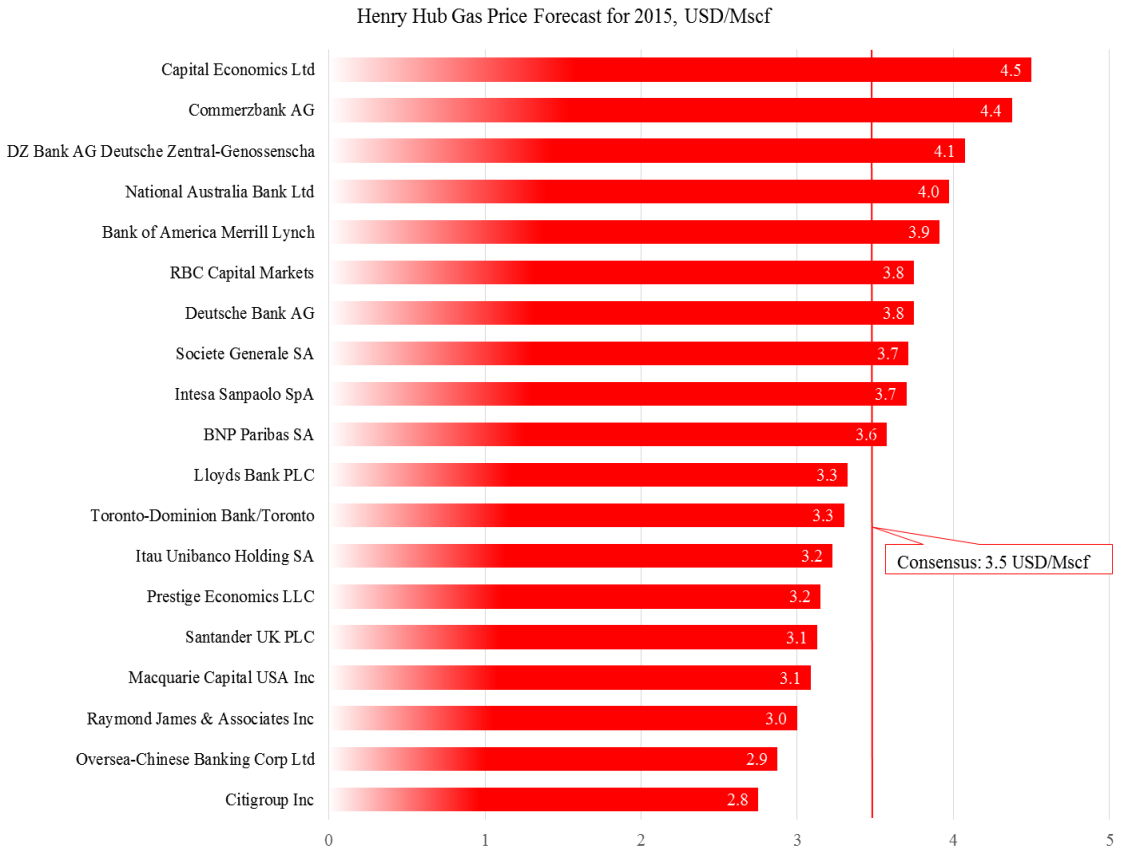

Fig. 2.10 – Henry Hub natural gas price forecast and consensus for 2015. Source: Bloomberg Professional Service

2.2.3 Economic Models Overview

When the prices are low and possible project's revenues shirk, the expense part of the project requires a closer look. Each company estimates project's Capex (generally associated with the drilling and completion operations and fracturing of horizontal well) and future Opex. However, before the recent fall in prices companies had a very little interest towards accurate estimation of the final cost of the well due to the high price of oil. Today, the proper cost estimation and precise well design optimization became key factors for low-marginal project; therefore, it is important to look at some examples of available cost models.

Gonzales and Callard (2011) optimized the completion and hydraulic treatment of horizontal well using very simplistic model. It requires two simple assumptions to be done: the cost of fracture and the total drilling costs. It does not allow the engineer to include fracture-associated costs (for example, proppant, fracture fluid and pumping costs) separately. The model also lacking distinction between drilling horizontal and vertical section of the well, so the immediate result of well length optimization is hard to control. The authors do not present the model itself, but based on the economic data presented, the cost model can be written as:

$$C_{well} = D_{total} + C_{frac} N_{frac} \quad \text{.....(1)}$$

where:

C_{well} = total well cost, USD

D_{total} = total drilling cost, USD

C_{frac} = cost of creating one fracture, USD/frac

N_{frac} = total number of fractures created

Britt and Smith (2009) updated the model described by **Eq. 1** through splitting total drilling costs into two separate groups: vertical and horizontal drilling costs. The authors also introduced stimulation cost coupled with the total fracture area created during the treatment and cost associated with the well completion. The model is lacking of the distinction between proppant, fracturing fluids and pumping costs and creating difficulties in coupling them with total fracture area and not using the total number of fractures instead. The proposed model is shown in **Eq. 2**:

$$C_{well} = D_{vert} + D_{horiz} + C_{compl} + C_{stim} A_{stim} \quad \text{.....(2)}$$

where:

C_{well} = total well cost, USD

D_{vert} = vertical section drilling cost, USD

D_{horiz} = variable horizontal section drilling cost, USD

C_{compl} = variable cost of completion, USD

C_{stim} = stimulation cost of frac area, USD/ft^2

A_{frac} = total stimulated frac area, ft^2

More transparent example of the cost model was presented by Aghighi et al. (2006). The authors divided the fracture costs into three basic components: required mass of proppant, volume of fluid and pumping pressure. Multiplication of these components by relevant estimated prices per unit yields the total cost of the treatment of a single fracture. This approach allows to control the change of costs associated with hydraulic fracturing when any changes are implemented in the treatment design. However, there is insufficient focus towards the drilling expenditures which are combined together into single parameter called "fixed costs". This creates difficulties if the company wants to see the immediate change of costs for longer or shorter horizontal well. The authors described the model as shown in **Eq. 3**:

$$C_{tr} = P_{fl}V_{fl} + P_{pr}M_{pr} + P_{pump}P_{av} + C_{fixed} \quad \text{.....(3)}$$

where:

C_{tr} = treatment cost, USD

P_{fl} = price of fracturing fluid, USD/gal

V_{fl} = volume of fracturing fluid, gal

P_{pr} = price of proppant, USD/lb

M_{pr} = mass of proppant, lb

P_{pump} = pumping cost, USD/psi

P_{av} = hydraulic power of the pump, psi

C_{fixed} = miscellaneous and fixed cost, USD

Marongiu-Porcu et al. (2009) optimized the treatment of horizontal well including both detailed drilling description and treatment variables. The authors split the fixed cost into vertical and horizontal drilling costs, as well as cost of mobilization/demobilization of the rig. Proppant mass and volume of fracturing fluid are introduced explicitly and coupled with associated prices, while pumping costs are now defined as a single component. The authors does not present the model itself, but based on the available economic input data we assume that it can be described by **Eq. 4**:

$$C_{tr} = D_{vert} + D_{horiz} + C_{pump} + C_{m/d} + P_{pr}M_{pr} + P_{fl}V_{fl} \quad \text{.....(4)}$$

where:

D_{vert} = cost of vertical section drilling and completion, USD

D_{horiz} = cost of horizontal section drilling and completion, USD

C_{pump} = cost of pumping, USD

$C_{m/d}$ = cost of mobilization and demobilization of the rig, USD

P_{pr} = price of proppant, USD/lbm

M_{pr} = mass of proppant, lbm

P_{fl} = price of fracturing fluid, USD/gal

V_{fl} = volume of fracturing fluid, gal

Juell and Whitson (2013) presented another cost model in optimization of liquid-rich shale well. The total cost of the model includes the vertical drilling costs (expressed as a single component) and horizontal drilling costs (by introducing variable for horizontal length of the well coupled with the average price for drilling a ft of this section). The fracture cost now presented as a single component and does not include the distinction between the required proppant mass, fracture fluid volume or required pumping pressure. Fracture cost is coupled with the total number of fractures in the treatment. In addition, the authors included non-linear increase of the treatment cost with increased treatment size by introducing empirical coefficient. The proposed model is presented by **Eq. 5**:

$$C_{well} = D_{vert} + d_{horiz} L_h + C_{frac} N_{frac} \left(\frac{x_f}{x_{f0}} \right)^a \quad \text{.....(5)}$$

where:

C_{well} = total well cost, USD

D_{vert} = cost of drilling vertical section of the well, USD

d_{horiz} = cost of drilling a foot of the horizontal section of the well, USD/ft

L_h = horizontal section length, ft

C_{frac} = cost of treatment of one fracture stage, USD

N_{frac} = number of fracture stages

x_f = new fracture half-length, ft

x_{f0} = fracture half-length which cost is initially estimated, ft

a = empirical constant determining how the cost of a fracture stage increases with treatment size

There are wide variety of cost models one can use for the estimation of Capex of a shale well. All of them have some advantages and disadvantage and the decision which one to use have to be done based on the available information about the treatment and experience from the previously drilled wells. **Table 1** consolidates all five models for a rapid comparison by the components they include.

TABLE 1 – COMPARING VARIOUS PROPOSED WELL COST MODELS BY COMPONENT

	Drilling costs		Frac costs			Number
Authors	Vertical	Horizontal	Proppant	Fluid	Pumping	of fracs
Gonzales and Callard	(✓)	(✓)	(✓)	(✓)	(✓)	✓
Britt and Smith	✓	✓	(✓)	(✓)	(✓)	(✓)
Aghighi et al.	×	×	✓	✓	✓	×
Marongiu-Porcu et al.	✓	✓	✓	✓	✓	×
Juell and Whitson	✓	✓	(✓)	(✓)	(✓)	✓

✓ indicates component is introduced to the cost model, × indicates component is not introduced to the cost model;
(✓) indicates component is introduced indirectly to the cost model

2.2.4 Economic Metrics Overview

When the expense part of the project is determined by selected cost model, one should decide how to specify the profit part. Apart from calculating revenues generated by a well, the company have to select reasonable economic metrics to judge the economic outcome of the project. This selection depends on a range of non-technical parameters (for example, availability of cash and current cost of capital and duration of the land-lease or production license) and individually prioritized by different companies. Usually, at the stage of treatment design the engineer does not operate with more than one to two metrics, but including several different metrics may help to justify the economy of the project and give another perspective what to call "optimized design".

Net Present Value (NPV) is a well-known and probably the most popular metric used for economic evaluation of the project. It shows the difference between the present value of the cash inflows and the present value of cash outflows over the time, specifying the total value of the investment if the project is implemented ("Financial Dictionary", 2015). Many authors use NPV as the only metric for economic justification of fracture treatment design (Aghighi et al., 2006; Marongiu-Porcu et al., 2009; Britt and Smith, 2009; Juell and Whitson, 2013; Yu and Sepehrnoori, 2014; Barree et al., 2015). The equation describing NPV is shown as:

$$NPV = \sum_{i=0}^{n} \frac{R_t}{(1+i)^t} - C_{well} \quad \text{.....(6)}$$

where:

$NPV =$ Net Present Value, USD

$R_t =$ cash flow on time *t*, USD

$i =$ discount rate, fraction

$t =$ time of cash flow (project time), year

$C_{well} =$ total well cost, USD.

From **Eq. 6** we notice that revenues to be calculated when the treatment is done, while total well cost solely driven by the cost model we select for the project. Different authors propose slightly different models for revenues calculations depending on the range of assumptions one is capable to apply. For example, Marongiu-Porcu et al. (2008) defines the annual revenues by including royalties, taxation and Opex payments as described by **Eq. 7**:

$$R_t = V_{HC} P_{HC} (1 - f_r)(1 - f_o)(1 - f_t) \quad \text{.....(7)}$$

where:

$R_t =$ annual revenue stream, USD

$V_{HC} =$ cumulative volume of produced hydrocarbons within the year, bbl or Mscf

$P_{HC} =$ hydrocarbon price, USD/bbl or USD/Mscf

$f_r =$ fracture of cash flow allocated to royalties, fraction

$f_o =$ fracture of cash flow allocated to operational expenditures, fraction

$f_t =$ fracture of cash flow allocated to taxes, fraction

Juell and Whitson (2013) omit using of taxation and royalty payments, but split the hydrocarbon revenues stream into cash flow from oil and gas production and includes the costs associated with disposal of produced water. The proposed revenues model is presented as:

$$R_t = Q_{o,t}P_o + Q_{g,t}P_g - Q_{w,t}P_w \quad \text{.....(8)}$$

where:

R_t = annual revenues stream, USD

$Q_{o,t}$ = cumulative oil production for sale within a year, bbl

P_o = price of oil, USD/bbl

$Q_{g,t}$ = cumulative gas production for sale within a year, Mscf

P_g = price of gas, USD/Mscf

$Q_{w,t}$ = cumulative water production for disposal within a year, bbl

P_w = cost of water disposal, USD/bbl

Fig. 2.11 represents typical NPV curve for different number of stages in hydraulic fracturing design. In this example, the maximum discounted cash flow observed with 30 and 45 stages for gas condensate and oil reservoirs respectively. At the point of maximum NPV, the marginal costs and marginal revenues from additional frac are equal, yielding economic optimum for the well. The left part from the optimum represents the situation when incremental revenues still overcome incremental cost from additional fracture, while the right part represents the opposite situation.

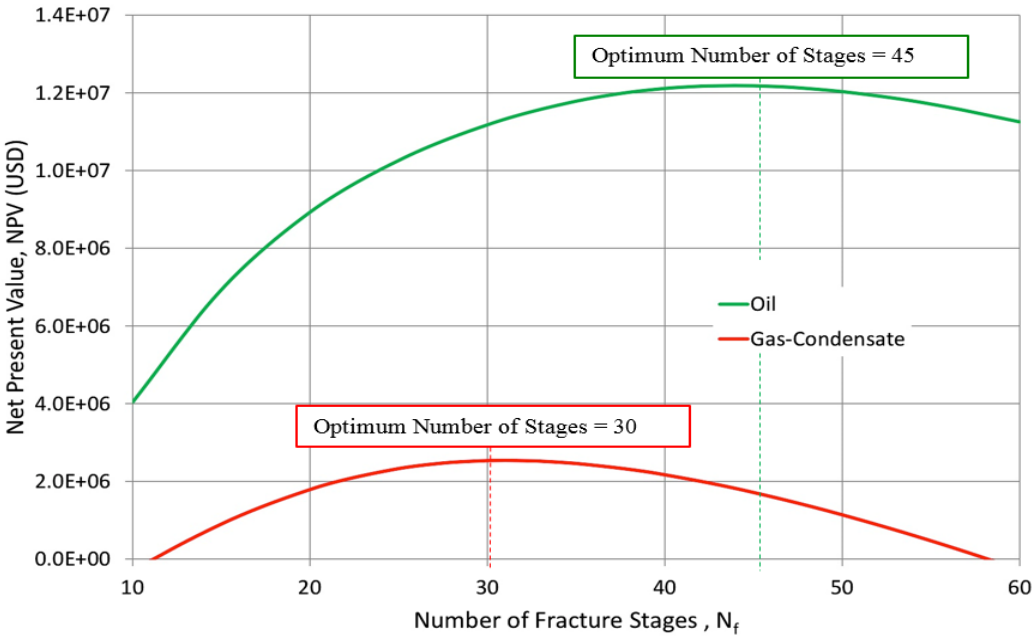

Fig. 2.11 – NPV calculations vs. total number of fracture stages. Adopted from: Juell and Whitson (2013)

Because of simple understanding and straight-forward explanation of the results, NPV proved to be a common tool in economic justification of the project. It has a clear explanation of the direct outcome of the investment measured in monetary units, however lacking of the project size (connection between the net present value with required total investments) is the main disadvantage of this metric (“Financial Dictionary”, 2015).

Discounted Profitability Index (DPI) is a metric which defines the relationship between future discounted cash flow and the required initial investments through their ratio ("Financial Dictionary", 2015). DPI tells how much value we receive per dollar avoiding the scale of investment and net cash flow. Coupled together with NPV, the metric allow understand the investment efficiency. If DPI is greater than 1.0, the project has a positive economy while the project with DPI less than 1.0 have to be rejected. DPI can be calculated in terms of discounted cash flow or NPV as shown in **Eq. 9** and **Eq. 10:**

$$DPI = \frac{\sum_{t=0}^{n} \frac{R_t}{(1+i)^t}}{C_{well}} \quad \text{.....(9)}$$

$$DPI = \frac{\sum_{i=0}^{n} NPV_i}{C_{well}} + 1 \quad \text{.....(10)}$$

where:

DPI = Discounted Profitability Index

NPV = Net Present Value, USD

R_t = annual revenue stream, USD

i = discount rate, fraction

t = time of the cash flow (project time), year

C_{well} = total well cost, USD

Lalehrokh and Bouma (2014) used both NPV and DPI in shale wells spacing optimization. In some cases, the maximum values of DPI and NPV corresponded to the same well spacing giving a single optimal solution. In other cases, the authors have to give a preference to one of the metric to select the final treatment design. **Fig. 2.12** shows the example of coupled NPV and DPI curves.

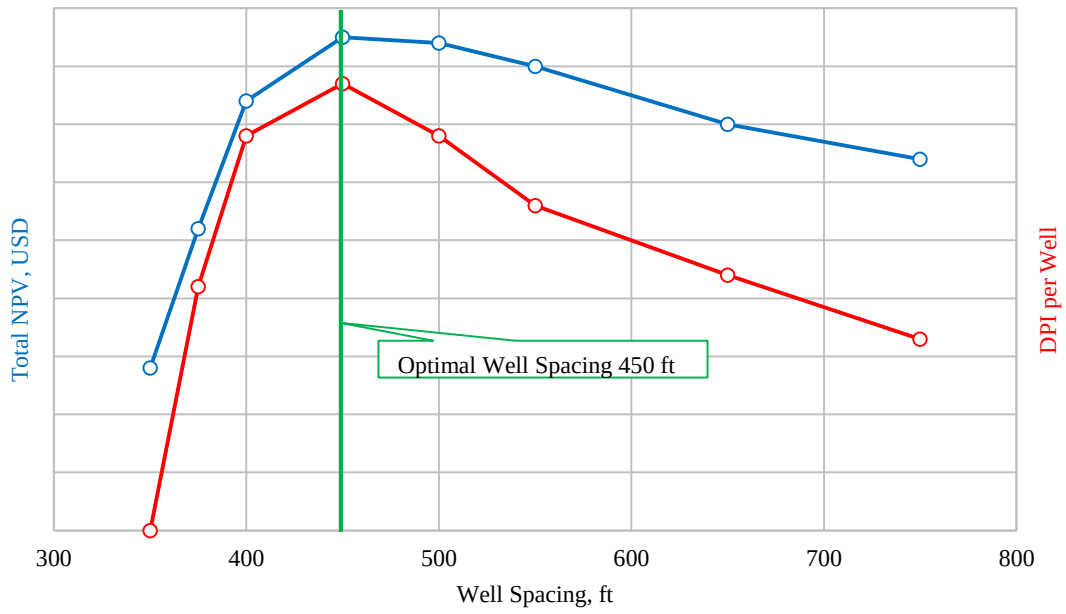

Fig. 2.12 – NPV and DPI calculations vs. well spacing. Adopted from: Lalehrokh and Bouma (2014)

Veatch (1986) and Rueda et al. (1994) used several additional indicators in comprehensive economic evaluation of the shale wells: Payout Time (PO) and Internal Rate of Return (IRR). Together with discussed NPV and DPI these two metrics allow the company to find the optimum economic solution based on internal financial constraints.

Payout time is a period of time when the expected revenues of the project will overcome the initial investments ("Financial Dictionary", 2015). Therefore, it is a moment when the well starts to generate net profit for the company and it is desirable to have payout time as short as possible. Fast production decline observed from the first months and reduced average lifetime of shale wells vs. conventional wells (7.5 years vs 12 years) denotes reasonable PO for shale wells around 3–5 years ("New Well-Productivity Data Provide US Shale Potential Insights", 2014). However, with favorable economy this time can be reduced down to 2–3 years.

Internal Rate of Return (IRR) is a specific discount rate at which the project NPV equals to zero ("Financial Dictionary", 2015). In other words, it shows the break-even cost of capital for the company and if IRR is higher than the companies discounting factor, the project should be accepted. In general terms, having mutually exclusive project, higher IRR indicates better project to invest in. Companies keep their internal rate of return as a commercial secret and always specify its minimum acceptable level for the project. Internal rate of return can be calculated using **Eq. 11:**

$$NPV = \sum_{t=0}^{n} \frac{R_t}{(1+r)^t} - C_{well} = 0 \quad \text{.....(11)}$$

where:

$NPV =$ Net Present Value, USD

$R_t =$ annual revenue stream, USD

$r =$ Internal rate of return to yield NPV = 0, fraction

$t =$ time of the cash flow (project time), year

$C_{well} =$ total well cost, USD

When several metrics applied for the economic evaluation of the project, the optimal well design solution could change. Rueda et al. (1994) showed that using of four metrics together with logical constrains can shift the optimum half-fracture length from the point of maximum NPV by around 40%. Since the financial department uses a wide range of economic metrics to assess the project, additional including of DPI, PO and IRR would help the engineer to find and justify the best shale well design.

THIS PAGE INTENTIONALLY LEFT BLANK

Chapter 3

Model Description and Initial Setup

The model represents a hydraulically fractured single well with completion typical for shale wells, including the horizontal section length, vertical depth and number of fracturing stages. The reservoir initial permeability and porosities are selected within typically observed shale plays in the US. The simulation is done for three different in-situ fluids (dry gas, gas condensate and oil) and includes a number of sensitivities related to well completion, initial reservoir parameters and combination of them.

Instead of simulating complete well model, the project deals with a single planar fracture. By upscaling of results by required number of fracture, we can estimate total well performance. This approach is valid assuming that all completion stages are identical along the wellbore and the reservoir is homogenous. Thus, the total simulation time is significantly reduced for this project.

There are several different industrial solution for economic evaluation of the projects for both conventional and unconventional reservoirs, for example *ARIES* by Halliburton or *Merak* by Schlumberger. However, they were not available at the university at a time of working on this thesis. Therefore, we combined several different solutions to perform numerical simulations and economic calculations.

All necessary setups and aggregation of the results are done by using Integrated Asset Modelling software *Pipe-It* by Petrostreamz AS. The software allows easy controlling the input data, gathering the results in a user-friendly way and making changes in the include files to the numerical simulator. *Shale Well Optimizer* for Pipe-It, kindly provided by Petrostreamz AS, was extensively used to complete the project. The numerical simulations are done by using compositional and black oil reservoir simulator *SENSOR* by Coats Engineering Inc. Post-processing visualization is done using *Tecplot RE* by Tecplot Inc.

3.1 Simulation Model and Base Case Scenario Description

The simulation model used in the project include one planar fracture shown **Fig. 3.1**. The wellbore located along X-axis, the fracture propagates along Y-axis in the middle of the model penetrating total thickness of the reservoir. Logarithmic gridding is done in X-direction along the wellbore starting from the fracture cell and in Y-direction beyond the fracture's tip. The blocks between the wellbore and the tip of the fracture are geometrically spaced in Y-direction.

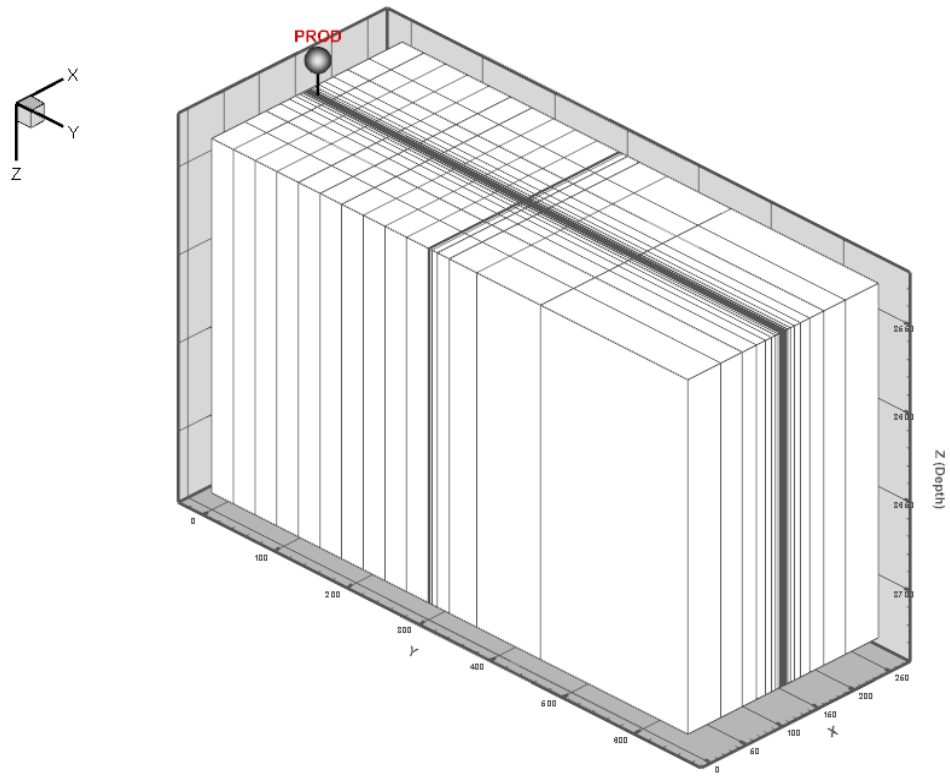

Fig. 3.1 – 3D view of simulation model. Wellbore located along X-axis. The fracture connection with the wellbore pinned with "PROD" label.

Shale's permeability and porosity can vary significantly between the reservoirs and even within the same shale play (Caputo, 2011; Walls and Sinclair, 2011). For example, in Eagle Ford formation porosity ranges between 2–11% and permeability changes 1–1,000 nd. Therefore, the selection of porosity of 7% and matrix permeability of 500 nd looks reasonable. One may argue that 500 nd is a very optimistic value, but we aimed to represent the well with average pay-out time within 16-24 months. Initial reservoir pressure is set to 7,500 psia on the 8,530 ft depth. The thickness of the reservoir selected to be 200 ft.

The 5,280 ft horizontal section is completed with 20 fractures with fracture half-length equal to 300 ft. Fracture width is set to 1 inch and physical fracture conductivity to be 1,000 md-ft. The well spacing of 160 acres yielding the single fracture drainage area of 4 acres. The summary of the initial reservoir parameters, fracture parameters and well completion for base case scenario simulation are shown in **Table 2**.

TABLE 2 – BASE CASE SCENARIO PARAMETERS		
Parameter	Value	Units
Matrix porosity, φ	0.07	
Matrix permeability, k	5,00	nd
Initial reservoir pressure, p_{ri}	7,500	psia
Reservoir thickness, h	200	ft
Reservoir temperature	135	°F
Reservoir vertical depth, H	8,530	ft
Horizontal well length, L_h	5,280	ft
Number of fractures, N_f	20	
Well drainage area	160	acre
Fracture spacing	264	ft
Wellbore diameter, horizontal section	4.5	inch
Wellbore diameter, vertical section	2.265	inch
Fracture half-length, x_f	300	ft
Fracture width	0.0833	ft
Fracture porosity	0.25	
Fracture conductivity	1,000	md-ft
Fracture drainage area	4	acre

3.2 Model Size and Gridding of Simulation Area

The dimensions of the model depend on two parameters: the spacing of fractures along the wellbore and single fracture drainage area. Fracture spacing is used to estimate the length of the simulation segment in X-direction, while single fracture drainage area used to estimate extend of the segment in Y-direction. Fracture spacing calculated simply as the distance between two neighbor fractures and can be expressed by **Eq. 12**:

$$x_{extend} = \frac{L_h}{N_{frac}} \quad \text{.....(12)}$$

where:

$x_{extend} =$ simulation model extend in X-direction (fracture spacing), ft

$L_h =$ horizontal section length of the well, ft

$N_{frac} =$ total number of fractures

The drainage area for a single fracture is determined by desirable well spacing and doubled number of fractures (fracture has a wing on each side of the well). From the fracture drainage area and known fracture spacing we can estimate the maximum model extend in Y-direction (**Eqs. 13–14**). Eqs. 12–14 yield the initial simulation model of 264 by 660 ft (**Fig. 3.2**)

$$A_{drain.\,frac} = \frac{A_{drain.well}}{2N_{frac}} \quad \text{.....(13)}$$

$$y_{extend} = \frac{43560 \cdot A_{drain.\,frac}}{x_{extend}} \quad \text{.....(14)}$$

where:

$A_{drain.\,frac}$ = fracture drainage area, acre

$A_{drain.well}$ = well drainage area, acre

N_{frac} = total number of fractures

y_{extend} = simulation model extend in Y-direction, ft

x_{extend} = simulation model extend in X-direction, ft

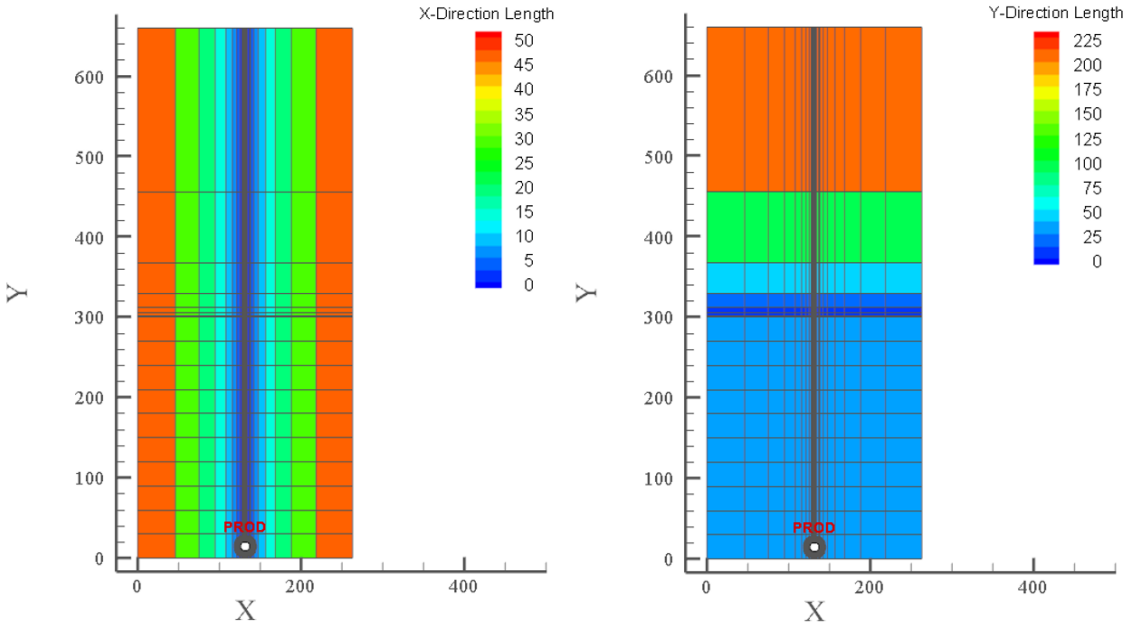

Fig. 3.2 – 2D view of simulation model. The dimensions are 264 by 660 ft in X and Y-directions respectively. The wellbore located along X-axis. The fracture connection with the wellbore pinned with "PROD" label.

The model has dimensions of 39×20×1 grid blocks yielding 780 blocks in total. The number of grid blocks in X-direction must be an odd number, so the fracture can be placed in the middle of the model. If the number of grid blocks was even, Pipe-It automatically rounded number down to the nearest odd value ("SensorGrid Documentation", 2012). The number of grid block in Y-direction can be any positive number.

The automatic gridding utility was used to refine the grid block sizes in X and Y direction. This is done to achieve better flow behavior in near-fracture region and have more accurate performance prediction. The distance from the fracture center towards the edge of a grid cell in X-direction can be estimated by using **Eqs. 15–16**. Gridding in Y-direction follows the same logic, but only for cells between the tip of the fracture and end of the model. The cell between the wellbore and the tip of the fracture has equal Y-direction size ("SensorGrid Documentation", 2012). **Fig. 3.3** shows flow regions within simulation model.

$$r_i = r_{i-1}\left(\frac{L}{w_f}\right)^{2/N} \quad \text{.....(15)}$$

$$r_0 = \frac{w_f}{2} \quad \text{.....(16)}$$

where:

$r_i =$ the distance from the center of the fracture to the edge of cell i

$L =$ the distance between two fractures, ft

$w_f =$ the fracture width, ft

$N =$ the number of the grid cells between two fractures

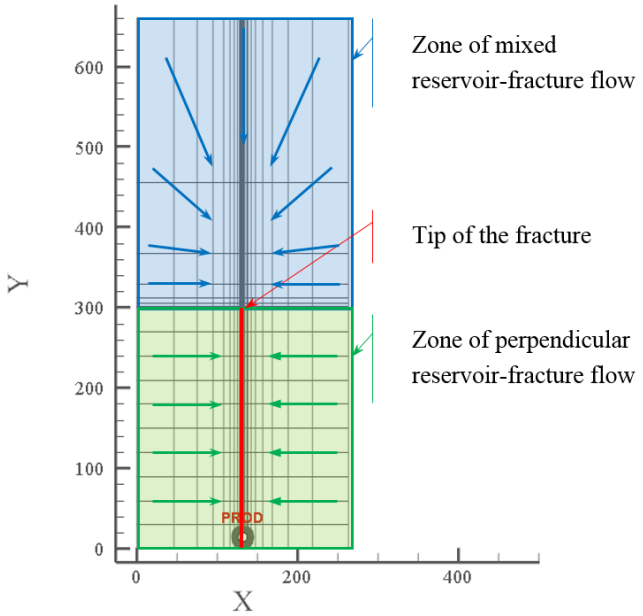

Fig. 3.3 – Schematic representation of the flow behavior within the model. Perpendicular reservoir-fracture flow occurs within the fracture half-length. Mixed flow occurs in between the tip of the fracture and the boundary of the model.

3.3 Relative Permeabilities

Permeability is a measure of rock's ability to transmit fluids through the porous media and, depending on the system of units, usually measured in millidarcies or squared meters. ("Oilfield Glossary", 2015). While the effective permeability is the rock property representing the capacity of immiscible fluid to flow through the rock, relative permeabilities are used to calculate the effective permeabilities of several fluids in the system with different particular saturations. Relative permeability is a dimensionless function of fluid's saturation ranging from 0 to 1.0 and calculated as shown in **Eq. 17**. When the system has only one fluid presented, the relative permeability of this fluid equals to 1.0. Calculations of relative permeabilities is important in multiphase flow and allow comparison of flow abilities of different fluids in the presence of each other ("Oilfield Glossary", 2015).

$$k_{ri} = \frac{k_i}{k_{abs}} \quad \text{.....(17)}$$

where:

k_{ri} = relative permeability of a phase *i*

k_i = effective permeability of a phase *i*, md

k_{abs} = absolute permeability of the rock, md

SENSOR simulator uses analytical Corey-type power law approximations for estimating relative permeabilities of the phases presented. The most important properties for calculation of relative permeabilities are end-point saturations and curvature exponents. **Eqs. 18–21** show used by SENSOR approximations when all three phases are present in a system ("Sensor Reservoir Simulator Manual", 2011). The required end-point saturations are: connate water saturation, residual oil saturation to water, residual oil saturation to gas and critical gas saturation. End-point relative permeabilities for water, oil and gas are equal to 1.0.

Two different sets of relative permeability curves are used for matrix and fracture flow. All matrix curvature exponent are equal 2.0, while for fracture flow the exponents are equal to 1.0 (giving straight line relative permeabilities). Another difference is that residual oil saturations to water and to gas are lower in the fracture than in matrix. **Table 3** consolidates the required data for relative permeability calculations. **Figs. 3.4-3.5** show the example of relative permeability curves depends on the curvature exponents ranging between 1.0 and 3.0 for matrix blocks.

$$k_{rw} = k_{rwro}\left[\frac{\left(S_w - S_{wc}\right)}{\left(1 - S_{orw} - S_{wc}\right)}\right]^{n_w} \quad \text{.....(18)}$$

$$k_{row} = k_{rocw}\left[\frac{\left(1 - S_{orw} - S_w\right)}{\left(1 - S_{orw} - S_{wc}\right)}\right]^{n_{ow}} \quad \text{.....(19)}$$

$$k_{rog} = k_{rocw}\left[\frac{\left(1 - S_{org} - S_{wc} - S_g\right)}{\left(1 - S_{org} - S_{wc}\right)}\right]^{n_{og}} \quad \text{.....(20)}$$

$$k_{rg} = k_{rgro}\left[\frac{\left(S_g - S_{gc}\right)}{\left(1 - S_{org} - S_{wc} - S_{gc}\right)}\right]^{n_g} \quad \text{.....(21)}$$

where:

S_w = water saturation, fraction

S_g = gas saturation, fraction

S_{wc} = connate water saturation, fraction

S_{orw} = residual oil saturation to water, fraction

S_{org} = residual oil saturation to gas, fraction

S_{gc} = critical gas saturation, fraction

k_{rwro} = relative permeability of water at $S_w = 1 - S_{orw}$ and $S_g = 0$, fraction

k_{rgo} = relative permeability of gas at $S_w = S_{wc}$ and $S_o = S_{org}$, fraction

k_{rocw} = relative permeability of oil at $S_w = S_{wc}$ and $S_g = 0$, fraction

n_w, n_{ow}, n_g, n_{og} = exponents for analytical relative permeabilities

TABLE 3 – RELATIVE PERMEABILITIES

Parameter	Matrix	Fracture
S_{wc}	0.2	0.2
S_{orw}	0.1	0.001
S_{org}	0.1	0.001
S_{gc}	0.1	0.1
$k_{rw}(S_{orw})$	1.0	1.0
$k_{rg}(S_{wc})$	1.0	1.0
$k_{ro}(S_{wc})$	1.0	1.0
n_w	2.0	1.0
n_{ow}	2.0	1.0
n_g	2.0	1.0
n_{og}	2.0	1.0

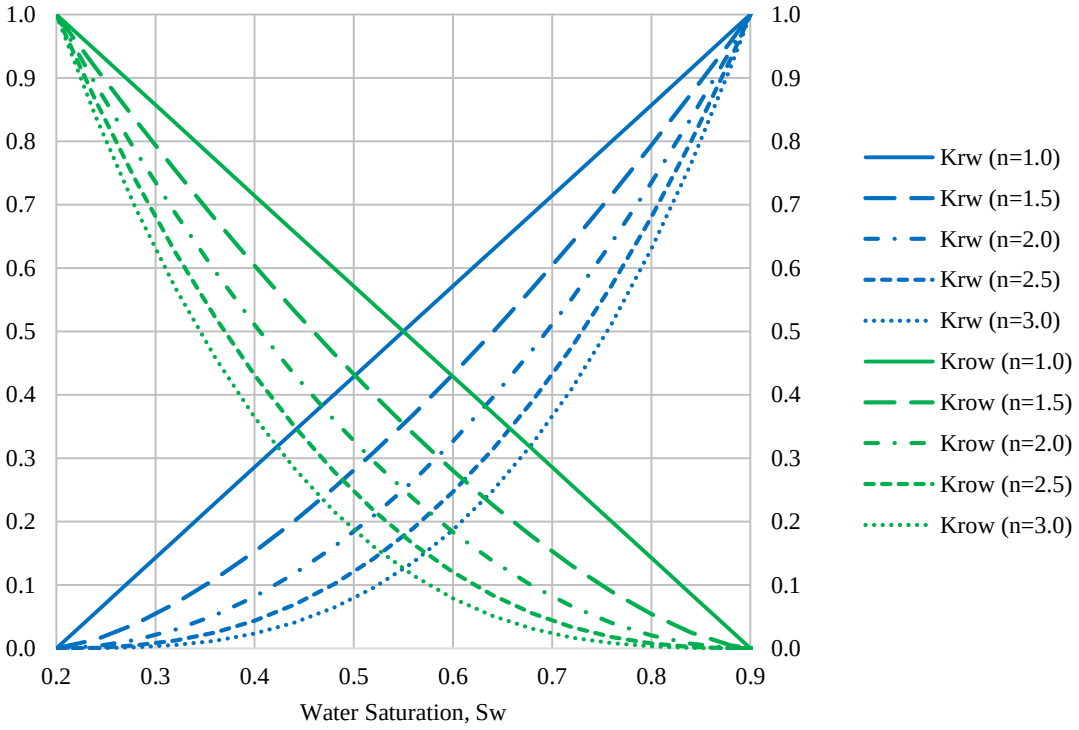

Fig. 3.4 – Water and oil-water relative permeability curves as functions of water saturation in matrix. ($n = n_w = n_{ow} = n_g = n_{og}$)

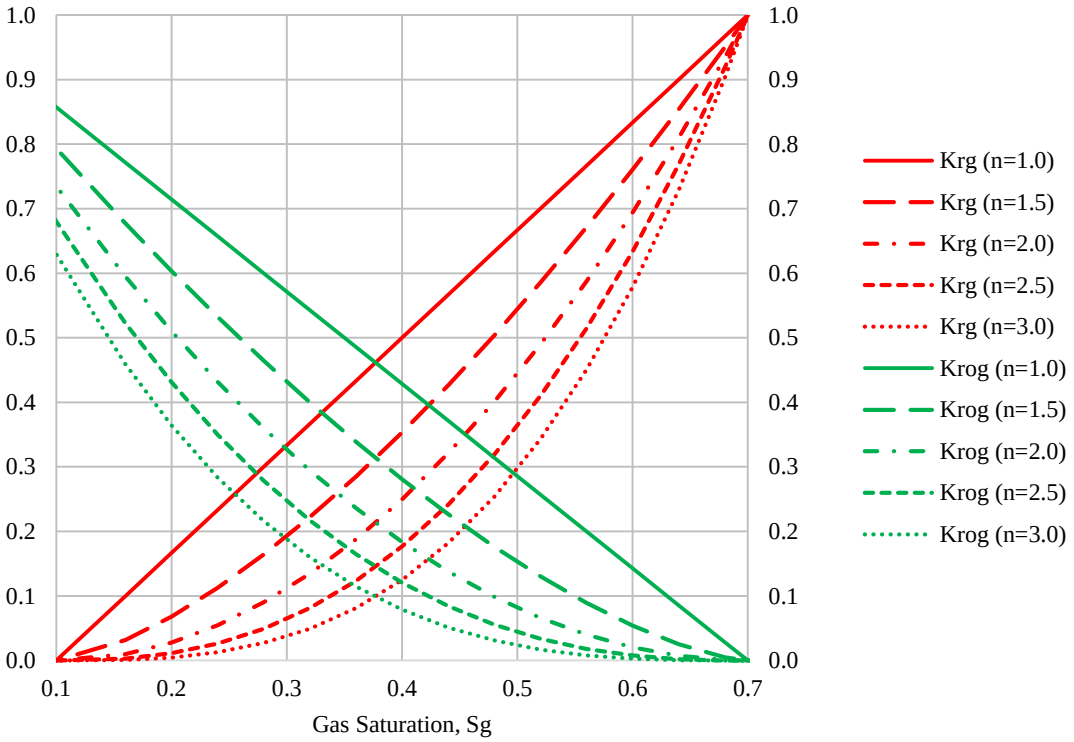

Fig. 3.5 – Gas and oil-gas relative permeability curves as functions of gas saturation in matrix. ($n = n_w = n_{ow} = n_g = n_{og}$)

3.4 Fluids Description and PVT

SENSOR simulator allows to use both compositional and black-oil fluid models. By compositional fluid model we refer to the model where oil and gas are represented by a range of hydrocarbon (C_1, C_2, C_3… C_{26+}) and non-hydrocarbon (N_2, CO_2, H_2S) components. The mass exchange between oil and gas phases controlled by thermodynamic balance and described by Equation of States (EOS). The black-oil model operates with oil and gas phases simplistically representing them with only two components: surface oil and surface gas. There is no compositional description for any of the phase. The mass exchange between two phases controlled by solution gas-oil ration which is a function of reservoir pressure. For this project we only used black-oil fluid model.

PVT black-oil tables were automatically generated by SENSOR based on 31 components Soave-Redlich-Kwong (SRK) EOS used for optimized well modeling of liquid-rich shale reservoirs by Juell and Whitson (2013). SENSOR uses Whitson and Torp (1983) method to internally generate required black-oil PVT tables from EOS data and then use them for the simulation. The method allows to elevate saturation pressures in generated tables above saturation pressure of the original reservoir fluid by adding bubble-point equilibrium gas ("Sensor Reservoir Simulator Manual", 2011). Resulting black-oil tables allow initializing the model with different in-situ fluids at any initial pressure. For this project, PVT tables covered the pressure range from 14.7 to 15,000 psia with critical pressure 4,906.4 psia at reservoir temperature. The first separation stage pressure and temperature are 150 psia and 100 °F. The second separation stage is 14.7 psia and 60°F. **Appendix B** describes the fluid composition and EOS used in this project.

3.5 Stress Dependent Transmissibility

In our model we introduced stress dependent transmissibility in the fracture. This dependence represents the reduction of the fracture area due to pressure depletion in the reservoir, restricting the flow to the wellbore. This effect is introduced by reduction in fracture permeability which, in the most severe case, will approach matrix permeability value. The relationship, representing the permeability reduction is given by **Eq. 22**:

$$\frac{k_f}{k_{fi}} = 10^{m\left(\frac{p-p_i}{1000}\right)} \quad \text{.....(22)}$$

where:

k_f = current fracture permeability, md

k_{fi} = initial fracture permeability, md

m = slope of stress dependent permeabilities

p = reservoir pressure, psia

p_{ri} = initial reservoir pressure, psia

Transmissibilities in three directions are then modified every time step based on the actual pressure in each grid block without any data extrapolation ("Sensor Reservoir Simulator Manual", 2011). The modification factor is equal to the fracture permeability reduction. Whitson and Sunjerga (2012) simulated different liquid-rich shale reservoirs assuming no stress dependence in fracture permeability. Their results show typical shale reservoir performance in terms of producing Oil-Gas Ratio. However, in following chapters we show the significant influence of stress dependent transmissibility on the shale performance in both gas condensate and oil reservoirs. Example of permeability reduction for slope *m* equals to 0.5 and initial pressure equals to 7,500 psia is shown on **Fig. 3.6.**

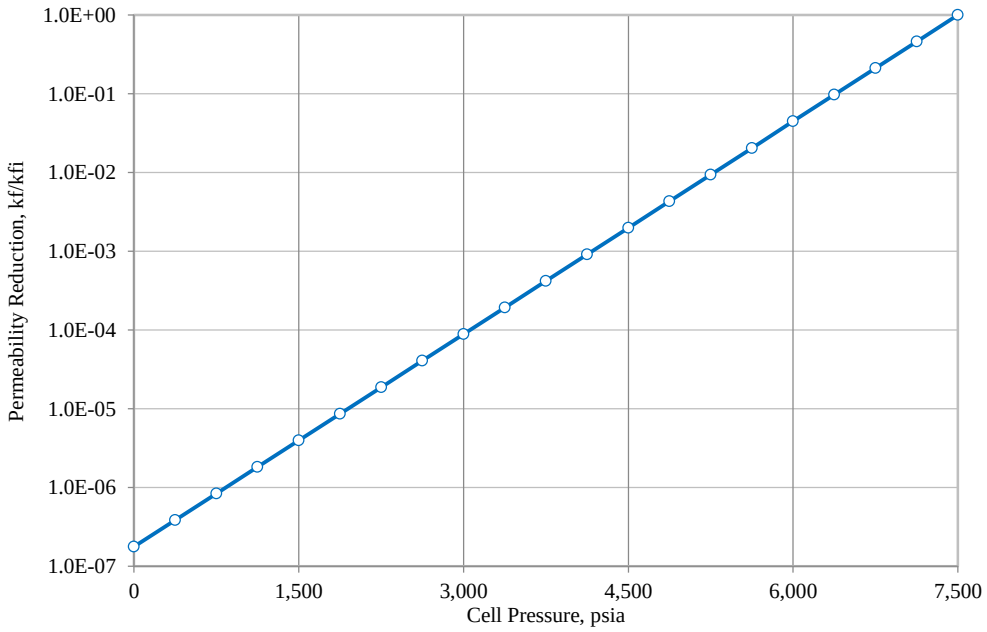

Fig. 3.6 – Permeability reduction as a function of current cell pressure. Greater slope *m* causes more severe effect on fracture permeability.

3.6 Other Simulation Setups

The simulation time for the model is set to five years. We decided that this time frame is of the highest interest for economic assessment of shale wells since the biggest share of the cash flow accumulated within first years. This decision is also supported by rapid production decline in first year and volatile hydrocarbon prices within the last 12 months. In addition, companies are interested in continuous drilling to keep the production rate stable; hence short-to-medium term evaluation of shale projects became vital.

The production forecast simulation is typically based on the assumption of constant BHP. For the base case, the pressure of 1,000 psia is selected. The maximum flowrate is set to unrealistically high number to control the well by constant bottomhole pressure only.

We used the cost model described by Eq.5 to calculate the well's Capex for the base case scenario and all sensitivity cases when the well completion design is changed. The only implemented adjustment is that the total vertical cost is now split into cost of drilling a ft of vertical section and the total vertical depth of the well. The cost of drilling a foot of vertical and horizontal sections are set to 150 USD/ft and 550 USD/ft respectively. Fracture treatment cost (including completion) is set to 240,000 USD/frac. The reference fracture half-length is set to 300 ft and the empirical cost-elevating coefficient *a* is set to 1.2. The total well cost for the base case described in Table 2 is USD 8,983,500.

Eq. 8 describes the selected revenues model for the project. The prices for oil and natural gas are selected along with the consensus price from Fig. 2.9-2.10. The oil price for revenues calculations is 65 USD/bbl and the price for natural gas is set to 3.5 USD/Mscf. The price of water disposal is set to 8 USD/bbl. The discount rate for NPV calculation is 10%. We excluded any operational expenditures from our model since its contribution to the final NPV is relatively small. For simplicity, any tax payment and royalties are set to 0. **Table 4** aggregated the input for cost and revenues models.

TABLE 4 – ECONOMIC PATAMETERS FOR BASE CASE SCENARIO

Parameter	Value	Units
Cost of drilling vertical section, d_{vert}	150	UDS/ft
Cost of drilling horizontal section, d_{horiz}	550	USD/ft
Fracture treatment cost, C_{frac}	240,000	USD/frac
Reference fracture half-length, x_{f0}	300	ft
Empirical cost-elevating coefficient, a	1.2	
Oil price, P_o	65	USD/bbl
Natural gas price, P_g	3.5	USD/Mscf
Water disposal cost, P_w	8	USD/bbl
Discount rate, i	10	%

3.7 Sensitivity Analysis Description

Sensitivity analysis is a powerful method to estimate variations of model performance depending on different input data. Such assessment is essential for narrowing project risks due to common data uncertainty. The typical approach used in sensitivity analysis is changing one parameter at a time and comparing the performance of the model with base case scenario. For this project, we divided all sensitivity parameters into three groups: (1) reservoir related parameters, (2) well completion parameters and (3) combined parameters.

Within initial reservoir parameters we particularly interested in initial reservoir pressure, reservoir thickness and matrix permeability. Well completion parameters cover different number of fractures, fracture's half-length, horizontal section lengths and bottomhole pressures. Under combined parameters we understand those where more than one parameter have to be changed to maintain another essential parameter as a constant value. For example, for constant productivity index (PI) we have to change both fracture half-length and reservoir permeability. Likewise, to keep fracture spacing constant with the single fracture drainage area, we needed to change total number of fractures, horizontal section length and well spacing.

Additional sensitivity analysis will be performed to see the difference in project economy assuming different price for oil and natural gas and change in well Capex. Also, we looked at the problem of optimal well spacing in a section of 1×2 mi comparing wells with different horizontal section length. For dry gas case we also evaluated the effect of including gas desorption process depending on different Langmuir volume and pressure on well performance. **Table 5** consolidates the range of variable parameters within all sensitivity analyses.

TABLE 5 – RANGE OF VARIABLES FOR SENSITIVITY ANALYSES

Parameter	Minimum value	Base case value	Maximum value	Units
Initial reservoir pressure, p_{ri}	2,500	7,500	14,500	psia
Matrix permeability, k_{matrix}	10	500	10,000	nd
Reservoir thickness, h	50	200	350	ft
Number of fractures, N_{frac}	5	20	50	
Fracture half-length, x_f	100	300	660	ft
Horizontal length, L_h	5,280	5,280	10,560	ft
Bottomhole pressure, p_{wf}	1,000	1,000	4,906.4	psia
Well spacing, A_{well}	40	160	320	acre
Grid cell for Y-direction logarithmic gridding	3	10	20	

3.8 Pipe-It Shale Well Optimizer Overview

Technical part of the thesis is mainly done by using Integrated Asset Modeling software Pipe-It. Pipe-It allows connection of different third-party software (numerical simulators, processing and flow assurance software, etc.) within a single project in a simple visual way. Required input data is usually introduced as text files or spreadsheets and then fed to the appropriate processes. Then, the output from the processes can be used as an input to the further stage, plotted or exported to

the file. By connecting several processes together, one can easily perform required simulation without changing input/output parameters in each of them. This project based on Shale Well Optimizer solution. **Fig. 3.7** shows the top-view of the project.

The project consist of four main composites: (1) Input Data, (2) Well Model, (3) Production History Matching and (4) Well Design Optimization. Composites are connected showing the data flow from one stage of simulation into another stage. For example, Input Data composite includes a spreadsheet with observed production rates from the well, a text file with desired well schedule and set of data for EOS generation. This data is then fed to Well Model and Production History Matching composite. When the numerical simulation are done and production rates are calculated, this data can be used for history matching of a well and for economic optimization by converting production volumes into a cash stream. Finally, at any stage of the project, any data can be extracted for further manual processing as it is done, for example, in a spreadsheet called Results Extraction.

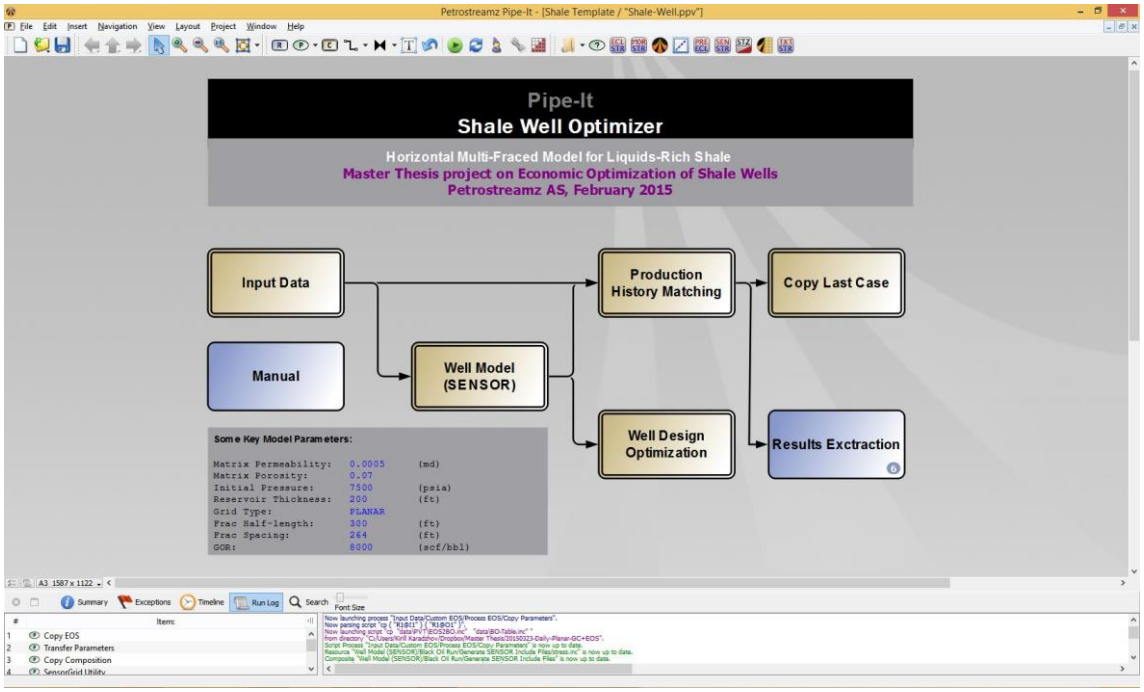

Fig. 3.7 – Top view on Shale Well Optimizer project in Pipe-It.

Inside of each composite we find a set of different resources used to process the input and output data, accumulate and aggregate results, prepare include filed for third-party software, etc. **Fig. 3.9** show the content of a Black Oil Run composite which is located in a Well Model composite of a top-level of the project. The main process – running of Sensor simulator – is fed with different include files. Some of them were prepared in Input Data composite and then transferred further, while the others (like gridding data and initial conditions) are generated by Pipe-It in a composite Generate Sensor Include Files. When the data is ready to use, Sensor performs required numerical simulations and provide results in different forms. Further, this data is processed by Pipe-It to compare results, history match the well, plot the data and optimize well's economy. Complex project like this may have many different include files which can be placed at different stages of simulations. To easily change required input data and control the model, Pipe-It introduced a control of any variables from a single location, called Optimizer window.

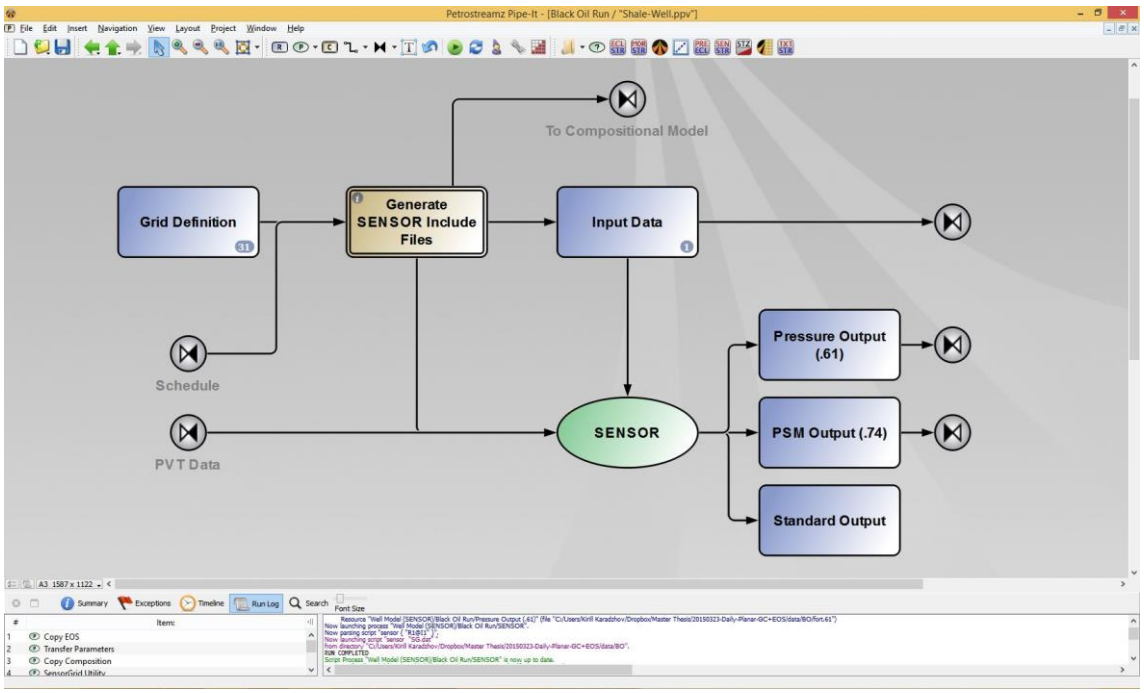

Fig. 3.8 – Black Oil Run composite of Shale Well Optimizer.

Fig. 3.9 shows a section of Optimizer window allowing to control and change any input parameter in data files. Any variable a user desires to control can be set from here. Variables are linked with an actual values data files and can be different types: user or optimizer defined input, constant and objectives. Each of the parameters may have upper and lower limits. Once the values are updated in Optimizer, they are transferred to the corresponding data files and updated before the model is executed. Optimizer allows to easily change the variables especially when performing a history matching and provides intuitive interface to control input and output data. It also, based on mathematical algorithms can optimize a target value by changing selected parameters and perform simulations sequentially.

File Edit Insert Solvers Optimization View Window Help

New Open Save Undo Redo Linkz History Reflection Active Solver Run Once Optimize

Composite to be executed: Shale Template

		Name	Role	Consti	Type	Lower	Value	Upper	Equation
1	☑	NX_Between_Fracs	AUX	☐	int	3	39	1000	NX_Between_Fracs
2	☑	NY_Total	AUX	☐	int	1	20	1000	NY_Total
3	☑	NY_Along_Frac	AUX	☐	int	1	10	1000	NY_Along_Frac
4	☑	Case_no	AUX	☐	int	1	1	22	Case_no
5	☑	SSQ_QG	CON	☐	real	0	1.315e+10	1	
6	☑	SSQ_QO	CON	☐	real	-1e+06	5.218e+07	1e+06	
7	☑	SSQ_QW	CON	☐	real	-1e+06	7.336e+18	1e+06	
8	☑	SSQ_PWF	CON	☐	real	-1e+06	0	1e+06	
9	☑	SSQ_PWF_BOUNDS	CON	☐	real	0	0	0	
10	☑	SSQ_CUMG	CON	☐	real	0	1.082e+16	0	
11	☑	SSQ_CUMO	CON	☐	real	0	2.967e+13	0	
12	☑	SSQ_Total	OBJ		real	--	**1.315e+10**	--	SSQ_PWF_BOUNDS+SSQ_QG
13	☑	Frac_Half_Length	VAR		real	100	300	660	
14	☑	Permeability_Rock	VAR		real	1e-05	0.0005	0.01	
15	☑	Porosity_Rock	VAR		real	0.07	0.07	0.07	
16	☑	GOR	VAR		real	100	8000	2e+04	
17	☑	m_dep_fracs	VAR		real	0	0.5	4	
18	☑	m_dep_matrix	AUX	☑	real	0	0	0	
19	☑	Well_PI	AUX	☐	real	0	6.708	0	Frac_Half_Length*sqrt(Permeability_Rock)
20	☑	ng	AUX	☐	real	2	2	3	ng
21	☑	nw	AUX	☐	real	2	2	3	nw
22	☑	now	AUX	☐	real	2	2	3	now
23	☑	nog	AUX	☐	real	2	2	3	nog

Fig. 3.9 – Section of Optimizer window in Pipe-It.

THIS PAGE INTENTIONALLY LEFT BLANK

Chapter 4

Dry Gas Simulation Results

For dry gas simulations the reservoir is initialized with undersaturated gas for all pressures. Required black-oil PVT table is generated by Pipe-It based on general gas properties calculations (real gas law, Lee's viscosity correlations, etc.) and introduced to SENSOR as an include file. The table of 38 entries covers the pressure range between 15 and 15,000 psia. Dry gas specific gravity is set to 0.748 with fluid composition described in **Table 6** of Appendix B. The molar fraction of components higher than C_6 is grouped together into C_{7+}. For sensitivity analysis we neglected the possible gas desorption processes in the reservoir. Initial water saturation S_{wi} is set to 0.4 and initial gas saturation S_{gi} is 0.6. Sensitivity analysis for dry gas cover different matrix permeabilities, initial reservoir pressures and thicknesses, number of fractures, fracture half-lengths, well horizontal lengths, constant productivity index and constant fracture spacing.

4.1 Matrix Permeability

Matrix permeability of shale reservoirs play an extremely important role in overall reservoir performance. We decided to simulate the range of 10 to 10,000 nd (10^{-5} to 0.01 md) to cover complete range of possible permeabilities and quantify the difference in performance of shales and conventional reservoirs.

Figs. 4.1–4.2 show the reservoir performance for different permeabilities in terms of NPV, DPI and IRR. Metrics are calculated on annual basis. Increase of reservoir permeability has a positive effect on the project economics monotonically. NPV varies in between -6 to 14.5 million USD for the range of 10–1,000 nd. The break-even reservoir permeability is about 90 nd for 5 years production period. DPI follows the trend of NPV since no change in well cost occurred and reaches maximum with 263%. That means that every invested dollar yields additional 1.63 dollars in net present value. IRR supports the break-even permeability with about 12% value for 4–5 years period. It is noticeable that higher permeability results generate lower increment in IRR in later periods. This happens due to the greater production contribution of first years to the total production form the well.

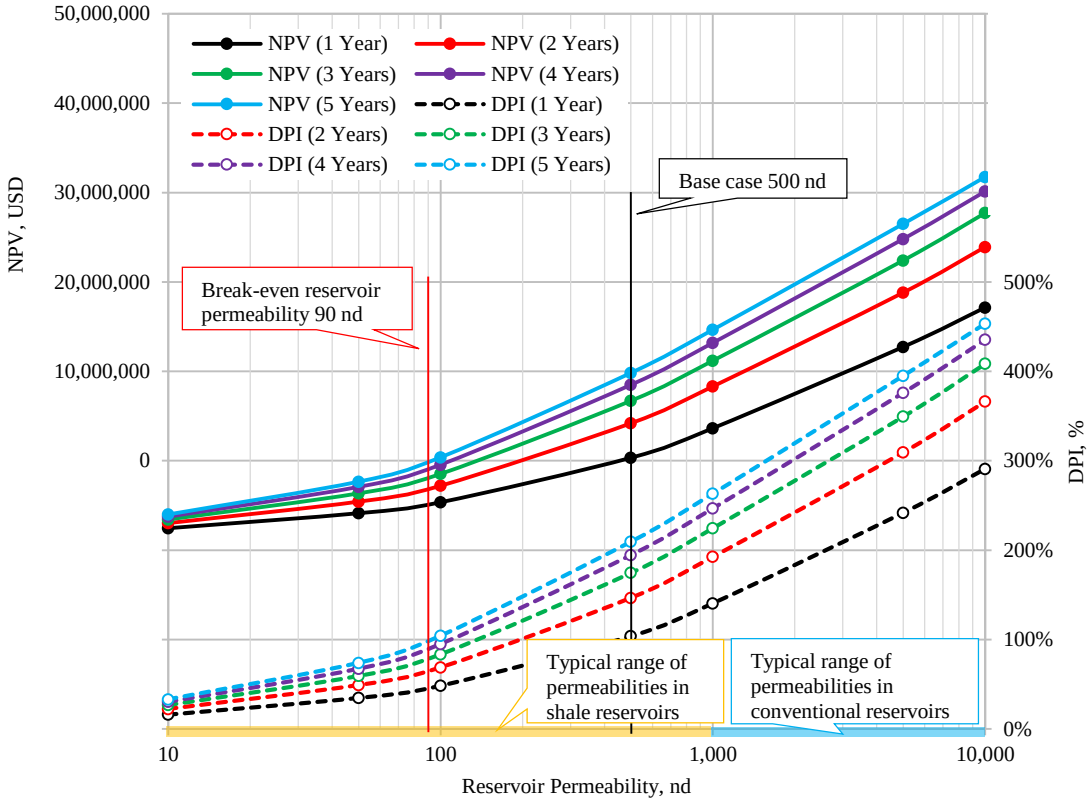

Fig. 4.1 – NPV and DPI in dry gas system for different reservoir permeabilities. Yellow and blue bars represent typical permeability ranges for shale and conventional reservoirs.

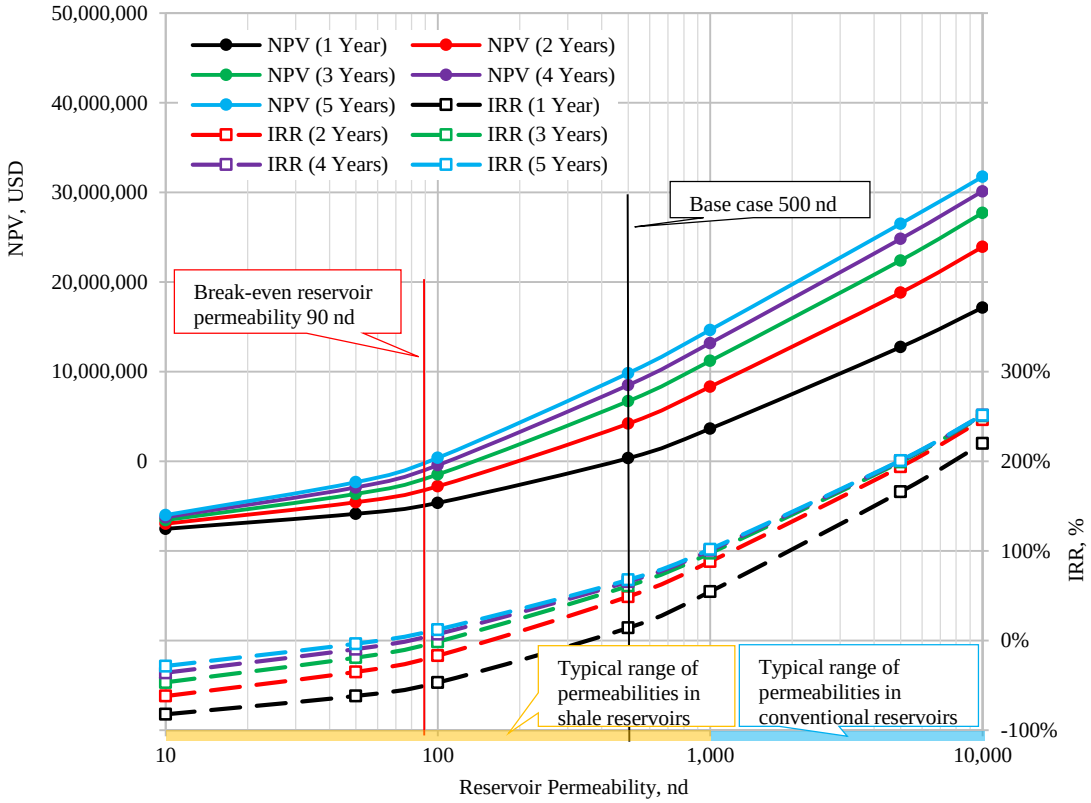

Fig. 4.2 – NPV and IRR in dry gas system for different reservoir permeabilities. Yellow and blue bars represent typical permeability ranges for shale and conventional reservoirs.

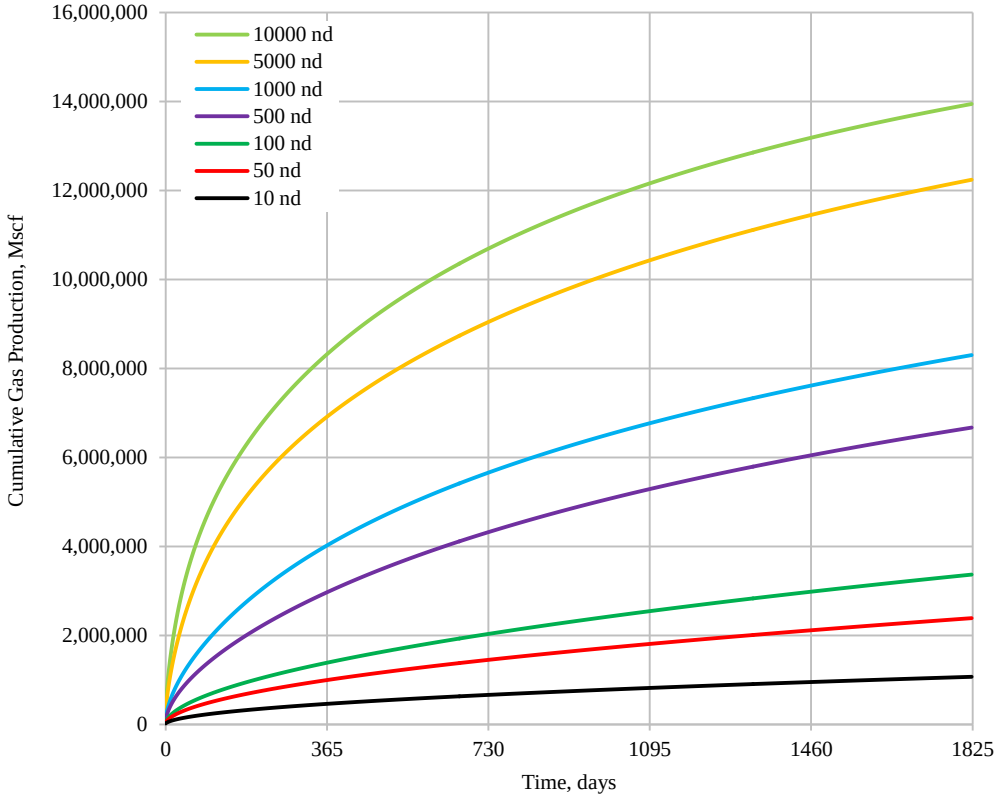

Fig. 4.3 – Cumulative gas productions in dry gas system for different reservoir permeabilities. Break-even permeability is 90 nd.

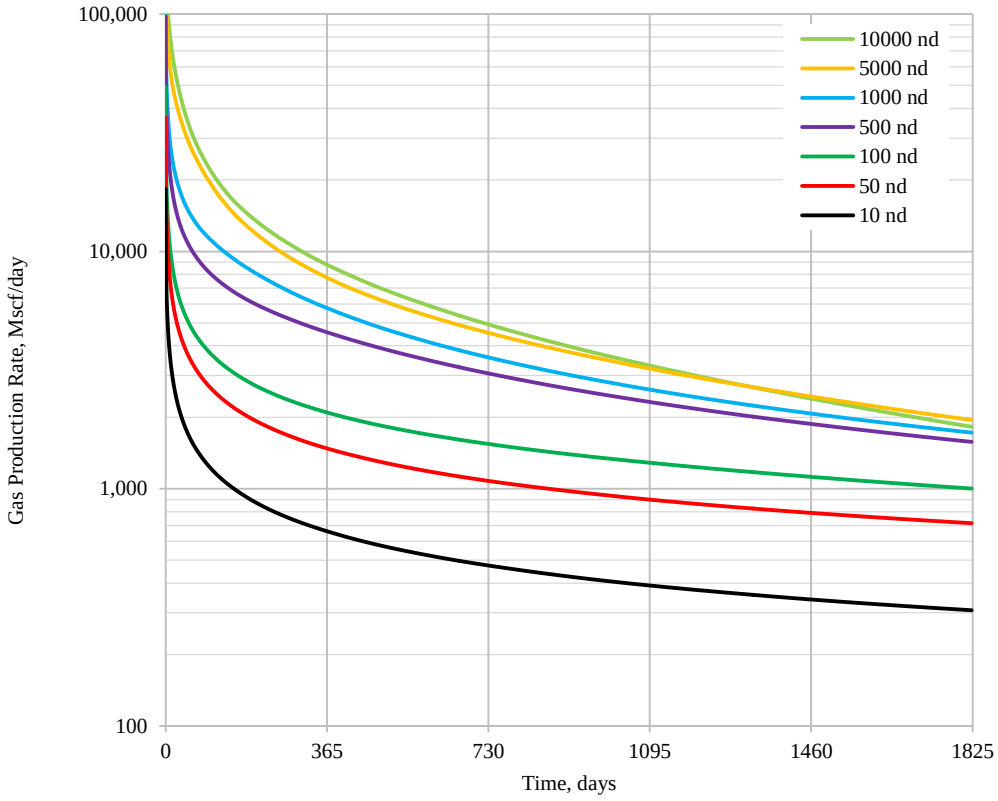

Fig. 4.4 – Gas production rates in dry gas system for different reservoir permeabilities. Decline rate for 1,000–10,000 nd reservoir is higher due to reaching the outer boundaries of the drainage area beyond fracture's tip.

Fig. 4.3 shows cumulative gas production for different permeabilities. It ranges between 1–14×10^6 Mscf of gas in 5 years with minimum required production of 3.3×10^6 Mscf to make the project profitable. **Fig. 4.4** shows the gas production rate curves. For the range of 10–1,000 nd all decline rate curves have identical decline exponents, indicating that none of the models reached outer boundaries of the drainage area beyond the fracture's tip. High permeable cases have a cross in production rate curves after 3.5 years due to rapid depletion of the model.

4.2 Initial Reservoir Pressure

Initial reservoir pressure has an impact not only on the production rates when the bottomhole pressure is kept constant. It also influences on the initial gas-in-place volume and the intensity of depletion of the simulation area.

Figs. 4.5–4.6 indicate that the best economic performance is achieved by the reservoirs with initial pressure ranges in 6,500–8,500 psia. Intuitively, we would assume that higher initial pressure will positively influence on the project economy. However, initial pressures higher than 10,000 psia showed worse economic performance. For example, with 14,500 psia reservoir NPV after 5 years will be only half of the base case scenario (DPI of 150% and 210% respectively). IRR follows the same trend, falling to 37% from base case 67%. The behavior is a result of increased pressure friction in the reservoir due to the increased gas viscosity which cannot be balanced by increased initial gas-in-place. (**Fig. 4.7**).

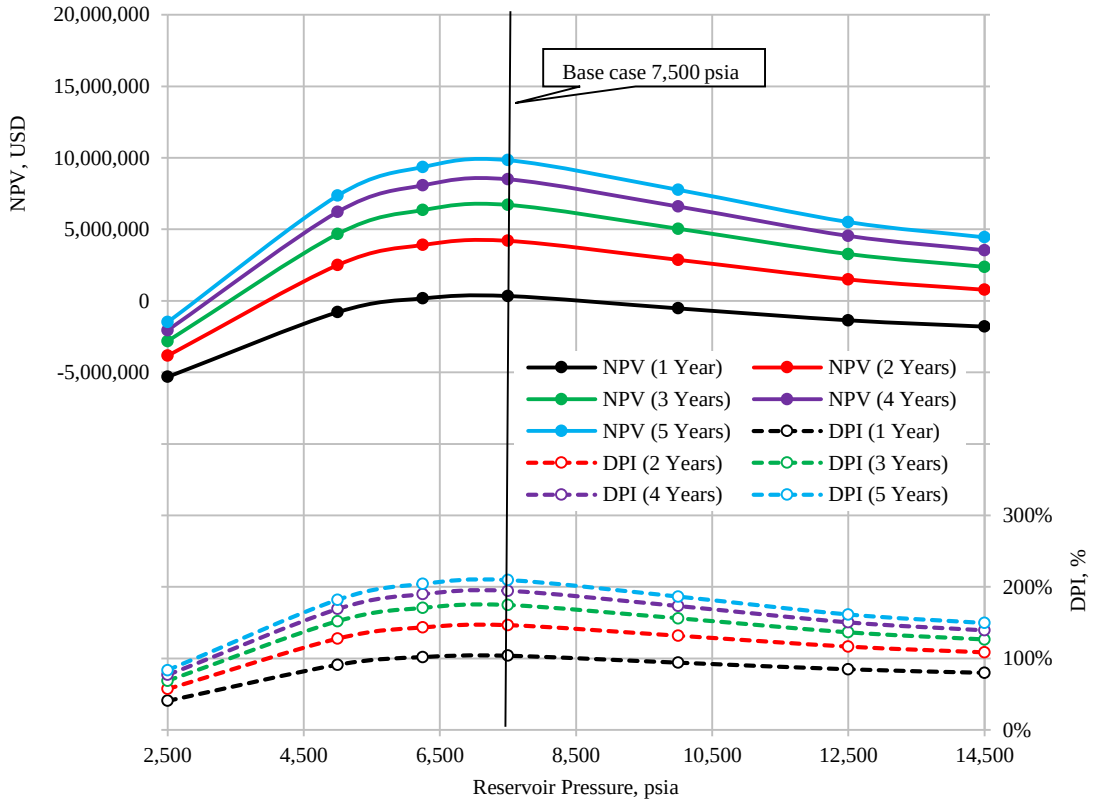

Fig. 4.5 – NPV and DPI in dry gas system for different initial reservoir pressure.

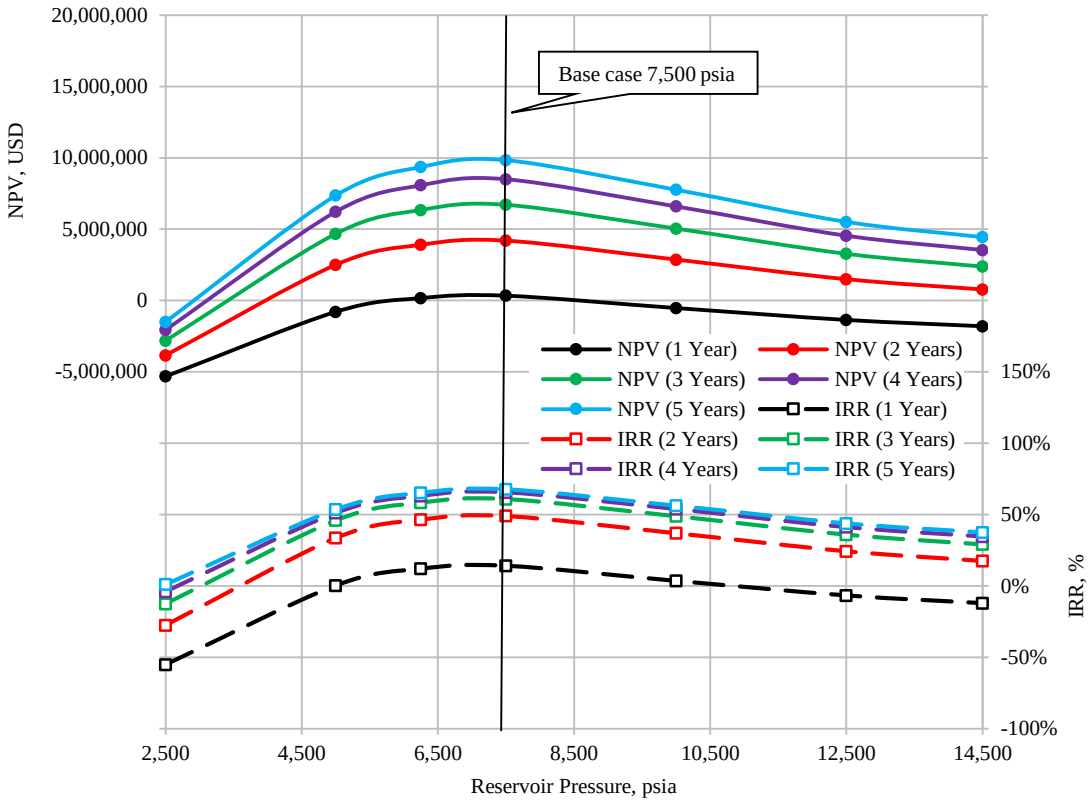

Fig. 4.6 – NPV and IRR in dry gas system for different initial reservoir pressure.

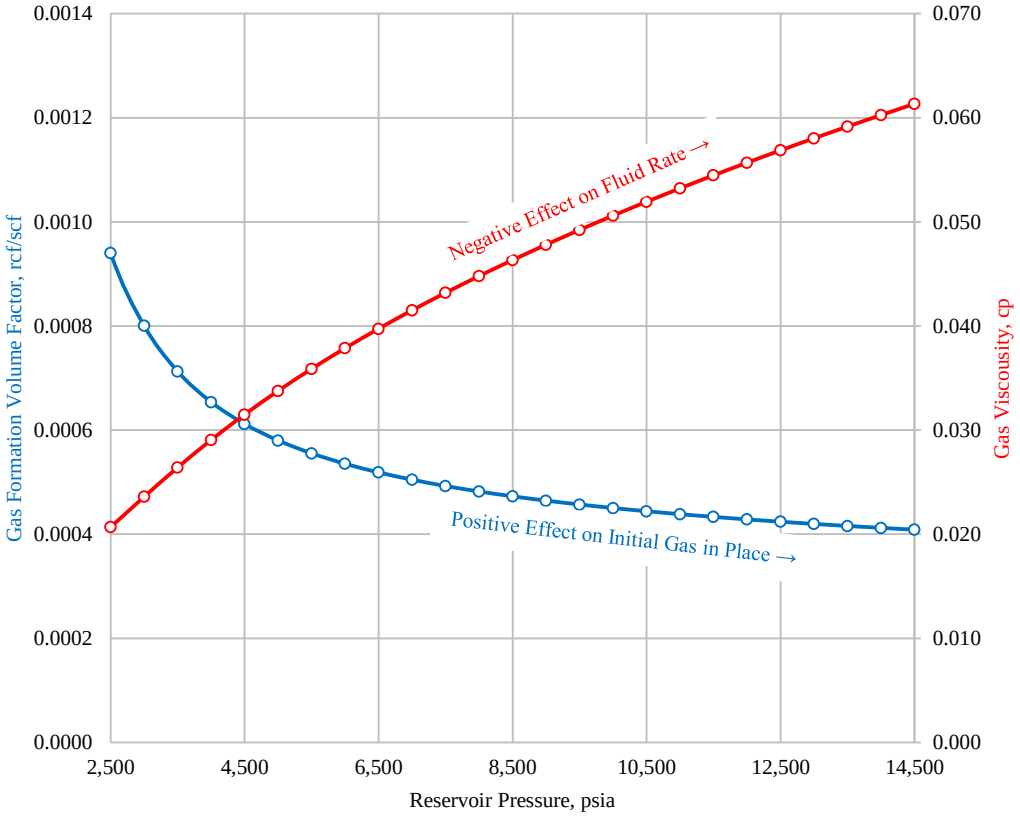

Fig. 4.7 – Gas formation volume factor and viscosity as functions of reservoir pressure.

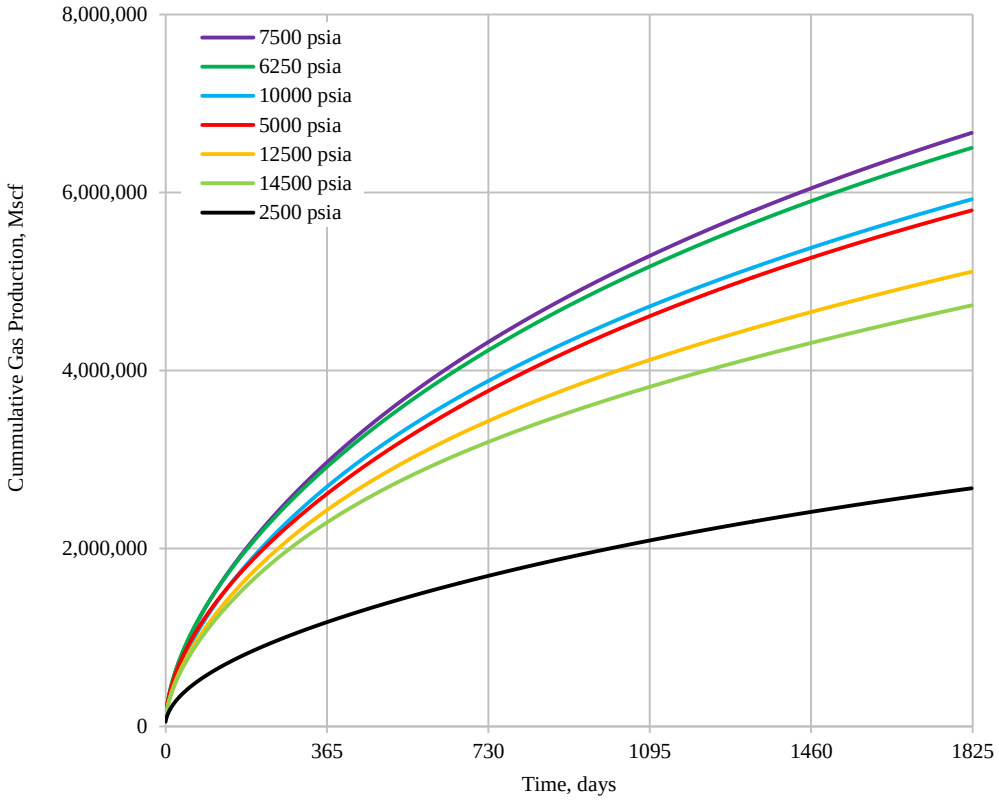

Fig. 4.8 – Cumulative gas production in dry gas system for different initial reservoir pressures. Production monotonically increases for 2,500–7,500 psia, then monotonically decreases for higher pressures

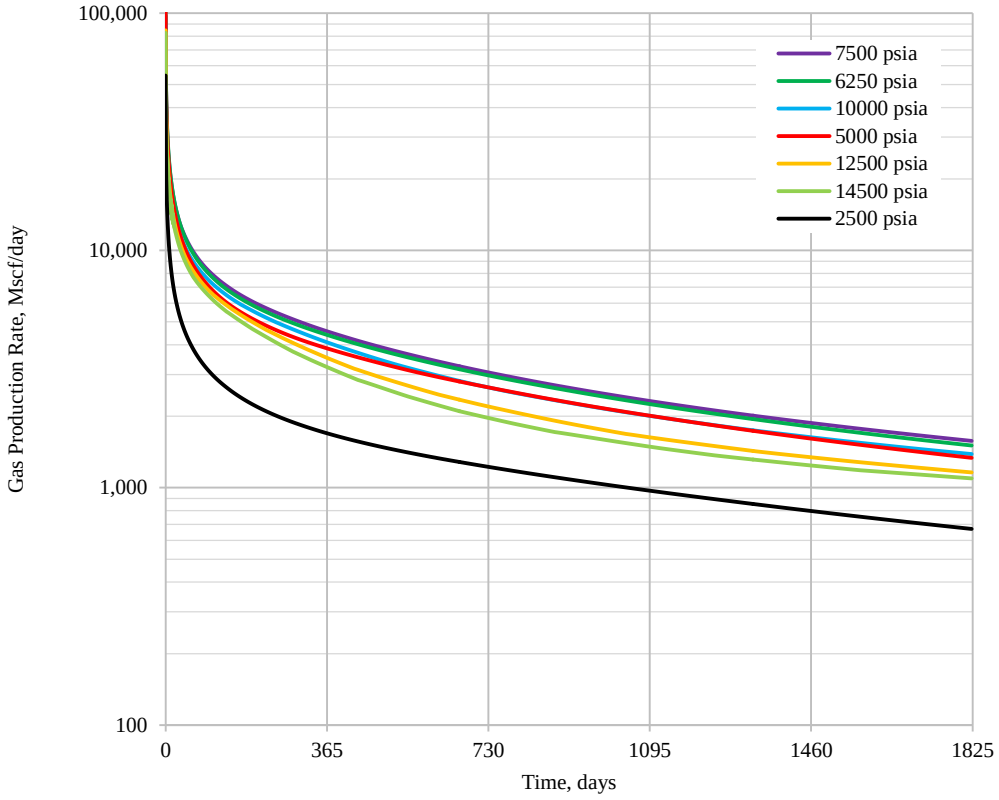

Fig. 4.9 – Gas production rates in dry gas system for different initial reservoir pressures. Decline rate for 10,000–14,500 psia is higher than for lower pressures.

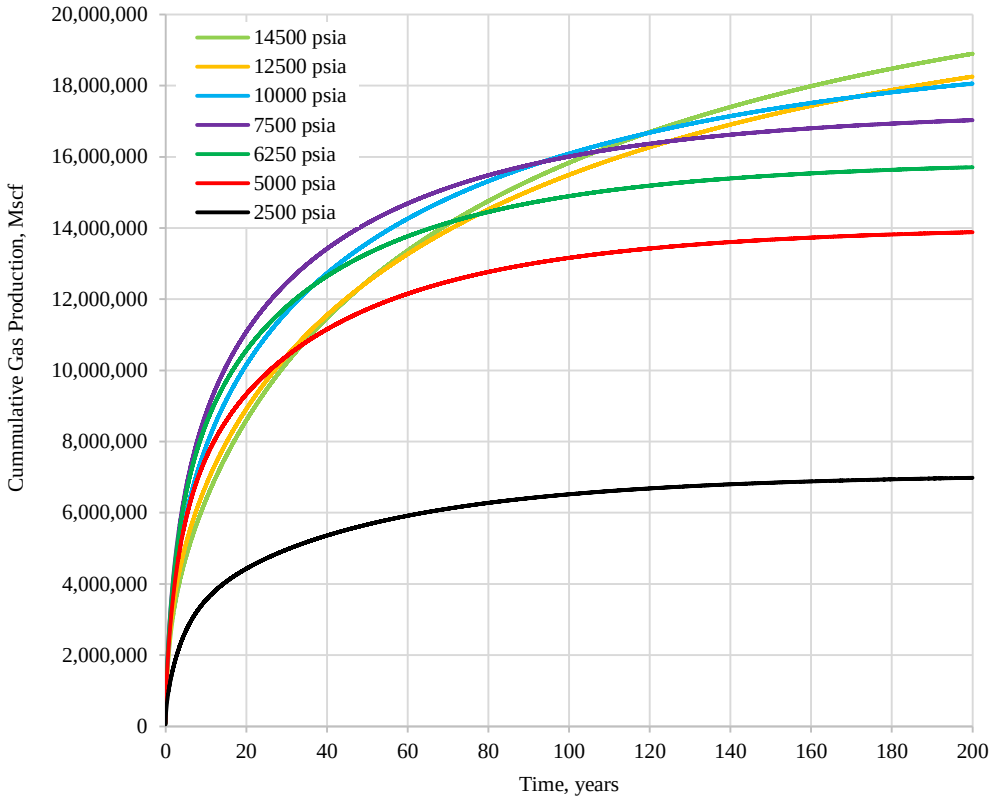

Fig. 4.10 – Cumulative gas production for different initial reservoir pressures in 200 years. 90–120 years of production is required to overcome negative effect of increased viscosity in reservoirs with initial pressure of 10,000–14,500 psia.

These non-monotonic results are supported by cumulative gas production data (**Fig. 4.8**). The 5 years production reaches maximum values for initial reservoir pressure around 7,500 psia with approximately 6.7×10^6 Mscf. Further increase of initial reservoir pressure to 10,000, 12,500 and 14,500 psia yields about 6.0×10^6, 5.1×10^6 and 4.7×10^6 Mscf of cumulative gas production. Production performance of 10,000 psia reservoir is almost the same as for 5,000 psia. The minimum production of 2.6×10^6 Mscf achieved with 2,500 psia due to small pressure drawdown between the well and the reservoir. **Fig. 4.9** indicates that the decline of gas production rate for high pressures is higher than for base case scenario. 5,000 and 10,000 psia reservoirs have identical production rates after 2 years.

Fig. 4.10 illustrates the effect of increased gas viscosity on cumulative production profile. Higher initial reservoir pressure positively influence on initial gas in place. However, it requires 90–120 years for reservoirs with 10,000–14,500 to achieve the same cumulative production as for the base case. Complete monotonic behavior in cumulative productions is observed only after 175 years. This indicates that negative effect from increased gas viscosity significantly overcomes the positive effect of increased gas in place in the reservoirs with high initial pressure.

4.3 Reservoir Thickness

In our model the thickness of the reservoir represented with one grid cell. Assuming that the fracture penetrates the whole reservoir in Z-direction, there is no vertical flow between different parts of the reservoir. Therefore, different reservoir thickness will only change the total hydrocarbon pore volume without affecting any other physical properties. The main interest is to evaluate the break-even reservoir thickness before the project turns into economically unattractive.

Figs. 4.11–4.12 clearly show the effect of reservoir thickness on economic performance of the well. Increased thickness monotonically contributes into higher production volumes, generating better economic results of the project. In our case, every additional 10 ft of the reservoir adds about 1 million USD for NPV, increasing DPI and IRR alike. The break-even thickness is about 90 ft for a production period of 5 years. In general, thicker reservoir will achieve more favorable economic results even without assumption of reservoir's complete penetration by fractures.

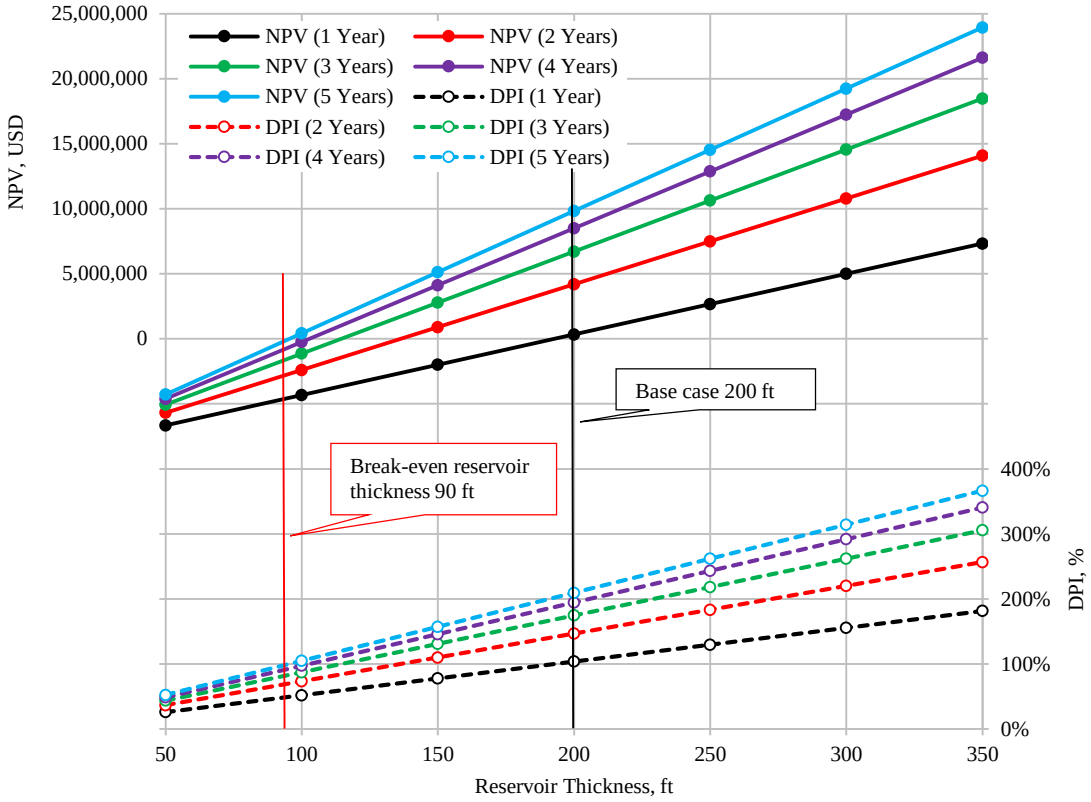

Fig. 4.11 – NPV and DPI in dry gas system for different reservoir thickness.

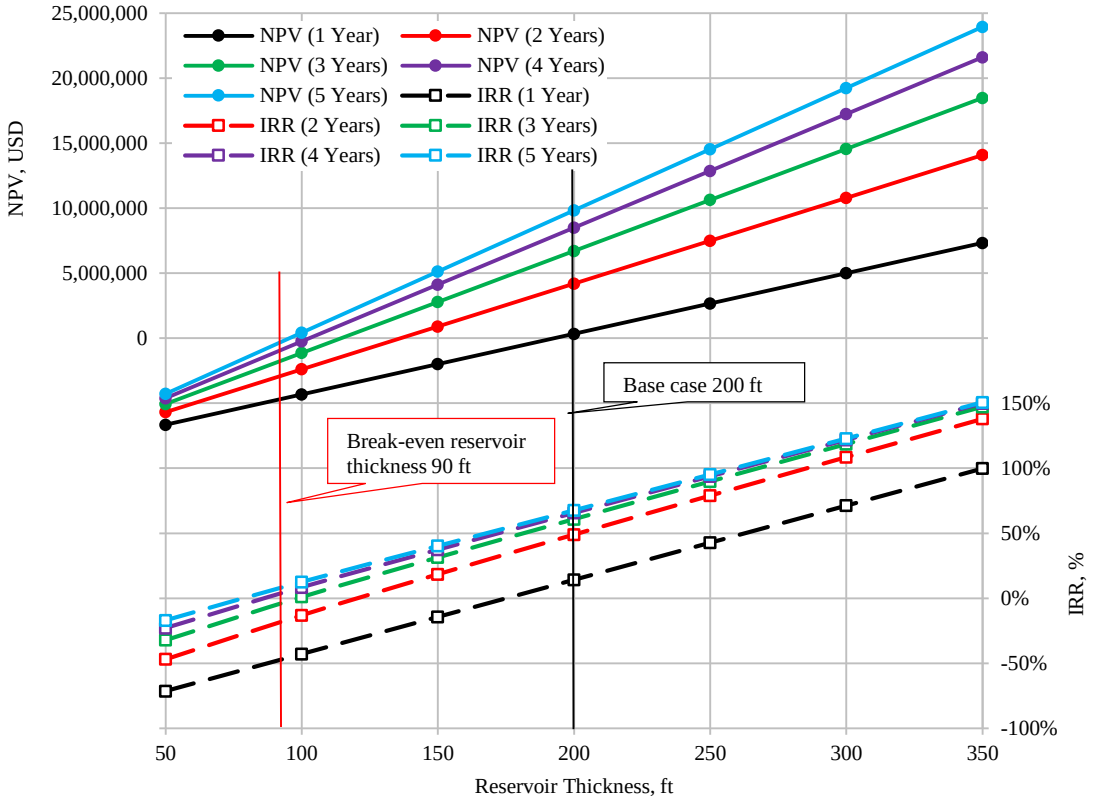

Fig. 4.12 – NPV and IRR in dry gas system for different reservoir thickness.

4.4 Number of Fractures

Number of fractures is one of the most important design parameters in hydraulic treatment completion. Increased number of fractures decreases the dedicated drainage area per fracture (if the well horizontal length is maintained constant) and accelerates production from the reservoir. This acceleration could increase the cash flow at the earlier stages, but later production could be negatively affected by increased pressure drop in the reservoir. In total, it may result in worse economics of the project if the number of fractures are not selected wisely. The general approach guides that the marginal revenues from the fracture should not overcome marginal cost of inducing one frac. However, comparing cash flows with required capital investments may lead into another optimal completion solution.

NPV and DPI as functions of number of fractures are shown on **Fig. 4.13**. The total number of fractures changes between 5 and 50 with constant horizontal length of the well. If company base their investment decision solely on NPV metric, the optimum number of fractures is in between 30 and 40 fracture with NPV equal to about 12.5 million USD. Using only DPI metric leads into optimized treatment design with 15–30 fracs with approximate investment effectiveness of 210%. Once can decide to which of the metrics company gives the highest priority and based on that information justify the completion design. Another approach would be using of both metrics and select compromised solution of 30 fractures, having 12.2 million USD of NPV and 206% of DPI. If the engineer goes for 40 fractures, the NPV will be 12.4 million USD, but DPI drops to 188%. Thus, completion with 10 less fractures yields almost the same NPV with 10% higher investment efficiency.

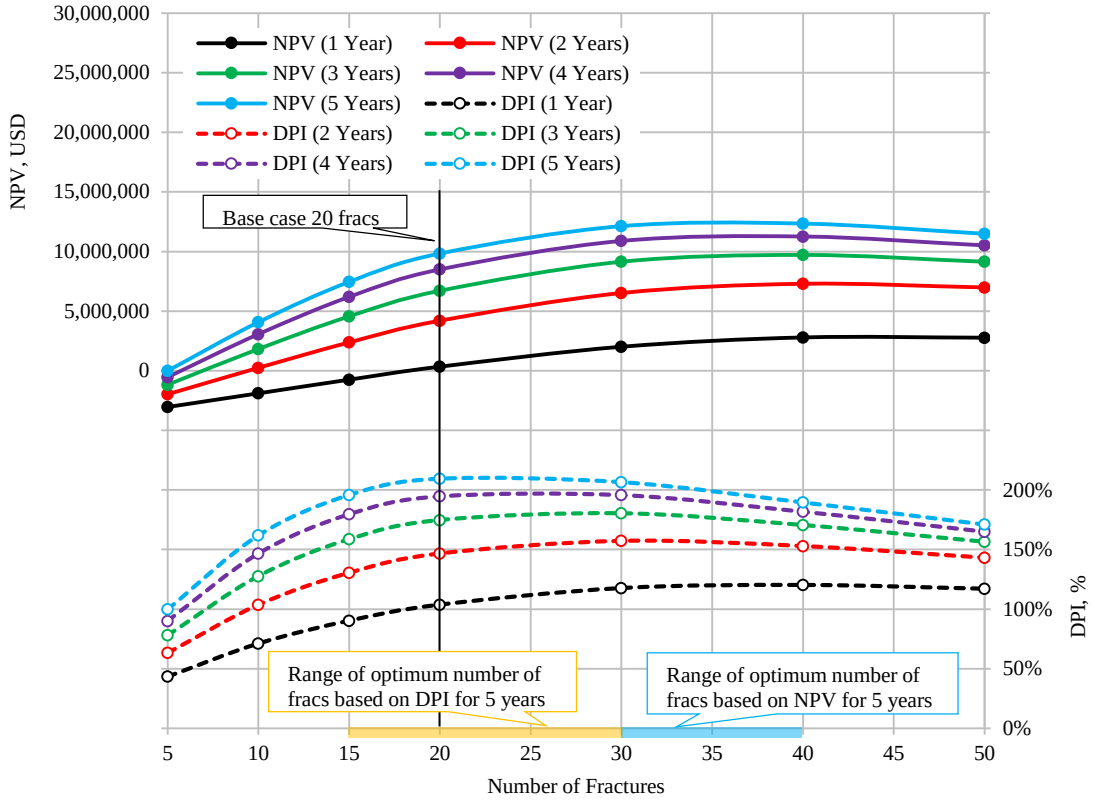

Fig. 4.13 – NPV and DPI in dry gas system for different number of fractures. Yellow and blue bars represent the optimum number of fracture based solely on DPI or NPV metrics

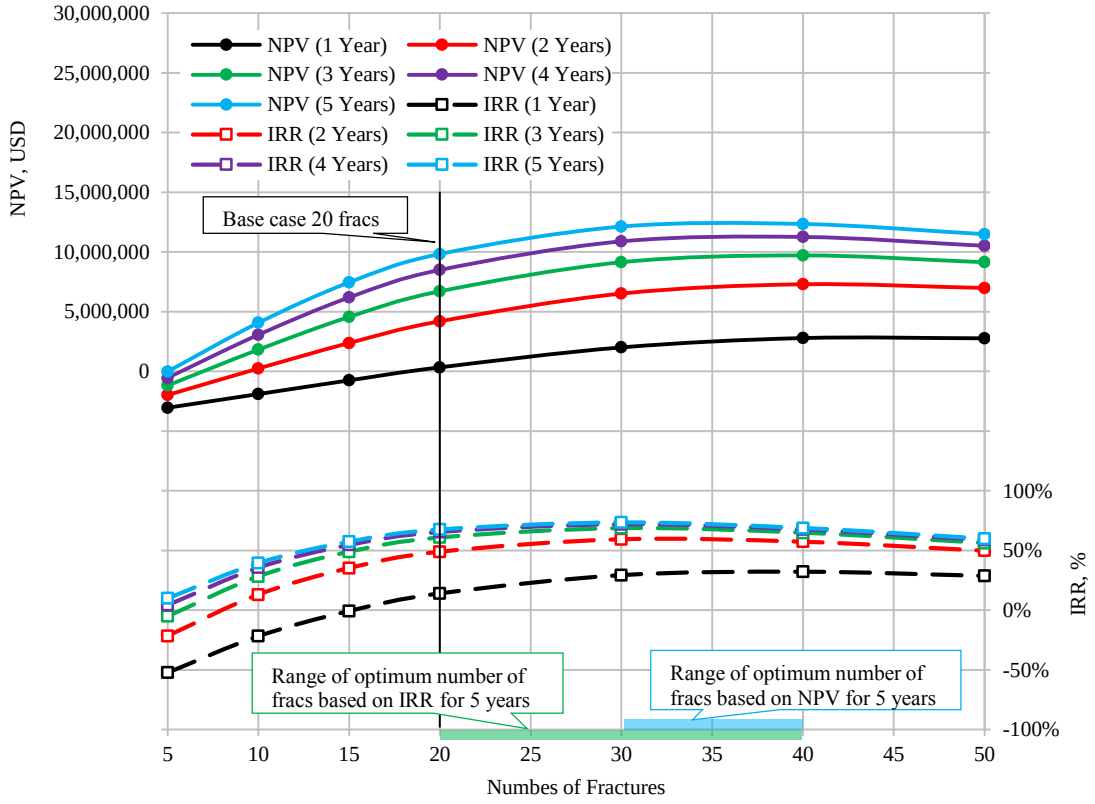

Fig. 4.14 – NPV and IRR in dry gas system for different number of fractures. Green and blue bars represent the optimum number of fracture based solely on IRR or NPV metrics

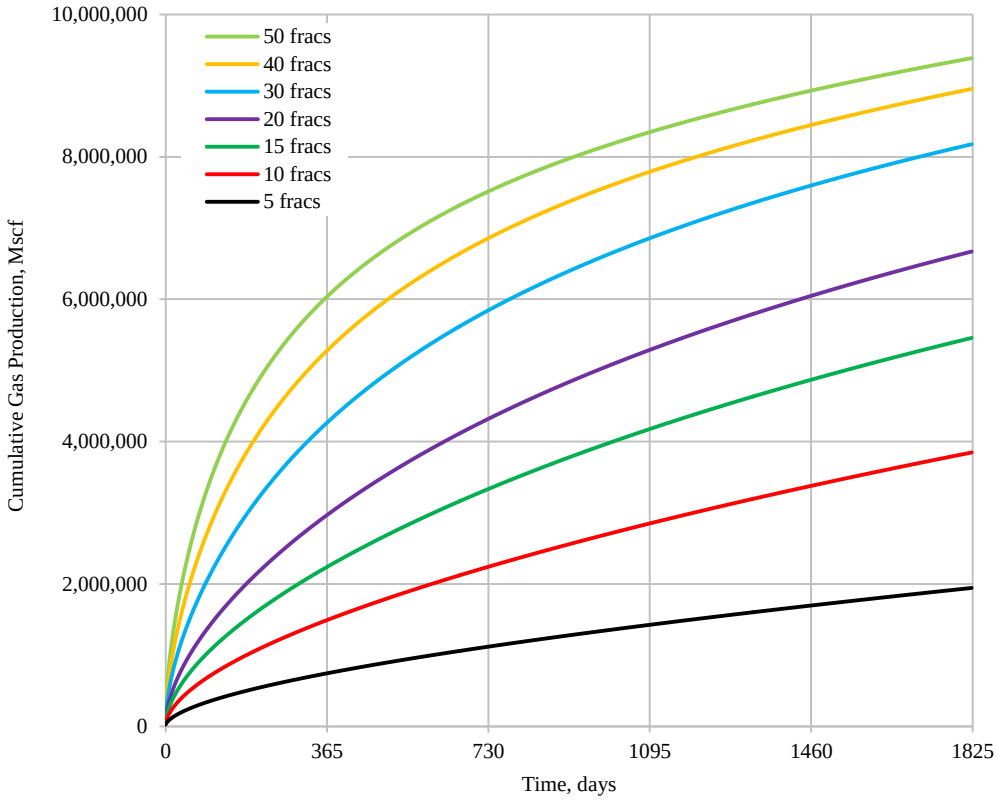

Fig. 4.15 – Cumulative gas production in dry gas system for different number of fractures.

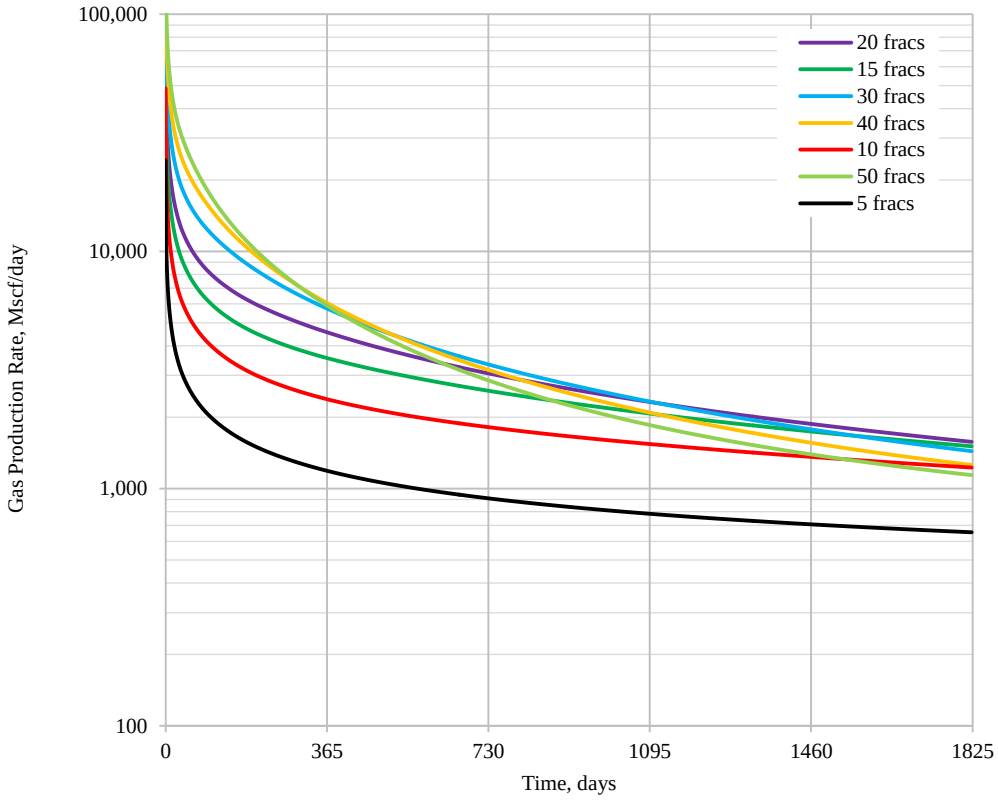

Fig. 4.16 – Gas production rates in dry gas system for different number of fractures.

Using both IRR and NPV could also make discussable what to call an optimal design (**Fig. 4.14**). For small companies it is important that IRR is as high as possible since the investors and banks will lend money with interest rate higher than for the big companies. We notice that

maximum IRR value shifts towards smaller number of fracs with 5 years period, while NPV optimum range is relatively the same. For example, comparing economic metrics after 2 years for 40 and 20 fractures we see clear difference in NPV (7.2 vs 4.2 million USD respectively) and in IRR (57.4% vs 49.1% respectively). The same observation done for NPV after 5 years still show the difference of 12.4 vs 9.8 million USD, but IRR value is almost constant for the range between 20 and 40 fracs. The combination of NPV, IRR and DPI yields the optimal design with 30 fracs; however if the company sticks to NPV as a sole criteria in economic assessment, 40 fractures will be preferred.

Cumulative production data and gas rates support the idea of using several metrics together (**Figs. 4.15-4.16**). Accelerated production for high number of fracs leads into high cash flow within first year, but negatively affect the production rates on later stages. Together with high initial investments, the efficiency of fractures in generating cash flow reduced with the higher number of fracs.

4.5 Fracture Half-Length

Fracture half-length is another important parameter controlled during hydraulic treatment. The expected length depends on the physical properties of the rock (horizontal and vertical stresses, Young modulus, etc.) and the treatment parameters (volumes of the hydraulic fluids and proppant, pressures created while fracturing the rock). It is assumed that the rock is homogeneous and induced fractures are identical. However, this assumption does not represent the real complexity of rock mechanics and processes ongoing during the treatment. Microseismics help to control the direction of extend of induced fractures, but often cannot provide accurate half-length, requiring history matching to be performed later. This makes fracture half-length one of the most important parameters for sensitivity analysis.

Total number of fractures and horizontal length of the well are kept the same, giving equal simulation area per frac in each case. Changing of half-length parameter increases the drainage within perpendicular fracture-reservoir flow, while reducing the drainage within mixed flow area (Fig. 3.3). **Figs. 4.17–4.18** show reservoir performance depends on different fracture half-lengths.

NPV optimal design suggests 500–660 ft fractures to achieve about 14 million USD with average DPI and IRR equal to 170% and 53% respectively. This result strongly differs from optimal fracture half-length based on DPI parameter. The maximum investment efficiency of about 210% achieved for fractures with 250–400 ft length. Corresponding average NPV is equal to 10.4 million USD and IRR is equal to 60%. Economic justification based on IRR gives a wide range of optimal fracture half-length in between 200 and 550 ft. DPI and NPV are changing significantly within this range (210–193% for DPI and 7.3–13.4 million USD for NPV). Combining of these three metrics will give an optimum fracture half-length within 400–500 ft.

Figs. 4.19–4.20 shows that doubling the size of the fracture does not yield doubled cumulative production. By increasing fracture from 300 to 600 ft, the cumulative production increases from 6.6 to 10.2×10^6 Mscf (or by 55% only). Therefore, additional fracture length does not increase production correspondingly causing lower investments efficiency in 5 years.

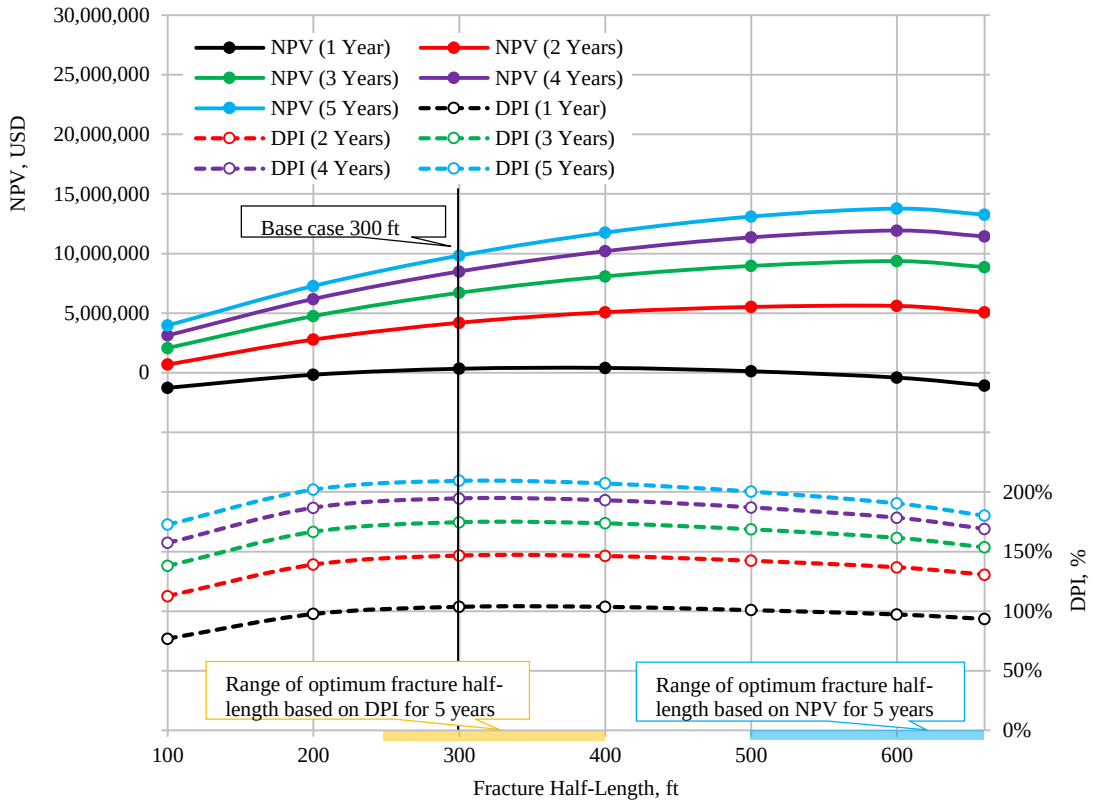

Fig. 4.17 – NPV and DPI in dry gas system for different fracture half-length. Yellow and blue bars represent the optimum number of fracture based solely on DPI or NPV metrics.

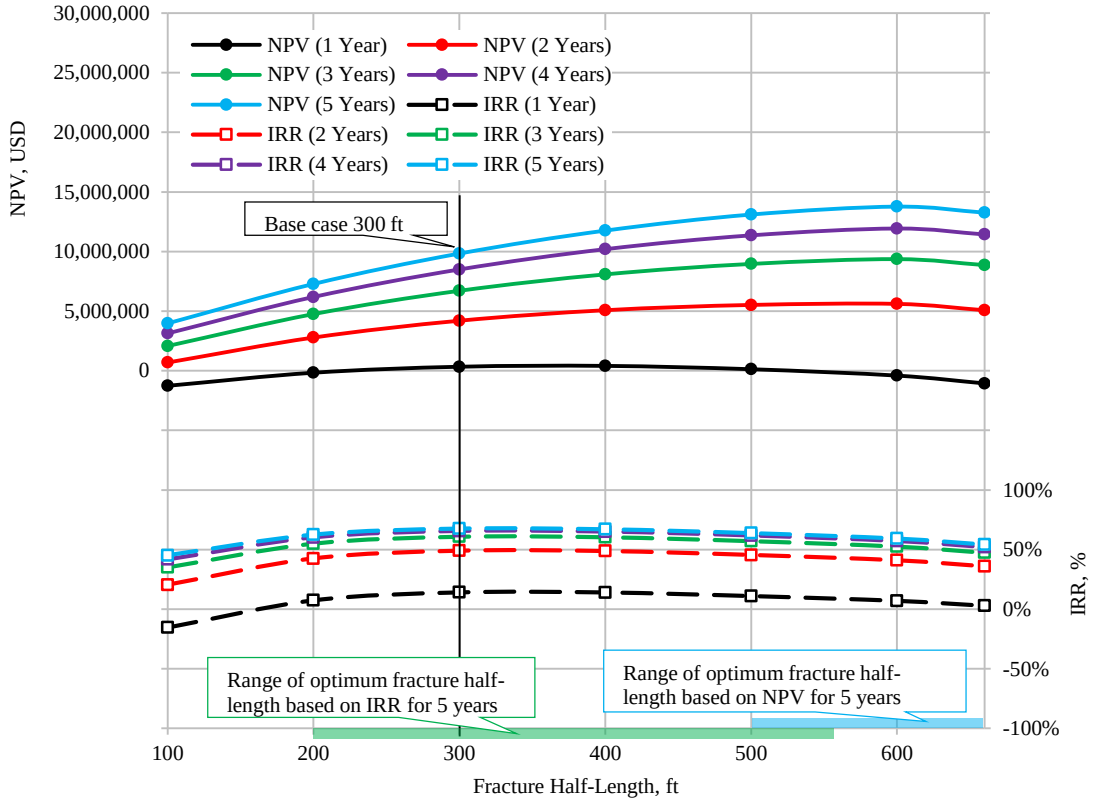

Fig. 4.18 – NPV and IRR in dry gas system for different fracture half-length. Green and blue bars represent the optimum number of fracture based solely on IRR or NPV metrics.

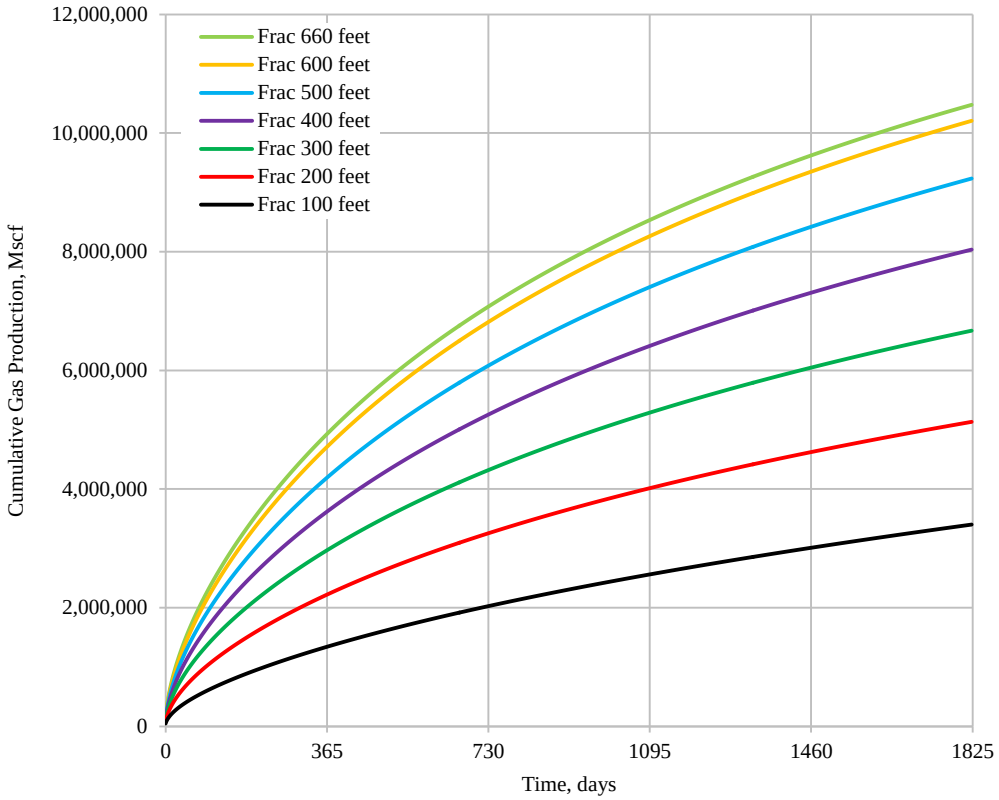

Fig. 4.19 – Cumulative gas production in dry gas system for different fracture half-length. The increase of length does not increase the cumulative production with the same magnitude.

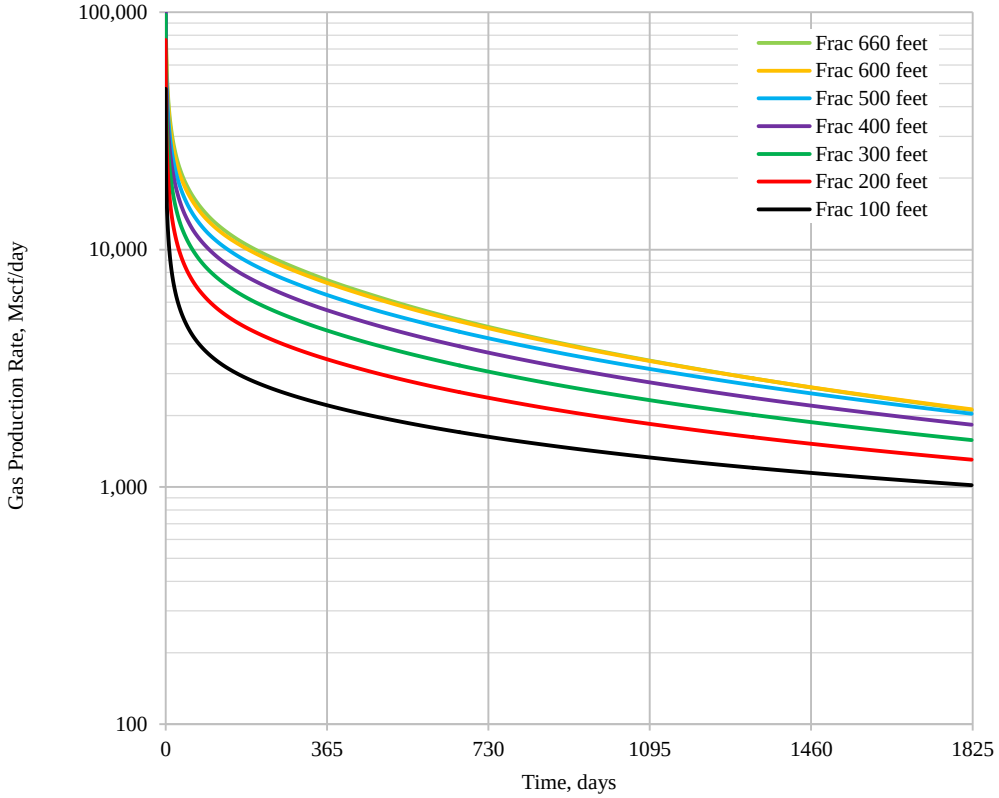

Fig. 4.20 – Gas production rate in dry gas system for different fracture half-length.

4.6 Well Horizontal Length

Longer well horizontal section allows involving into drainage bigger reservoir volumes without drilling additional well. Together with total number of fractures it defines the total drainage area assigned for one fracture. For this sensitivity, the number of fracture is kept constant while horizontal length changes from 5,280 to 10,560 ft. Placing 20 fractures along the wellbore yields fracture spacing between 264 and 528 ft. This case is not very realistic since usually both horizontal length and number of fractures are changed, but it helps understand if the effect of boundaries on the flow.

Figs. 4.21–4.22 shows the performance of the model for different horizontal lengths of the well. In 5 years, the NPV of the model stays around 10 million USD regardless the variable length. However, the investment efficiency drops down from 209% at 5,280 ft to 179% at 10,560 ft. Internal rate of return behave similarly decreasing from 67.6% to 47.7%. A slightly noticeable NPV maximum achieved for about 7,000 ft horizontal section with 10.4 million USD. However, the DPI and IRR is lower than base case with 204% and 61.7% respectively. This indicated that incremental costs from increased horizontal length (or fracture spacing) are higher than incremental revenues.

Figs. 4.23–4.25 show that difference in model performance become noticeable after 1 year of production. This can be explained that at this point the pressure in the model with 264 ft fracture spacing is significantly lower than for 528 ft spacing model. This maintains higher production rates in the model yielding higher total cumulative gas production. However, the incremental gas production from increased fracture spacing is too small to positively influence the project's economy.

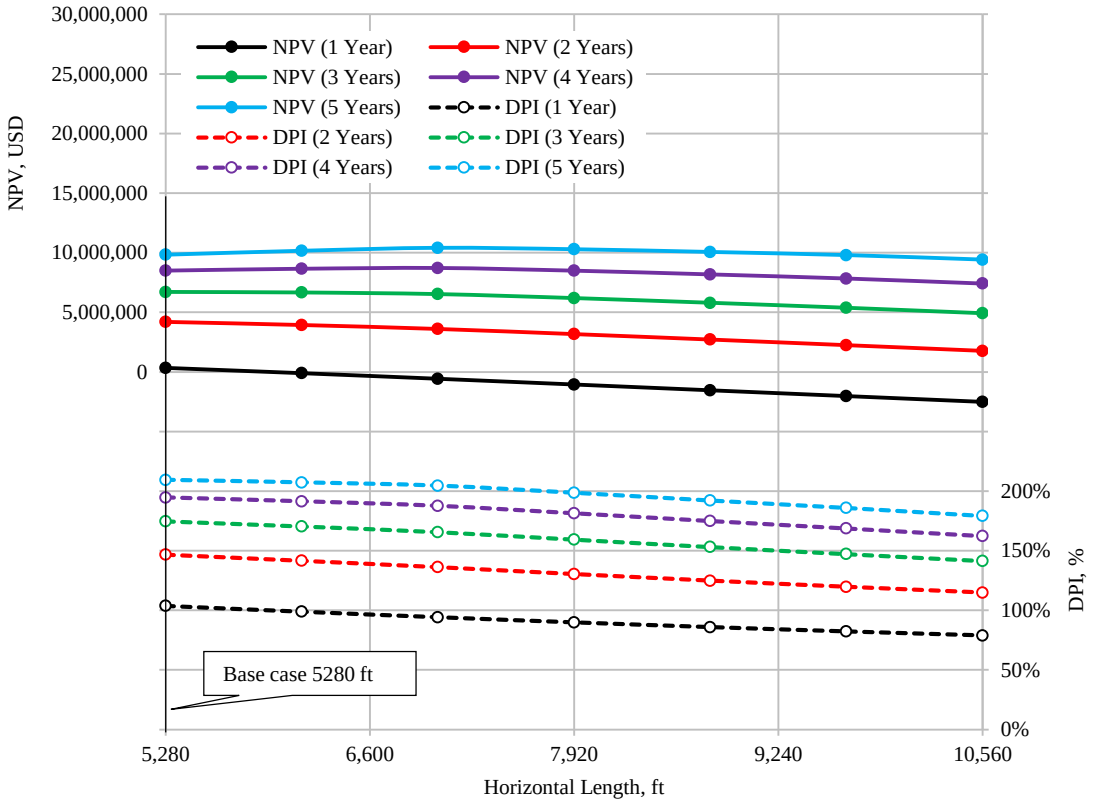

Fig. 4.21 – NPV and DPI in dry gas system with different horizontal length of the well.

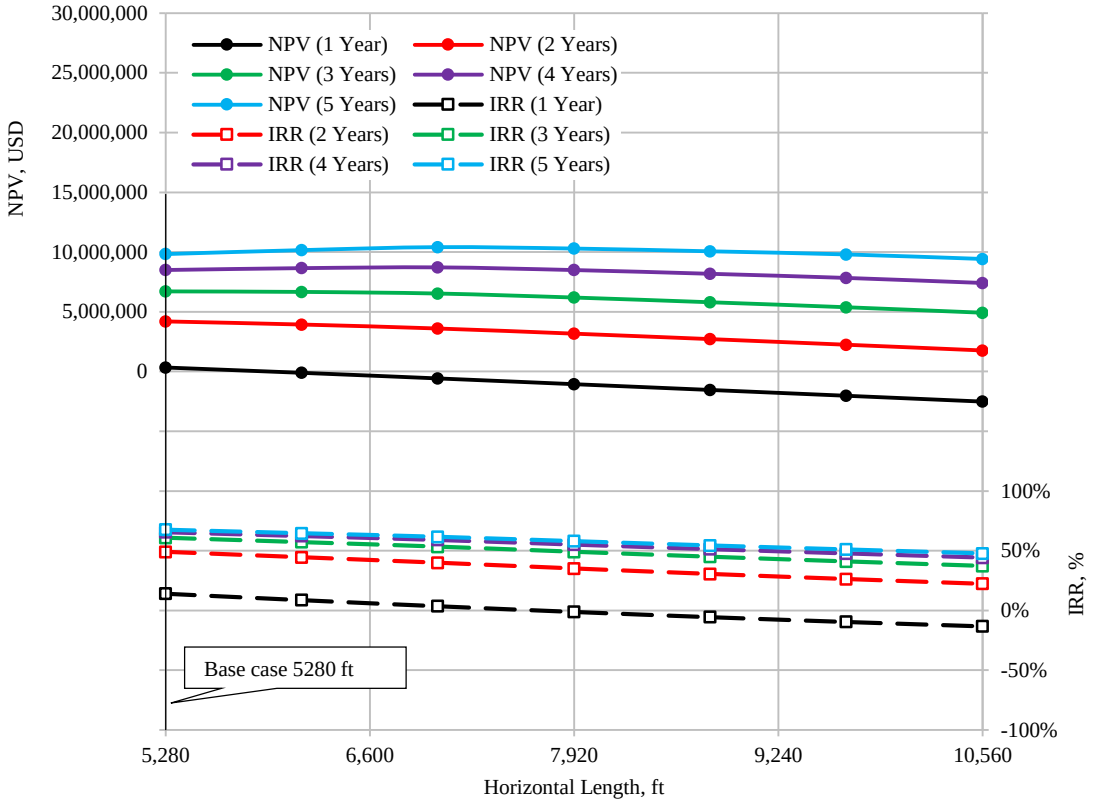

Fig. 4.22 – NPV and IRR in dry gas system with different horizontal length of the well.

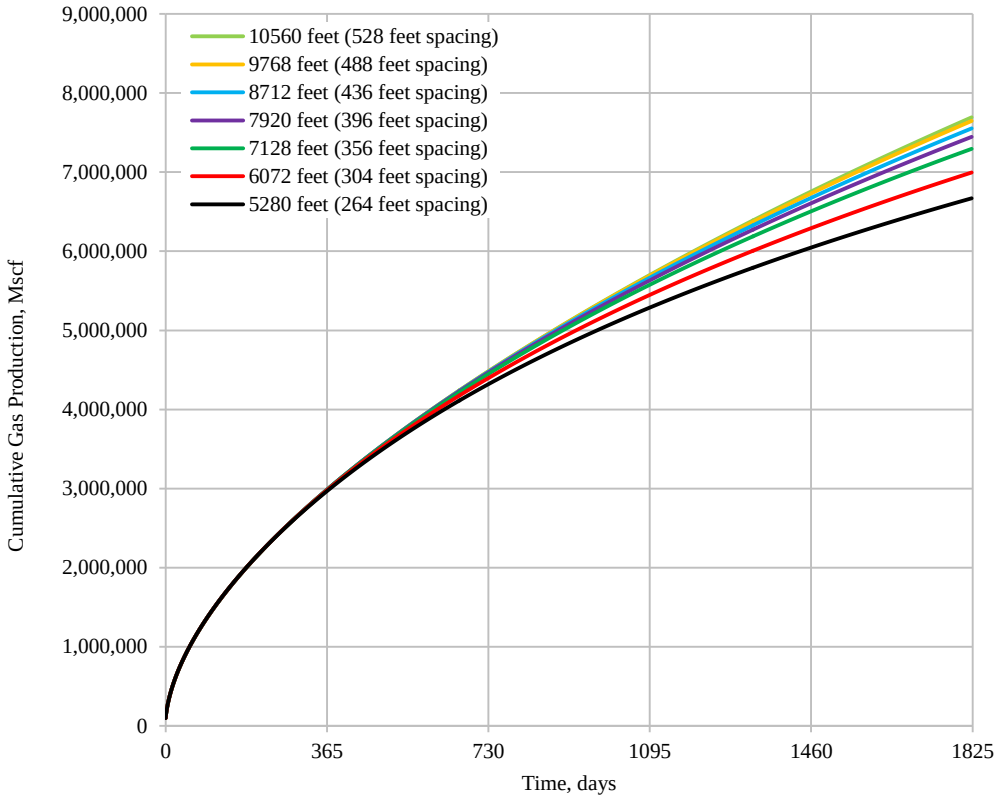

Fig. 4.23 – Cumulative gas production in dry gas system for different horizontal length of the well. The incremental production becomes insignificant with length longer than 7,920 ft (fracture spacing more than 396 ft)

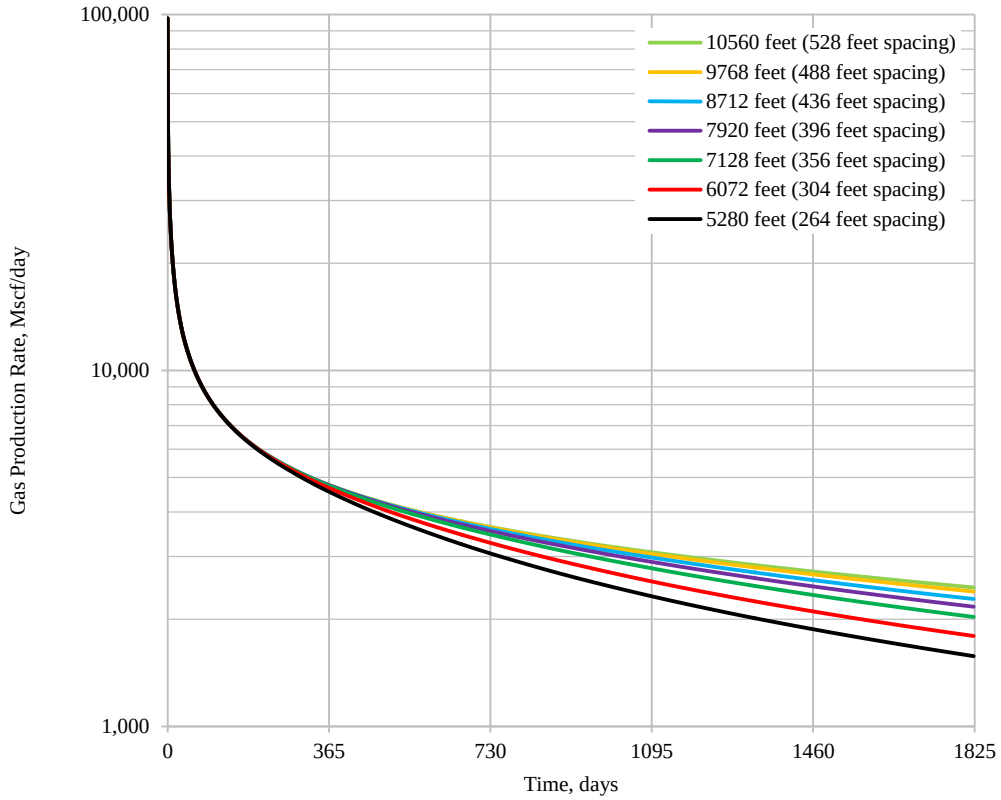

Fig. 4.24 – Gas production rate in dry gas systems for different horizontal length of the well. The increment to gas rate become insignificant with length longer than 7,920 ft (facture spacing more than 396 ft)

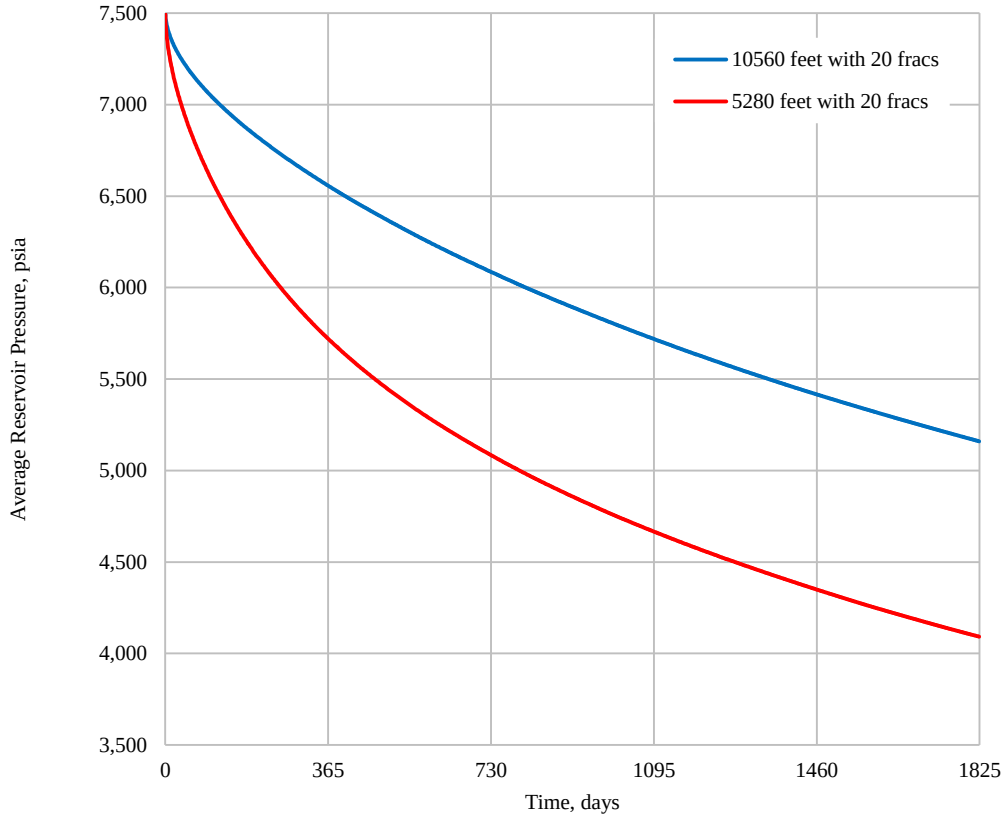

Fig. 4.25 – Average reservoir pressure for models with different horizontal length of the well. Other cases have pressure in between these two extreme cases.

4.7 Constant Fracture Spacing

As a logical continuation of previous sensitivity run, we maintained constant fracture spacing for different horizontal lengths of the well. The horizontal section is in between 5,280 and 10,560 ft with changing number of fractures 20 to 40. This yields a constant fracture spacing of 264 ft.

Figs. 4.26-4.27 indicate the monotonic linear trend in reservoir performance with constant fracture spacing. The maximum achieved NPV is equal to 20.9 million USD with 225% DPI and 76% IRR. Monotonically increasing behavior shows the surplus of marginal revenues over marginal costs for all cases since. The linear behavior is explained by definition of cost model for the project. We assume that the price of one fracture and price for drilling one foot of horizontal section are constant regardless the total number of fractures or total horizontal length. Therefore, the total reservoir performance will indicate a linear behavior.

By having constant fracture spacing together with keeping all other parameters unchanged, the performance of a single fracture is identical in all of the cases. **Figs. 4.28–4.29** illustrate that the model transformed into scaling problem model, where the difference in performance depends only on the final multiplication number. Thus, without introducing change in incremental cost for higher number of fracs or longer horizontal section, the solution will be trivial; if incremental revenues are higher than incremental costs for base case scenario, the best solution is to have longer well with more fractures.

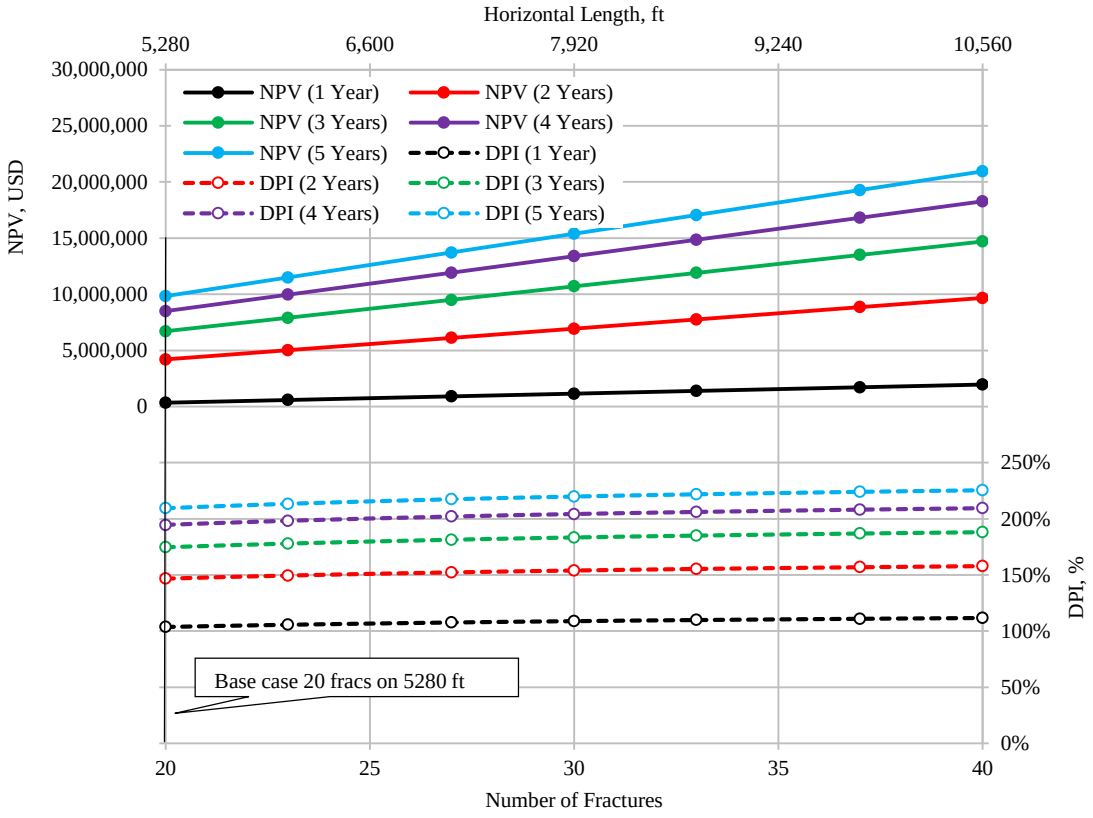

Fig. 4.26 – NPV and DPI in dry gas systems with constant fracture spacing.

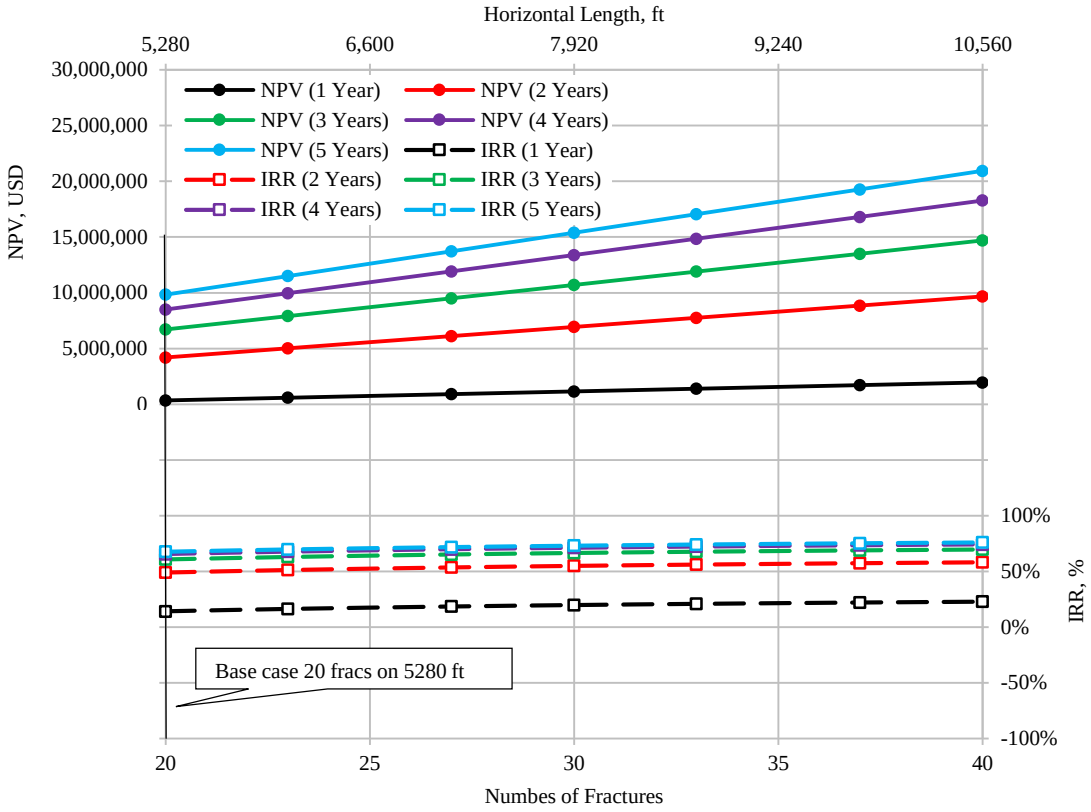

Fig. 4.27 – NPV and IRR in dry gas system with constant fracture spacing.

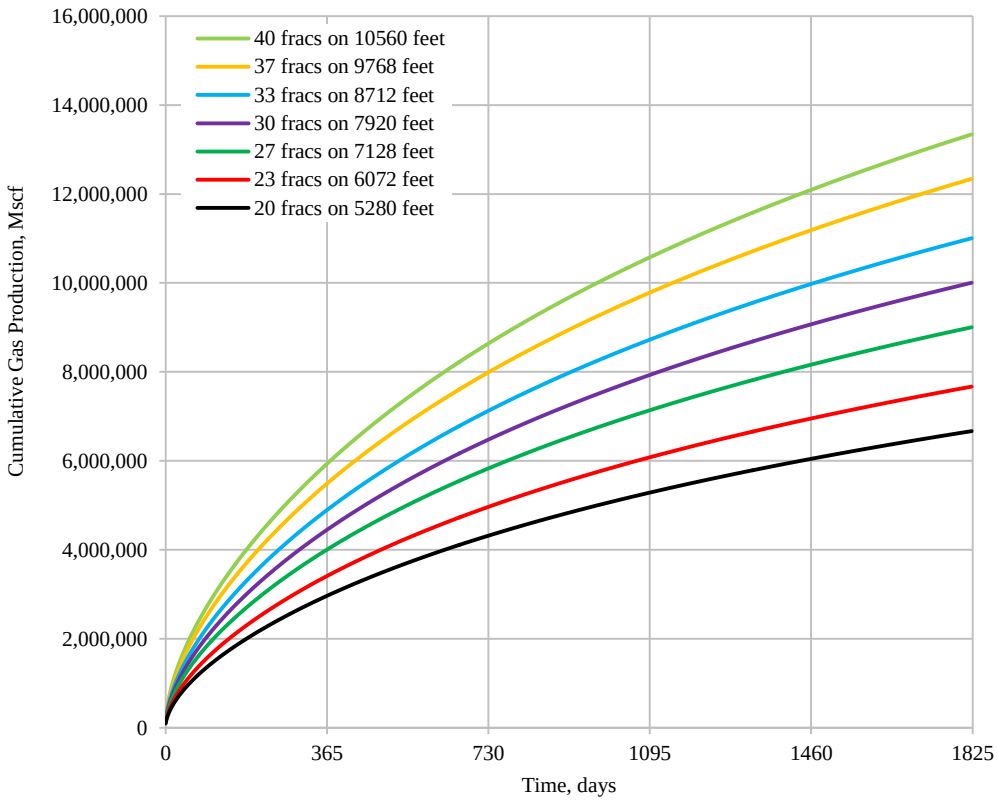

Fig. 4.28 – Cumulative gas production in dry gas system with constant fracture spacing. The production is scaled by the number of fractures.

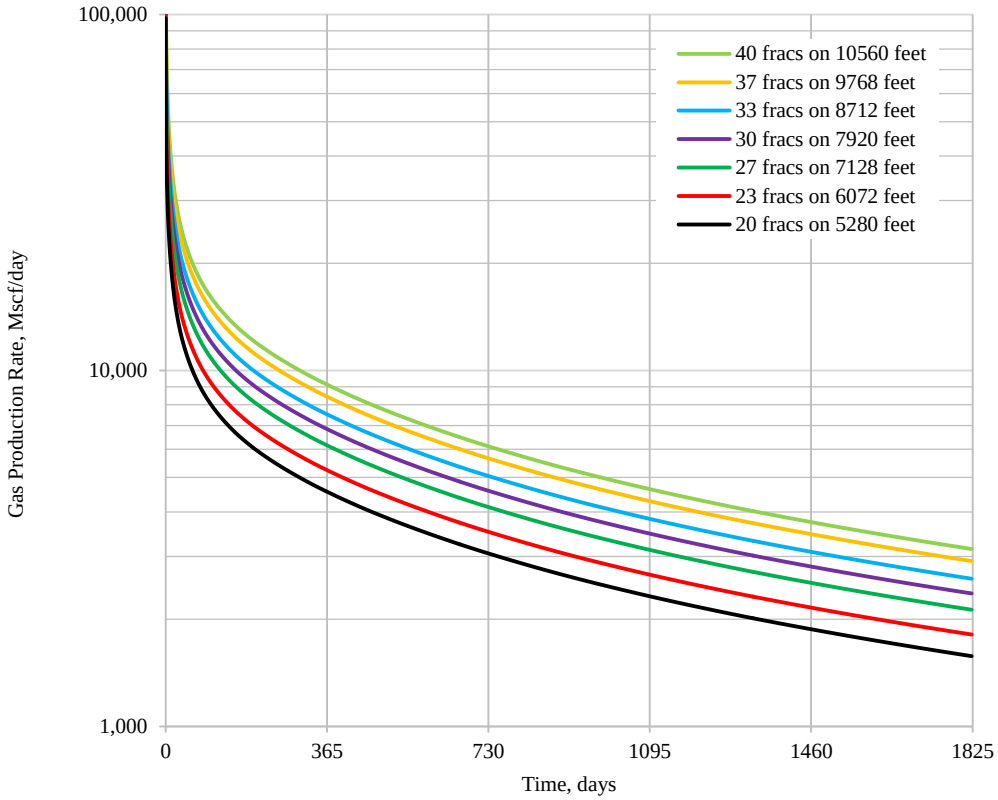

Fig. 4.29 – Gas production rate in dry gas system with constant fracture spacing. Decline of production rates is identical for all cases. The rates are scaled by the number of the fractures.

4.8 Productivity Index

Productivity index of shale wells is commonly expressed as a parameter calculated by multiplication of total fractured area by the squared root of permeability (Lalehrokh and Bouma, 2014). Productivity index shows the ability of the reservoir to deliver the flow to the wellbore ("Oilfield Glossary", 2015). For planar model, assuming the width of the fracture is constant, the fractured area can be substituted by fracture half-length, yielding:

$$PI = x_f \sqrt{k_m} \quad \text{.....(23)}$$

where:

$PI =$ linear flow, infinite-acting productivity index, √ft-md

$x_f =$ fracture half-length, ft

$k_m =$ matrix permeability, md

For this sensitivity analysis, we were changing fracture half-length and matrix permeability in order to keep constant base case scenario PI is equal to 6.71. The fracture half-lengths selected between 100 and 660 ft, giving the corresponding reservoir permeabilities of 4,500–103 nd. **Figs. 4.30–4.31** show calculated NPV, DPI and IRR for this reservoir.

The effect of reduced matrix permeability significantly influences on the economy of the project. With the permeability of about 1,000 nd (corresponding fracture half-length is 212 ft), the best NPV is about 12.1 million USD, the highest DPI is 260% and the highest IRR is 100%. However, going down in permeability of 125 nd drops down project's NPV to 2.5 million USD, DPI to 116% and IRR to 18%. Maintaining constant productivity index does not allow to keep the project economy on acceptable level in low-permeability reservoirs within 5 years. It is possible that longer production period (for example, 10 years) could slightly change the project economy in a better way, but due to the discounting effect this change may not drastically change the overall picture.

Figs. 4.32–4.33 illustrate that increase of the fracture half-length can help to maintain approximately the same production rates and cumulative gas production in a range of 103–1,125 nd. However, the cost of fracture treatment increases significantly with increased fracture half-length. For example, using Eq. 5 with economic input from Table 4, the cost for well completion will vary between 5.5 million USD for 100 ft fracs and 16.5 million USD for 660 ft fracs. The incremental cost of maintaining constant PI is much higher than incremental revenues from increased fracture half-length. It could be suggested to have more fractures with shorted half-length to keep project economy on higher level.

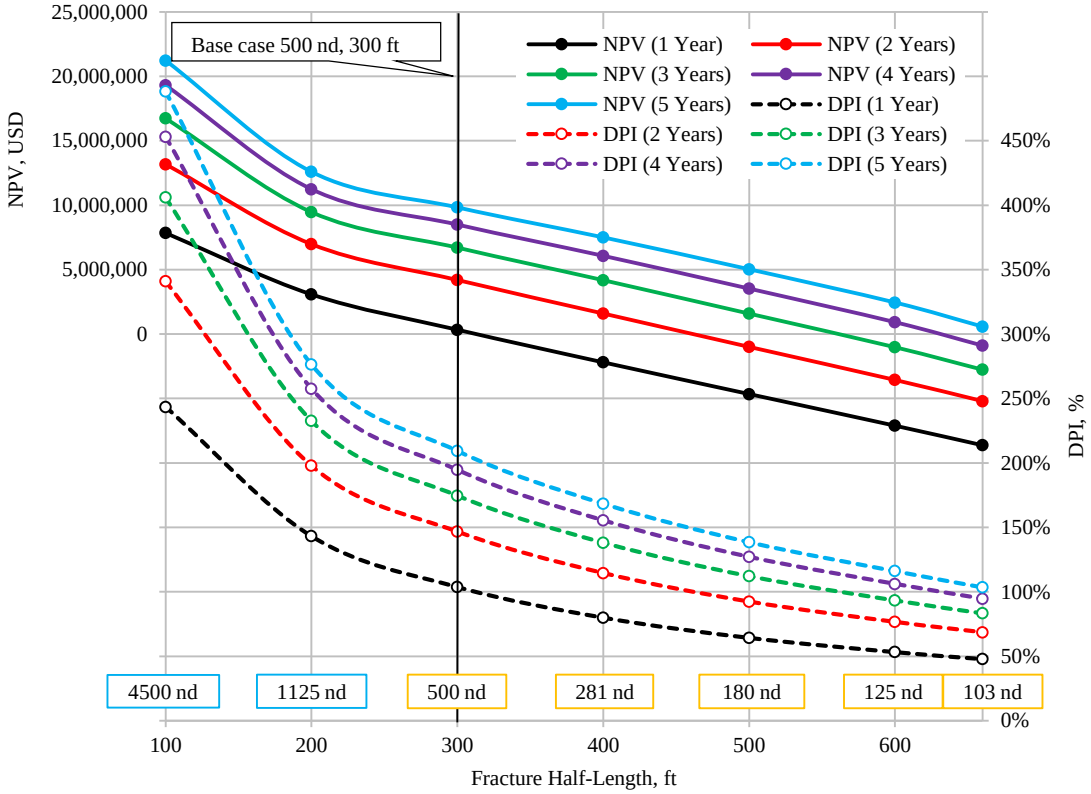

Fig. 4.30 – NPV and DPI in dry gas system with constant PI. Fracture half-length and reservoir permeability are changed simultaneously. Yellow and blue boxes represent the permeabilities typical for shale and conventional reservoirs respectively.

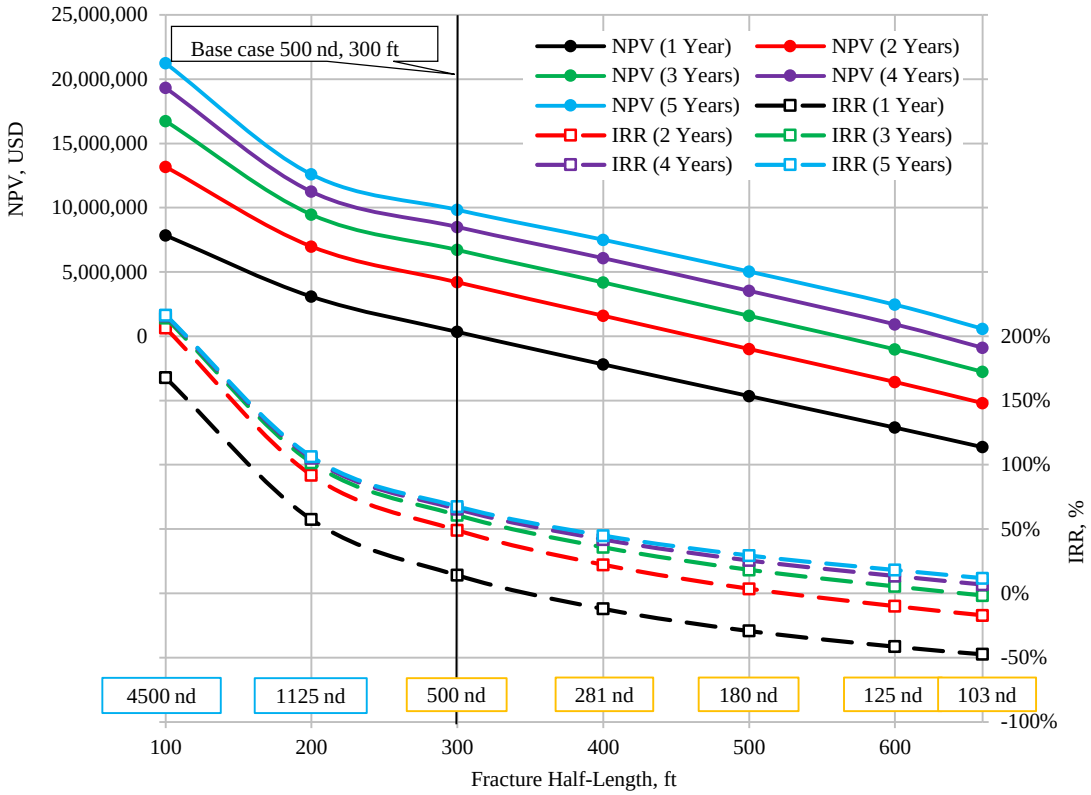

Fig. 4.31 – NPV and IRR in dry gas system with constant PI. Fracture half-length and reservoir permeability are changed simultaneously. Yellow and blue boxes represent the permeabilities typical for shale and conventional reservoirs respectively.

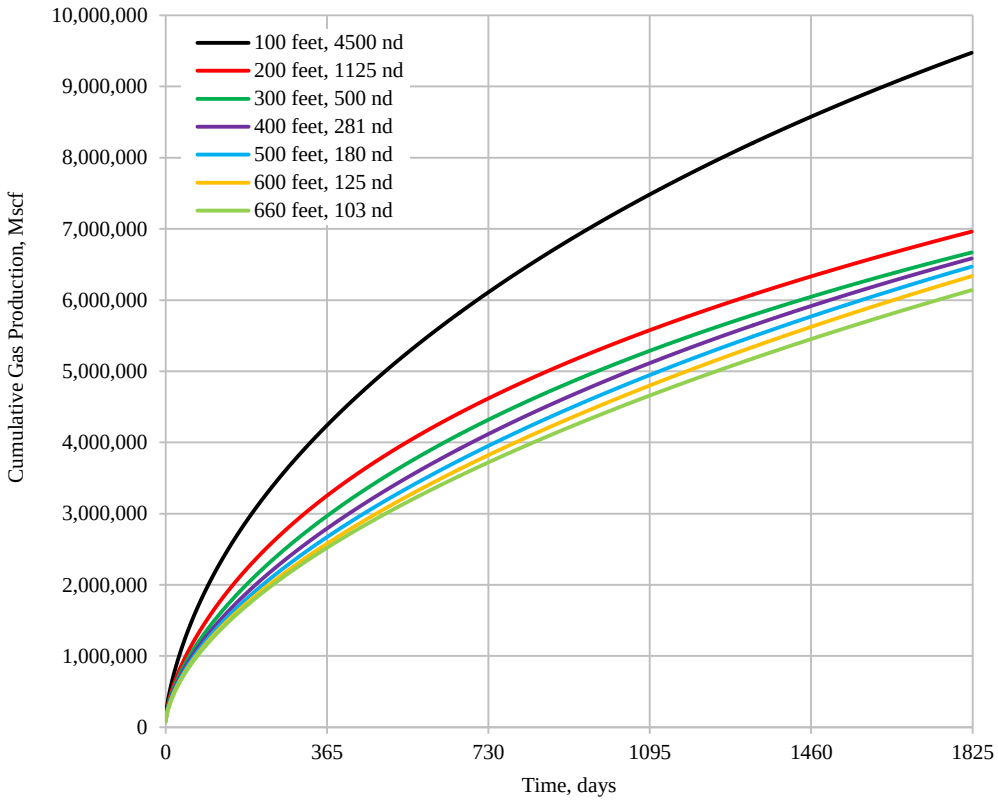

Fig. 4.32 – Cumulative gas production in dry gas system with constant PI. Total cumulative production is almost the same for 300–660 ft fractures.

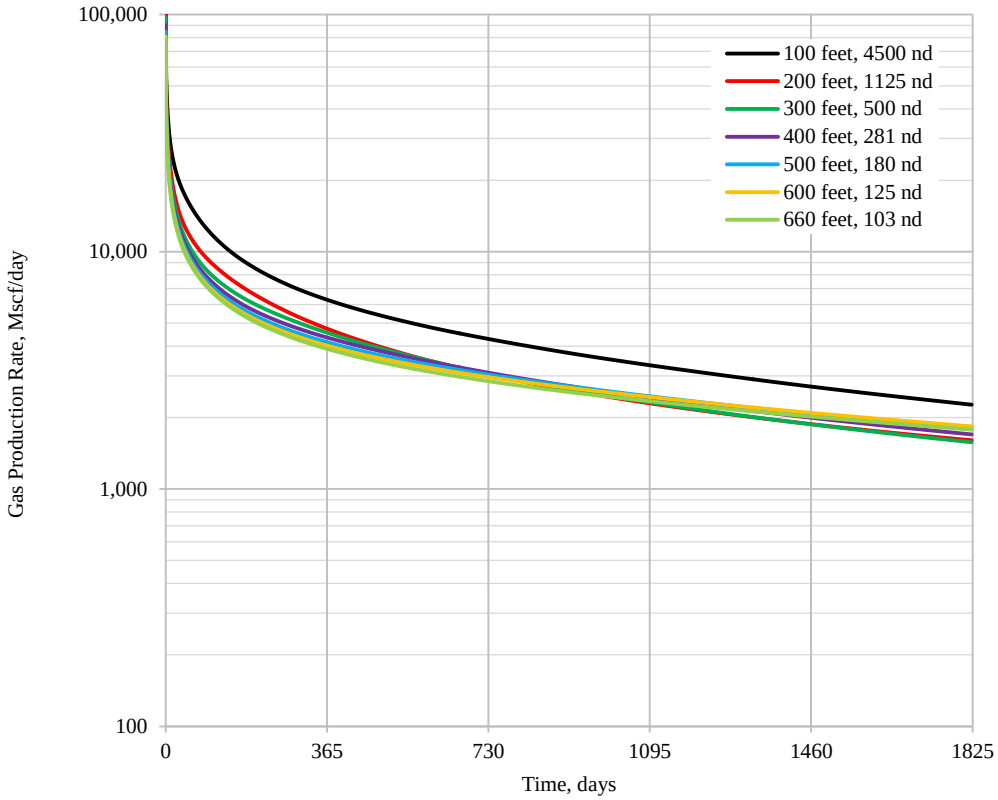

Fig. 4.33 – Gas production rate in dry gas system with constant PI. Performances for 300-660 ft fracs are almost the same

THIS PAGE INTENTIONALLY LEFT BLANK

Chapter 5

Gas Condensate Simulation Results

Gas condensate simulation case initialized with undersaturated gas in the reservoir. PVT black-oil tables generated automatically by SENSOR based on Equation-of-States described in Appendix B using Whitson and Torp (1983) method. Black-oil tables consist of saturated data covering pressure range from 14.7 to 4,906.4 psia and a set of undersaturated data up to 15,000 psia for each of the saturation data pressures. EOS uses 31 components for table generation. Initial water saturation S_{wi} is set to 0.4, initial gas saturation S_{gi} is set to 0.6. Initial GOR of the system is 8,000 scf/STB (OGR is 125 STB/MMscf). Comparing with dry gas results, gas condensate includes the sensitivity on different flowing bottomhole pressure.

5.1 Matrix Permeability

Figs. 5.1–5.2 show reservoir performance with different matrix permeability of the system. The best performance in shales achieved for permeability of 1,000 nd with 16.5 million USD for NPV, 284% of DPI and 111% IRR. High permeability range of 1,000–10,000 nd showed much better performance for gas condensate than dry gas reaching maximum NPV of 39.8 million USD, 540% of DPI and 320% of IRR. The performance in ultra-right shales with permeabilities of 10–100 nd was lower for gas condensate due to significant liquid drop-out around fracture area. The oil presence reduces the relative permeability of gas and in synergy with small active drainage area negatively influences the economy of the well. In a range of 100–1000 nd, gas condensate model shows relatively equal results to dry gas. For base case, NPV reached 9.9 million USD, investment efficiency was 211% with project's IRR of 67%. The break-even permeability for gas condensate achieved at 120 nd (33% higher than for dry gas model).

Figs. 5.3–5.5 shows that high economic results in 1,000–10,000 achieved due to great amount of produced condensate. Even with lower cumulative gas production, the cash contribution from sold oil raised gas condensate model performance over the dry gas model. Fast depletion of the reserves at the early stages caused later intensive condensation in the reservoir confirmed by low produced OGR and faster decline of oil rates.

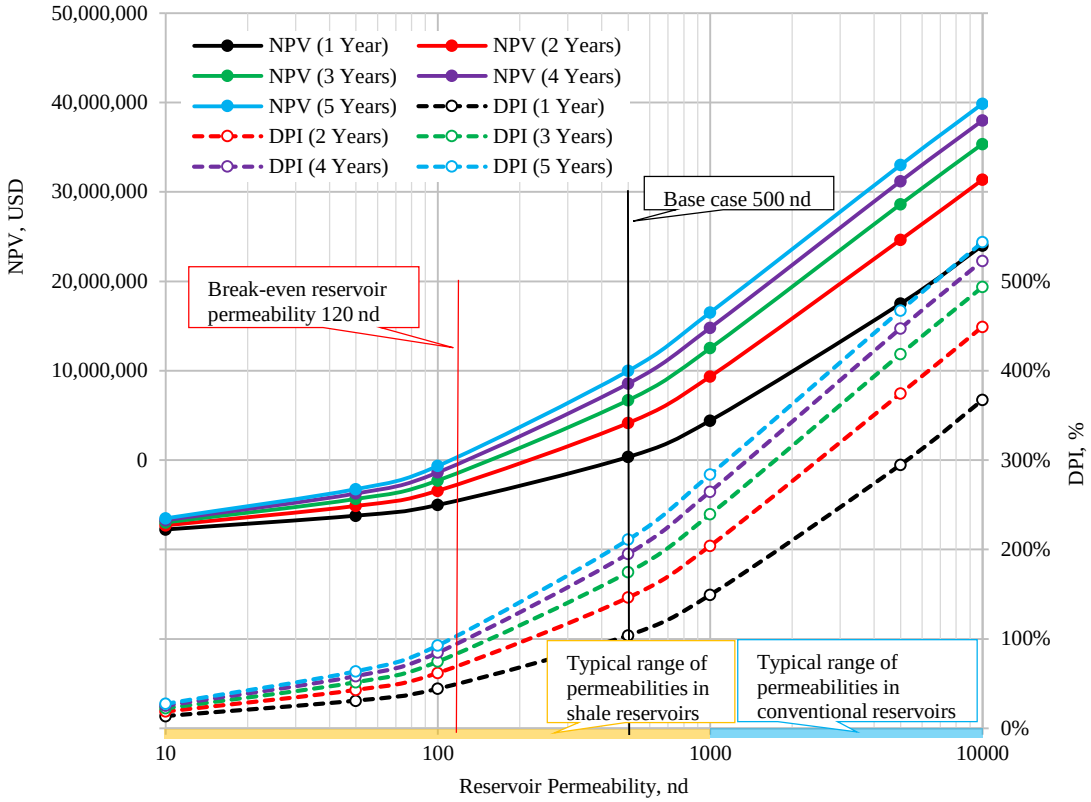

Fig. 5.1 – NPV and DPI in gas condensate system for different reservoir permeabilities. Yellow and blue bars represent typical permeability ranges for shale and conventional reservoirs.

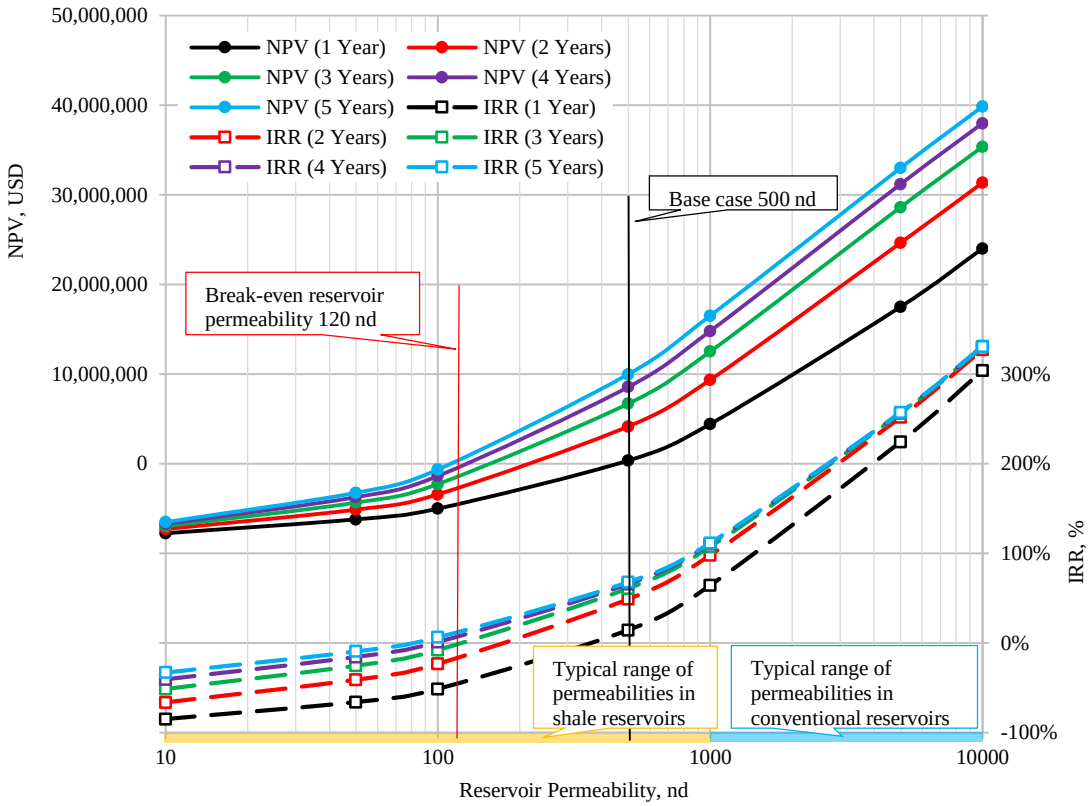

Fig. 5.2 – NPV and IRR in gas condensate system for different reservoir permeabilities. Yellow and blue bars represent typical permeability ranges for shale and conventional reservoirs.

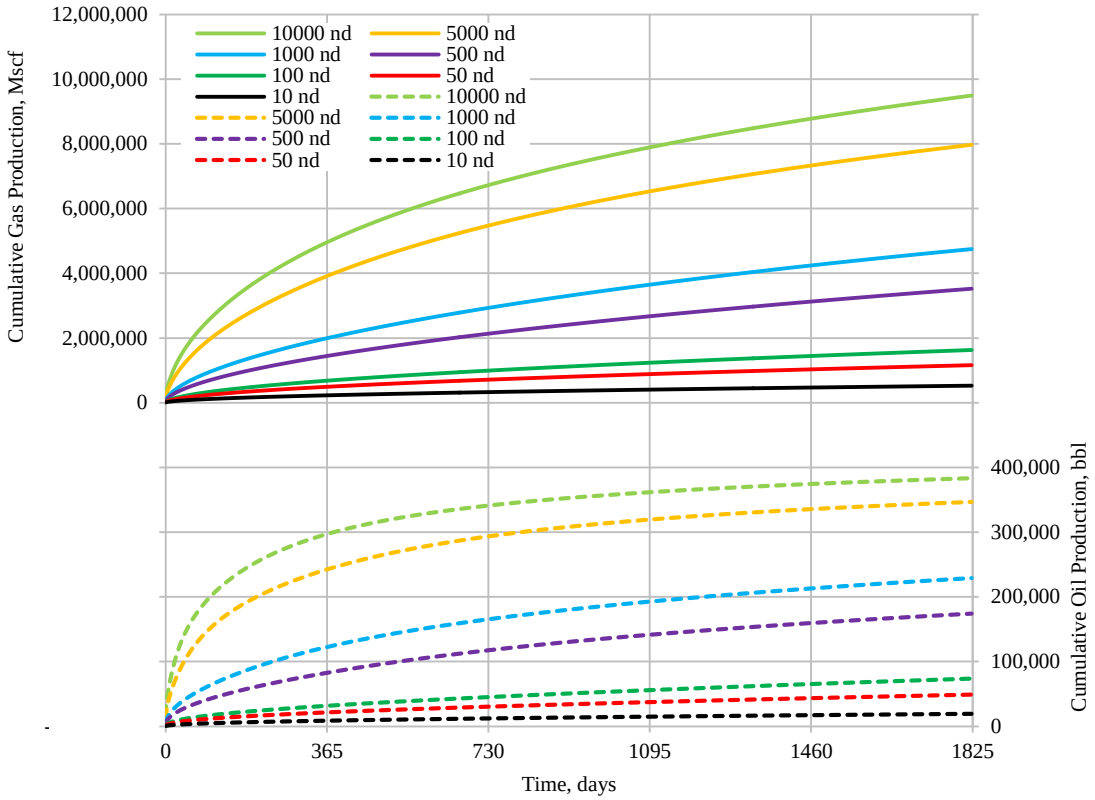

Fig. 5.3 – Cumulative oil and gas production in gas condensate system for different reservoir permeabilities. Break-even reservoir permeability is 120 nd.

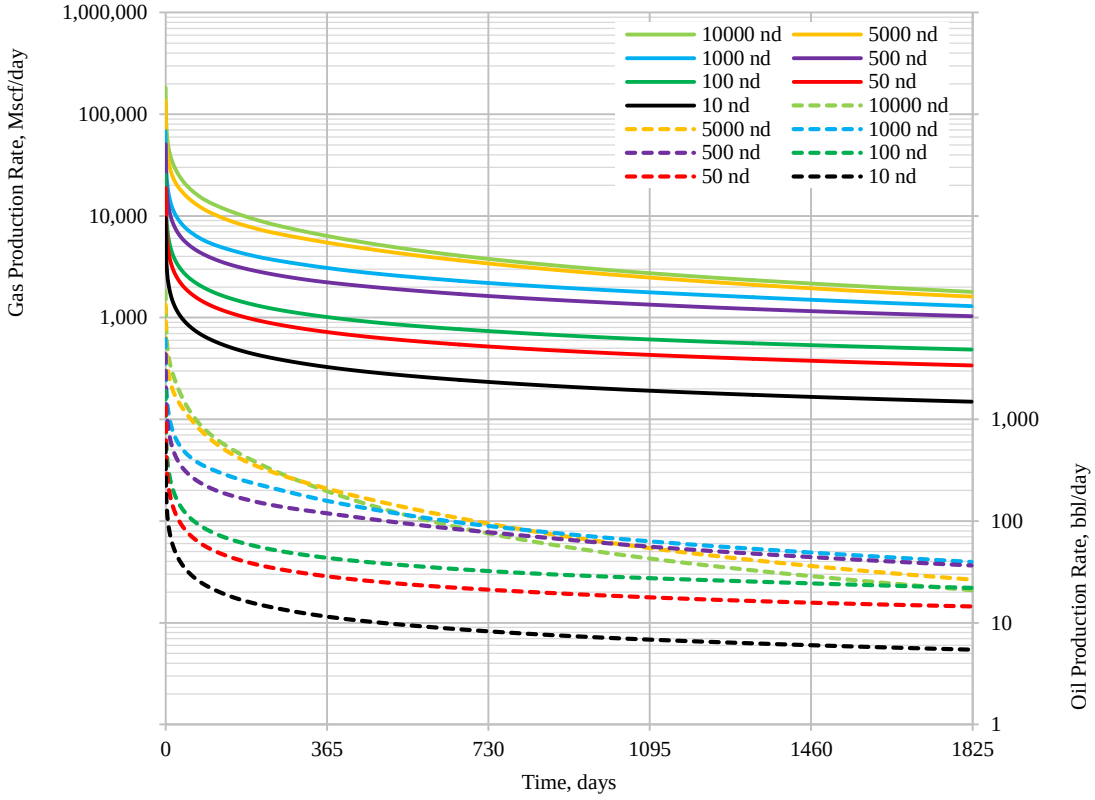

Fig. 5.4 – Oil and gas production rates in gas condensate systems for different reservoir permeabilities.

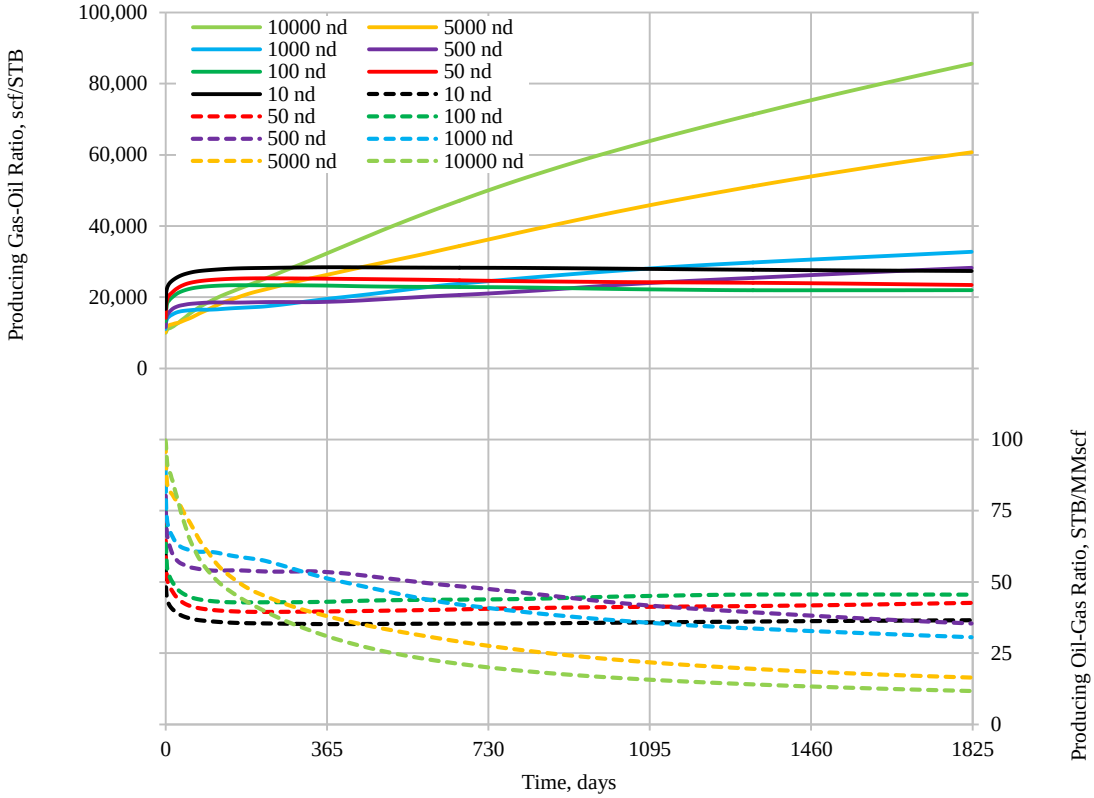

Fig. 5.5 – Producing GOR and OGR in gas condensate system for different reservoir permeabilities.

100–1,000 nd cases showed slightly lower cumulative gas production comparing to dry gas case. Produced OGR was decreasing from the beginning of the production from about 65 to 30 STB/MMscf within 5 years. However, the amount of produced condensate was sufficient to substitute the missing cash from reduced cumulative gas production. Ultra-tight shales (10–100 nd) showed worse performance due to very high liquid drop-out inside the reservoir keeping OGR in a range of 35–45 STB/MMscf. The gas relative permeability is severely reduced and the total gas production was twice lower than for dry gas case.

5.2 Initial Reservoir Pressure

Figs. 5.6–5.7 indicate maximum reservoir performance achieved at pressures around 12,500 psia. The highest NPV is 18.1 million USD with investment efficiency of 300% and project's IRR of 120%. From 10,000 psia and below we observe steep decline in all metrics. The pressures yielding high reservoir performance are in between 9,500 and 14,500 psia. It's a wider range of pressures comparing with dry gas model where maximum performance achieved with 6,500–8,500 psia. This behavior of gas condensate model can be explained by extremely low liquid drop-out in the reservoir since the average reservoir pressure stays above saturation pressure (4,906.4 psia). The mobility reduction from increased gas viscosity has less influence on the economy due to cash substitution from produced oil. In pressure range below 7,500 psia, gas condensate model showed worse performance than dry gas model because of significant liquid drop-out in the reservoirs from the beginning of the production, causing gas mobility reduction.

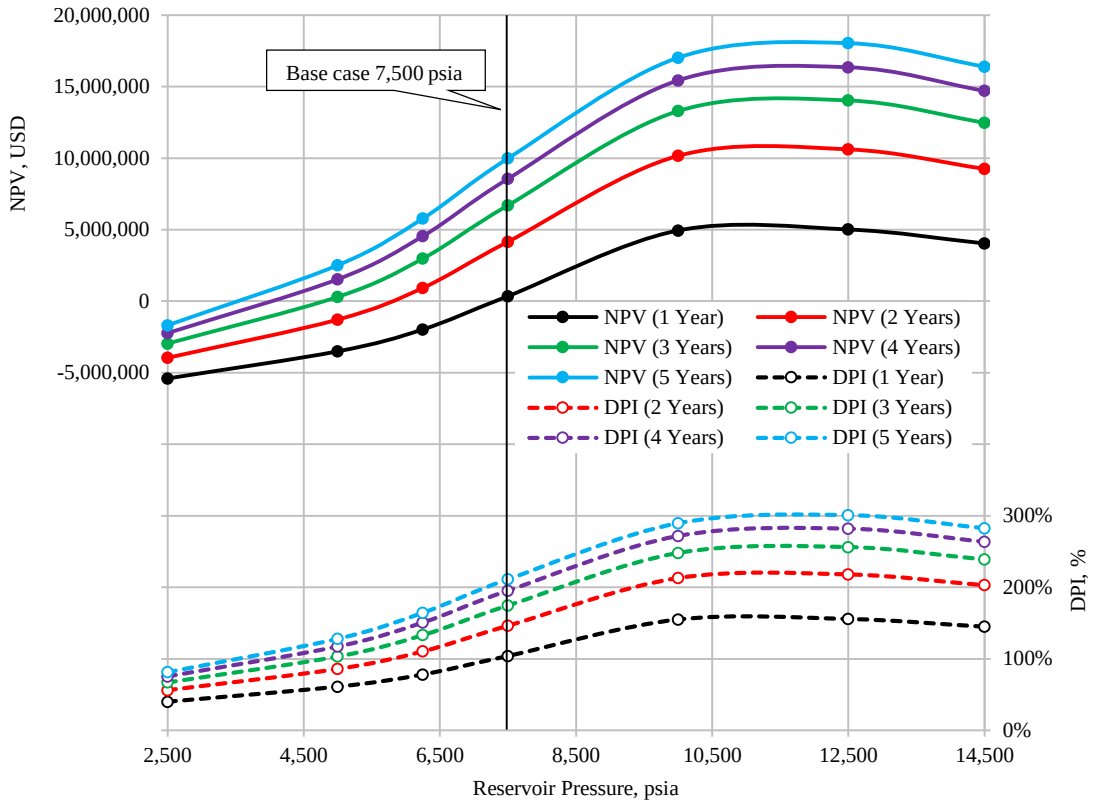

Fig. 5.6 – NPV and DPI in gas condensate system for different initial reservoir pressure.

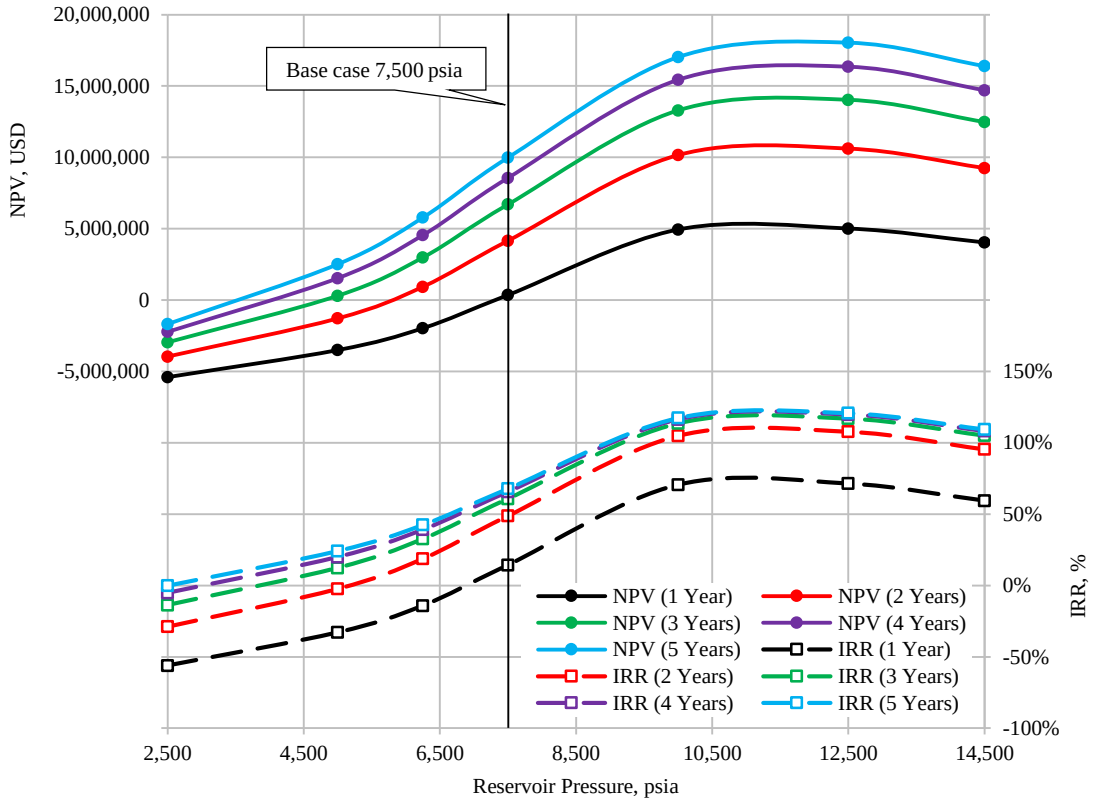

Fig. 5.7 – NPV and IRR in gas condensate system for different initial reservoir pressure.

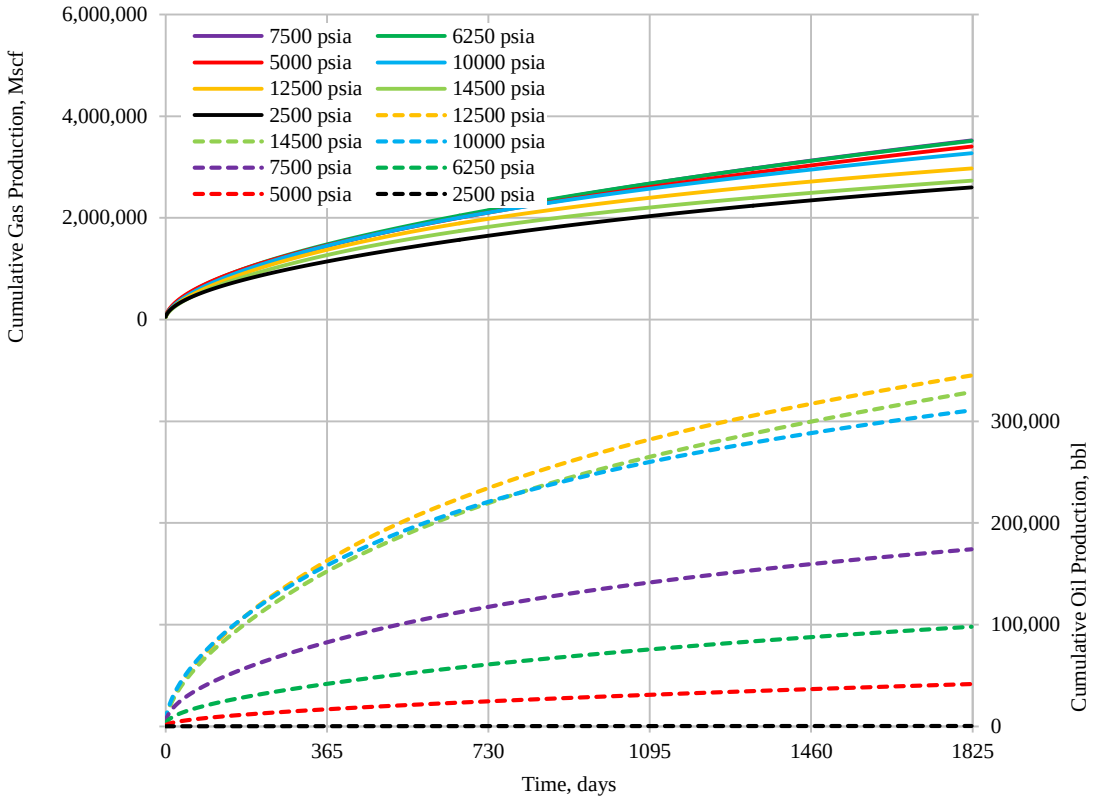

Fig. 5.8 – Cumulative oil and gas production in gas condensate system for different initial reservoir pressures. Gas production monotonically increases for 2,500-7,500 psia, then monotonically decreases for higher pressures. Oil production increases for 2,500-12,500 psia.

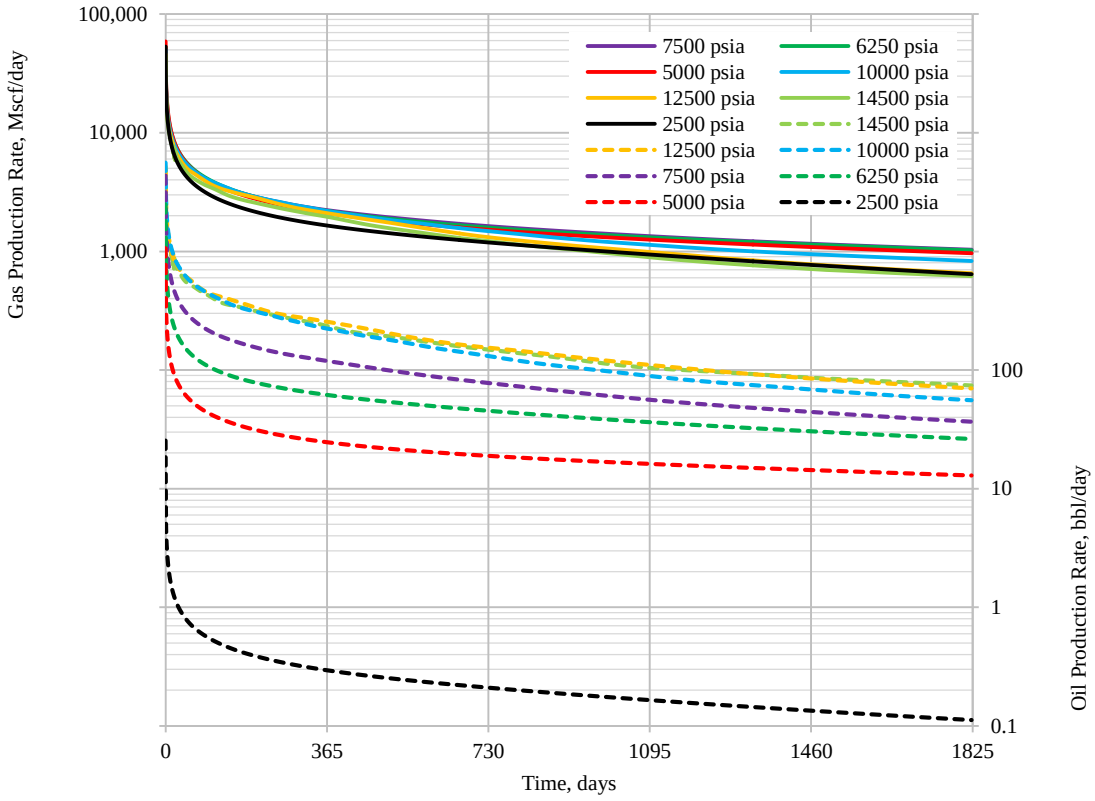

Fig. 5.9 – Oil and gas production rates in gas condensate system for different initial reservoir pressures. Oil decline curves for 12,500 and 14,500 psia are almost identical.

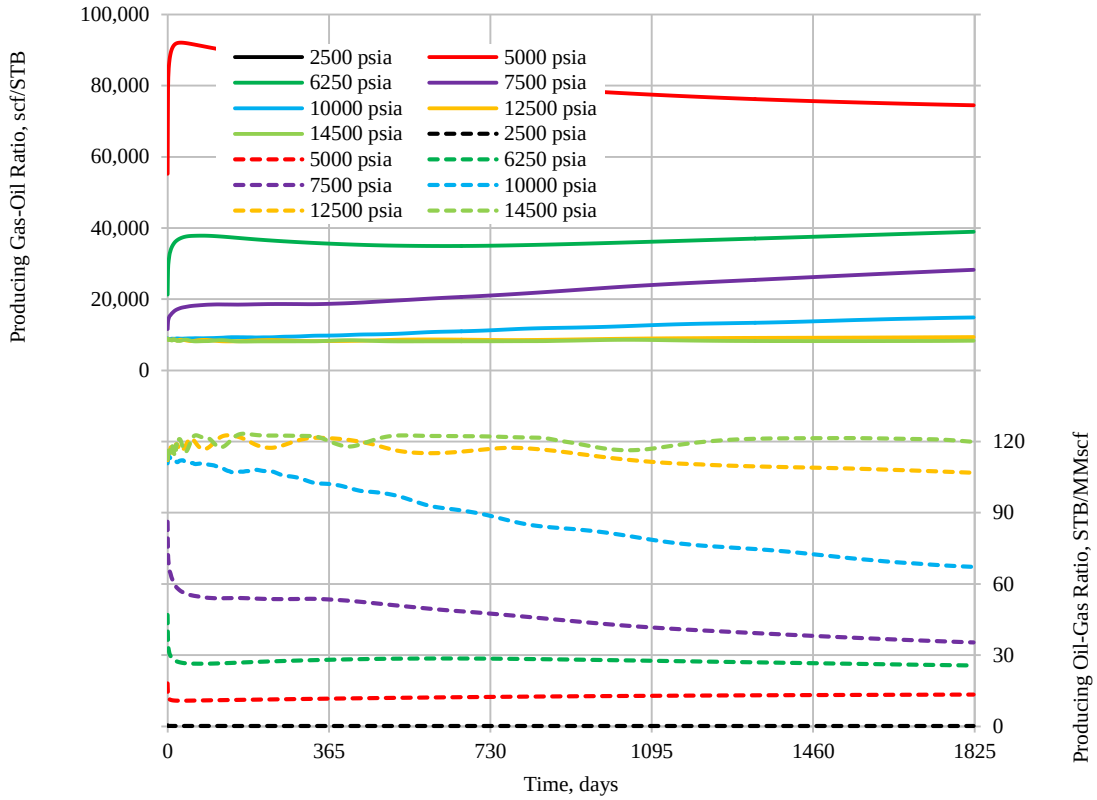

Fig. 5.10 – Producing GOR and OGR in gas condensate system for different initial reservoir pressures. 12,500 and 14,500 psia show OGR variation around initial 125 STB/MMscf.

Figs. 5.8–5.10 clearly show additional oil production caused by high initial reservoir pressure. We observe monotonic growth in cumulative oil production for complete range of pressures. Gas cumulative production monotonically increases until 7,500 psia and then decreases. However, the cash flow obtained from additionally produced oil overcomes the losses from reduced gas production between 7,500 and 12,500 psia. We notice that since the gas production rate are reasonably identical, the main contributor to the difference in economic performance is produced oil. After one year, oil production rate varies from 2 to 250 bbl/day for 2,500 and 14,500 psia and this significant different observed through all simulation time. OGR fluctuations around 120 STB/MMscf show that the average pressure in the reservoir is above the critical saturation pressure. It allows to use condensate potential on maximum and generate more cash. On the other hand, extremely low production OGR and cumulative oil production for 2,500 psia indicates that once the oil is trapped by the reservoir, it stays there and will never be produced.

5.3 Reservoir Thickness

Figs. 5.11–5.12 indicate the same performance behavior as we observed for dry gas case. The same break-even thickness of 90 ft achieved since cash flow in gas condensate model is almost identical to cash flow in dry gas model (the difference is within 1.5%). The base case scenario NPV is 9.9 million USD, investment efficiency is 211% and project IRR is 68% after 5 years production. Additional 10 ft increases NPV by 1 million USD, adding about 10.5% to DPI and 8% to IRR of the project.

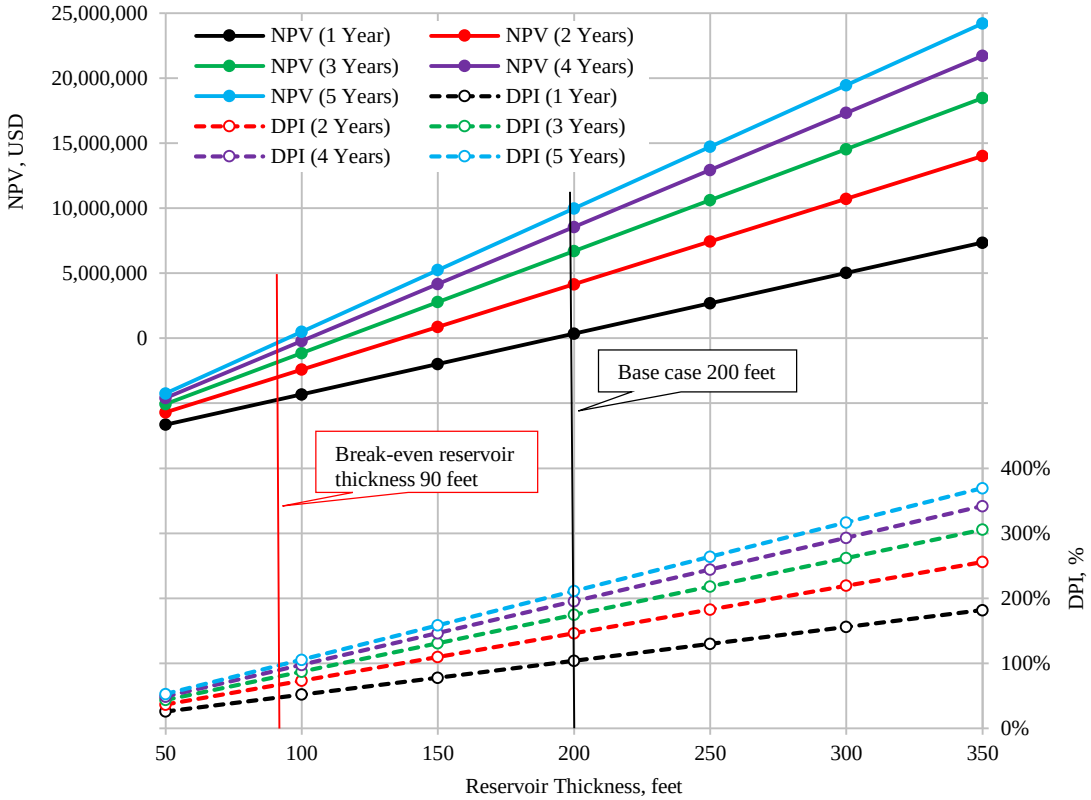

Fig. 5.11 – NPV and DPI in gas condensate system for different reservoir thickness.

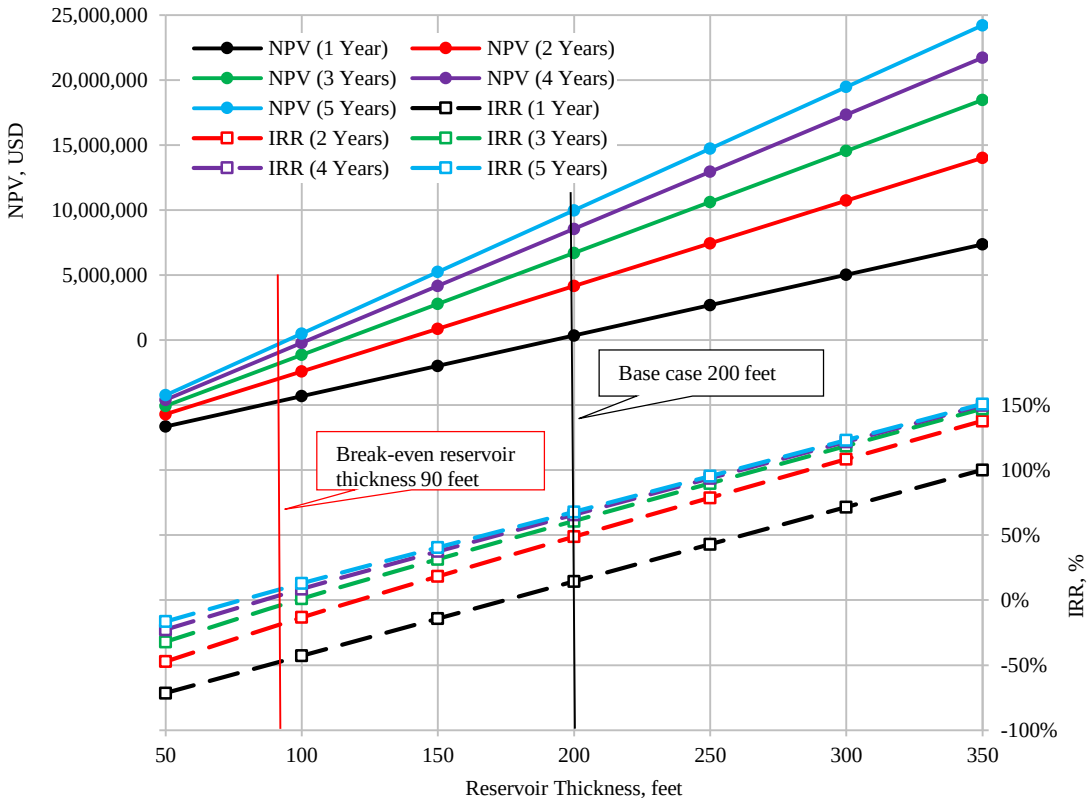

Fig. 5.12 – NPV and IRR in gas condensate system for different reservoir thickness.

5.4 Number of Fractures

Fig. 5.13 shows range of optimal number of fractures based on NPV and DPI. Accelerated depletion with 40–50 fracs yields the highest NPV value for the project with about 15.6 million USD after 5 years while base case scenario with 20 fractures yields 30% less net present value. On every dollar invested we will get just above two dollars back. DPI metric shows that the optimum number of fractures is in between 20 and 40 fracs, giving the highest 220% of investment efficiency. This mean that having 30 fractures allow us using the investment with 10% higher efficiency comparing with 50 fractures case. Combination of these two metrics suggest 40 fractures as the most optimal completion solution with 15.4 million USD of NPV and 212% of DPI.

If company tends to rely on IRR as a second metric for investment decision, the optimal range may be different (**Fig. 5.14**). We again noticed the shift of maximum IRR value towards smaller number of fractures with time. The maximum achieved IRR is 80% for 35 fractures, but flat behavior of the curve allow us to choose optimal range of fracture in between 25 and 45. IRR value for this range changes from 73% to 80%. Coupling both metrics, the agreed optimal number of fracs is between 40 and 45. However, including DPI as a third metric will narrow the solution to 40 fractures per well. That mean of company rely only on NPV as an assessment criteria, they will gain additional 0.3 million USD of NPV (comparing 50 vs 40 fractures), but investment efficiency and IRR drop by 17% and 7% respectively.

Cumulative oil and gas data shows monotonic increase in produced volumes, supporting NPV results (**Fig. 5.15**). We observe the significant flattering in oil production after 2 years for 40 and 50 fractures cases. It can be explained by accelerated depletion of the reservoir causing earlier pressure drop below saturation pressure and significant oil condensation inside the matrix.

Figs. 5.16–5.17 indicate rapid decline in oil rate within first two years while gas production rate is less affected during the same period. OGR drops down to the lowest value of 20 STB/MMscf in 2 years. 5 years period indicates that oil production rate for 5 and 50 fractures are identical. The surplus from accelerated production positively influence on cash flow, but additional expenses make the project less investment efficient. After about 30 fracture, the difference between marginal revenues and marginal costs from every additional fracture shrinks.

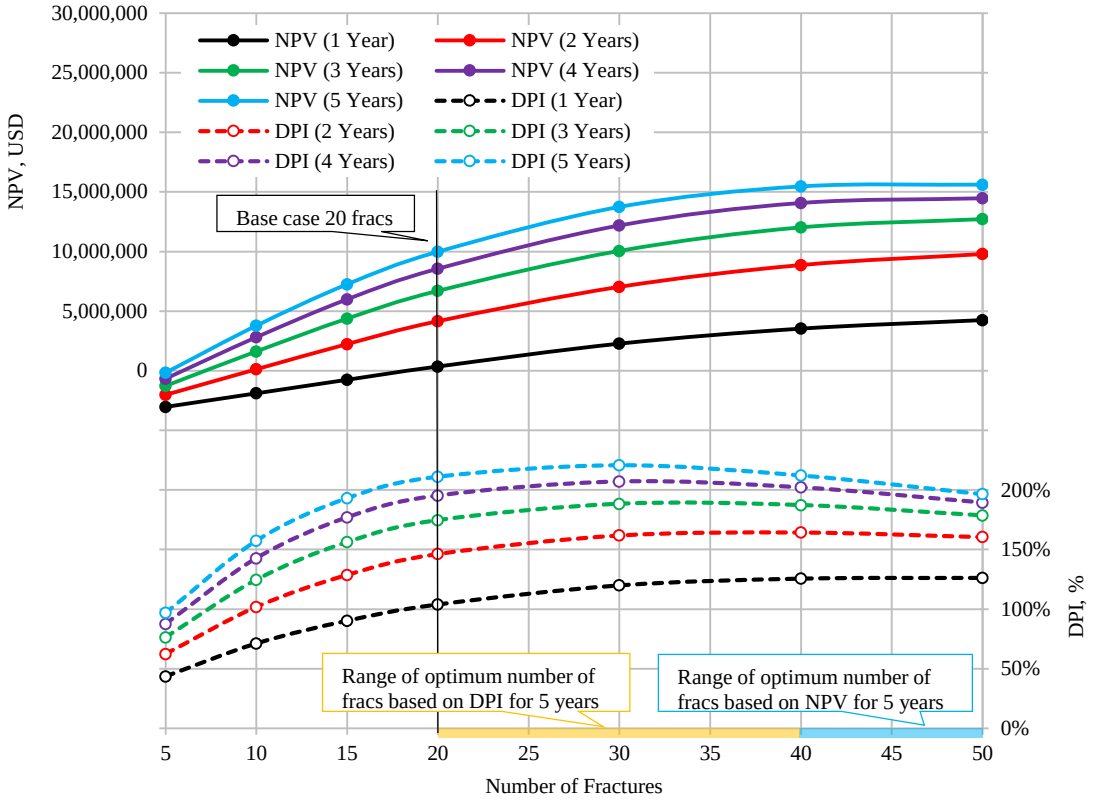

Fig. 5.13 – NPV and DPI in gas condensate system for different number of fractures. Yellow and blue bars represent the optimum number of fracture based solely on DPI or NPV metrics.

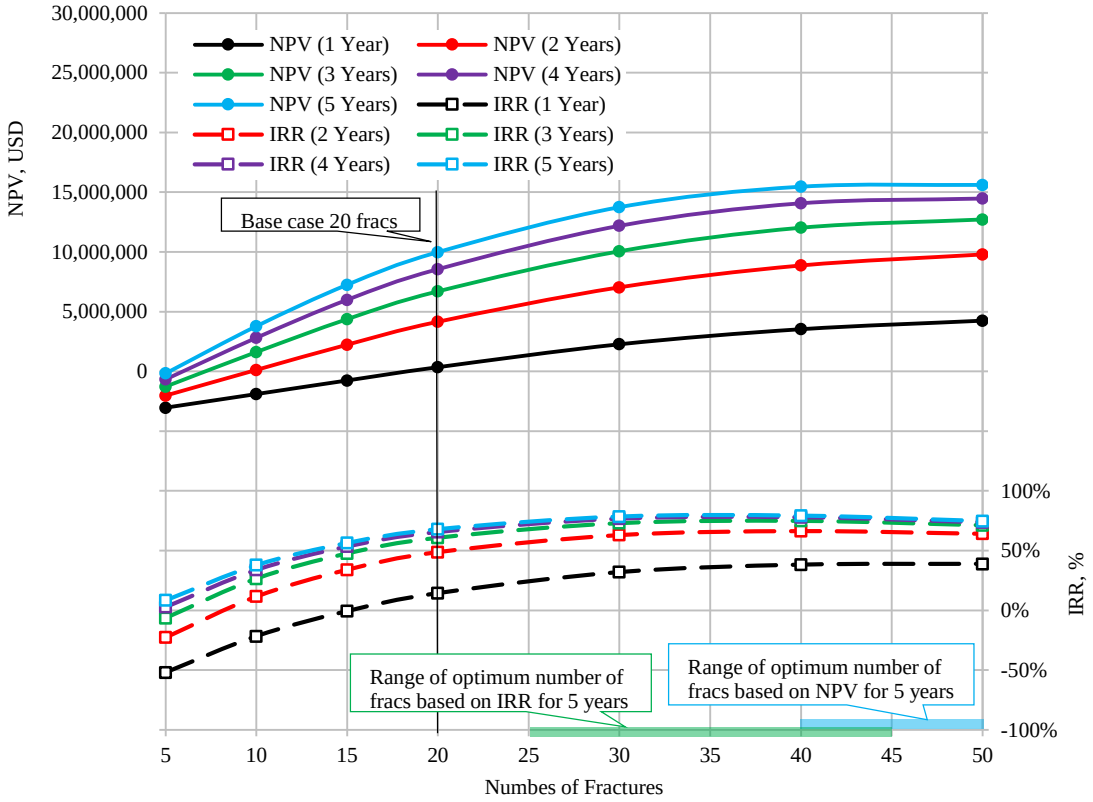

Fig. 5.14 – NPV and IRR in gas condensate system for different number of fractures. Green and blue bars represent the optimum number of fracture based solely on IRR or NPV metrics.

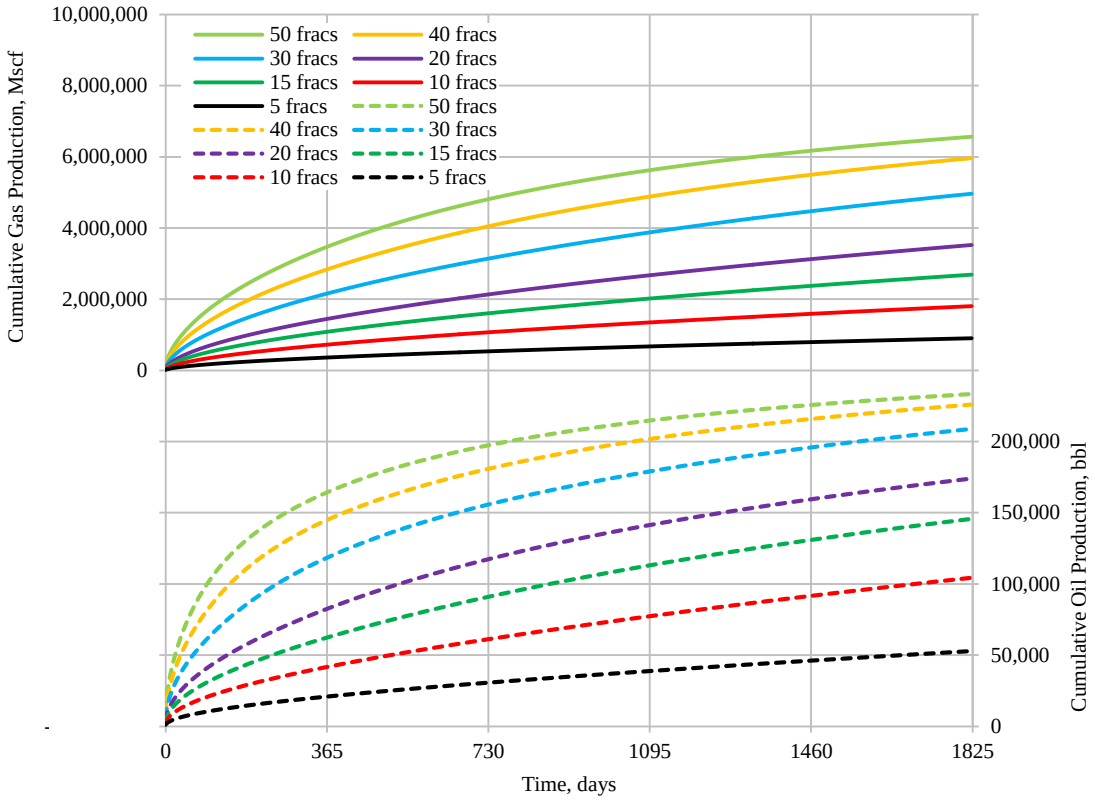

Fig. 5.15 – Cumulative oil and gas production in gas condensate system for different number of fractures.

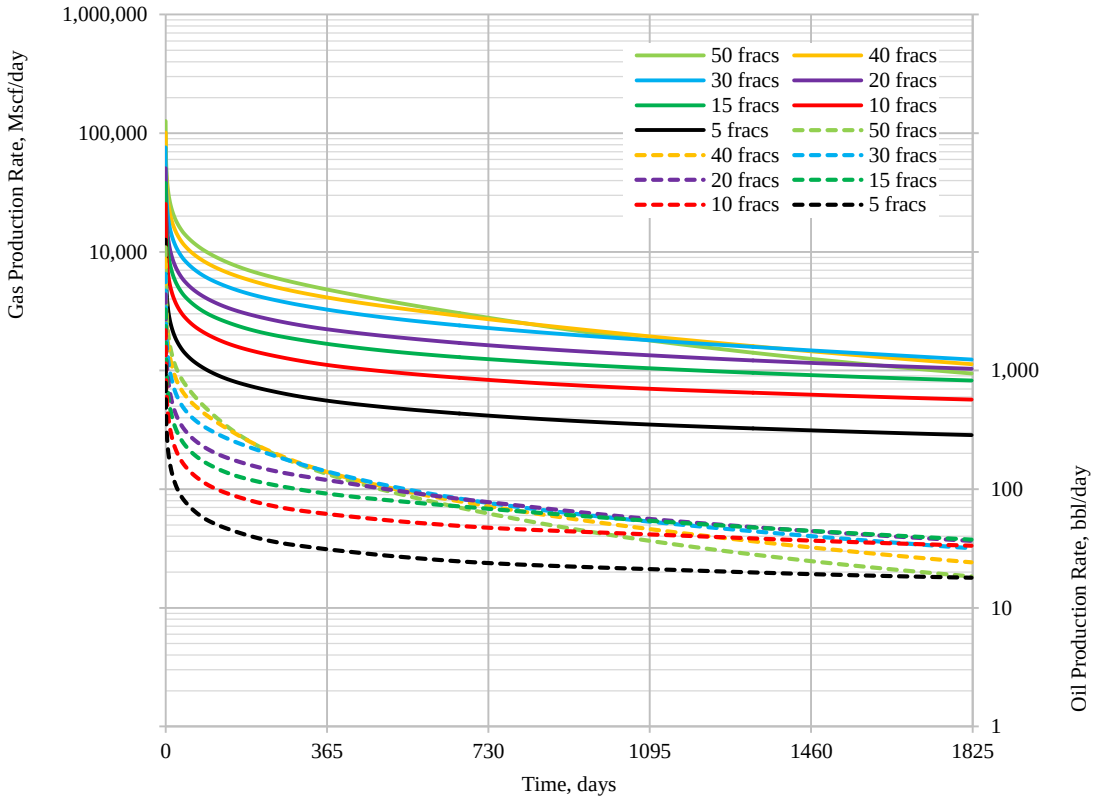

Fig. 5.16 – Oil and gas production rates in gas condensate system for different number of fractures. Significant decline in oil rate observed for 40 and 50 fracs after 2 years. After 5 years, 5 and 50 fracs show the same oil production rate.

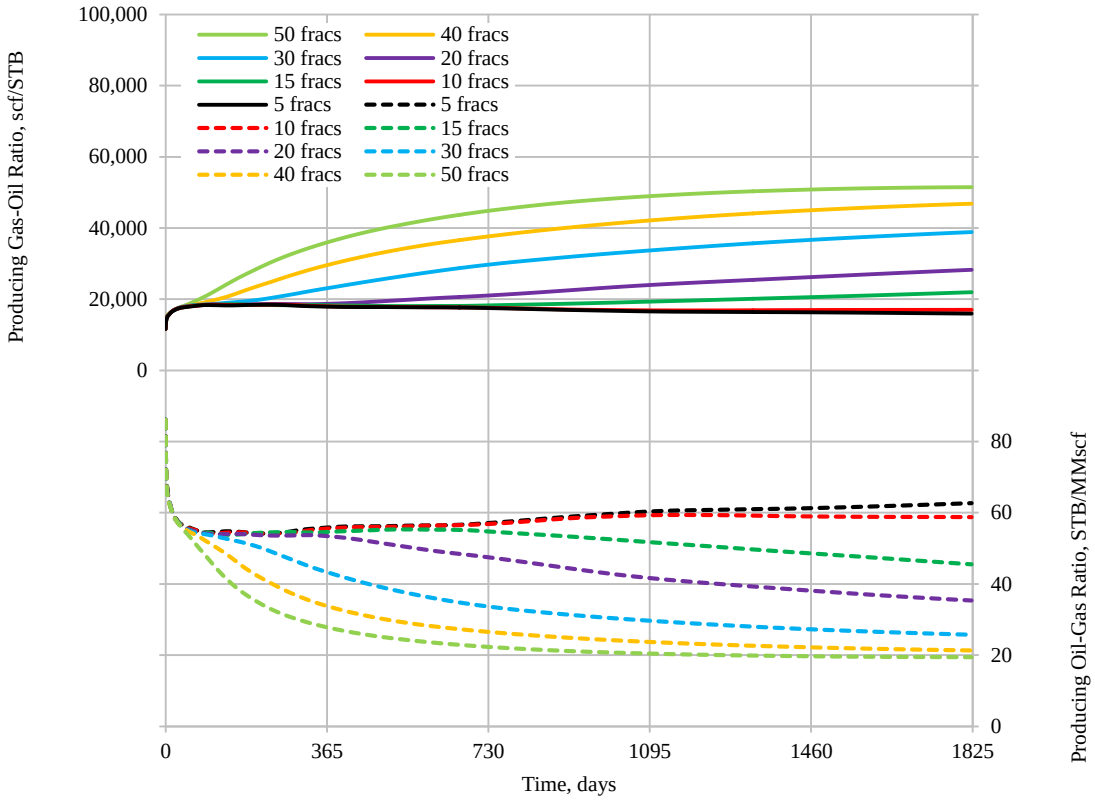

Fig. 5.17 – Producing GOR and OGR in gas condensate system for different number of fractures. OGR of 40 and 50 fractures drops significantly after 2 years and remains low.

5.5 Fracture Half-Length

Sensitivity results for fracture half-lengths presented on **Figs. 5.18–5.19**. Maximum NPV achieved with fractures of 600 ft yielding 17.7 million USD. Corresponding investment efficiency is about 215% with internal rate of return of 74%. On the other hand, giving priority to investment efficiency, maximum DPI achieved by 400 ft fracs with 219%. Corresponding NPV is about 12.9 million USD and IRR is roughly the same as for 600 ft case. By maximizing IRR (75.1%) we should decide on 500 ft fractures with project's NPV of 15.6 million USD and 218% investment efficiency. Optimal ranges for fracture half-length for different metrics are the following: based on NPV the optimum achieved for 550–660 ft; based on DPI the optimum varies between 300–600 ft and based on IRR the optimum is in a range of 400–600 ft. Taking into account all three parameters, the best solution will be to complete the well with 600 ft fractures.

Figs. 5.20–5.22 support the above mentioned results. Steady increase in both cumulative gas and oil production overcome the additional expenses from longer fracs. Reaching the limit of simulation area, fracture with 660 ft half-length could not maintain sufficient cash flow to overcome incremental costs comparing with 600 ft fracture. OGR behavior shows significant liquid drop-out for all cases; however 100 and 200 ft cases show increase in producing OGR (from 40 to 60 STB/MMscf) within first 2 years. This behavior associated with involvement of area beyond the fracture tip and causes temporary increase in OGR, followed by steady decrease in next 3 years.

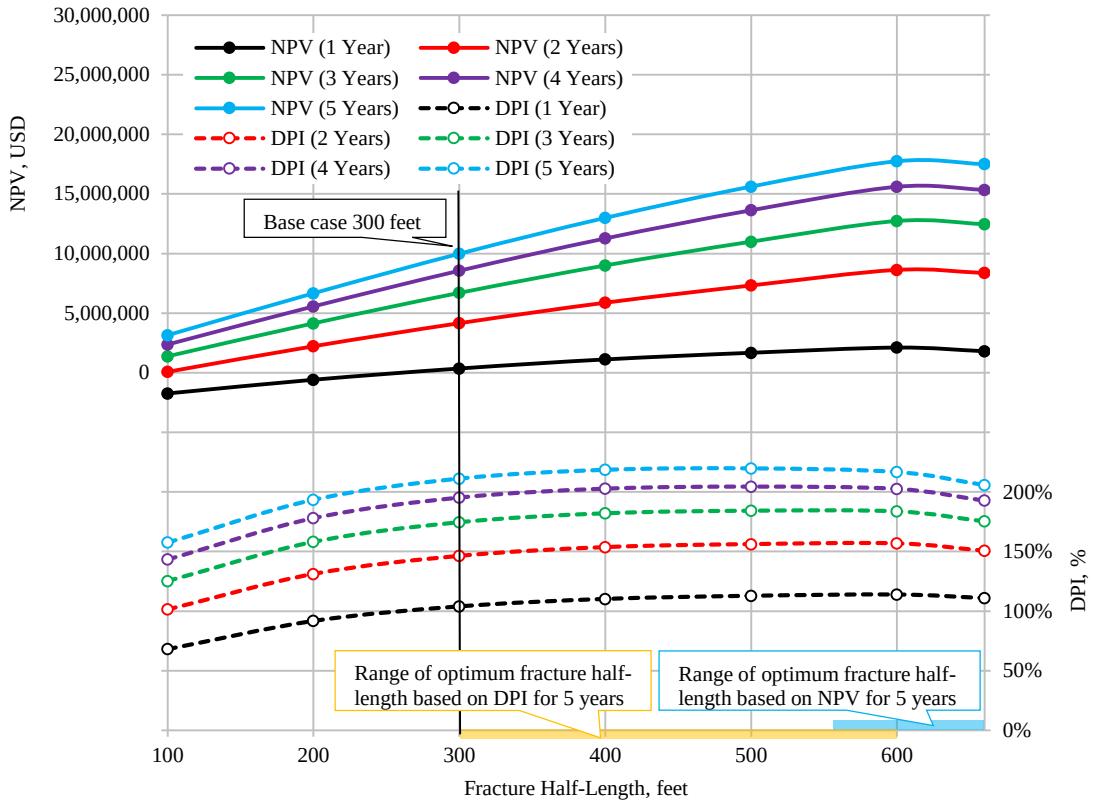

Fig. 5.18 – NPV and DPI in gas condensate system for different fracture half-length. Yellow and blue bars represent the optimum number of fracture based solely on DPI or NPV metrics

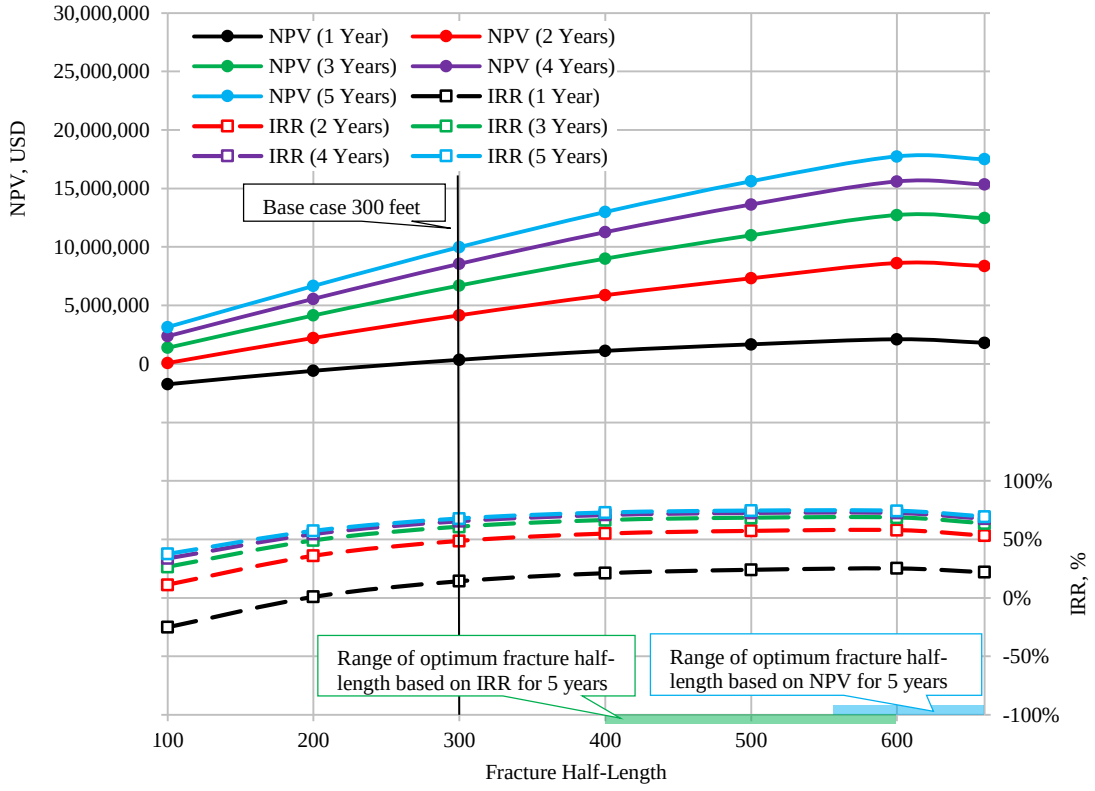

Fig. 5.19 – NPV and IRR in gas condensate system for different fracture half-length. Green and blue bars represent the optimum number of fracture based solely on IRR or NPV metrics

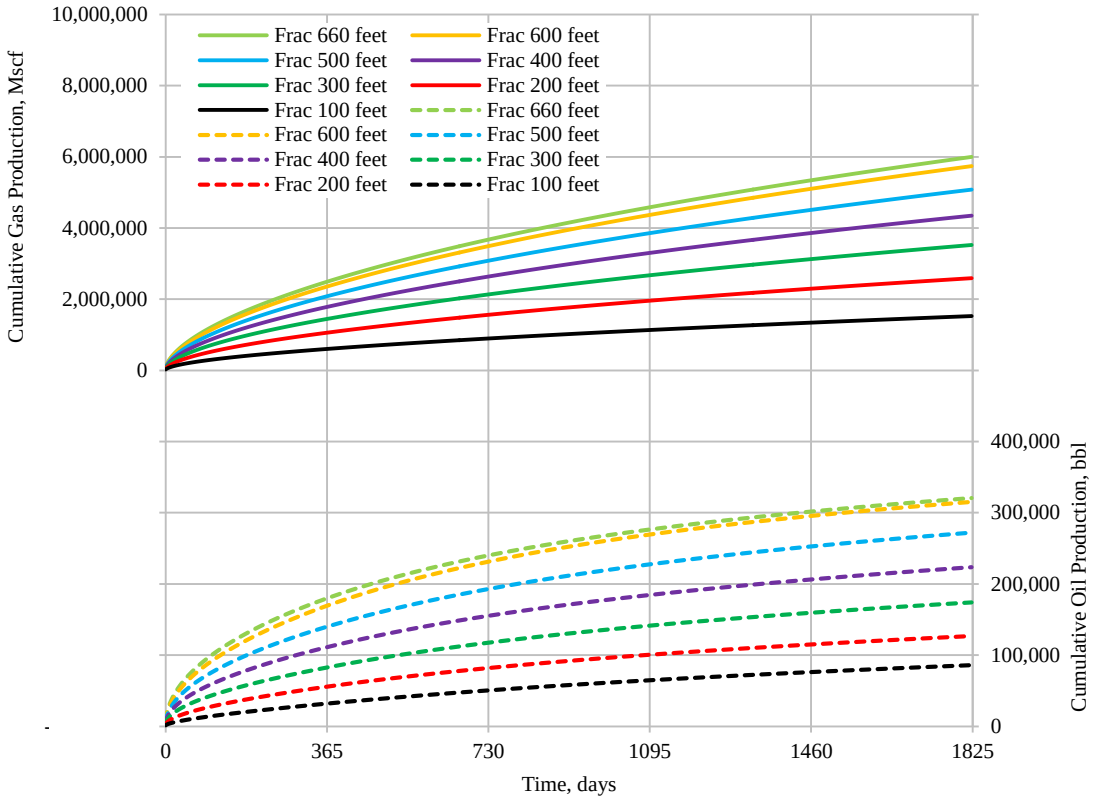

Fig. 5.20 – Cumulative oil and gas production in gas condensate system for different fracture half-length.

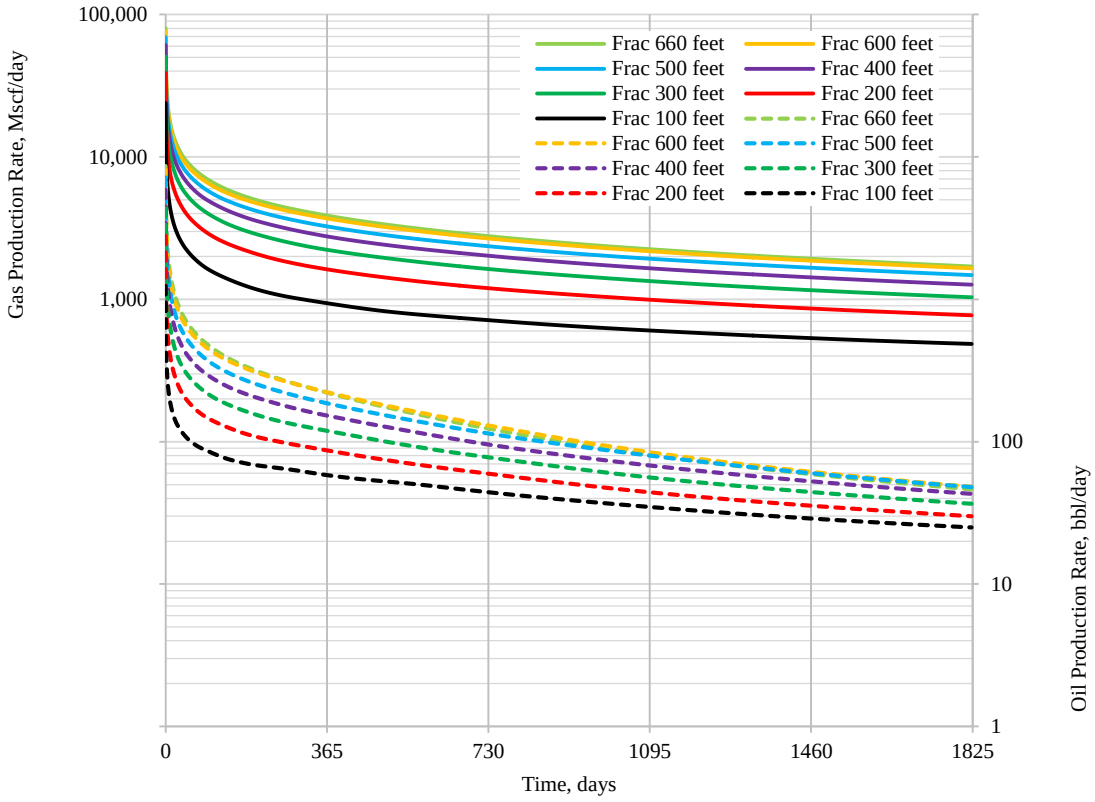

Fig. 5.21 – Oil and gas production rates in gas condensate system for different fracture half-lengths.

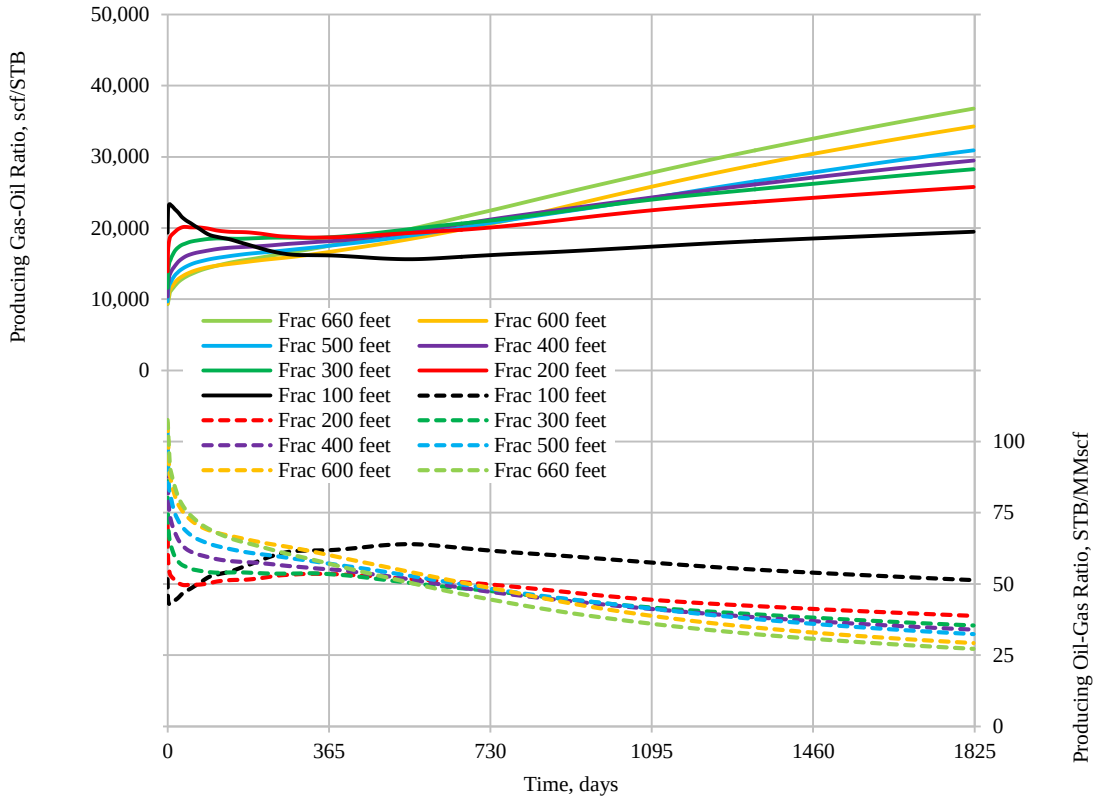

Fig. 5.22 – Producing GOR and OGR in gas condensate system for different fracture half-lengths. OGR for 100 and 200 ft cases show increase in first 2 years, followed by steady decrease due to drainage from area beyond the fracture tip. 660 ft case OGR gradually decreases since it has steady increase only in perpendicular direction.

5.6 Bottomhole Pressure

Sensitivity analysis of initial reservoir pressure clearly showed the negative effect of liquid condensation in the reservoir. However, the initial reservoir pressure is not a flexible parameters to control depletion process in the reservoir and the amount of liquid losses in the reservoir. Since the average pressure in the reservoir cannot be effectively changed for shales, the importance of careful selection of flowing bottomhole pressure arises. Whitson and Sunjerga (2012) previously confirmed string correlation of producing GOR (or reverse OGR) with flowing BHP and degree of undersaturation. This behavior in shales differs significantly from conventional reservoirs performance, where GOR is proven to be strongly depended on average reservoir pressure (Lei et al., 2014).

Figs. 5.23–5.24 show performance of the model with different constant BHP. For three metrics we see monotonic decrease in all range of pressures. The best results are achieved for 500 psia BHP with NPV of 10.1 million USD, 212% of investment efficiency and about 68% of IRR after five years. The worst results are achieved with BHP equal to saturation pressure (4906.4 psia). For this case, NPV dropped down to 4.7 million USD with 152% DPI and 41% IRR. However, if we look at first-year performance we don't see significant change for BHP range between 500 and 3500 psia. That mean that the cash decrease from unproduced amount of gas due to higher BHP was balanced by cash earned from additionally produced oil from the reservoir.

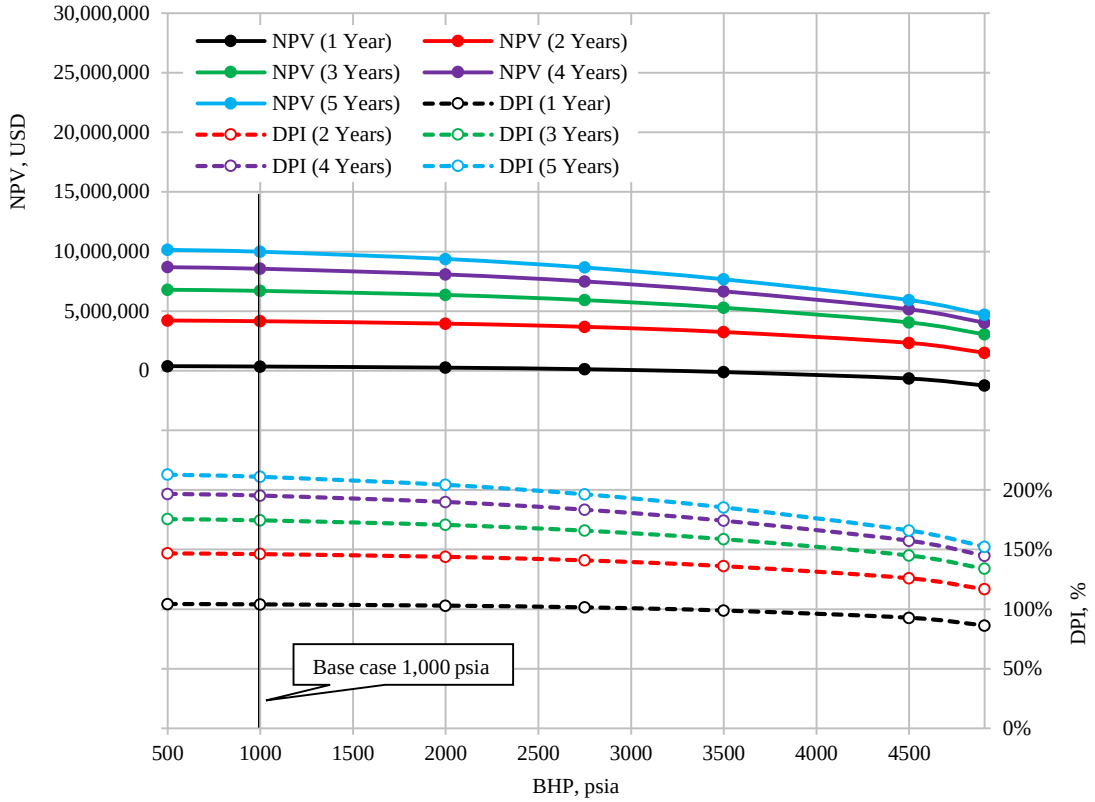

Fig. 5.23 – NPV and DPI in gas condensate system for different bottomhole pressures. The performance after 1 year for 500-3,500 psia is almost identical.

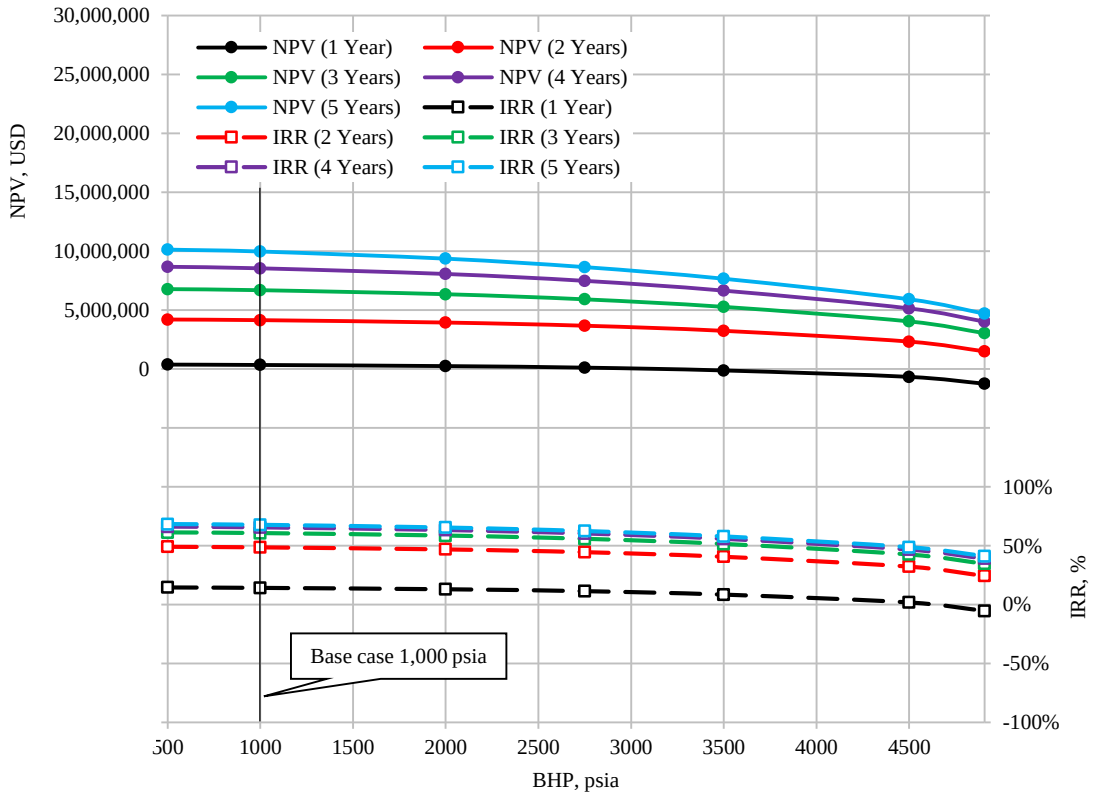

Fig. 5.24 – NPV and IRR in gas condensate system for different bottomhole pressures. The performance after 1 year for 500-3,500 psia is almost identical

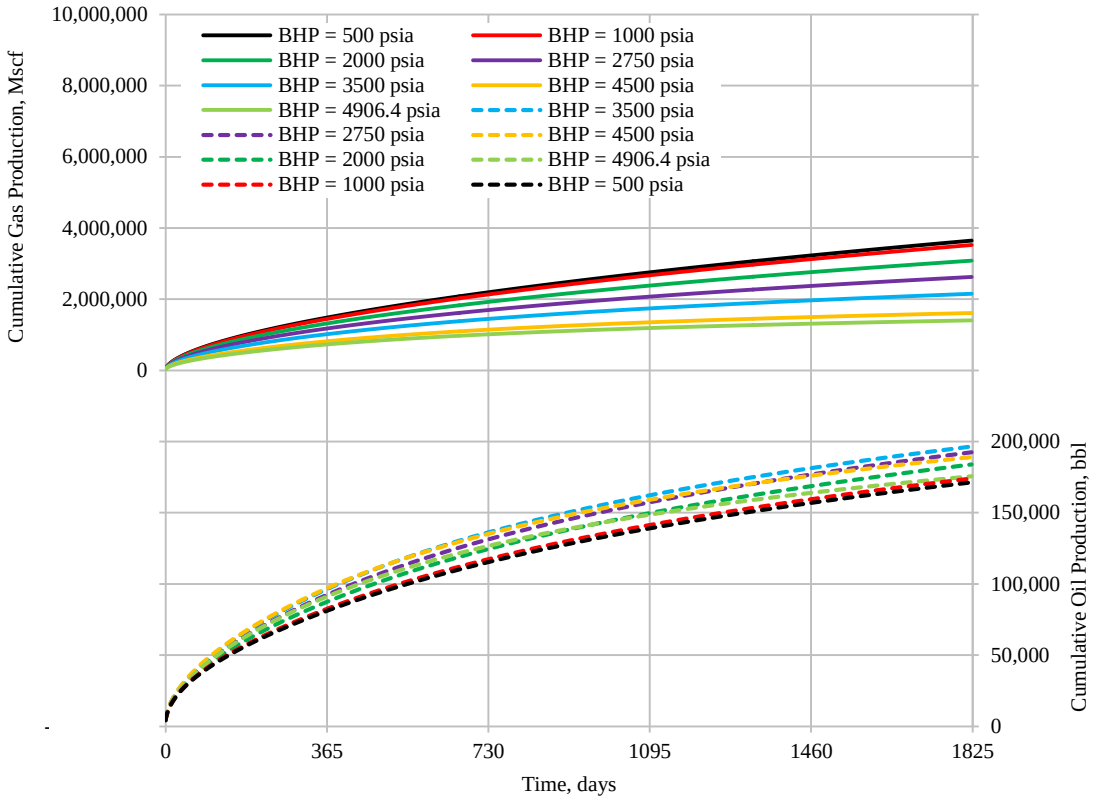

Fig. 5.25 – Cumulative oil and gas production in gas condensate system for different bottomhole pressures. Gas cumulative production shows monotonic behavior, while oil cumulative production is non-monotonic.

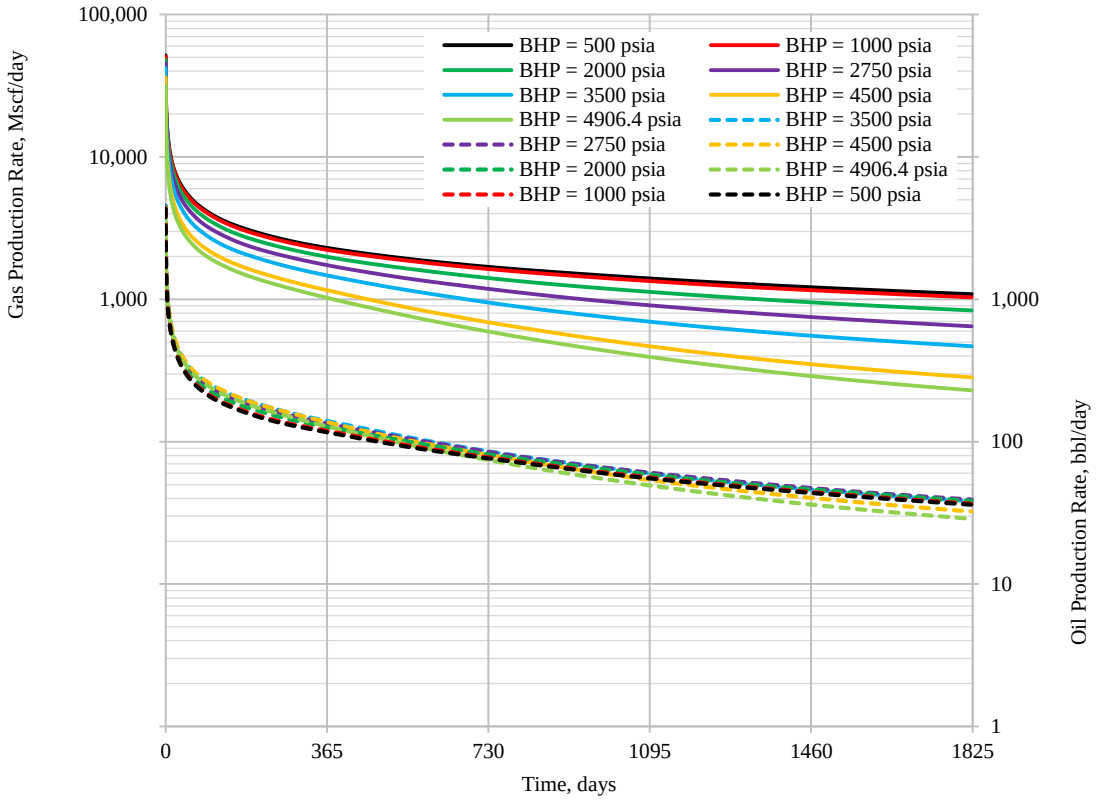

Fig. 5.26 – Oil and gas production rates in gas condensate system for different bottomhole pressures. Gas rates differ significantly, while oil rates are relatively the same.

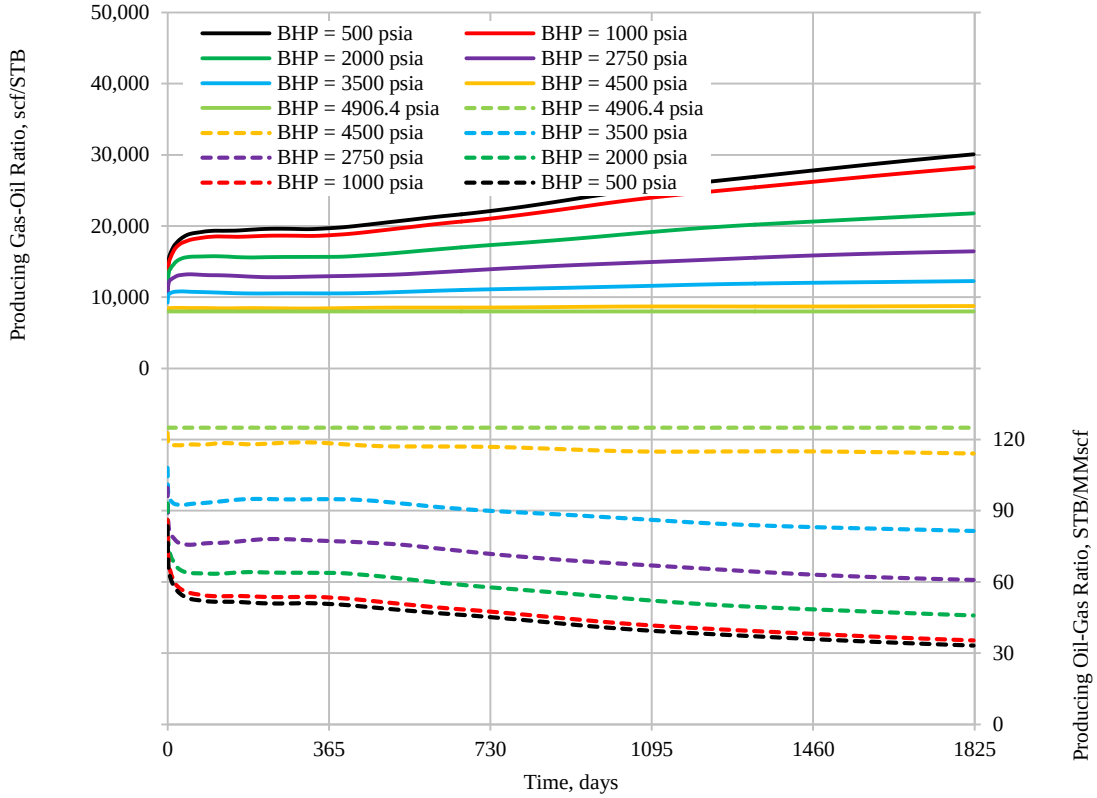

Fig. 5.27 – Producing GOR and OGR in gas condensate system for different bottomhole pressures. Initial reservoir GOR is 8,000 Mscf/STB (OGR is 125 STB/MMscf)

Figs. 5.25–5.27 indicate that increase of BHP decreases gas production rate significantly, yet keeping the oil production rates close for all cases. While gas cumulative production monotonically increases with lower BHP, oil cumulative production shows non-monotonic behavior. Firstly, it grows in a range of 500-3,500 psia, but then the trend is changing and cumulative production decreases for higher BHP. Additional oil production with 3,500 psia was by 25,000 bbl higher than for 500 psia. Results show that initial low BHP immediately influences on the producing OGR. While for high BHP (4,500 and 4,906.4 psia) it fluctuates around 120 STB/MMscf, lowering BHP caused drop of OGR in time. Lowering bottomhole pressure to 2,750 psia caused average producing OGR to be half of the initial 125 STB/MMscf. More significant drawdown cause even lower OGR in the system.

The suggestion would be to keep close attention on bottomhole pressure selection while producing liquid-rich gas condensate shales. Keeping BHP just on saturation pressure level may not have positive economic effect due to lower gas production. Lei (2012) showed that for a wide range of permeabilities and initial GOR, the contribution of oil to the total revenues at the beginning of the production may vary between 30–95%!. Therefore, the well requires a special attention for selecting BHP to maximize ultimate reservoir value.

5.7 Well Horizontal Length

Figs. 5.28–5.29 show the performance of the model for different horizontal section lengths. The maximum NPV, DPI and IRR values are achieved for base case scenario with 5,280 ft section. Net present value reached 9.9 million USD, investment efficiency is 211% and internal rate of return is 68%. Increased horizontal length has negative effect on all economic metrics regardless increased production. For 10,560 ft case project's NPV slightly shrinks to 8.8 million USD, DPI decreases to 175% and IRR stays just above 45%. Additional production from higher fracture spacing could not overcome the increased costs associated with drilling longer well.

Figs. 5.30–5.32 show the difference in gas production due to difference in average pressure in the models. Gas production rates and cumulative gas production is only slightly different after 5 years for all models. Higher average reservoir pressure for the models with longer horizontal section resulted in increased producing OGR. For 10,560 model average OGR stays over 60 STB/MMscf while for base case scenario it decreases to around 40 STB/MMscf. The synergy of 50% increase of OGR and almost constant gas rate yielded higher cumulative oil production. However, this 35,000 bbl of oil could not turn the economy of this case and incremental costs still overpass the incremental revenues. The average pressure for 5,280 ft model was 17% lower than in 10,560 ft model after 5 years (**Fig. 5.33**).

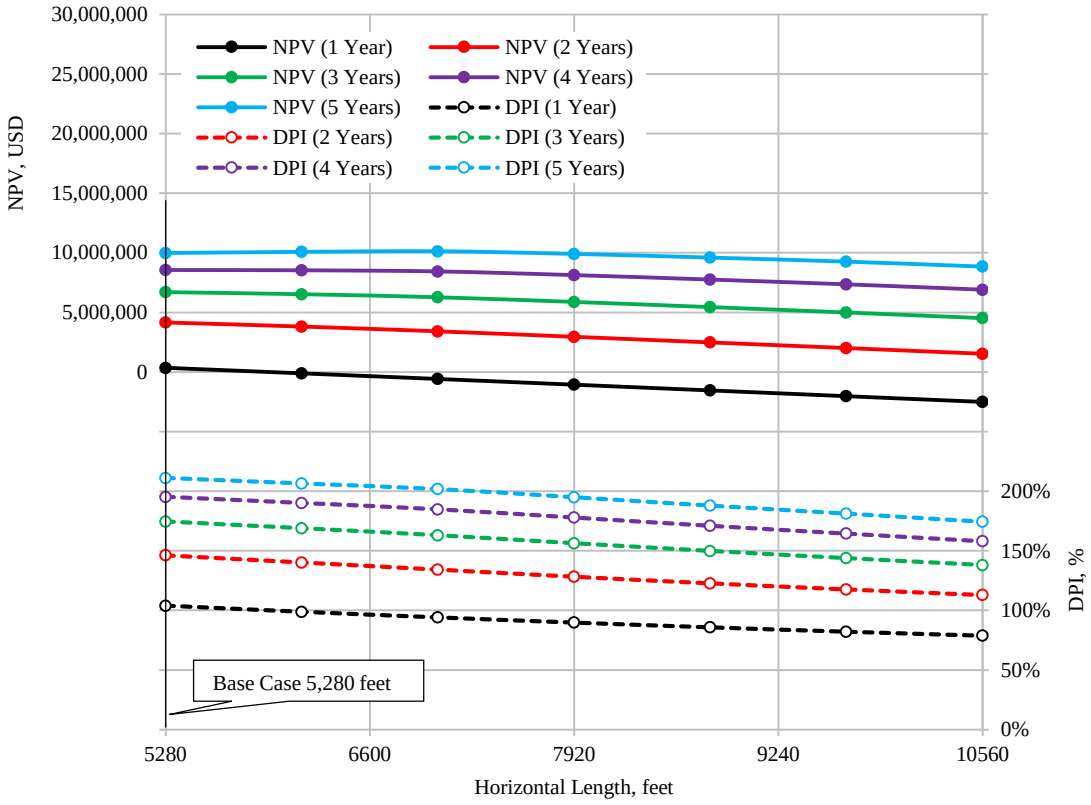

Fig. 5.28 – NPV and DPI in gas condensate system with different horizontal section length.

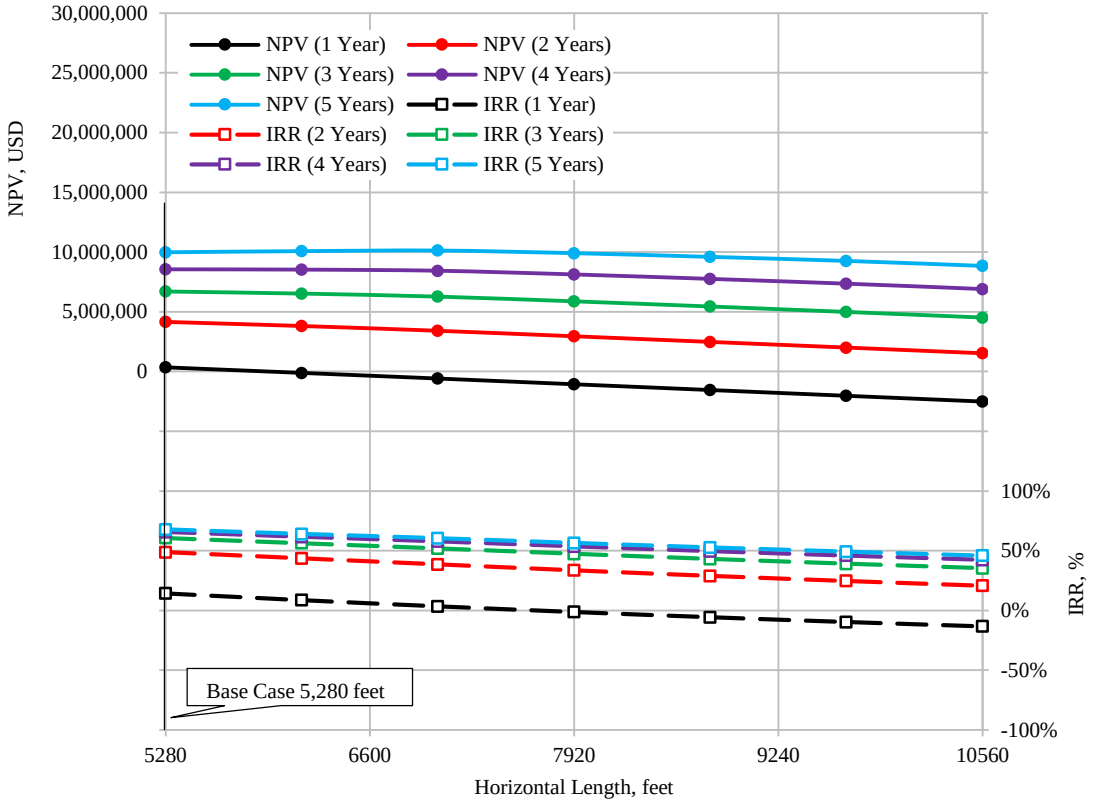

Fig. 5.29 – NPV and IRR in gas condensate system with different horizontal section length.

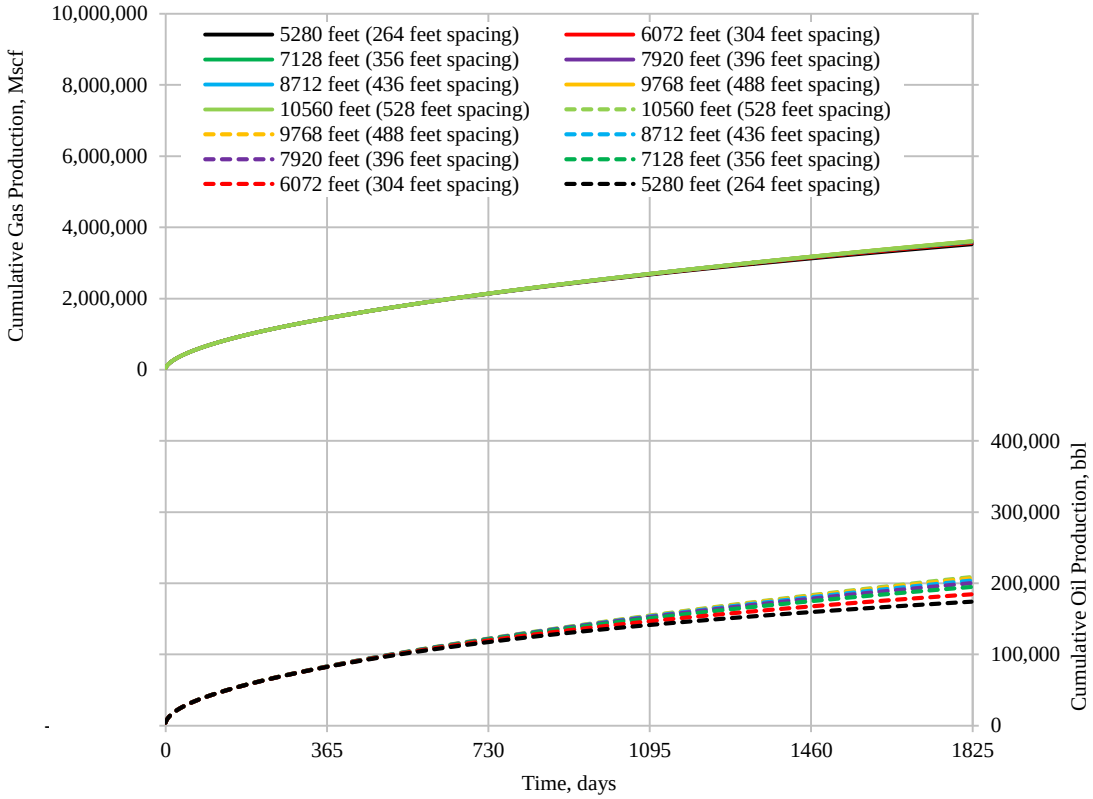

Fig. 5.30 – Cumulative oil and gas production in gas condensate system with different horizontal section length. Cumulative gas production is almost the same for all the cases. Cumulative oil production is higher with longer horizontal length.

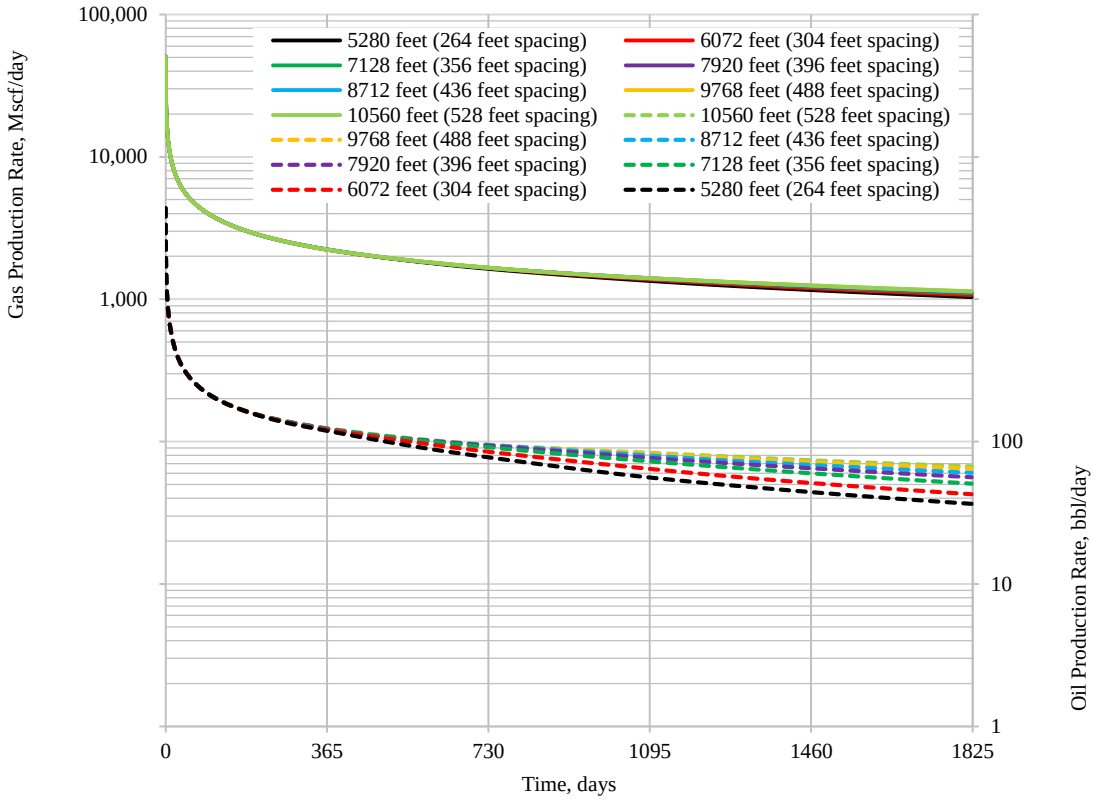

Fig. 5.31 – Oil and gas production rates in gas condensate system with different horizontal section length. Gas production rates are identical for all cases. Oil production rates are higher due to increased OGR for longer horizontal length.

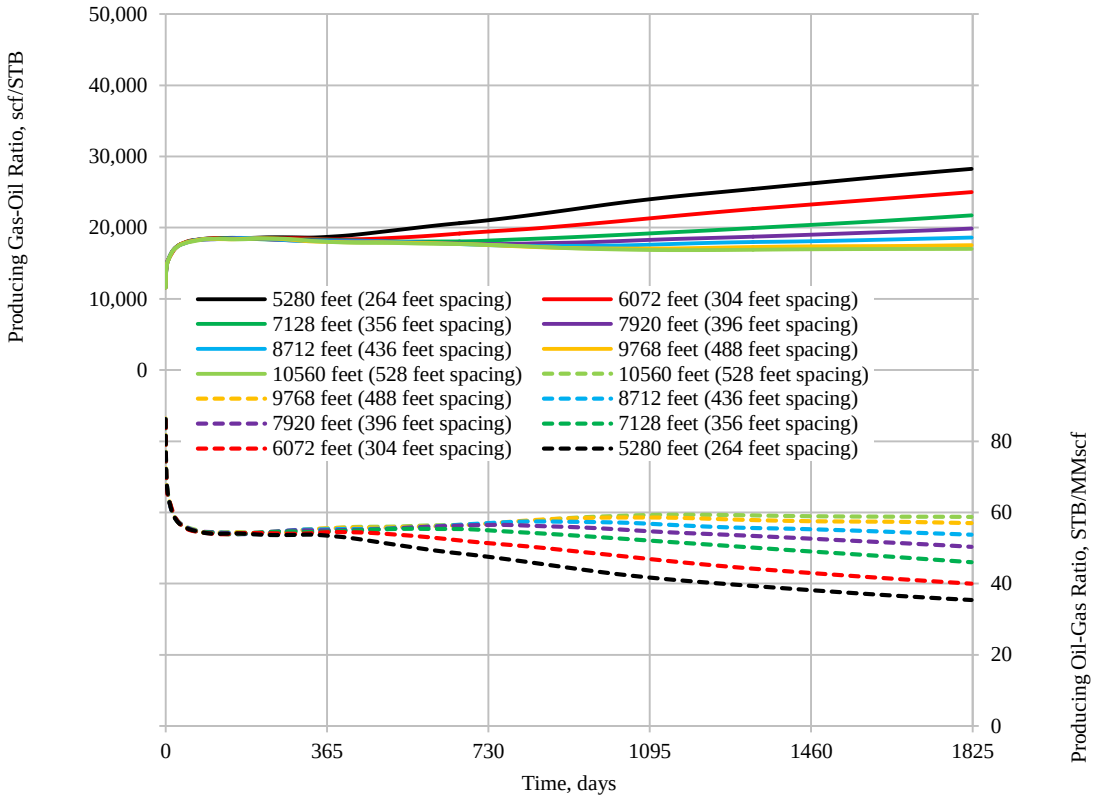

Fig. 5.32 – Producing GOR and OGR in gas condensate system with different horizontal section length. OGR in cases with longer horizontal section is higher than for base case model.

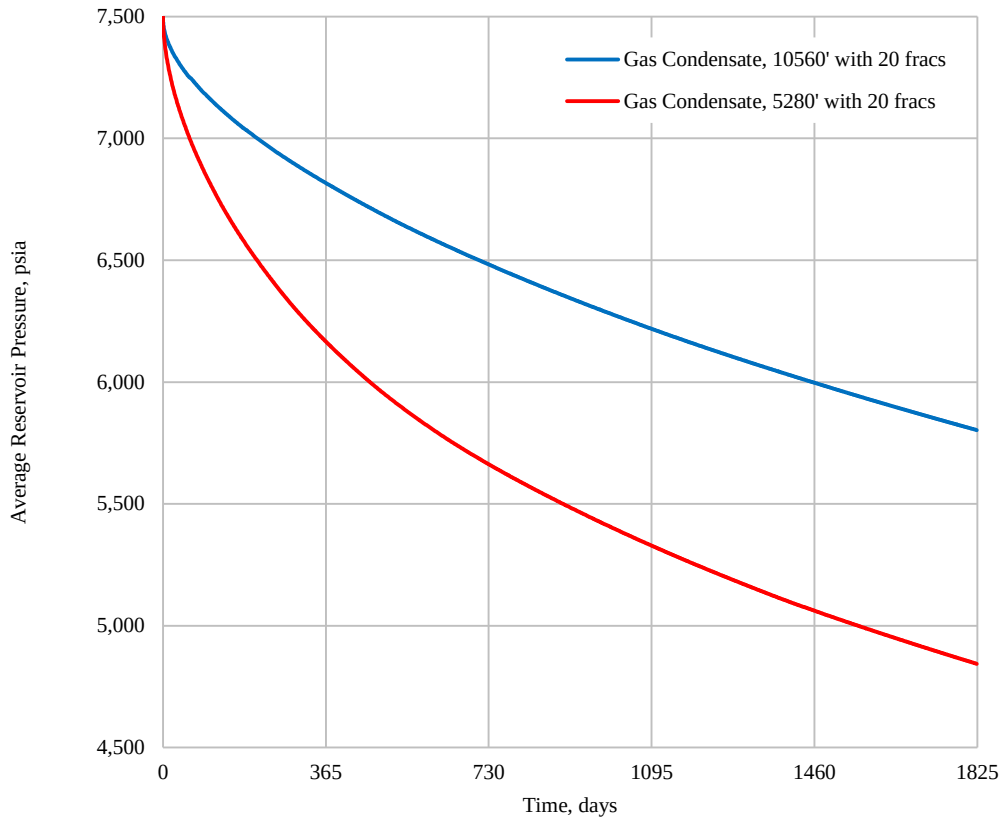

Fig. 5.33 – Average reservoir pressure in dry gas system for different horizontal section length.

5.8 Constant Fracture Spacing

Constant fracture spacing setup follows the same procedure as described for dry gas system. **Figs. 5.34–5.35** indicate the best economic performance of long horizontal section with 40 fractures. Net present value, investment efficiency and internal rate of return achieved maximum at 21.2 million USD, 227% and76% respectively. Since the incremental costs for additional fractures and horizontal length are kept constant, the cost dependence of the model is linear. At the same time, since the drainage area dedicated to one fracture is constant, the overall performance of the model depends only on the total number of fractures.

Figs. 5.36–5.38 illustrate and support the idea of identical single fracture performance of all the models. Absolutely equal producing OGR values indicate that oil and gas production rates at any time are equal for all sensitivity cases. Therefore, cumulative production for every case changes only due to difference in total number of fractures in the model. Incremental revenues are higher than incremental costs yielding positive economic outcome with longer horizontal section.

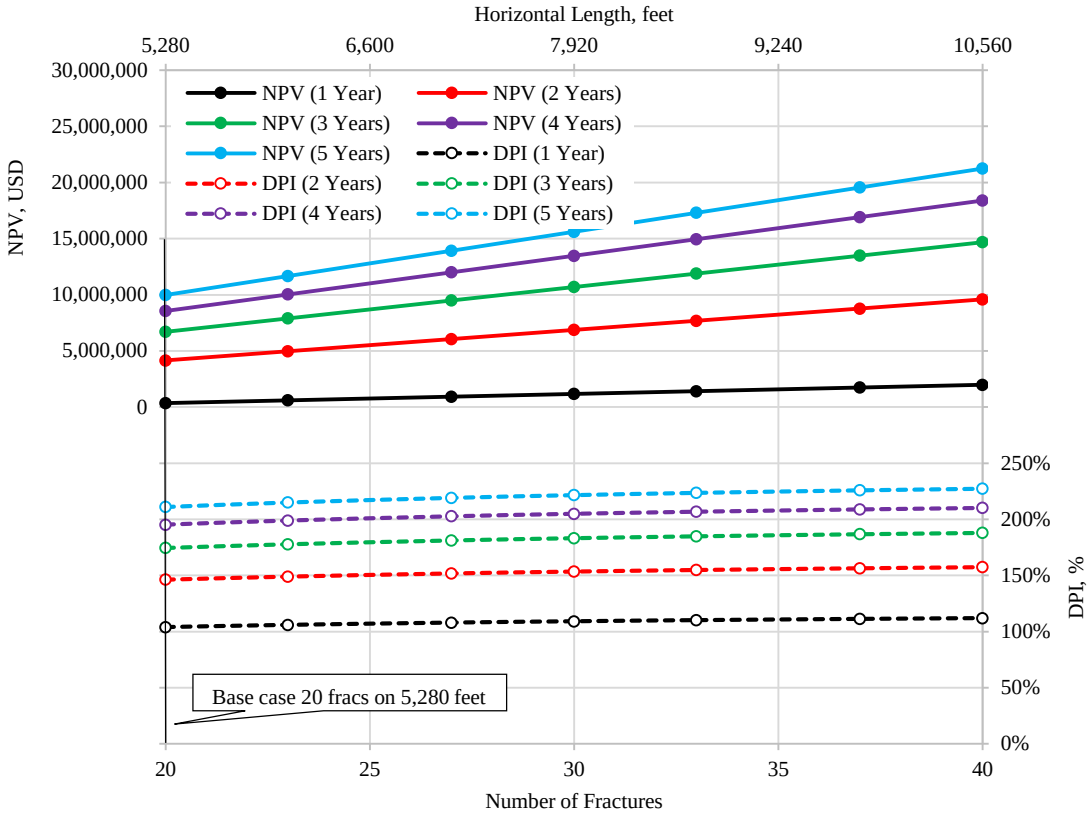

Fig. 5.34 – NPV and DPI in gas condensate system with constant fracture spacing.

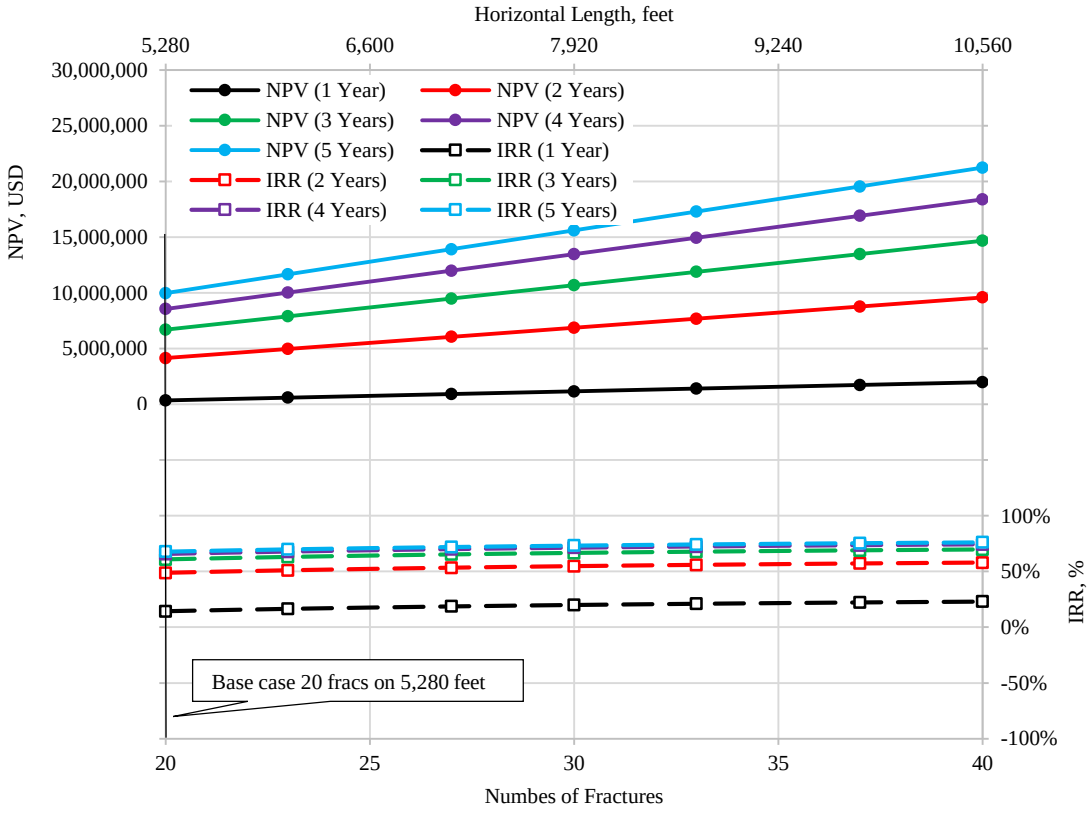

Fig. 5.35 – NPV and IRR in gas condensate system with constant fracture spacing.

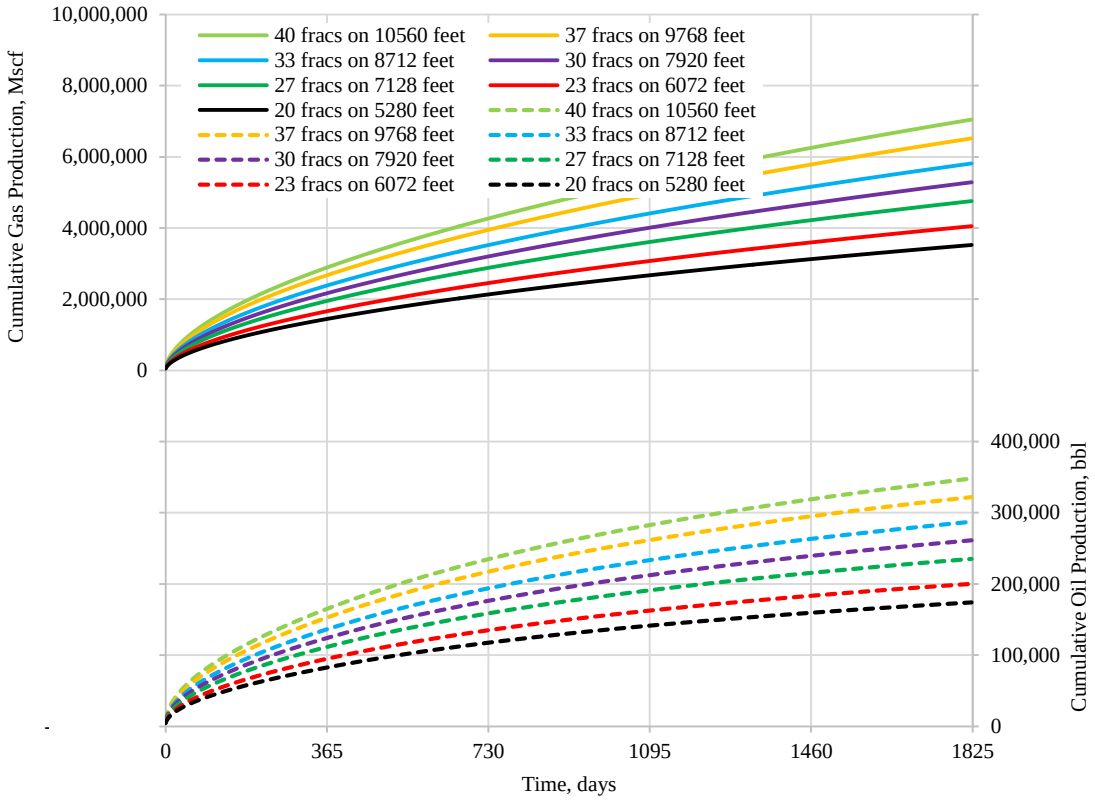

Fig. 5.36 – Cumulative oil and gas production in gas condensate system with constant fracture spacing. The production is scaled by number of fractures.

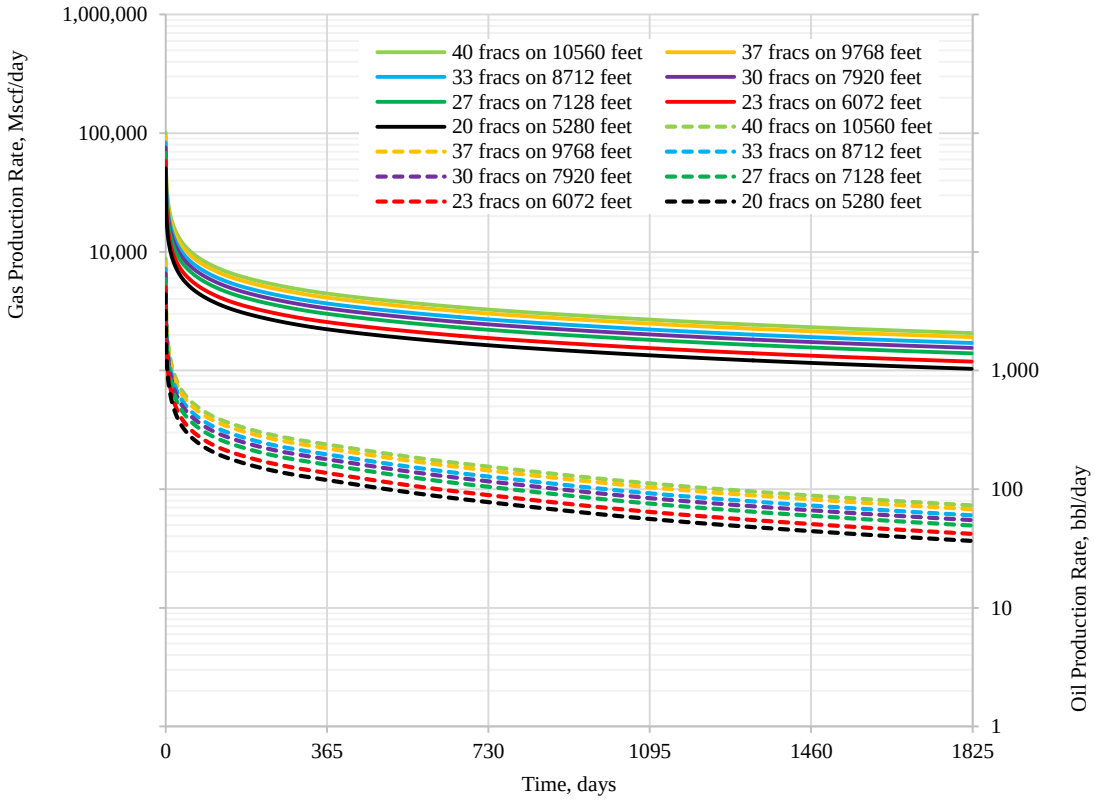

Fig. 5.37 – Oil and gas production rates in gas condensate system with constant fracture spacing. Decline of production rates is identical for all cases. The rates are scaled by the number of the fractures.

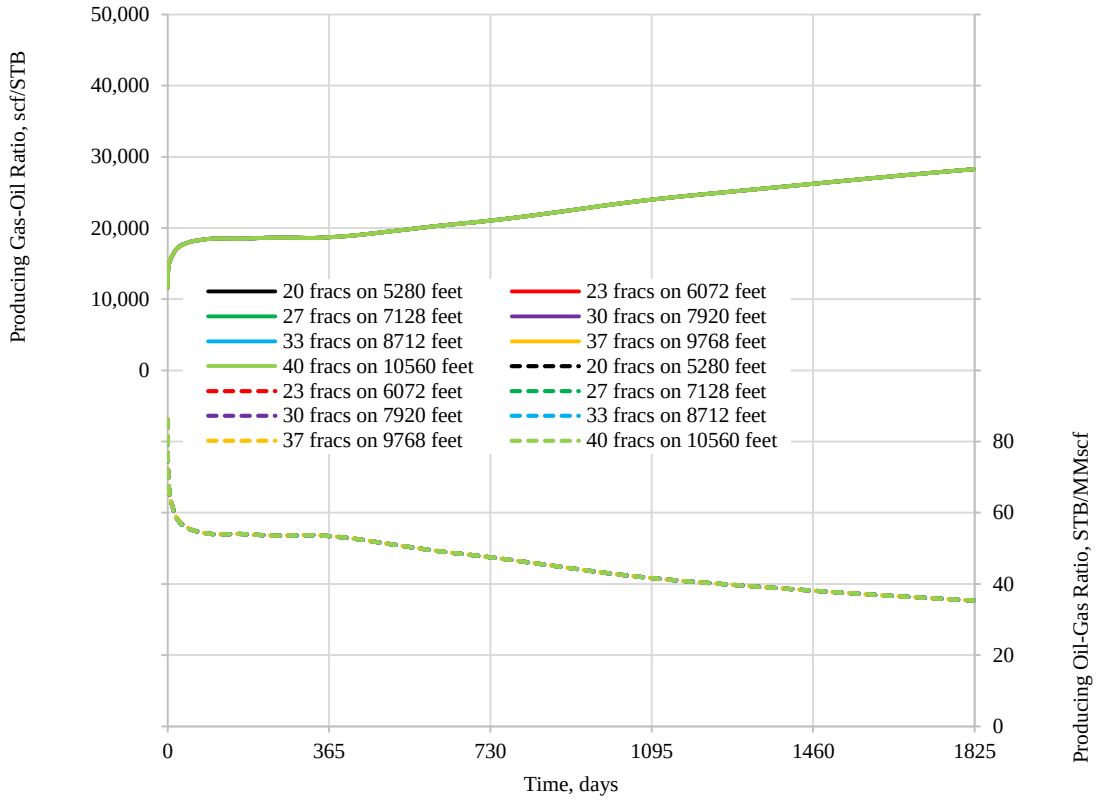

Fig. 5.38 – Producing GOR and OGR in gas condensate system with constant fracture spacing. The performance of all cases is completely identical.

5.9 Productivity Index

Reservoir performance for gas condensate model with constant productivity index is shown on **Figs. 5.39–5.40**. Gas condensate model indicated similar performance as for dry gas case. Base case yielded 9.9 million USD of net present value with 211% of investment efficiency and 68% of internal rate of return. Higher permeabilities turned better economy of the project due to synergy effect of increased oil and gas production and lower costs associated with fracture half-length. Having conventional reservoir with 4,500 nd permeability achieving NPV equal to 20.3 million USD, DPI is 411% and IRR is 211%. Low-permeable shales with 103 nd almost eliminate economic value of the project with net cash flow of 0.5 million USD, investment efficiency of 102% and internal rate of return equal to 11.5%.

Increased fracture half-length helps to maintain cumulative gas production at almost the same level when permeability changes in between 103 and 500 nd. More noticeable different achieved for 1,125 and 4,500 nd reservoir (**Figs. 5.41–5.42**). Cumulative oil production slightly varies for 103–1,125 nd cases and significantly higher for 4,500 nd. Gas production rates are monotonically increases together with the reservoir permeability, while oil production rates indicate non-monotonic behavior after about 3.5 years. OGR fall from initial 125 STB/MMscf to 25–50 STB/MMscf indicate excessive oil condensation in the reservoir (**Fig. 5.43**). The short increase in producing OGR for 100 and 200 ft fractures indicates that the drainage area extends beyond the end of the tip only after reaching the interfracture boundaries.

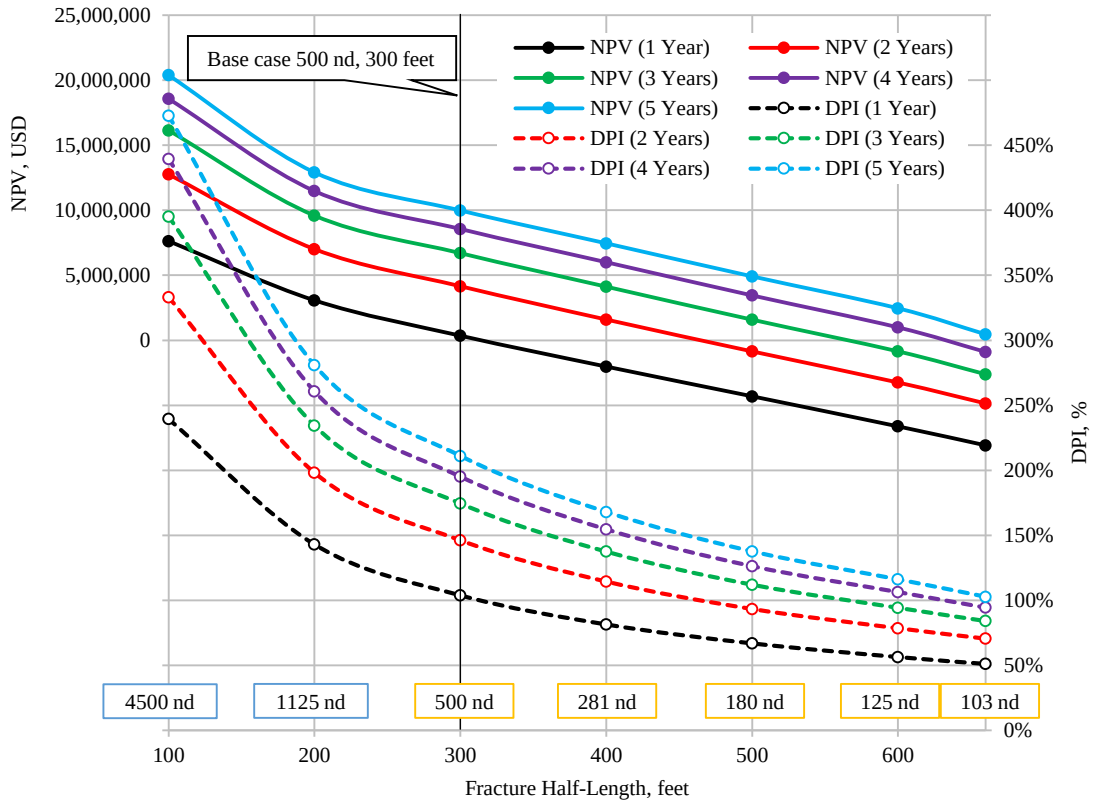

Fig. 5.39 – NPV and DPI in gas condensate system with constant PI. Fracture half-length and reservoir permeability are changed simultaneously. Yellow and blue boxes represent the permeabilities typical for shale and conventional reservoirs respectively.

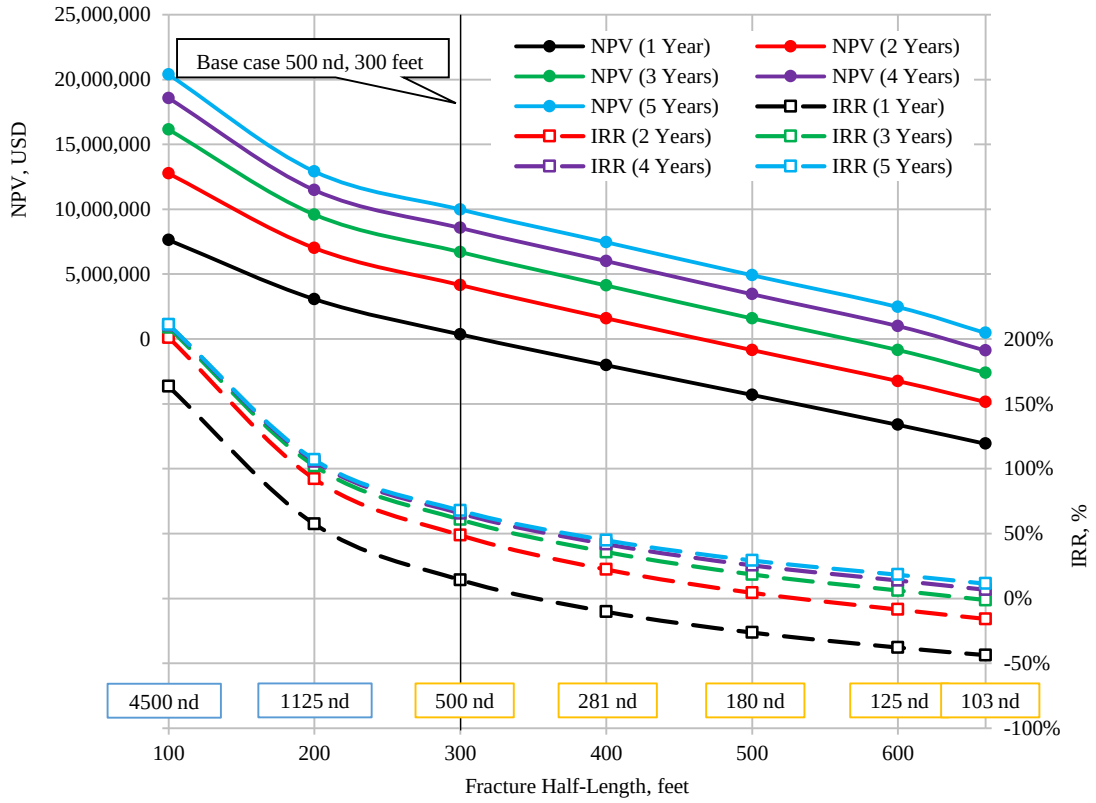

Fig. 5.40 – NPV and IRR in gas condensate system with constant PI. Fracture half-length and reservoir permeability are changed simultaneously. Yellow and blue boxes represent the permeabilities typical for shale and conventional reservoirs respectively.

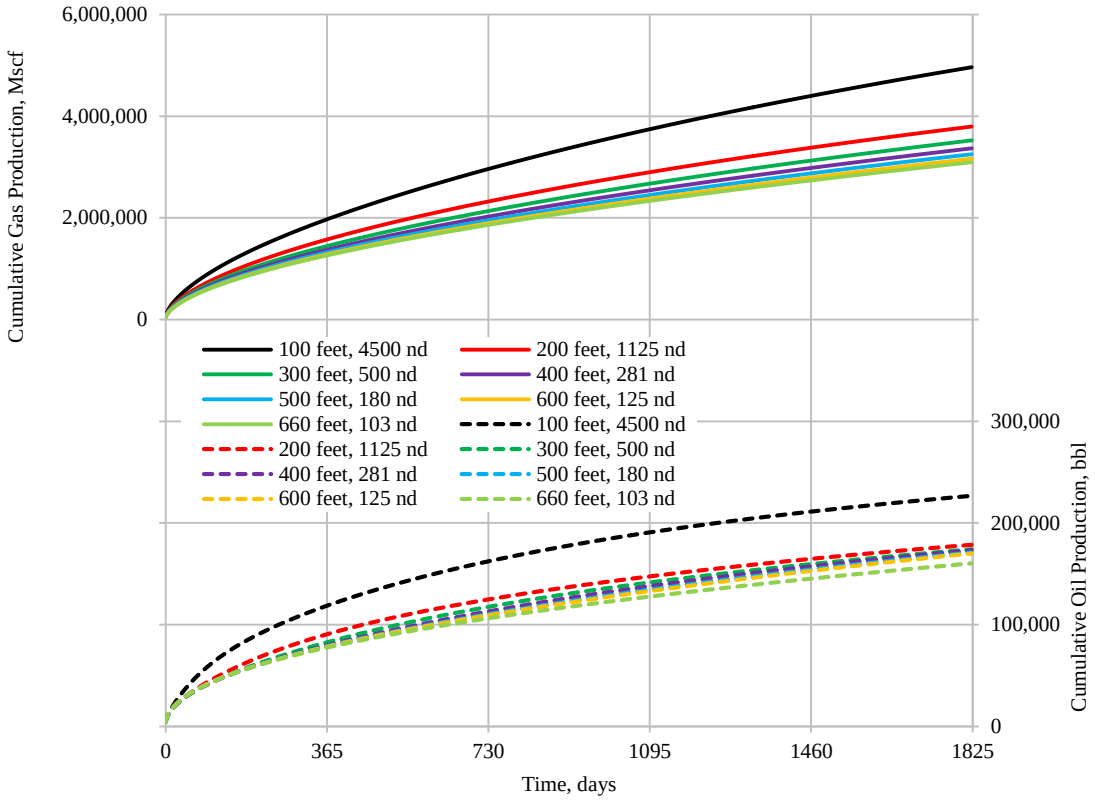

Fig. 5.41 – Cumulative oil and gas production in gas condensate system with constant PI. Values monotonically increases from low-permeable to high-permeable cases.

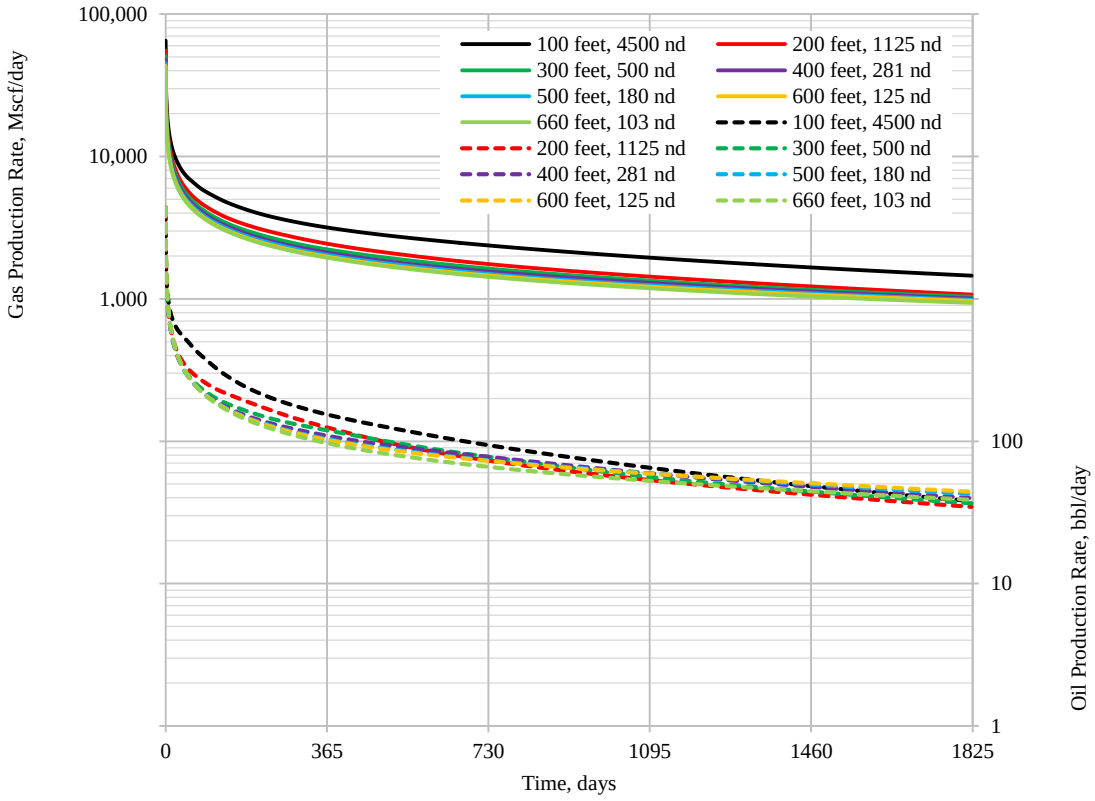

Fig. 5.42 – Oil and gas production rates in gas condensate system with constant PI. Gas rates monotonically increase for all permeabilities during 5 years. Oil rates show non-monotonic behavior after about 4 years of production.

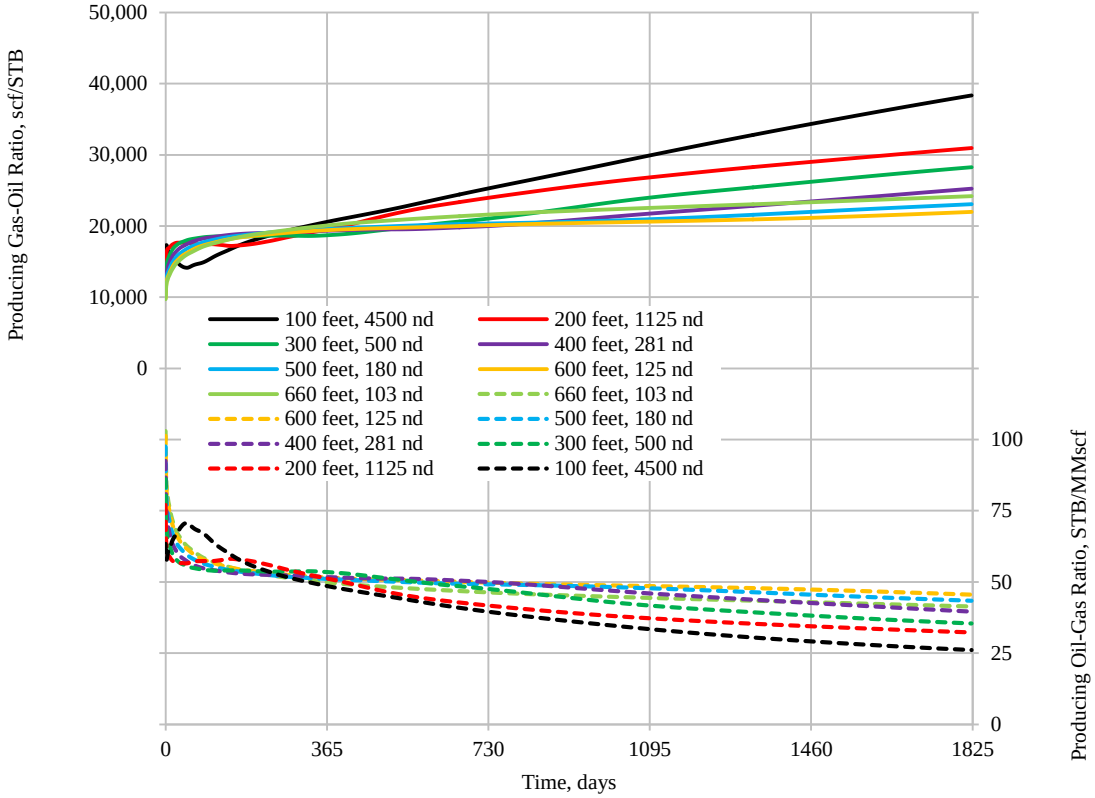

Fig. 5.43 – GOR and OGR in gas condensate system with constant PI. OGR performance in 103–281 nd is identical. 4,500 nd case has more significant liquid drop-out in the reservoir.

Chapter 6

Oil Simulation Results

Oil simulation model is initialized with undersaturated oil. PVT table are generated by SENSOR using the same 31 component EOS. Saturated data covers pressure range from 14.7 to 4,906.4 psia and a set of undersaturated data covers pressures up to 15,000 psia. Initial water saturation S_{wi} is set to 0.4, initial oil saturation S_{oi} is set to 0.6. Initial GOR of the system is 500 scf/STB (OGR is 2000 STB/MMscf). From the thesis we exclude sensitivity analysis on fracture constant spacing because the results correspond with dry gas and gas condensate results, turning the sensitivity into simple scaling problem. We also exclude bottomhole pressure sensitivity due to clear effect of it on the total production in oil systems.

6.1 Matrix Permeability

Figs. 6.1–6.2 presents the performance of oil system for different matrix permeabilities. The base case scenario achieved NPV of 7.9 million USD, DPI reached 188% and IRR equal to 52%. Oil model showed about 20% worse performance than gas condensate model. The best results within shale permeability range obtained for 1,000 nd case with 13.6 million of net present value, 252% of investment efficiency and 75% of internal rate of retunes. The break-even permeability is about 130 nd which is higher than for gas condensate case (120 nd) and dry gas case (90 nd). Maximum achieved economic metrics for conventional permeabilities are in 10,000 nd model with 34.7 million USD, 486% of DPI and 250% of IRR. This, for example, indicated that best performance for oil system is lower by 15% comparing with gas condensate case.

Figs. 6.3–6.5 show oil and gas production for different cases. Production rates and cumulative production grows monotonically in accordance with increased permeability. High-permeable models (5,000 and 10,000 nd) indicated faster decline in both oil and gas production from the beginning of the simulation. After 4 years, oil and gas production rates for reservoirs with 500–10,000 nd were almost equal. The volume of cumulative produced gas depends solely on the amount of produced oil through GOR. Average reservoir pressure does not drops below saturation pressure resulting in presence of undersaturated oil only in the model. Same GOR (OGR) behavior is observed for all other sensitivity results and, therefore, not presented any further.

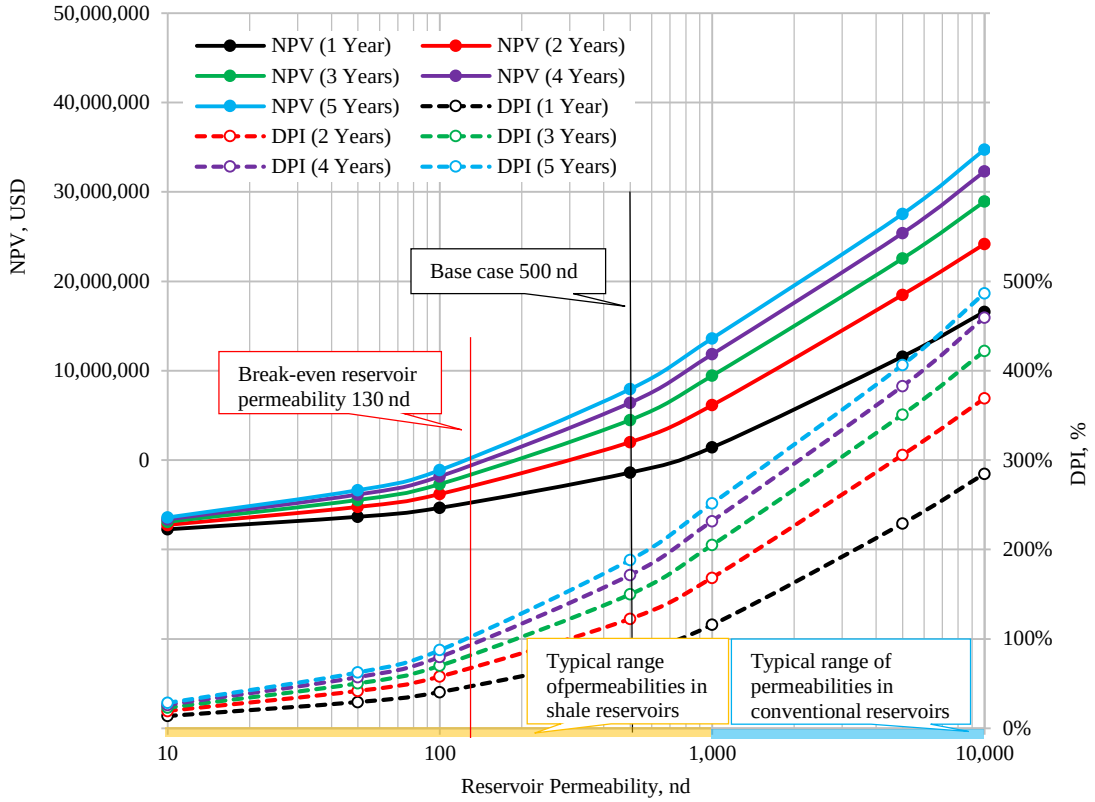

Fig. 6.1 – NPV and DPI in oil system for different reservoir permeabilities. Yellow and blue bars represent typical permeability ranges for shale and conventional reservoirs.

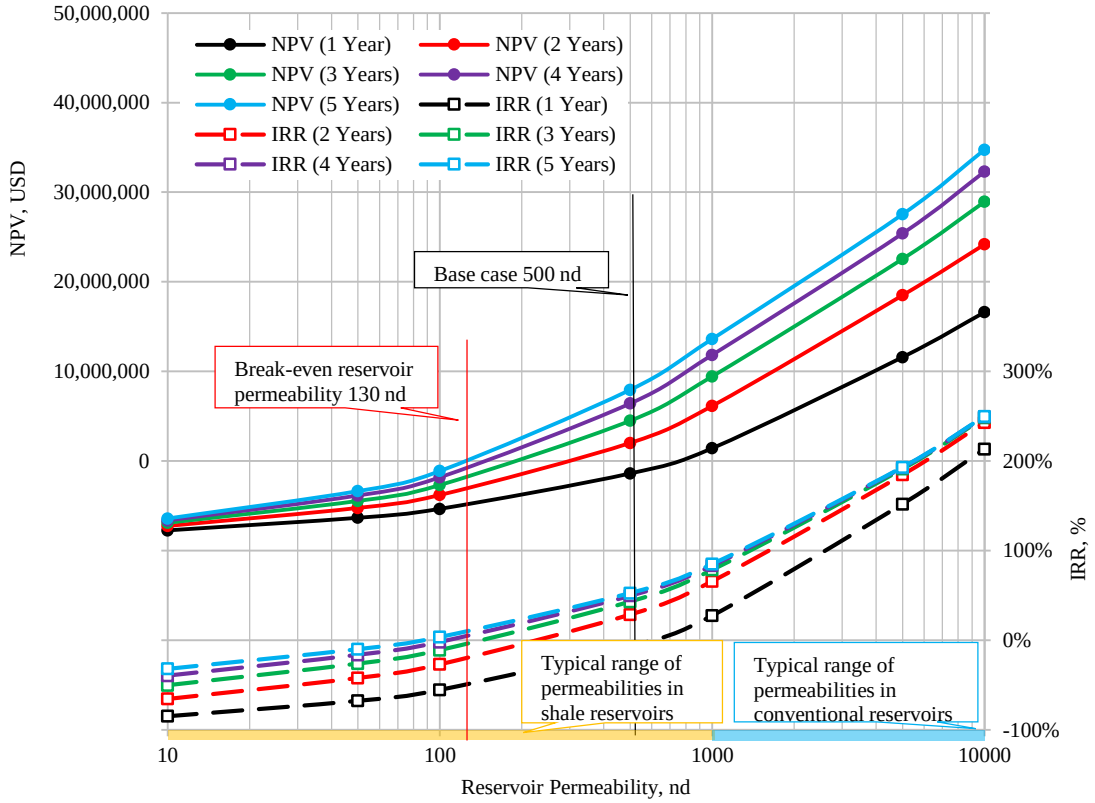

Fig. 6.2 – NPV and IRR in oil system for different reservoir permeabilities. Yellow and blue bars represent typical permeability ranges for shale and conventional reservoirs.

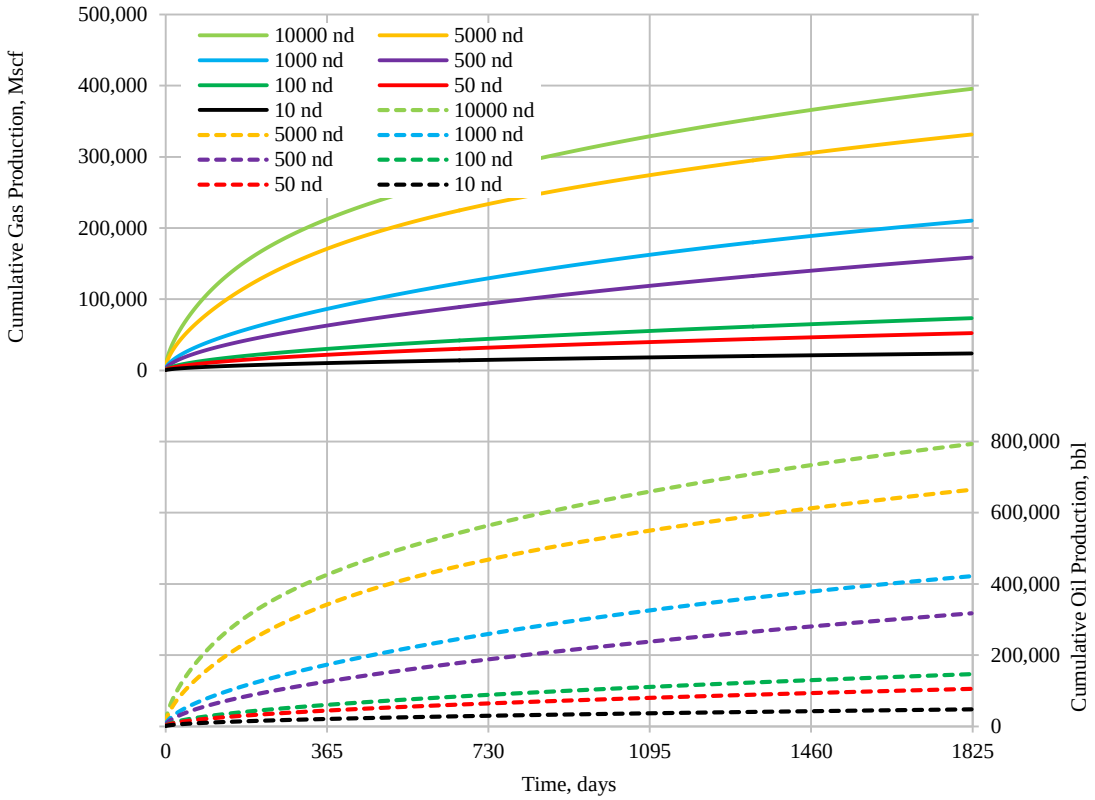

Fig. 6.3 – Cumulative oil and gas production in oil system for different reservoir permeabilities. Cumulative gas production is equal to cumulative oil production multiplied by GOR.

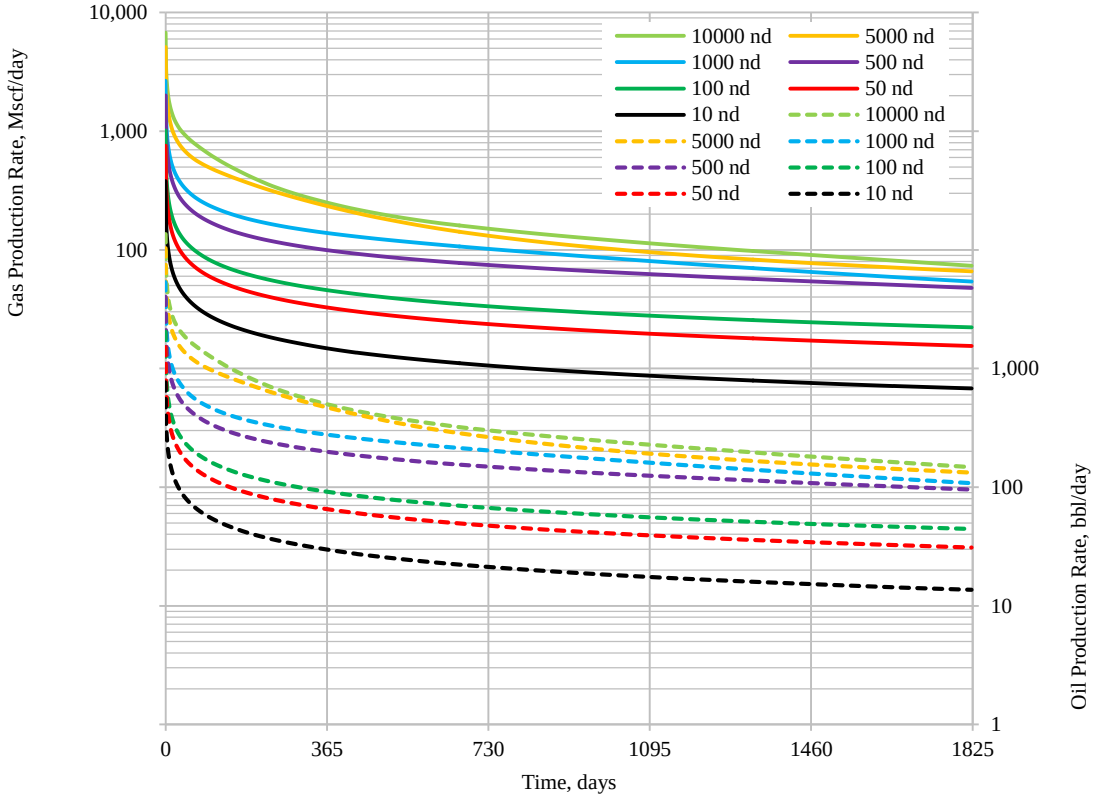

Fig. 6.4 – Oil and gas production rates in oil system for different reservoir permeabilities. After 4 years both oil and gas rates in 500–10,000 nd models are almost equal

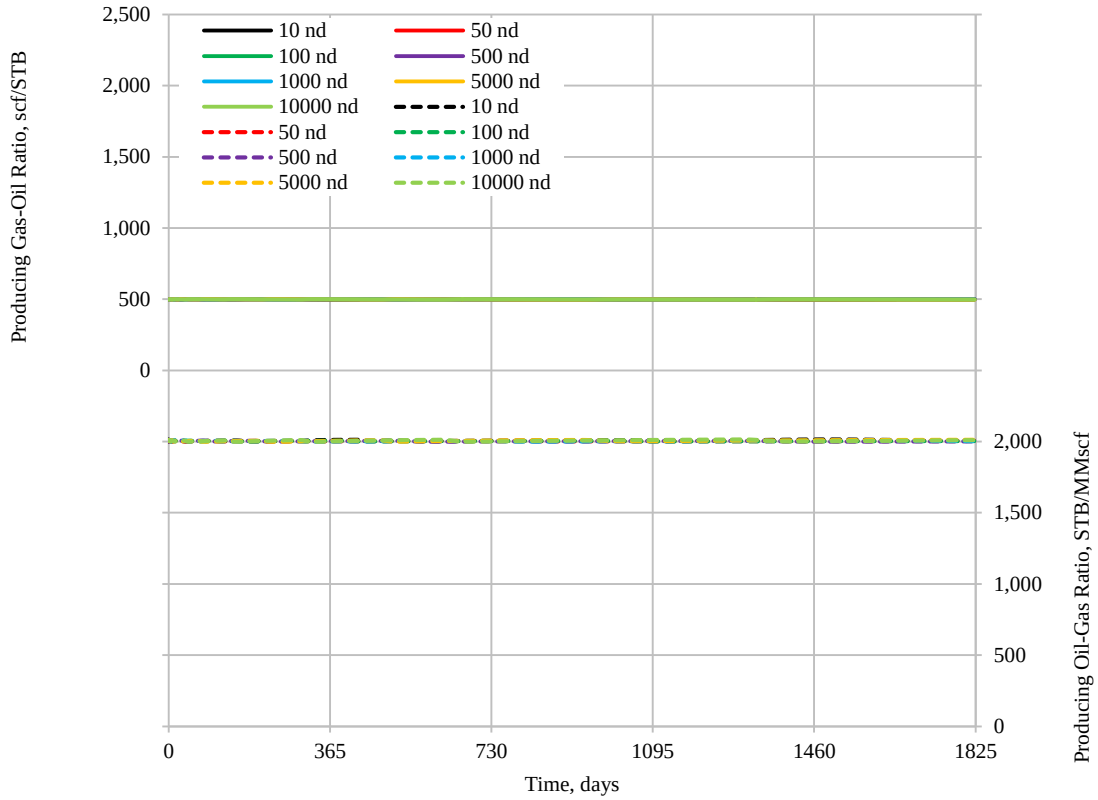

Fig. 6.5 – Producing GOR and OGR in oil system for different reservoir permeabilities. Constant values indicate that the model has undersaturated oil at any time

6.2 Initial Reservoir Pressure

Figs. 6.6–6.7 illustrate the performance difference in oil models depending on initial reservoir pressure. Just like in dry gas cases, the best reservoir performance achieved for the reservoirs with pressure around 7,500 psia. Corresponding NPV is 7.9 million USD, DPI is 188% and IRR is 52%. Higher pressure decreases project's net present value, investment efficiency and internal rate of return. For 14,500 psia corresponding economic metrics are 4.1 million USD, DPI is 146% and IRR is 33% This is caused by increased pressure drop in high pressure reservoir. This pressure drop overcomes the positive effect from increased initial oil-in-place volumes and turns production rates and cumulative production behave non-monotonically. The pressures below 7,500 psia were not sufficient to provide enough flow of oil and gas to the well and reinforce the project's economy.

Oil and gas cumulative productions monotonically increases for the reservoirs from 2,500 to 7,500 psia (**Figs. 6.8–6.9**). After that, higher initial pressures allow to produce less hydrocarbons from the model due to increased pressure drop within first months of the production. 5,000, 12,500 and 14,500 psia cases produced almost equal cumulative volumes of oil and gas after 5 years. However, this was about 20% lower result comparing with best case 7,500 psia model.

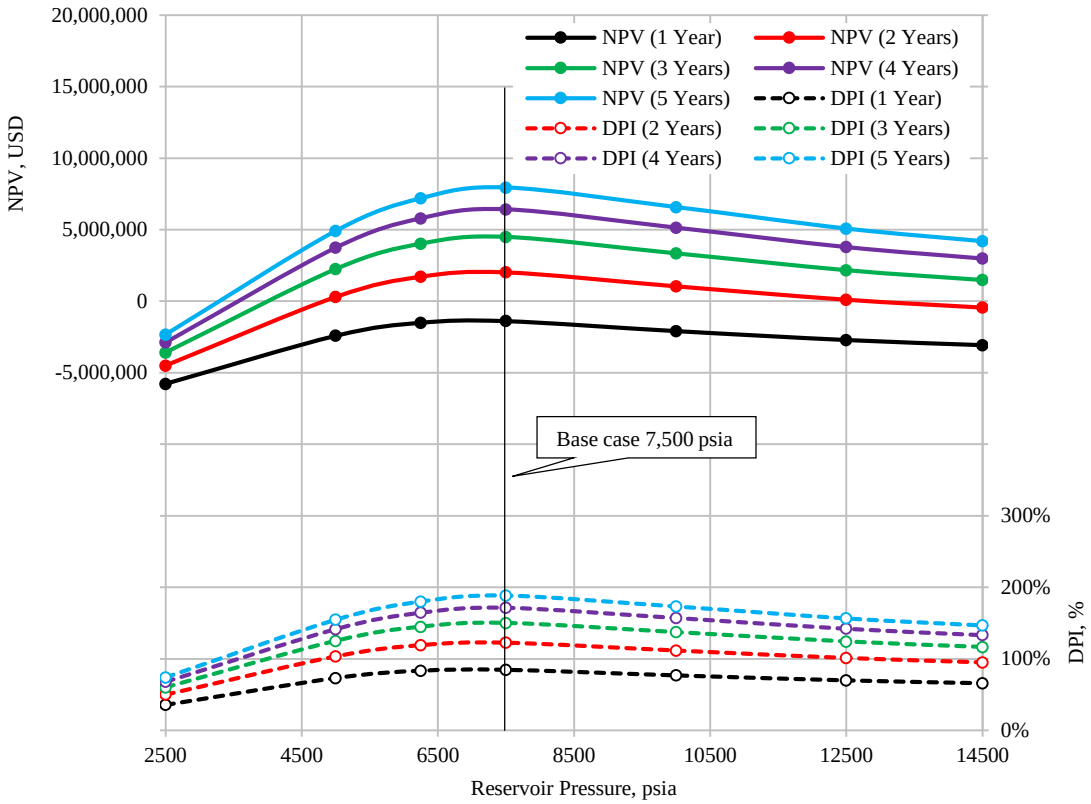

Fig. 6.6 – NPV and DPI in oil system for different initial reservoir pressures.

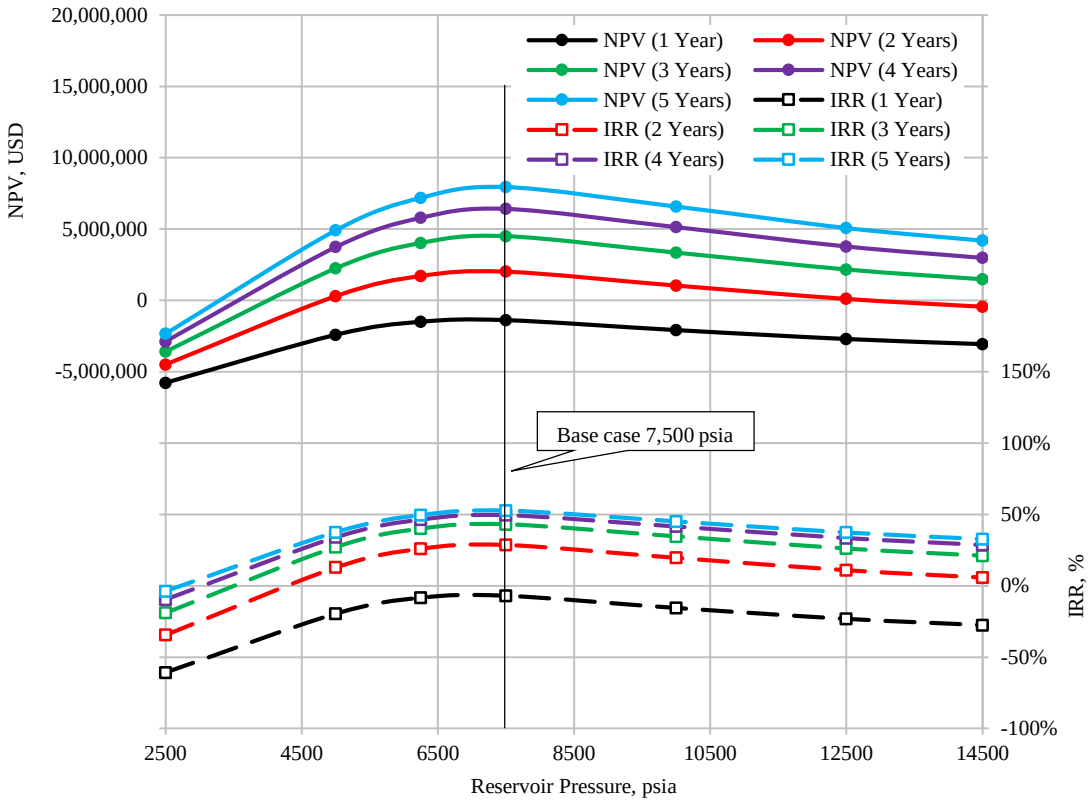

Fig. 6.7 – NPV and IRR in oil system for different initial reservoir pressures.

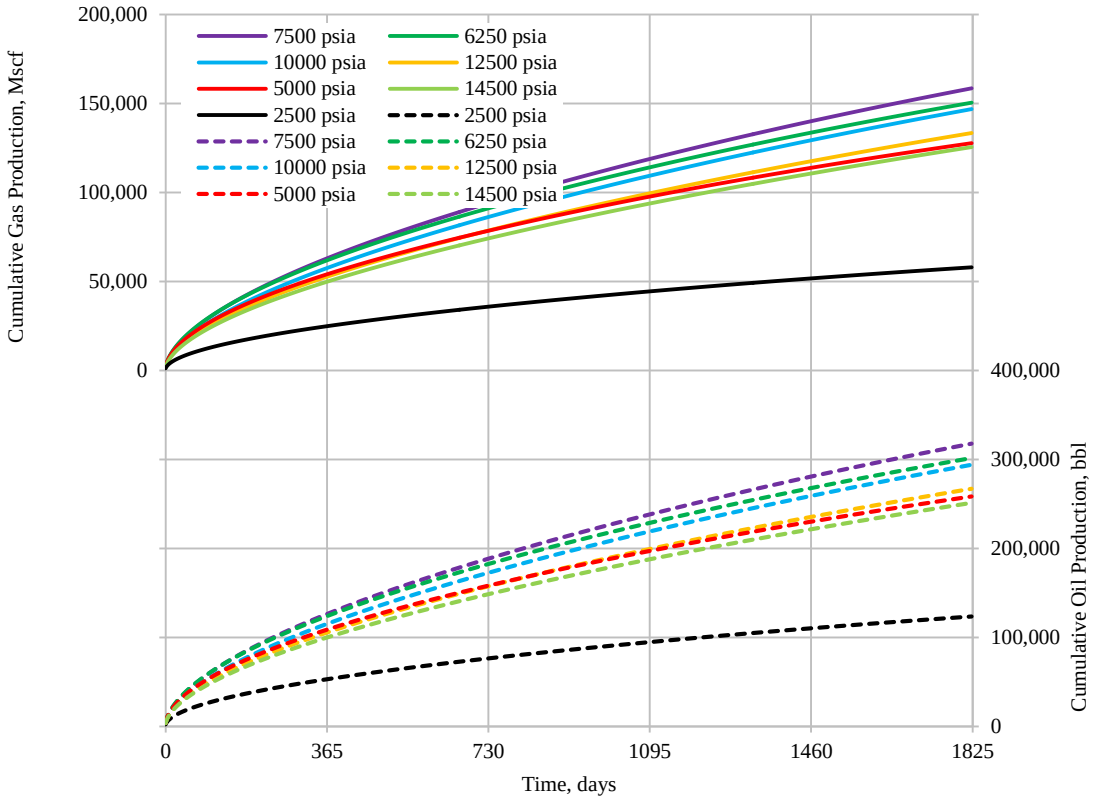

Fig. 6.8 – Cumulative oil and gas production in oil system for different initial reservoir pressures. Cumulative production for 5,000, 12,500 and 14,500 psia is almost the same after 5 years.

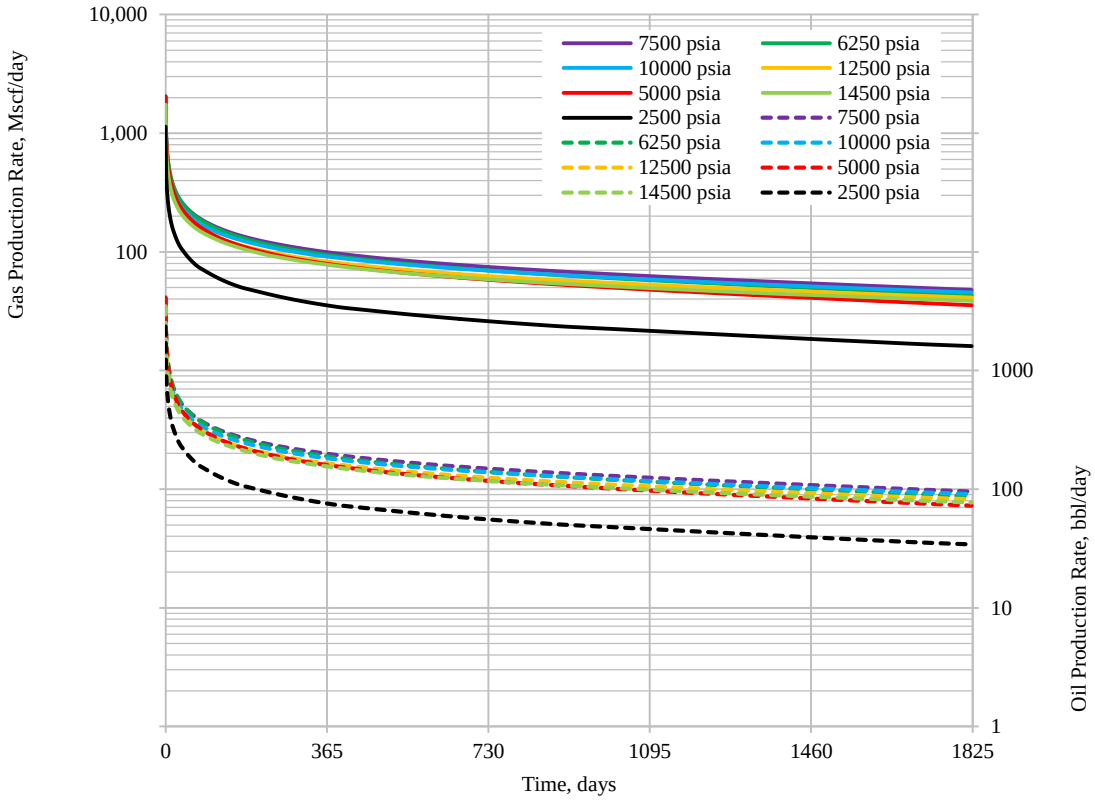

Fig. 6.9 – Oil and gas production rates in oil system for different initial reservoir pressures.

6.3 Reservoir Thickness

Figs. 6.10–6.11 show the model performance for different reservoir thickness. Break-even reservoir thickness is 110 ft, which is by 22% higher than break-even thickness for dry gas and gas condensate models. The base case scenario achieved net present value of 7.9 million USD, investment efficiency of 188% and internal rate of return equal to 52%. Since the model has only one layer in Z-direction and the fracture penetrate whole thickness of the model, the only difference in models are associated with change of hydrocarbon pore volume. Every 10 additional ft of reservoir thickness give about 0.7 million of additional net present value for the project.

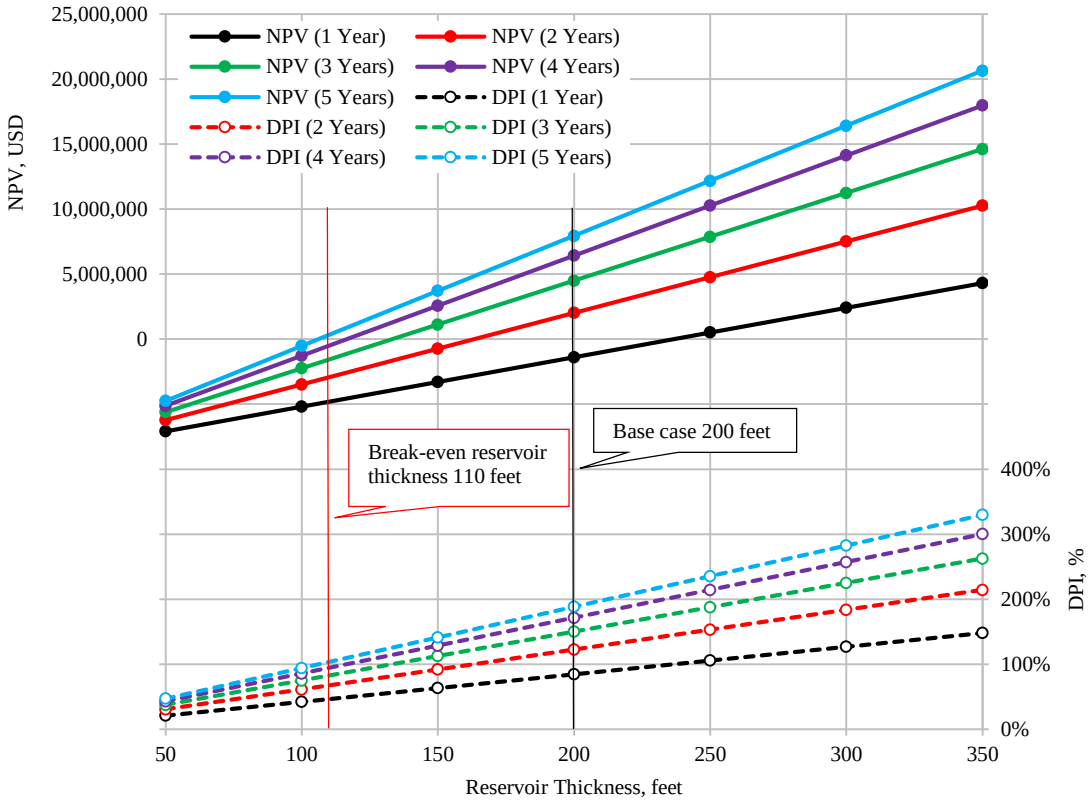

Fig. 6.10 – NPV and DPI in oil system for different reservoir thickness.

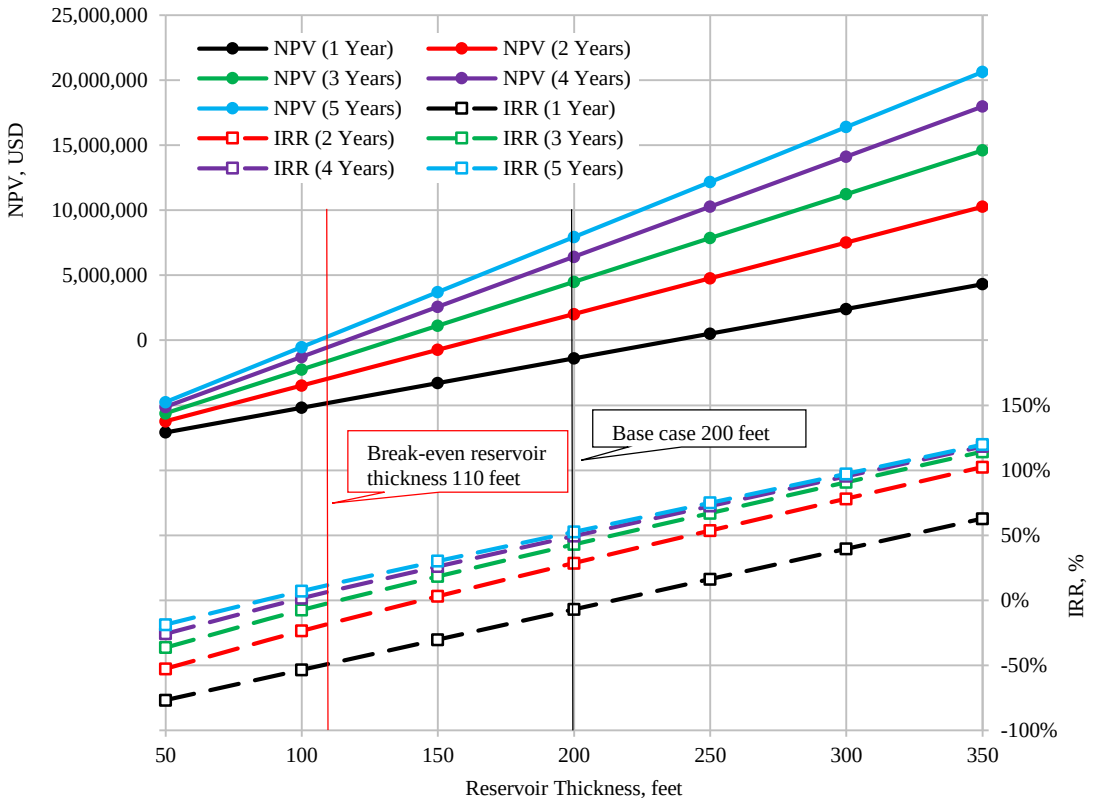

Fig. 6.11 – NPV and IRR in oil system for different reservoir thickness.

6.4 Number of Fractures

Figs. 6.12–6.13 show the performance of the model for different number of fractures. Based solely on NPV metric, the optimal well design will require 40–50 fractures for completion to achieve NPV about 14 million USD after 5 years. That would yield corresponding investment efficiency about 187% and internal rate of return for the project around 66%. On the other hand, once the company decided to achieve maximum investment efficiency, DPI metric should be prioritized among others. Thus, maximum achievable DPI is about 207% giving the recommended range of fracs in between 26 and 38 per well. For 30 fractures, corresponding NPV would be about 12.2 million USD (-13% of maximum net present value) and IRR would be 65.9% (almost no change from maximum value). Attempt to achieve the highest internal rate of return would yield maximum 65–66% values for a wide range of fractures (27–47 fracs). Corresponding NPV and DPI vary significantly within this range.

Coupling all three metrics would help to justify the well with 35–37 fractures providing high investment efficiency (about 205%), high internal rate of return (more than 69%) and high net present value (13.4 million USD). Flat behavior of IRR for bigger number of the fractures after 4–5 years explained by small incremental income from additional fracs at a later production stage and, therefore, small influence on the projects internal rate of return.

Figs. 6.14–6.15 show that acceleration of the production is not significantly affected by additional fractures. 40 and 50 fractures cases have a rapid decline in production rates and does not allow achieving better investment efficiency.

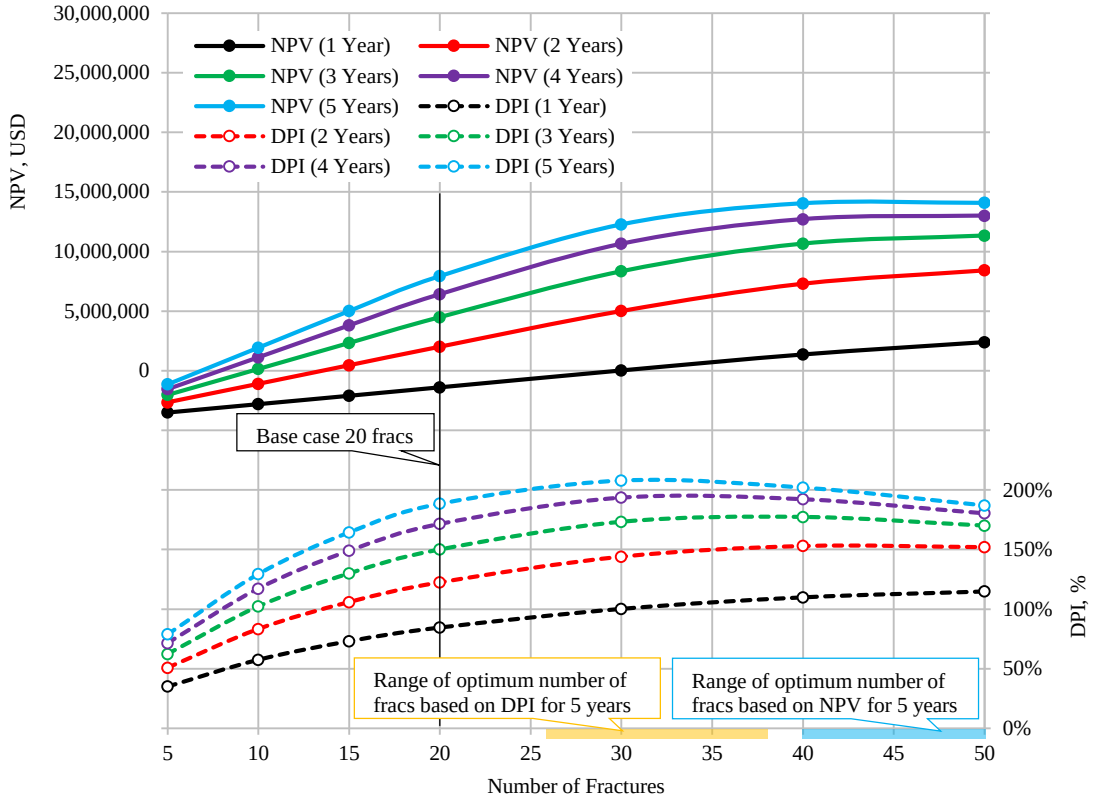

Fig. 6.12 – NPV and DPI in oil system for different number of fractures. Yellow and blue bars represent the optimum number of fracture based solely on DPI or NPV metrics.

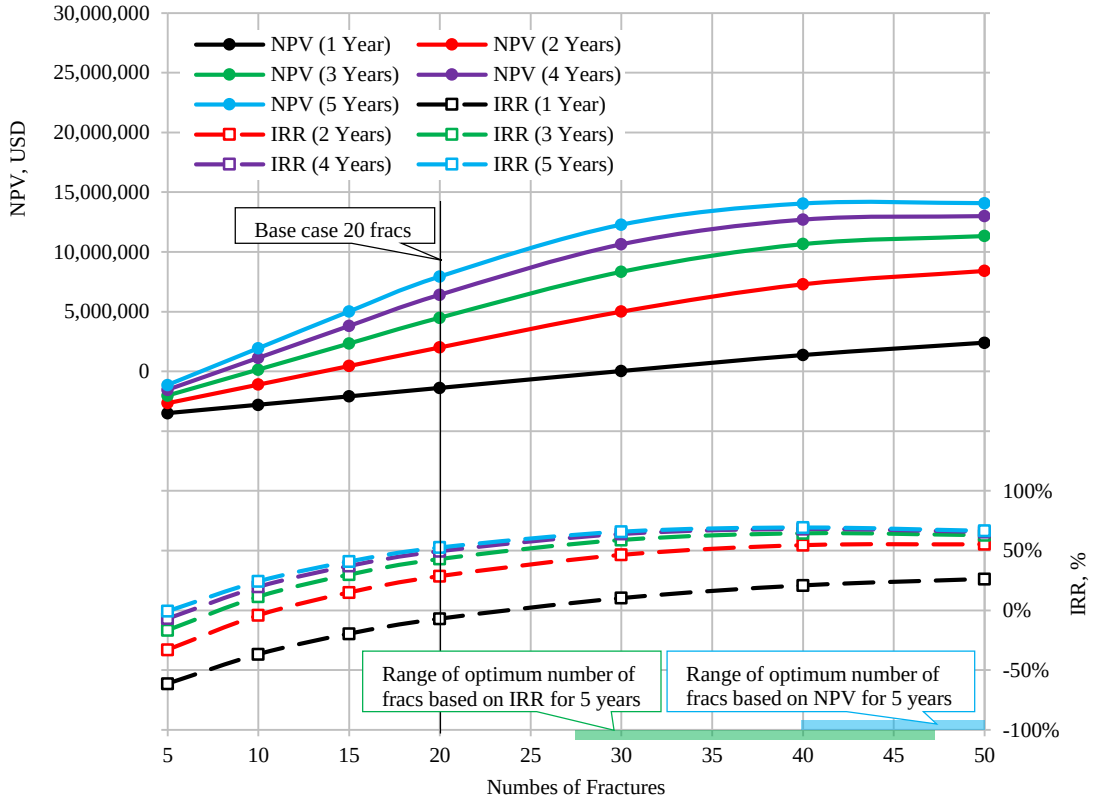

Fig. 6.13 – NPV and IRR in oil system for different number of fractures. Green and blue bars represent the optimum number of fracture based solely on IRR or NPV metrics.

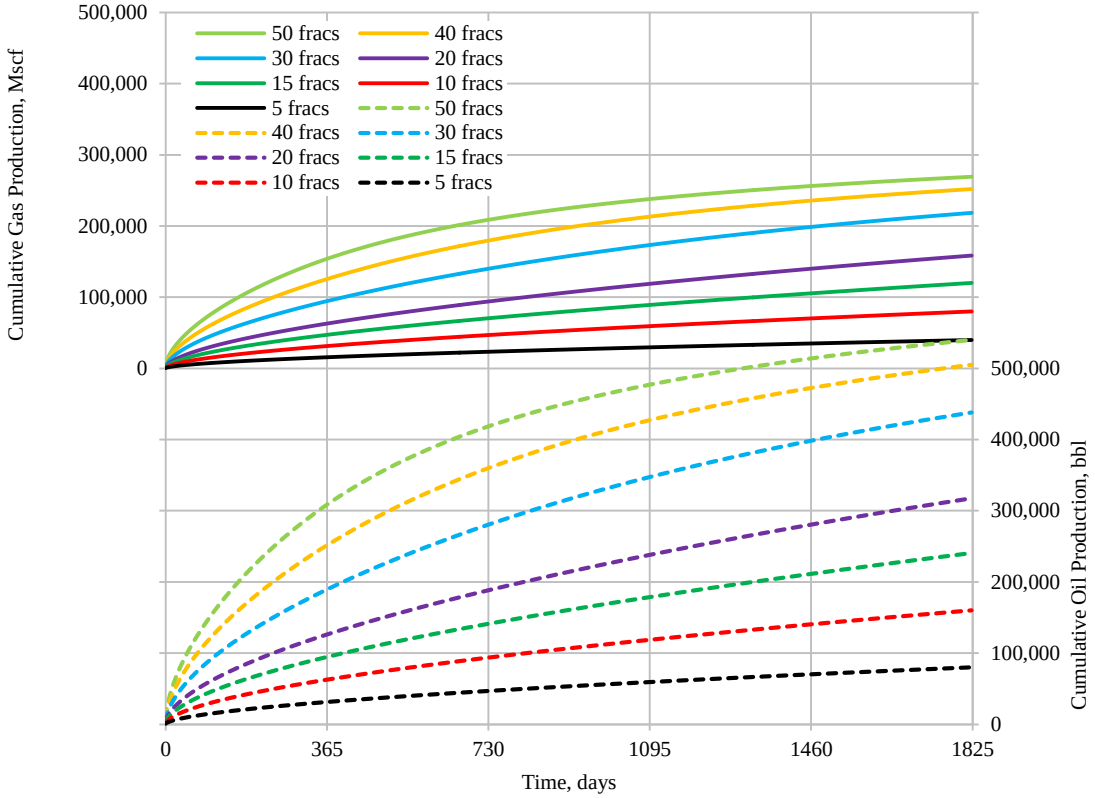

Fig. 6.14 – Cumulative oil and gas production in oil system for different number of fractures.

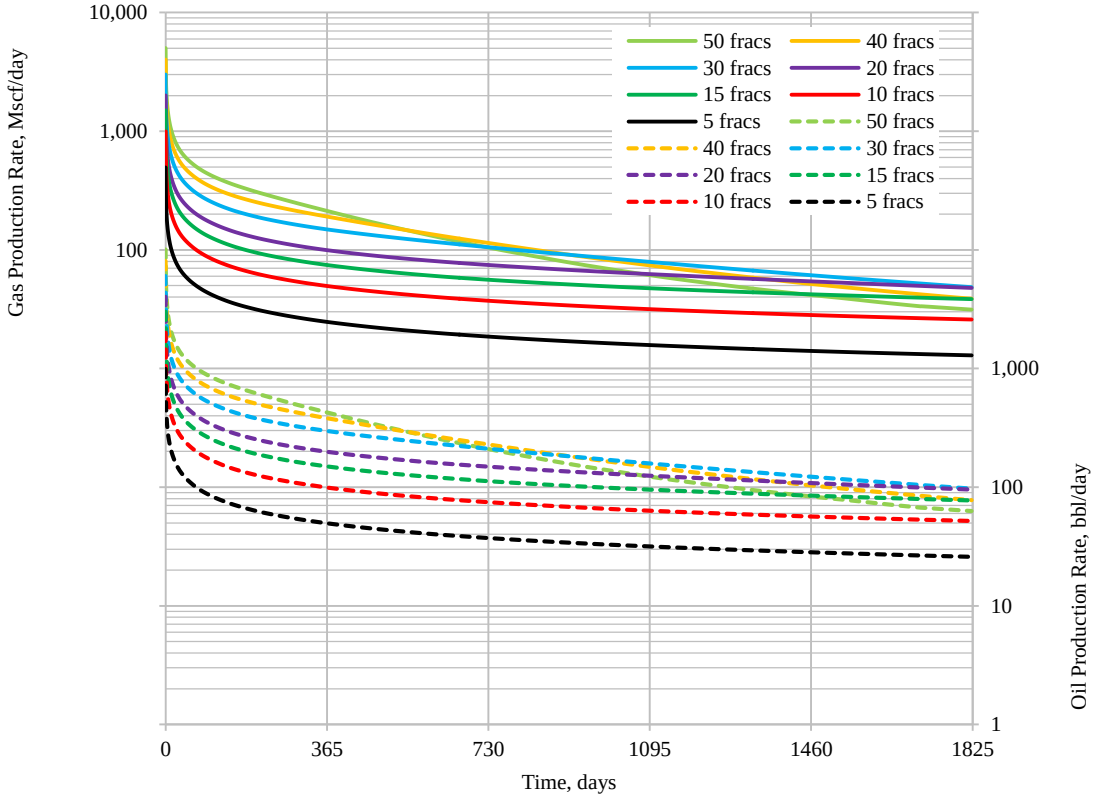

Fig. 6.15 – Oil and gas production rates in oil system for different number of fractures. For 40 and 50 fractures cases the decline rate is higher than for the rest of the models.

6.5 Fracture Half-Length

Figs. 6.16–6.17 present performance of the model depending on the different fracture half-length. Maximum achievable NPV is about 11.5 million USD and require fractures of 550–660 ft long. Corresponding values for DPI and IRR would be 169% and 43% respectively. However, a higher investment efficiency and internal rate of return can be achieved by sacrificing a part of net present value.

Maximum achievable DPI for the model is about 188% with 300 ft fractures. Fractures with half-length from 250 to 450 ft yield approximately the same result for DPI. Corresponding NPV could shrink down to 7.3 million USD for 250 ft and 10.1 million USD for 450 ft fracs. Corresponding IRR is in a range of 50-52%.

Maximizing IRR could be possible with 350 ft fractures achieving 52%. Since IRR does not significant change after 5 years for the majority of the cases, the optimum range of fractures half-length could be between 200–550 ft. NPV changes significantly from 5.5 million USD for 200 ft up to 11.3 million USD for 550 ft fracture. Minimum and maximum DPI values are 177% and 188% for selected range of fracture half-lengths.

Figs. 6.18–6.19 show monotonic increase in both cumulative production and production rates. Incremental revenues from increased fracture half-length are hardly cover incremental costs for 500–600 ft fractures. After 600 ft half-length, incremental costs overtake incremental revenues due to non-linear increase in treatment of longer fractures yielding lower economic performance of the project.

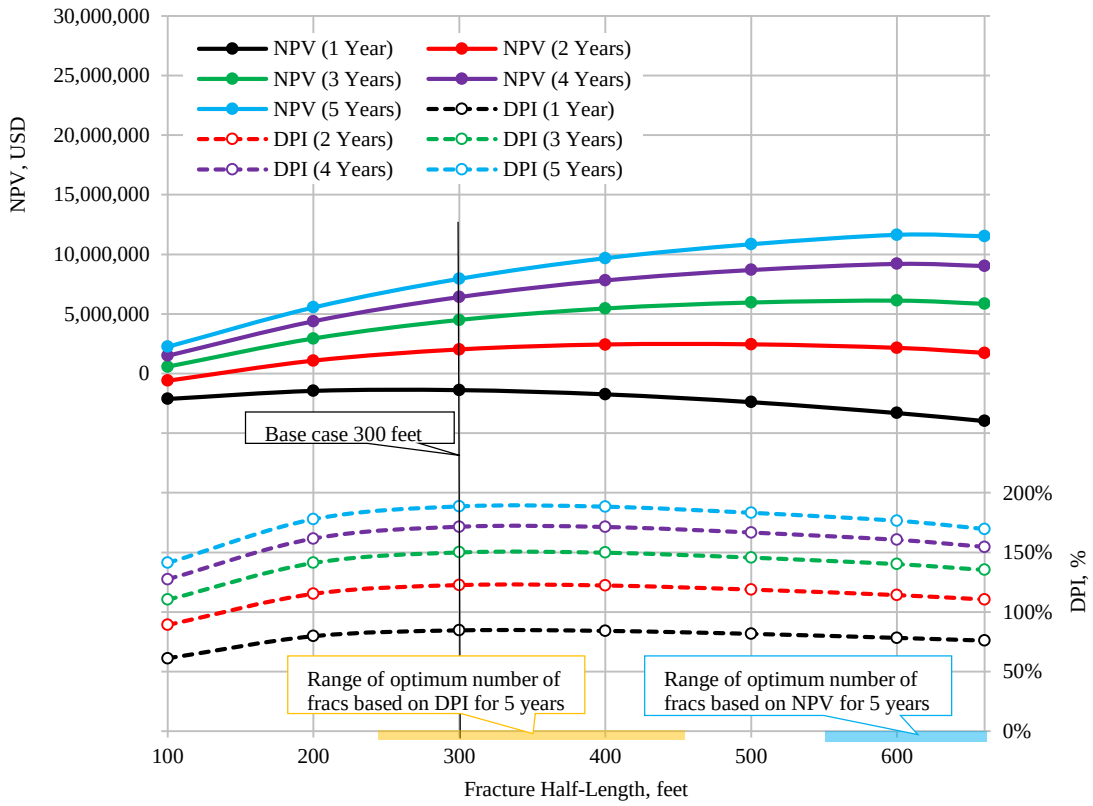

Fig. 6.16 – NPV and DPI in oil system for different fracture half-length. Yellow and blue bars represent the optimum number of fracture based solely on DPI or NPV metrics.

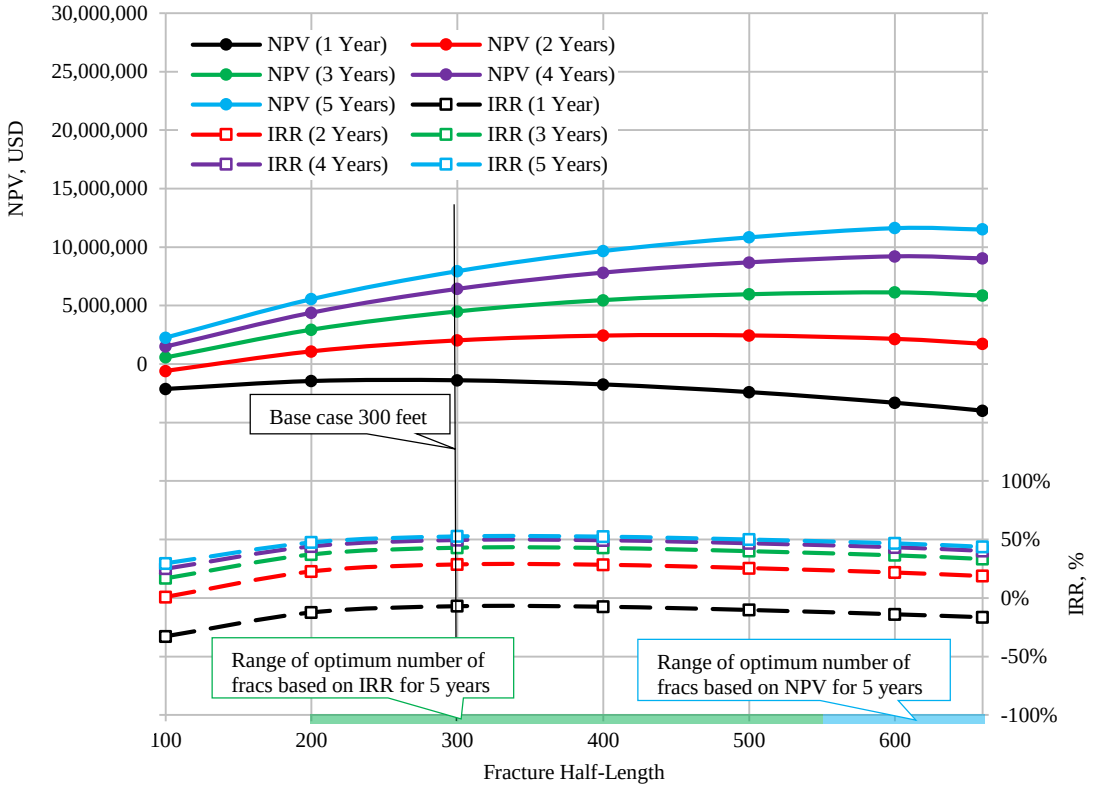

Fig. 6.17 – NPV and IRR in oil system for different fracture half-length. Green and blue bars represent the optimum number of fracture based solely on DPI or NPV metrics.

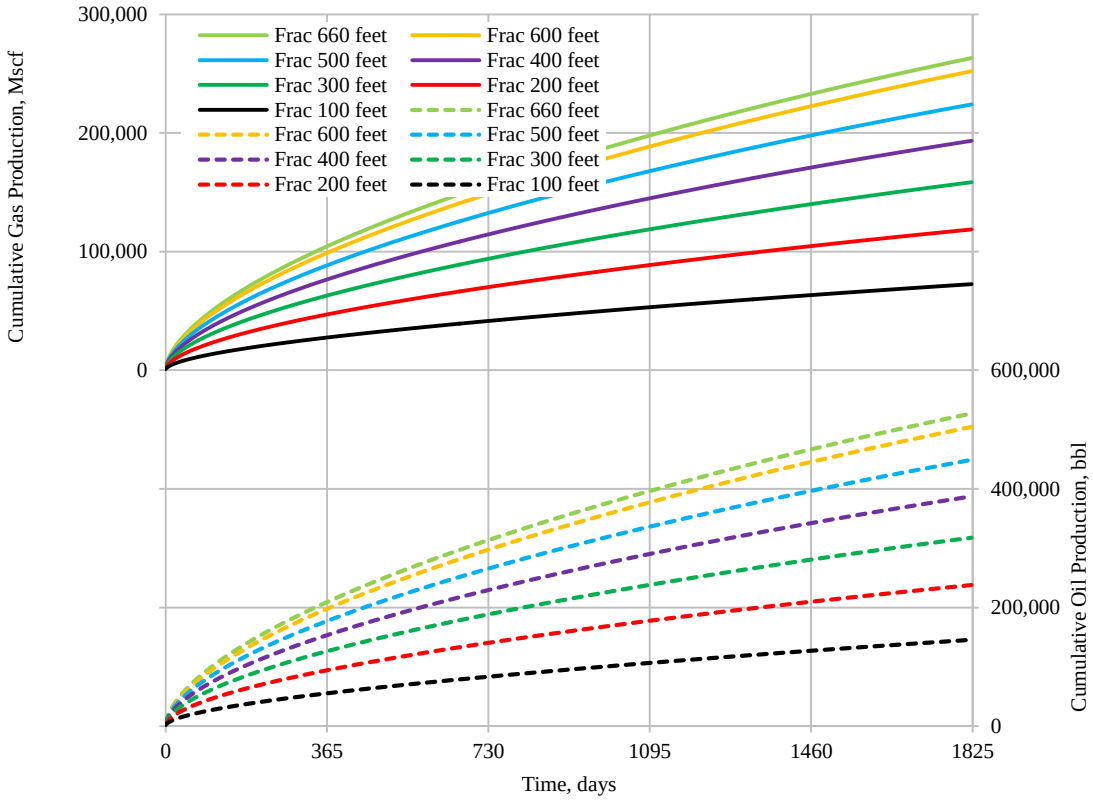

Fig. 6.18 – Cumulative oil and gas production in oil system for different fracture half-lengths.

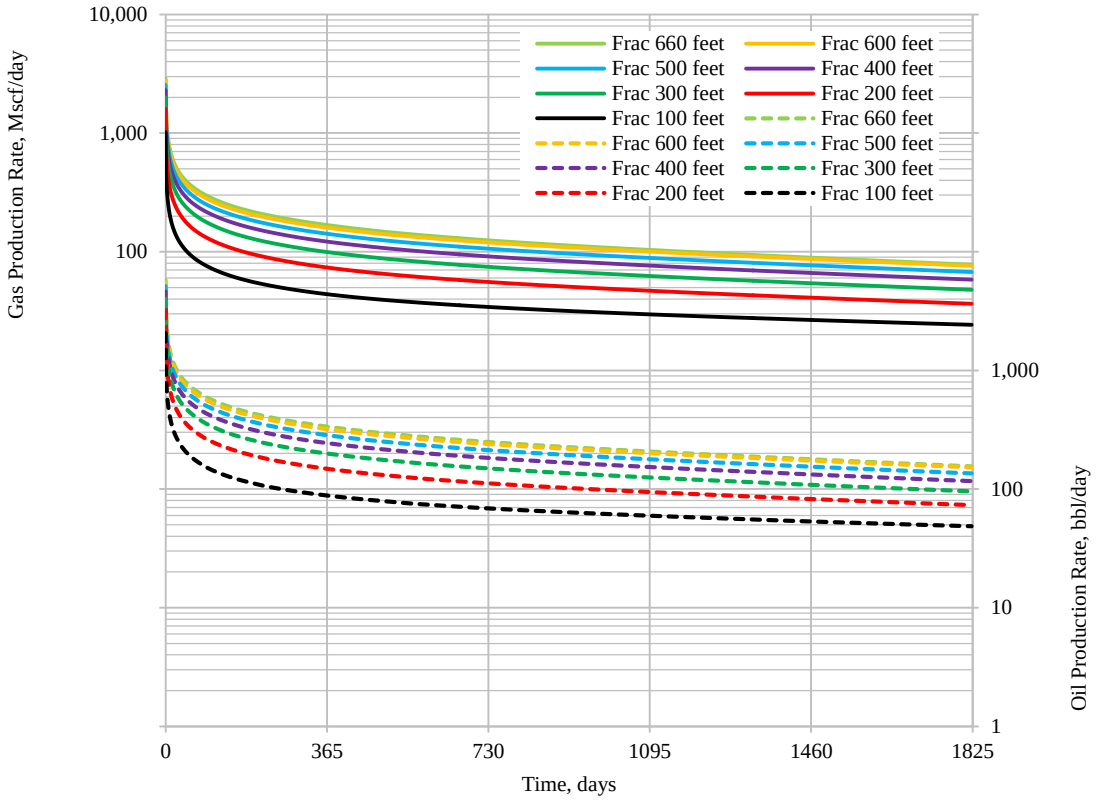

Fig. 6.19 – Oil and gas production rates in oil system for different fracture half-lengths

6.6 Well Horizontal Length

Figs. 6.20–6.21 show the model performance depending on different horizontal section lengths. Best performance achieved for base case scenario is 5,280 ft section with NPV of 7.9 million USD, DPI of 188% and IRR of 52%. Increased horizontal length and, therefore, fracture spacing showed negative trend for all three metrics. The model with 10,560 ft section showed the worse performance among others achieving only 5.1 million USD for net present value, investment efficiency is around 144% and internal rate of return is around 32%. The behavior for DPI and IRR metrics correspond with dry gas and gas condensate cases. Unlike observed for two other models, NPV metric for oil shows distinct negative trend for any time for the production. This is cause by infinite-acting behavior of the model when oil model does not reach the interfracture boarders at a first place. Therefore, increased fracture spacing (which causes increase in single fracture drainage area) almost does not influence the production within 5 years.

Figs. 6.22–6.23 support the idea presented above. We observe that the same cumulative amount of oil and gas were produced within 5 years for each of the models. A very small difference could be noticed after 4 years in oil production but for extremely different cases (5,280 vs 10,560 ft). Production rates for all cases show identical performance indicating the infinite-action behavior of the model.

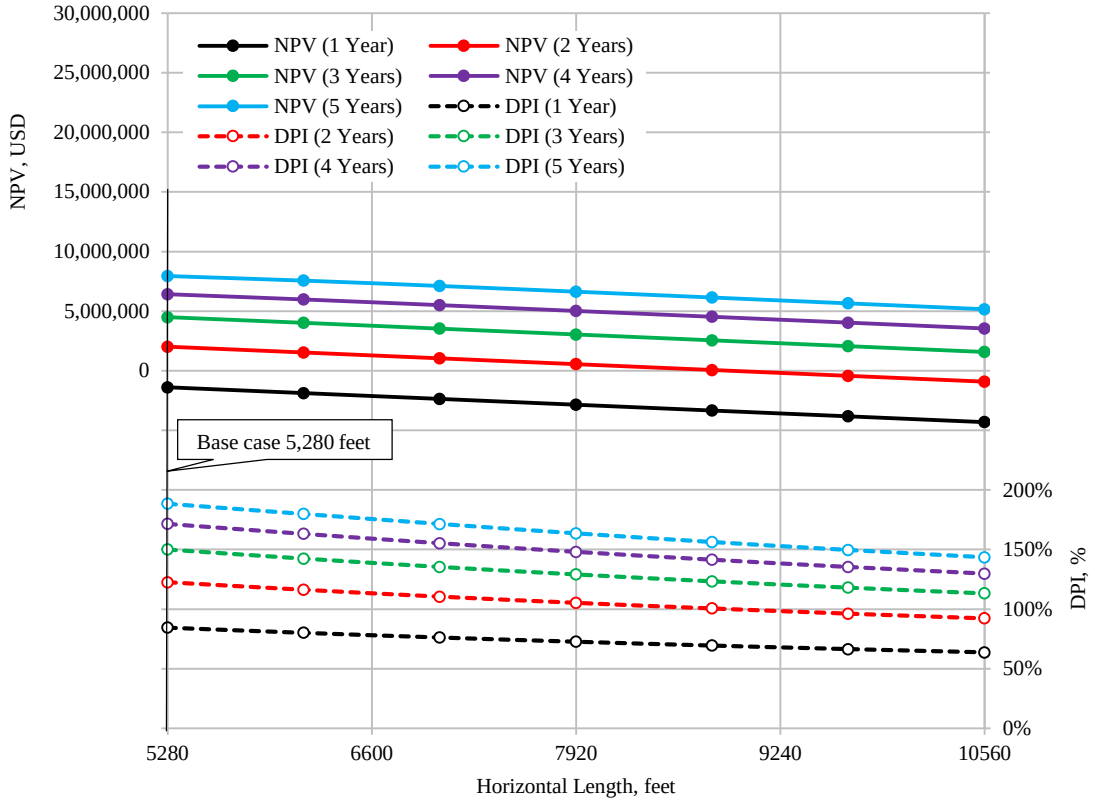

Fig. 6.20 – NPV and DPI in oil system with different horizontal section length.

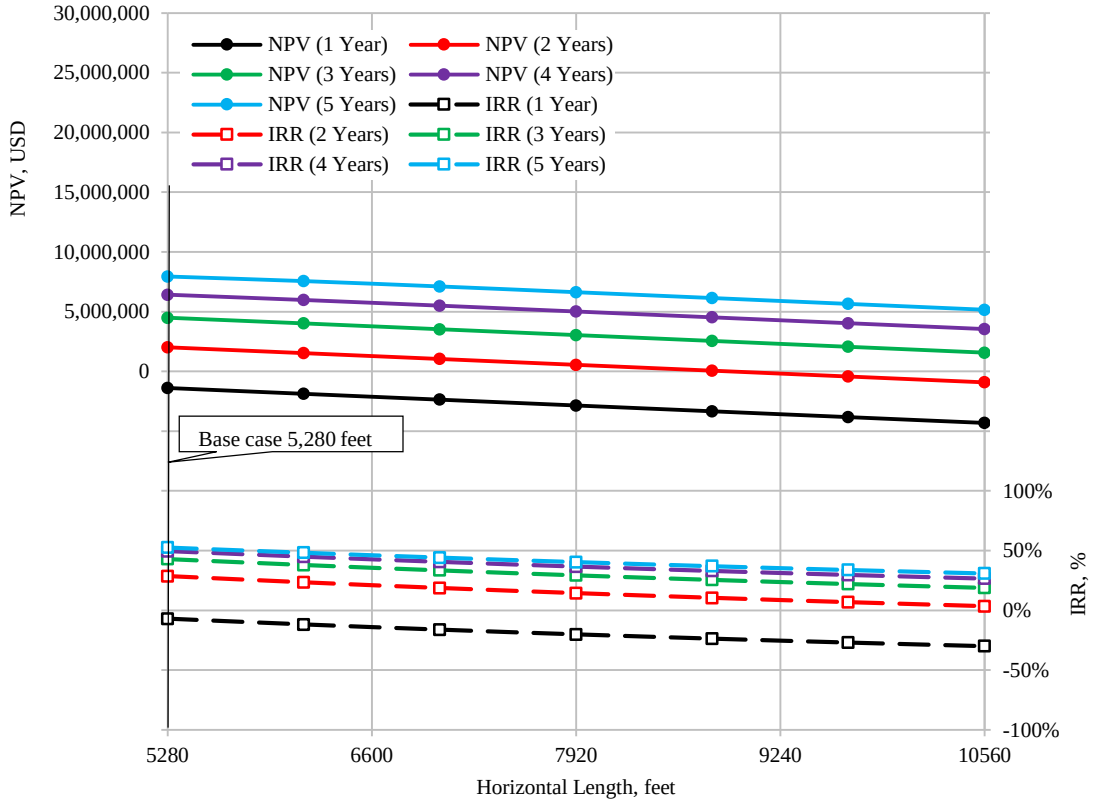

Fig. 6.21 – NPV and IRR in oil system with different horizontal section length.

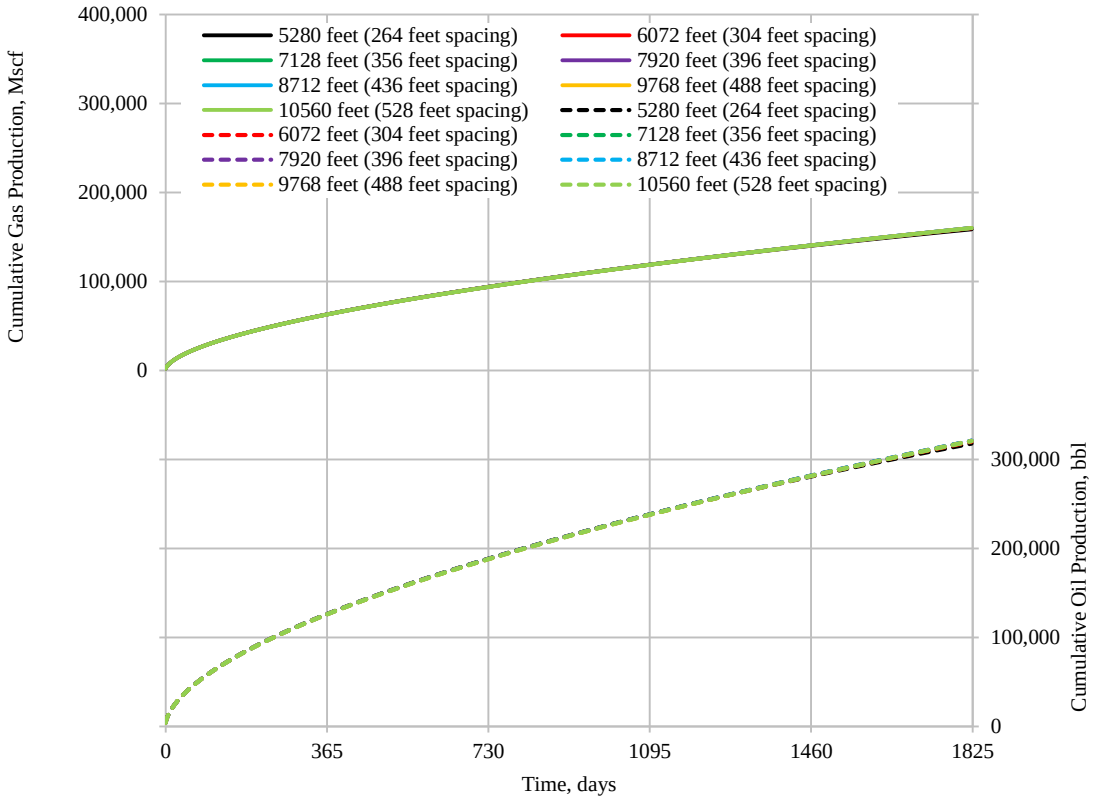

Fig. 6.22 – Cumulative oil and gas production in oil system with different horizontal section length. All cases show near infinite-acting behavior for the first 5 years.

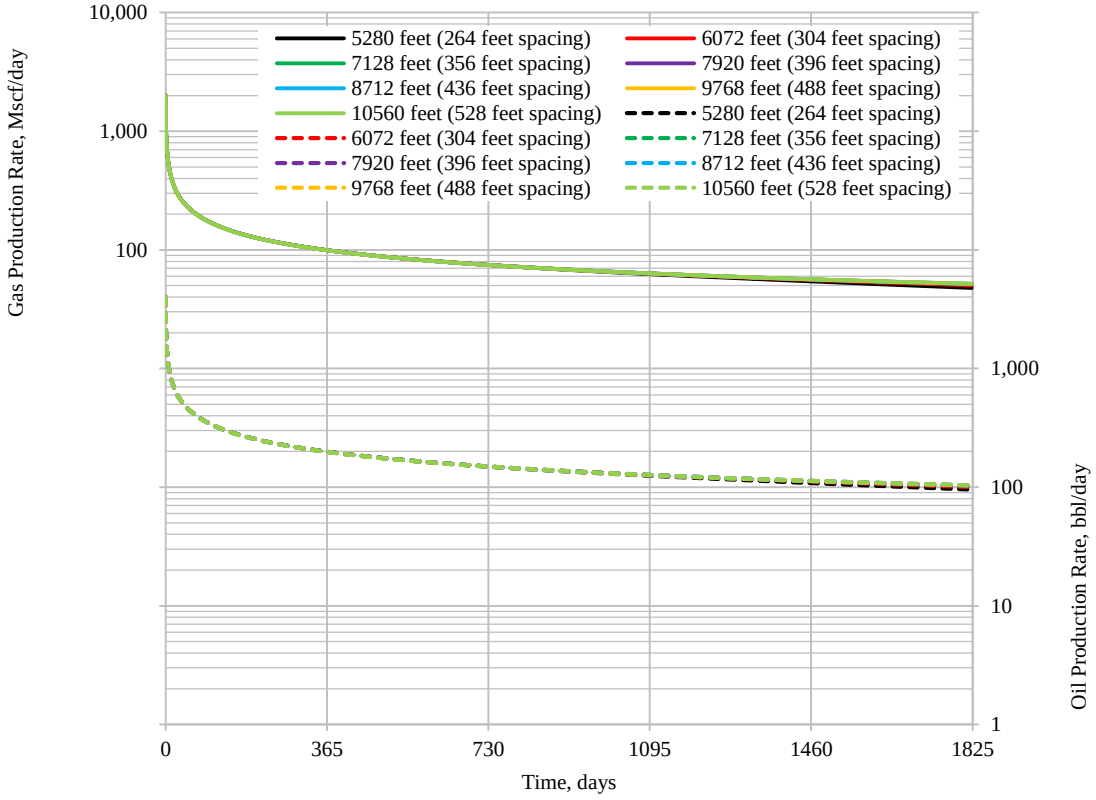

Fig. 6.23 – Oil and gas production rates in oil system with different horizontal section length. All cases show near infinite-acting behavior for the first 5 years.

6.7 Productivity Index

Figs. 6.24–6.25 present oil model performance with constant PI when permeability of the reservoir and fracture half-length are changes simultaneously. Base case net present value equals to 7.9 million USD, investment efficiency is 188% and internal rate of return is equal to 52%. Increased reservoir permeability yields better economic performance by the synergy of increased cumulative oil and gas production and reduced costs for the completion of the well. The maximum NPV is 18.4 million USD, DPI is 438% and IRR is 177% achieved for 4,500 nd reservoir with 100 ft fractures. Oppositely, the reduced reservoir permeability turns down the economic performance of the model. For example, 180 nd reservoir with 500 ft fractures will yield only 2.2 million USD of net present value, with 177% investment efficiency and 18% internal rate of return. Model with reservoir permeability equal to 135 nd and fracture half-length of about 580 ft will not yield positive project's economy within 5 years.

Figs. 6.26–6.27 indicate that constant PI allow the models to produce fairly equal cumulative amount of oil and gas, except for high-permeable cases. Oil and gas production rates in 4,500 nd is significantly higher than in other cases during all simulation period. At the same time, there is almost no difference in production rates in models with 103–1,125 nd reservoir permeability after 4 years.

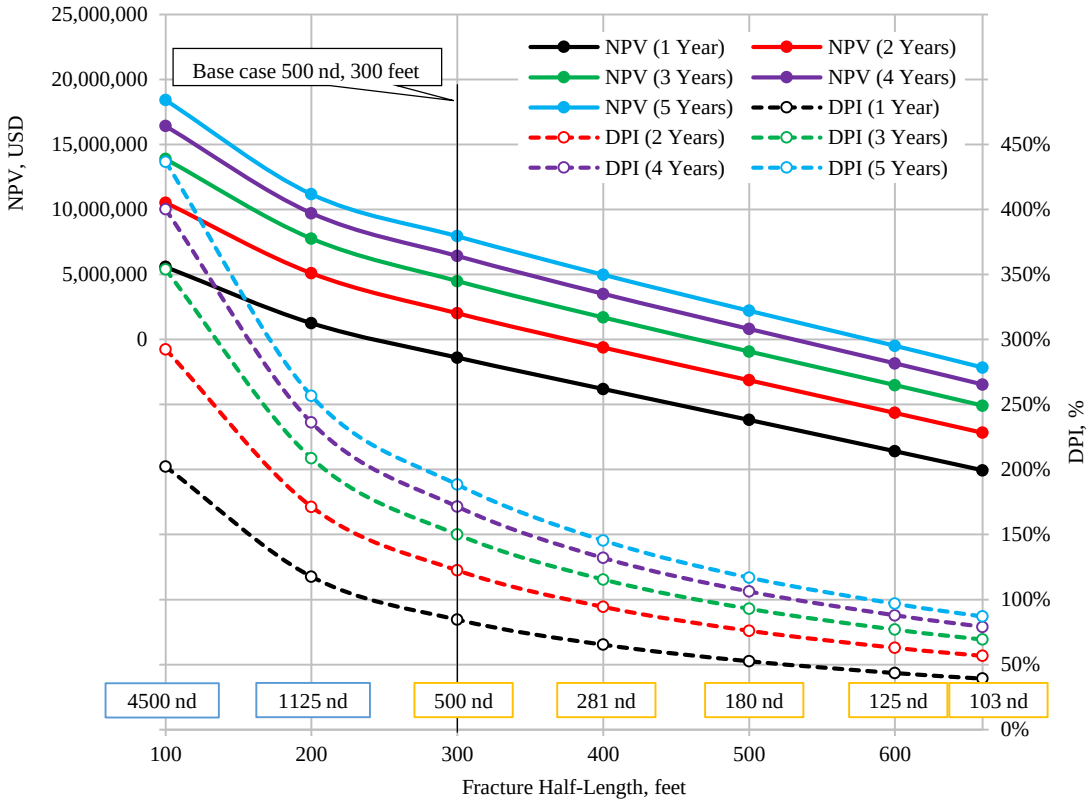

Fig. 6.24 – NPV and DPI in oil system with constant PI. Fracture half-length and reservoir permeability are changed simultaneously. Yellow and blue boxes represent the permeabilities typical for shale and conventional reservoirs respectively.

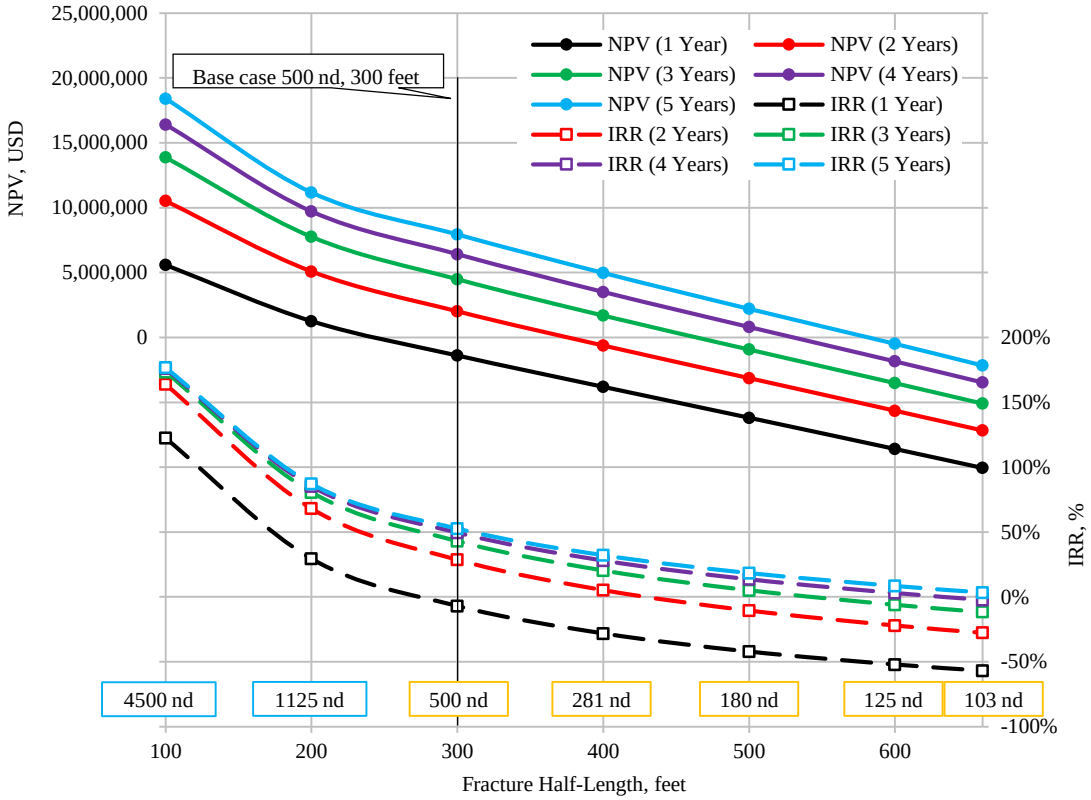

Fig. 6.25 – NPV and IRR in oil system with constant PI. Fracture half-length and reservoir permeability are changed simultaneously. Yellow and blue boxes represent the permeabilities typical for shale and conventional reservoirs respectively.

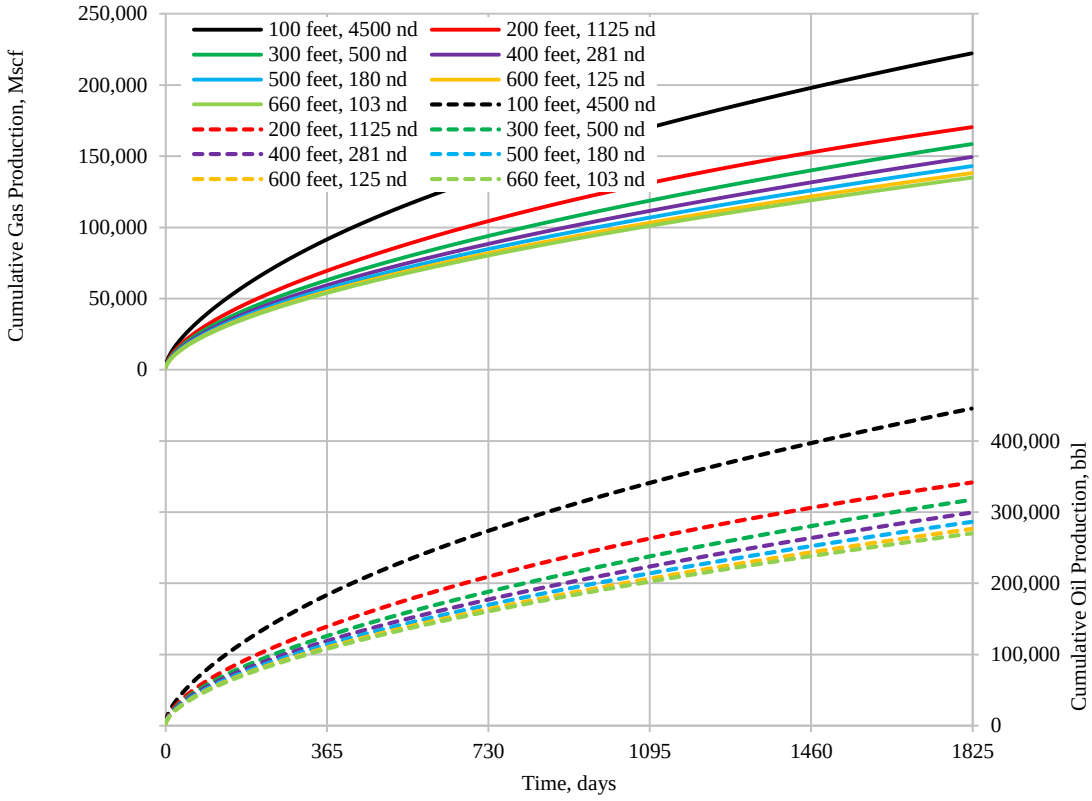

Fig. 6.26 – Cumulative oil and gas production in oil system with constant PI. Values monotonically increase from low-permeable to high-permeable cases.

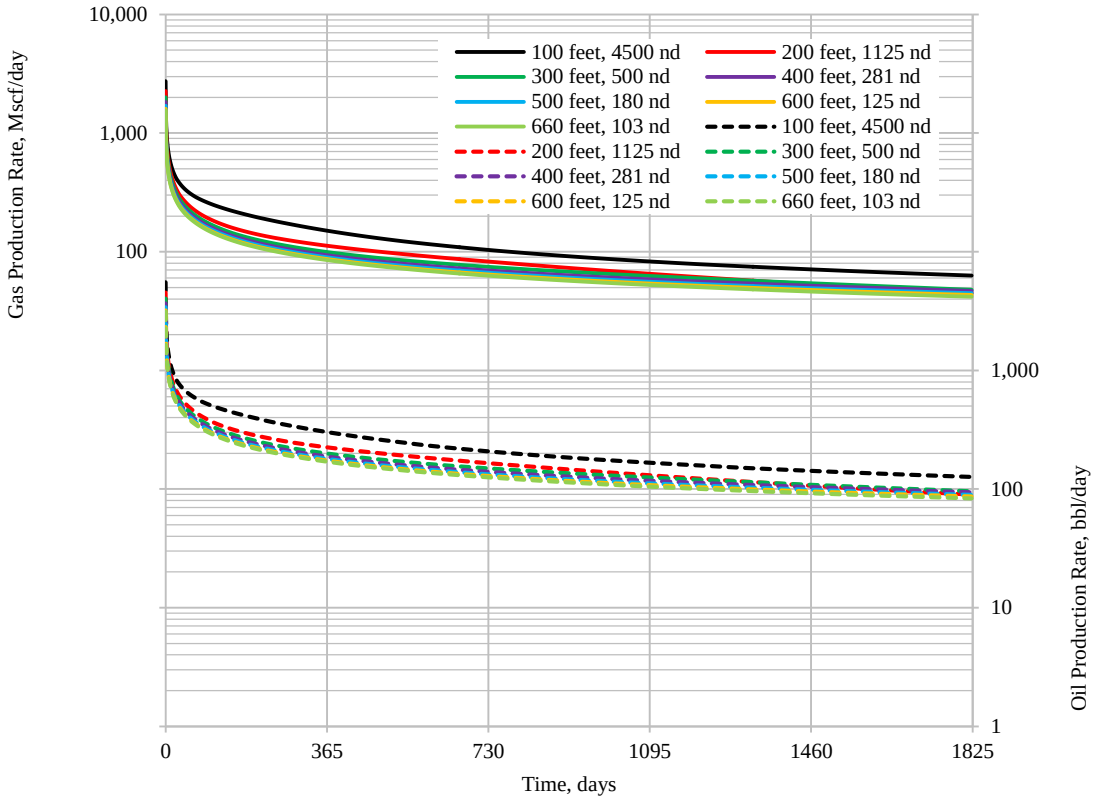

Fig. 6.27 – Oil and gas production rates in oil system with constant PI. Rates monotonically increase from low-permeable to high-permeable cases. Oil and gas rates for 103–1,125 nd cases are almost identical after 4 years.

Chapter 7

Additional Simulations Results

7.1 Effect of Gas Desorption in Dry Gas System

Gas desorption is a process of releasing gas adsorbed on the surface of rock matrix. This effect was carefully studied in coalbed methane reservoirs where the amount of free gas is very low (due to low porosity and high initial water saturation) and the gas production solely depends on the gas desorption from the matrix (Jukes et al., 2012). The same principle can be applied for shale gas reservoirs with low porosity and permeability. Including desorption effect into simulation model could positively change the project's economy by increased gas production.

Typically, the desorption processes is described by Langmuir isotherm curve (Yu and Sepehrnoori, 2014; Jukes et al., 2012; Marongiu-Porcu et al., 2013). Isotherm curve depends on two important parameters: Langmuir volume and Langmuir pressure. Langmuir volume is the maximum amount of gas that can be adsorbed to coal or shales at infinite pressure. Langmuir pressure specifies pressure at which half of the Langmuir volume can be adsorbed ("Langmuir Isotherm", 2014). **Eq. 24** describes Longmuir isotherm as:

$$C_g = \frac{V_L p}{p_L + p} \quad \text{.....(24)}$$

where:

$C_g =$ Volume of adsorbed gas, scf/ton

$V_L =$ Langmuir volume, scf/ton

$p_L =$ Langmuir pressure, psia

$p =$ reservoir pressure, psia

One of the assumption behind Langmuir isotherm is at the maximum adsorption only a monolayer of gas can be created ("Adsorption Isotherm", 2015). SENSOR simulator implements adsorption effect by including a trace of immobile oil in the model to represent the monolayer and saturate it with adsorbed gas ("Sensor Reservoir Simulator Manual", 2011). By introducing immobile oil saturation in order of 0.001, PVT black-oil table values for solution gas should be recalculated according to **Eq. 25:**

$$R_s = C_g \frac{0.17525\rho_s}{\phi S_o} \quad \text{.....(25)}$$

where:

$R_s =$ solution gas, scf/STB

$C_g =$ volume of adsorbed gas, scf/ton

$\rho_g =$ bulk shale density, g/cm^3

$\phi =$ porosity, fraction

$S_o =$ artificial oil saturation, recommended 0.001, fraction.

Yu and Sepehrnoori (2014) stated that Langmuir pressure has less effect on the production performance of the reservoir than Langmuir volume. Early production was less affected by gas desorption due to high average reservoir pressure. In a longer period the total additional contribution from gas desorption to the cumulative production was about 10% after 30 years.

We performed analysis to assess the contribution of desorption to the cumulative gas production in 5 years period and compute the economic effect from it. Three different Langmuir pressure and volumes are used for the sensitivity: 25, 50 and 75 scf/ton for Langmuir volume and 1,000, 1,500 and 2,000 psia for Langmuir pressure.

Figs. 7.1–7.2 show cumulative gas production with different Langmuir volumes and pressures. We can observe that change in Langmuir volume has more significant effect than change in Langmuir pressure. Increase of Langmuir volume by 25 scf/ton yield increase in cumulative by 2.5% in average. At the same time, increase of Langmuir pressure by 1,000 psia would only increase production by about 1%. This mean that cumulative production more sensitive to changes of volume rather than pressure.

Figs. 7.3–7.4 show model performance depending on different adsorption parameters. Maximum incremental NPV of 1.6 million USD achieved for Langmuir pressure of 1,500 psia and Langmuir volume of 75 scf/ton. Average incremental NPV for all six cases is 1.1 million USD. Best DPI yields 227% which is higher than no adsorption case by 18%. Average increment in DPI equal to 12%. Best increment of IRR is 8.5% with average increment for six cases equal to 5.6%

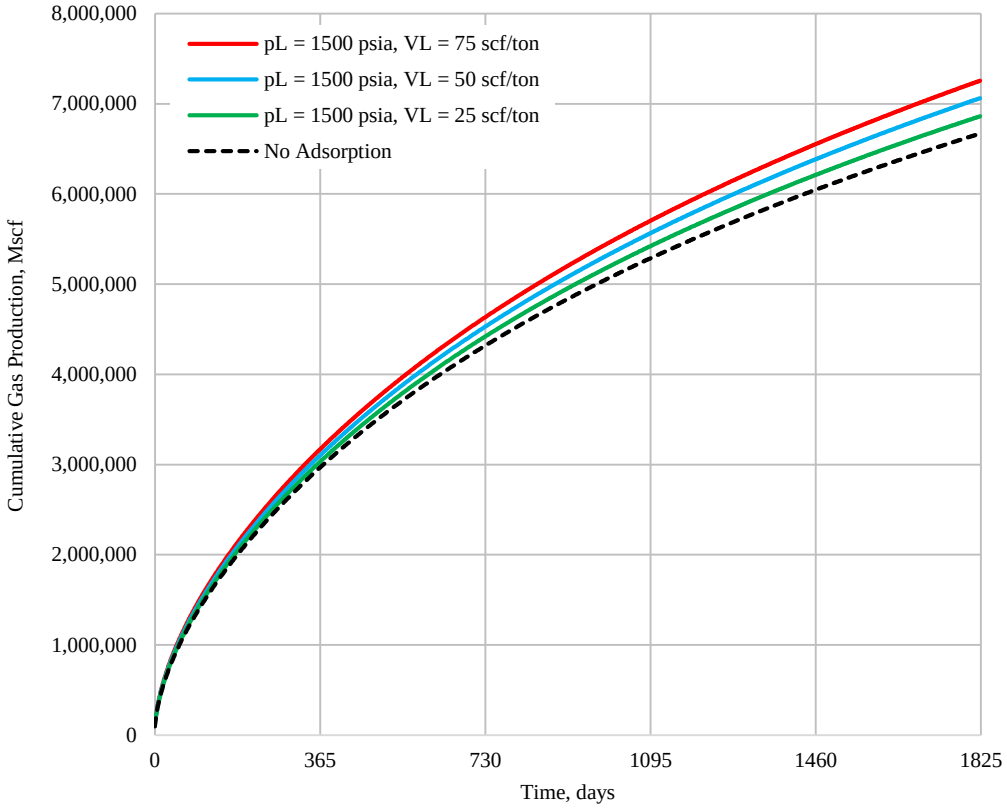

Fig. 7.1 – Cumulative gas production in dry gas system with adsorption and constant Langmuir pressure.

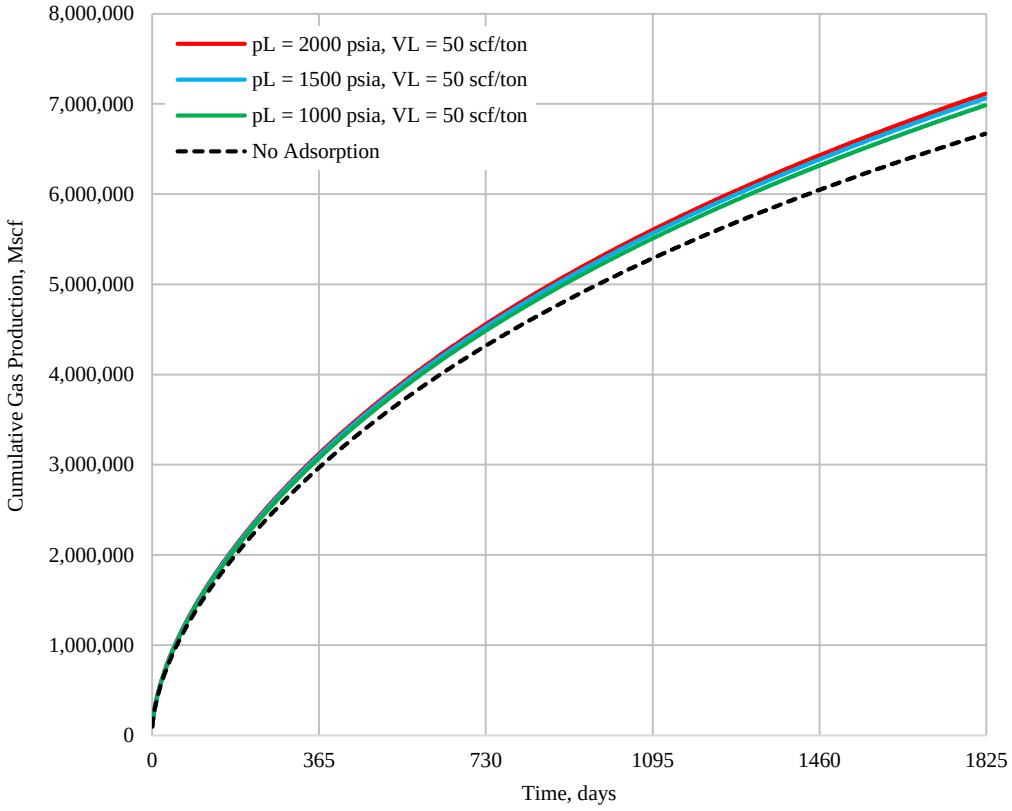

Fig. 7.2 – Cumulative gas production in dry gas system with adsorption and constant Langmuir volume.

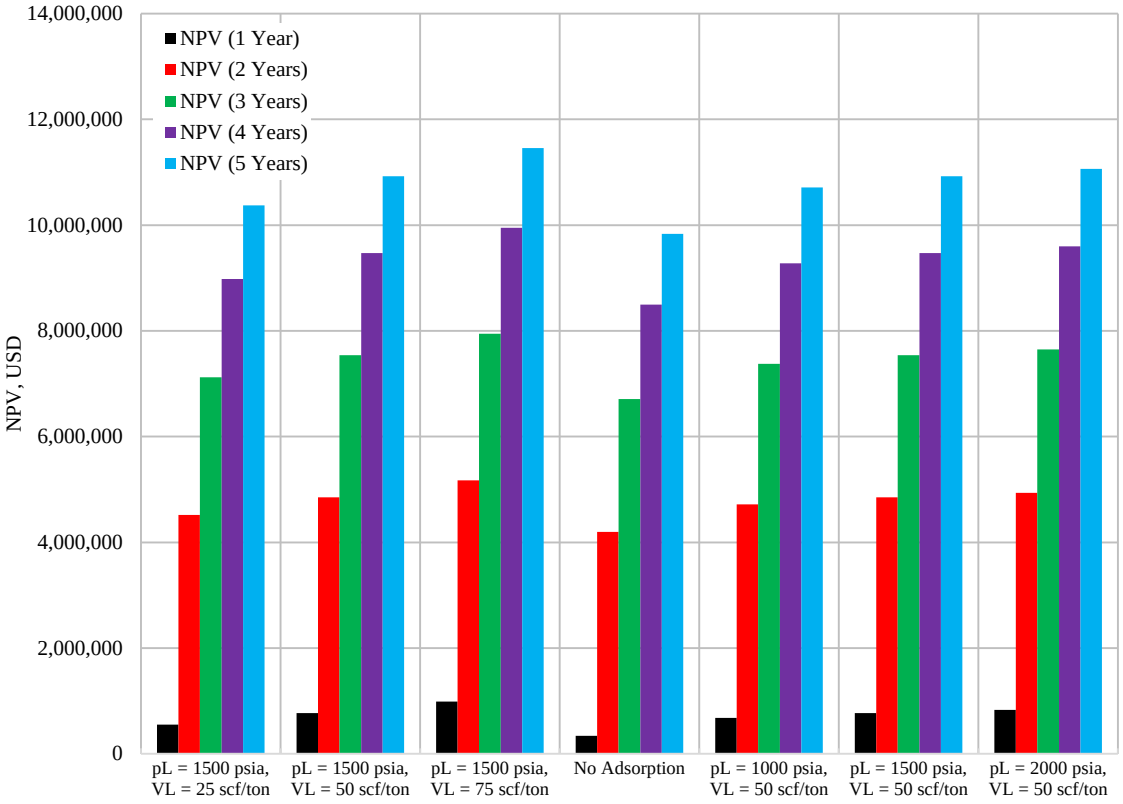

Fig. 7.3 – NPV in dry gas system with adsorption and different Langmuir pressures and volumes.

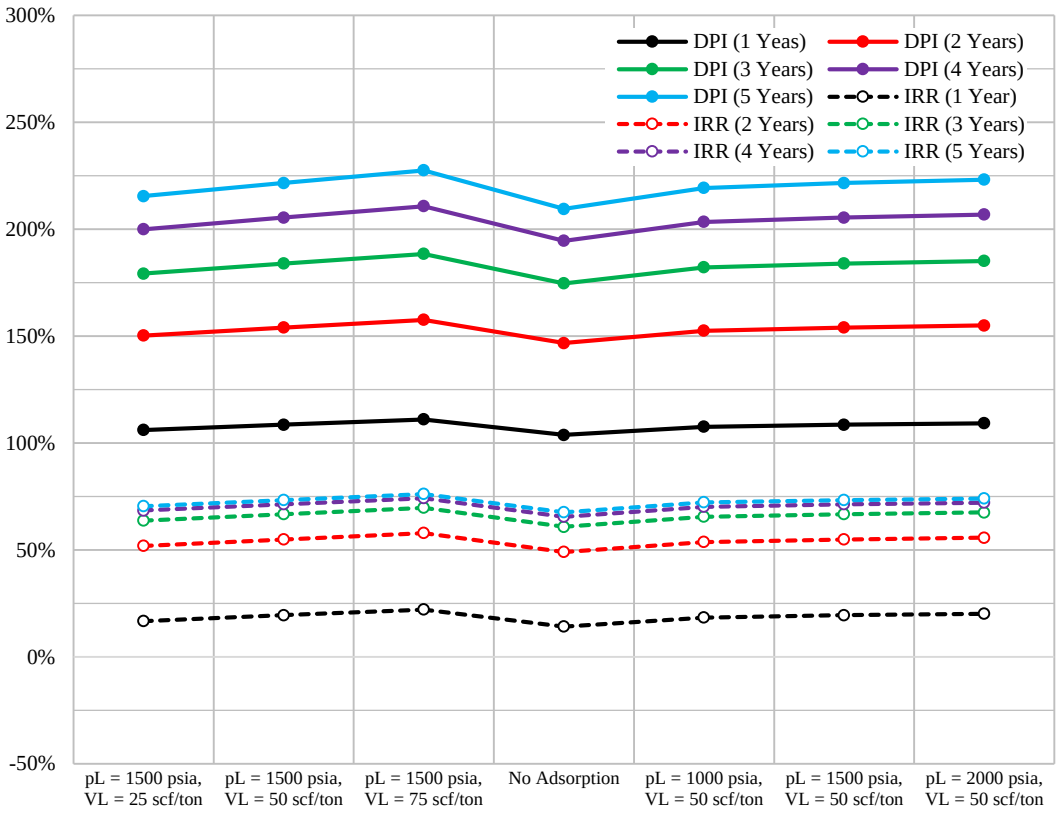

Fig. 7.4 – DPI and IRR in dry gas system with adsorption and different Langmuir pressures and volumes.

7.2 Commodities Price and Capex Changes

Global economy and market situation, political decisions, regional instability and many other factors have direct and indirect influence on the commodities prices. In the last 8 years, global market was shocked twice by rapid fall in crude oil prices (Fig. 2.7). Only 6 years passed since recession caused by World Economic Prices and again BRENT oil price falling from stable 100–110 USD/bbl to 50–60 USD/bbl. This instability requires careful assessment of shales economy assuming the prices for oil and gas could change significantly. Therefore, it is important to quantify the effect of changed hydrocarbon prices on project's economy.

We assumed three different scenarios: low prices, base case and high prices. Base case assumes oil price equal to 65 USD/bbl and natural gas price equal to 3.5 UDS/Mscf. Low and high price scenarios are based on the most pessimistic and optimistic forecast from Figs. 2.9–2.10. Thus, low prices assume oil price of 50 USD/bbl and gas price of 2.8 USD/Mscf. High price scenario based on oil price of 85 USD/bbl and gas price of 4.5 USD/Mscf. In addition, we introduced capital expenditures as a variable for both high and low scenario. The total costs can be higher or lower by 15% and 30%. Unfortunately, we could not find any publication regarding the correlation between the commodities prices and drilling and completion costs. However, we assume that Capex variation within 30% covers possible real situation.

Figs. 7.5–7.6 show NPV, DPI and IRR of gas condensate base case well completion with different oil and gas prices and Capex change. While base case yields about 9.8 million USD of NPV, minimum and maximum achievable NPV are 5.7 and 15.5 million USD. Monotonic growth of NPV indicates that commodities prices have higher effect on net present value change than Capex correction with 30%. Comparing base case and low price scenario without Capex correction we observe decrease of NPV by about 43% following change in oil and gas prices by -23% and -20% respectively. Increased oil and gas prices by 30% and 28% would add about 56% to NPV comparing with base case.

DPI and IRR does not show monotonic behavior for all cases. Base case yields about 211% of investment efficiency and 67% of internal rate of return. The worse performance achieved 164% and 43% for DPI and IRR, while the best performance yields 273% and 100% respectively. It is noticeable that high price case indicate higher NPV comparing with base case, but correction of Capex by 30% eliminate difference in DPI and IRR. Therefore, increase of oil and gas prices by 30 and 28% does not change project investment efficiency and internal rate of return if Capex prices grow as well. Likewise, to maintain DPI and IRR at the same level in case of low prices, capital expenditures should be reduced by about 22-23%.

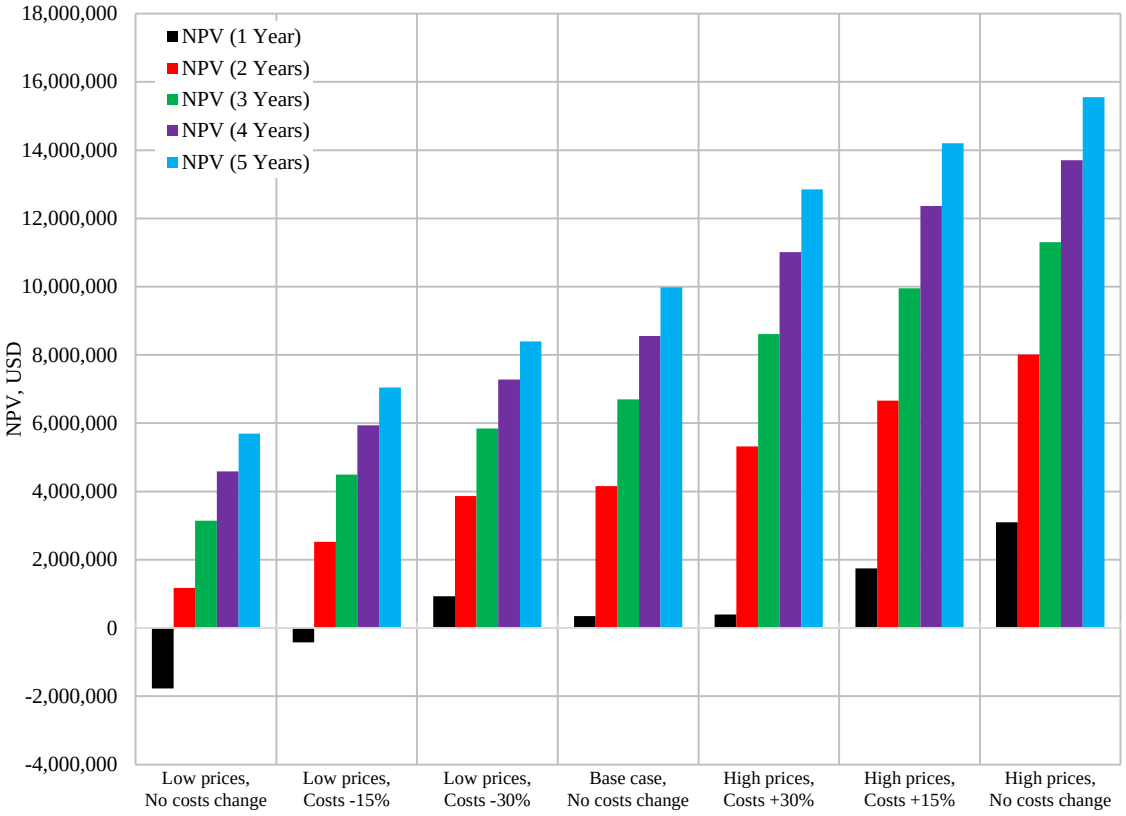

Fig. 7.5 – NPV in gas condensate system for different commodities prices and Capex.

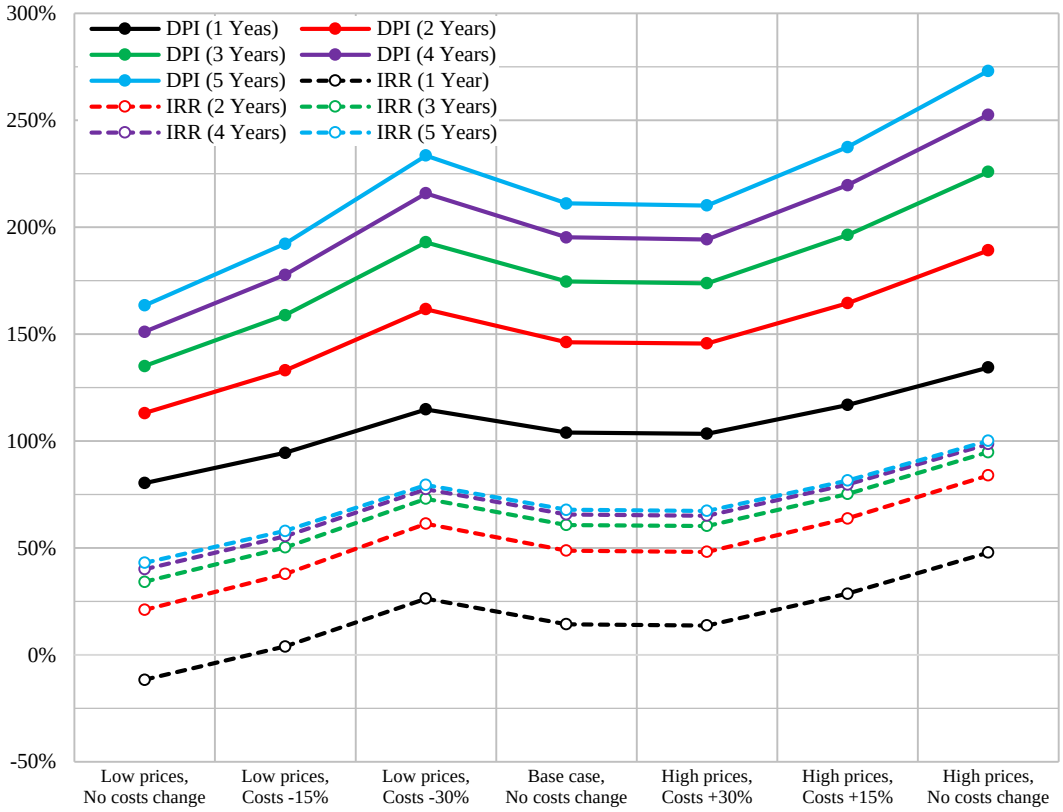

Fig. 7.6 – DPI and IRR in gas condensate system for different commodities prices and Capex. Increase of Capex by 30% together with high oil and gas prices yields the same performance as for base case.

7.3 Optimal Well Spacing

For this sensitivity we look for the best completion design for a development area of 1×2 mi to find the optimal numbers for shale production. We analyze economic performance for two type of wells: short completion with 5,280 ft horizontal section and 20 fractures and long completion with 10,560 ft section and 40 fractures. Based on sensitivities shown in Chapters 4–6, we assume the performance of both well completions identical if the fracture half-length is kept constant. We specified three different sets of well with fracture half-lengths of 660, 330 and 165 ft giving well spacing of 1,320, 660 and 330 ft. One long well or two short wells required to cover extend of the development area. Then the performance of a single well multiplied by the total number of wells on the segment. The example of short well placement with 660 feet fractures is shown on **Fig. 7.7**.

Depending on the maximum fracture half-length, there are three options for total number of wells required per development area: (1) 4 long wells or 8 short wells with 660 ft fracture half-length; (2) 8 long or 16 short wells with 330 ft fracture half-length; (3) 16 long and 32 short with 165 ft fracture half-length. Total associated costs for all wells are shown on **Fig. 7.8.**

Figs. 7.9–7.10 show NPV, DPI and IRR in dry gas system for different well completion scenario and number of wells. After 5 years, the best NPV performance corresponds to 330 ft fracture half-length (660 ft well spacing). Total revenues is 135.9 million USD for long well scenario and 125.7 million USD for short well scenario. Best DPI metric achieved for long completion with 195% investment efficiency. Corresponding IRR equals to 64%. However, short completion with the same acreage show DPI and IRR performance lower than long and short completion with fracture half-length of 660 ft.

Figs. 7.11–7.12 show the same metrics in gas condensate system. 5 years NPV shows that both 330 and 660 ft fractures indicate relatively close results ranging between 129.1 and 145.4 million USD. The best performance achieved for long completion with 660 ft fracs with 145.4 million USD. Both short completion with 660 ft fracs and long completion with 330 ft fracs indicated almost identical results of 139.2 million USD. However, DPI and IRR has a distinct preferable option. Long and short completion with 660 ft fractures achieve investment efficiency between 206% and 214%. Corresponding IRR is about 72% in average. Other acreage options show significant decrease in DPI and IRR metrics and less preferred for gas condensate systems.

Figs. 7.13–7.14 present performance of oil model. Best NPV performance indicated for long and short completion with 330 ft fractures and long completion for 165 ft fractures. Corresponding net present values are 130.7, 120.5 and 118.9 million USD. Highest investment efficiency achieved for long and short completion with 330 ft fractures and long completion with 660 ft fractures. DPI values for these options are 192%, 179% and 176% with corresponding internal rate of return in between 47–55%. Therefore, optimal solution would be based on fracture half-length of 330 ft with long completion.

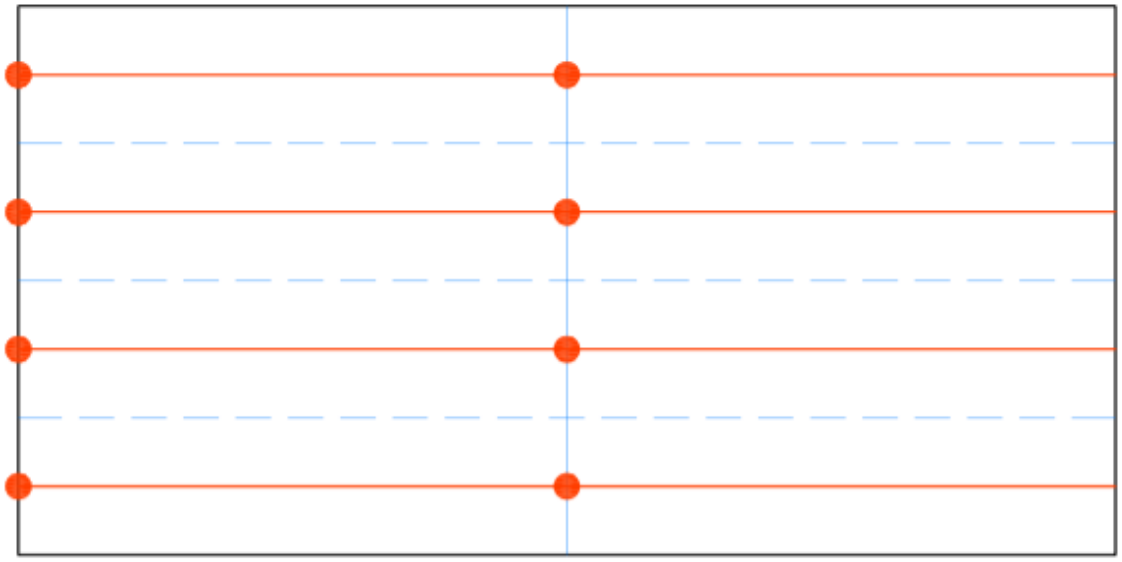

Fig. 7.7 – Example of placement of 8 short wells with 660 ft fractures (well spacing is 1,320 ft).
Black area represents 1×2 mi segment, blue dash line represent single well drainage area, red line shows wellbore, red dot shows wellhead.

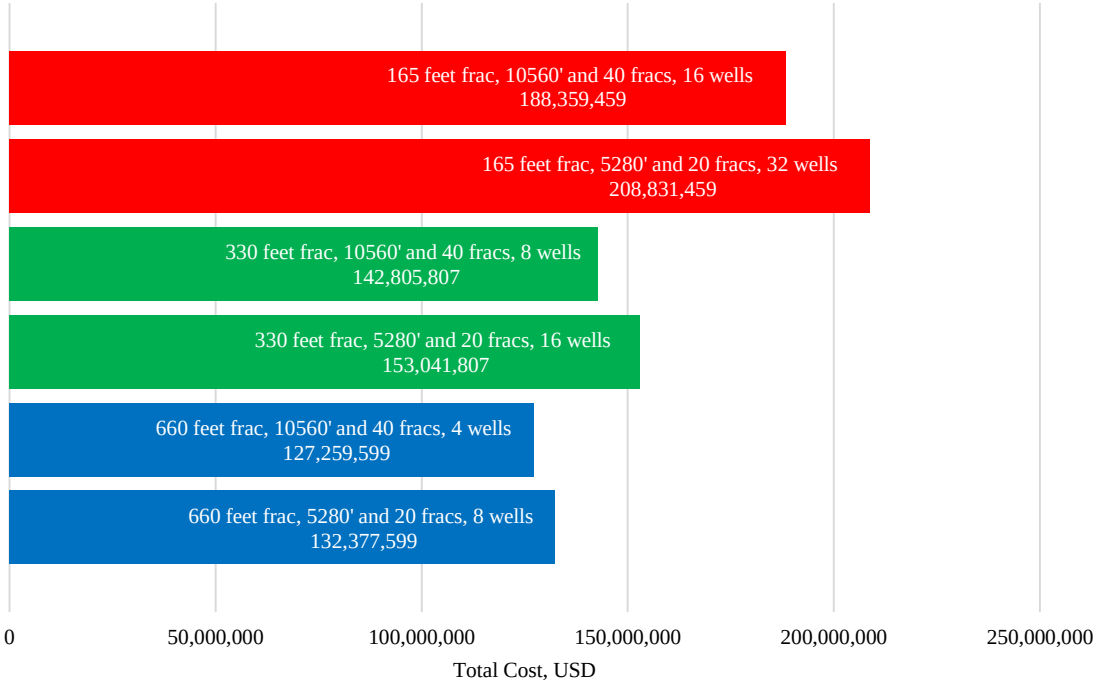

Fig. 7.8 – Total Capex for long and short wells to cover development area of 1×2 mi with different fractures.

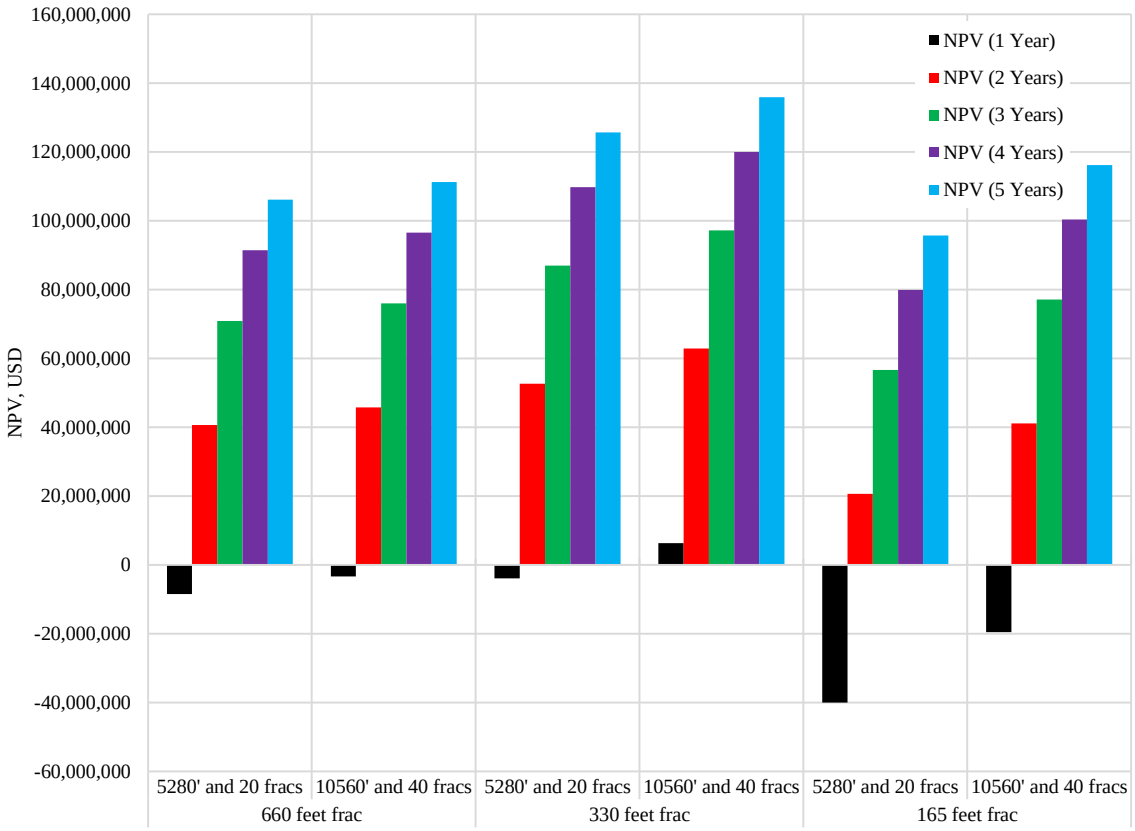

Fig. 7.9 – NPV in dry gas system for different single well acreage and long or short completion. Best performance achieved for10,560 ft completion with 330 ft fractures.

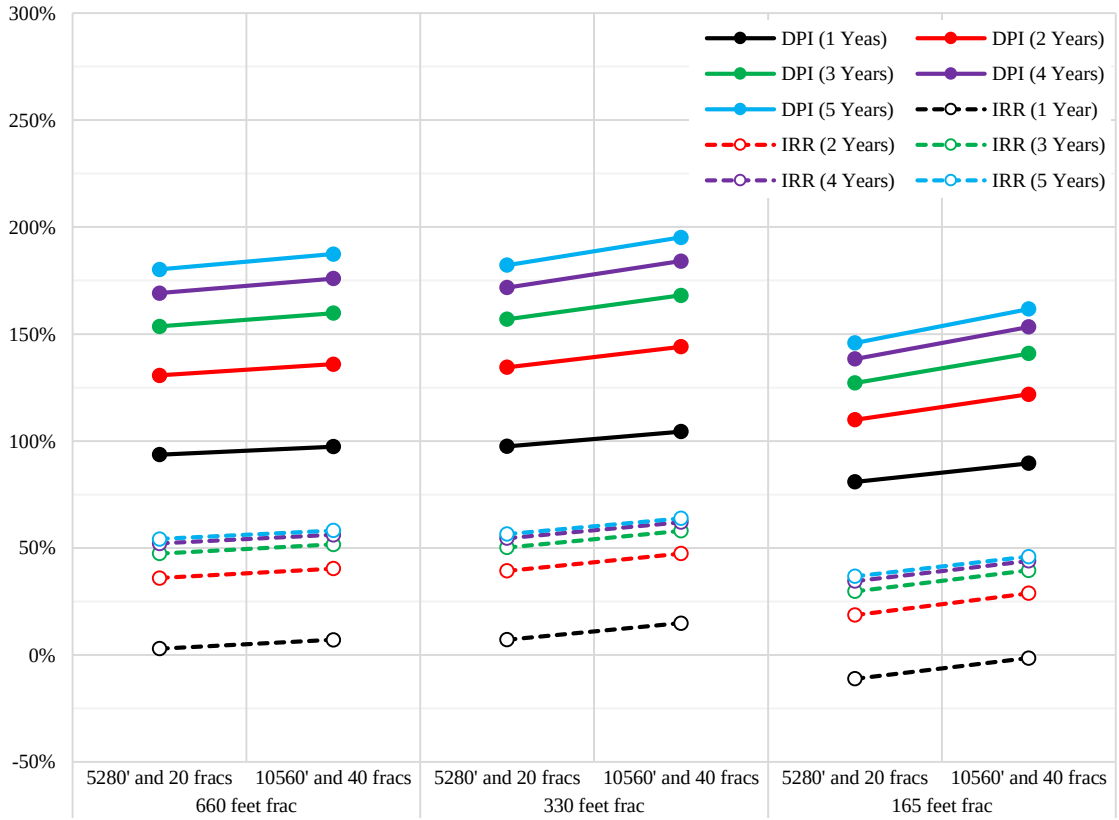

Fig. 7.10 – NPV and IRR in dry gas system for different single well acreage and long or short completion. Best performance achieved for 10,560 ft completion with 330 ft fractures.

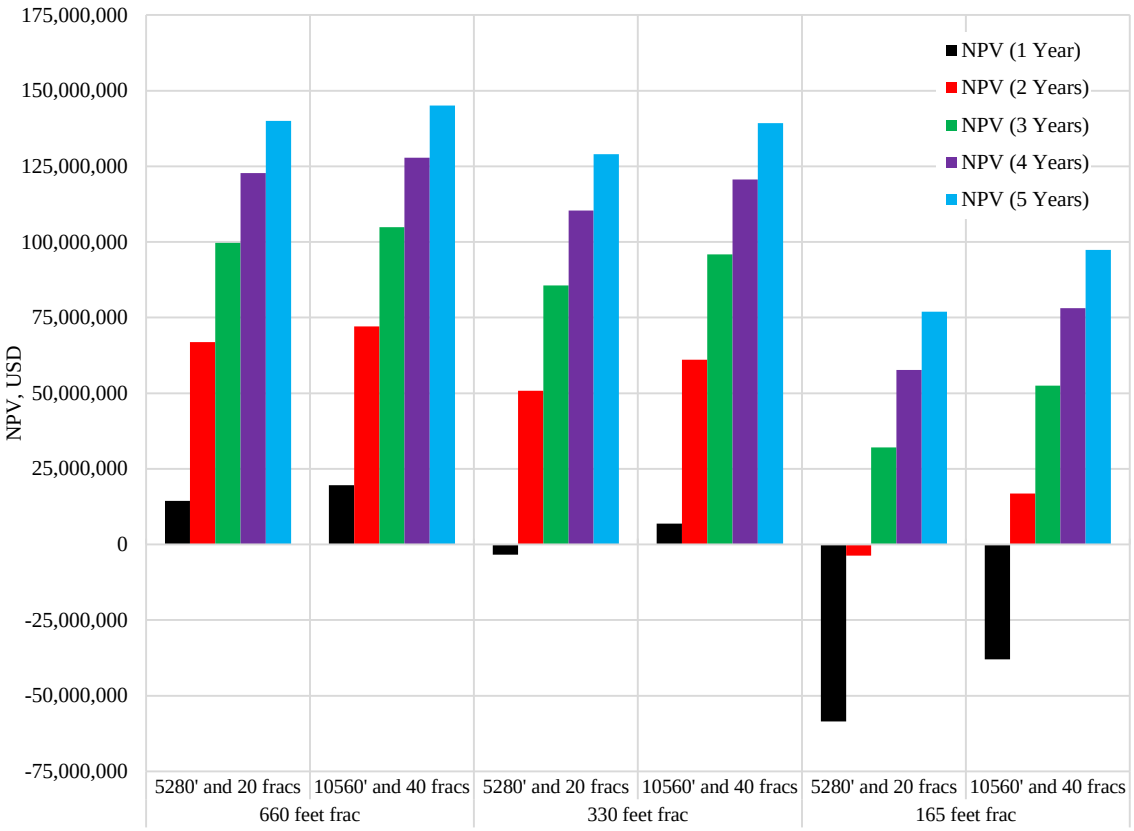

Fig. 7.11 – NPV in gas condensate system for different single well acreage and long or short completion. Best performance achieved for 10,560 ft completion with 660 ft fractures.

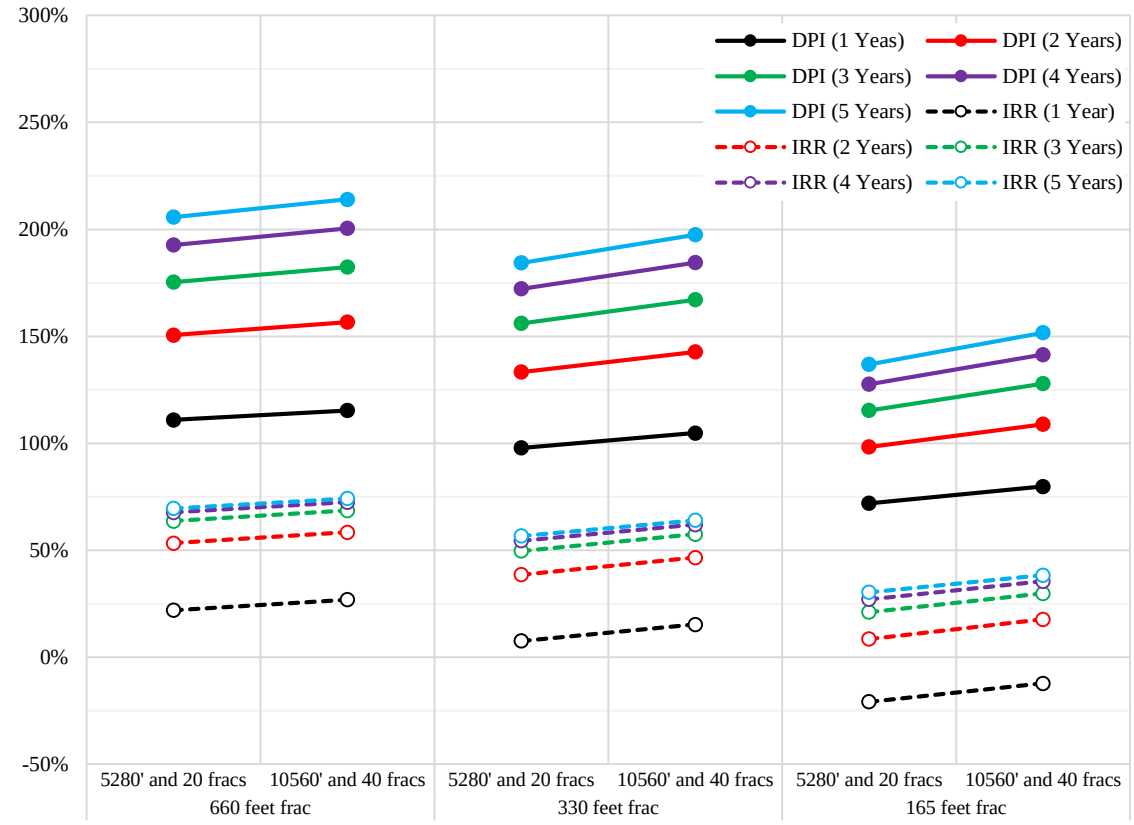

Fig. 7.12 – NPV and IRR in gas condensate system for different single well acreage and long or short completion. Best performance achieved for 10,560 ft completion with 660 ft fractures.

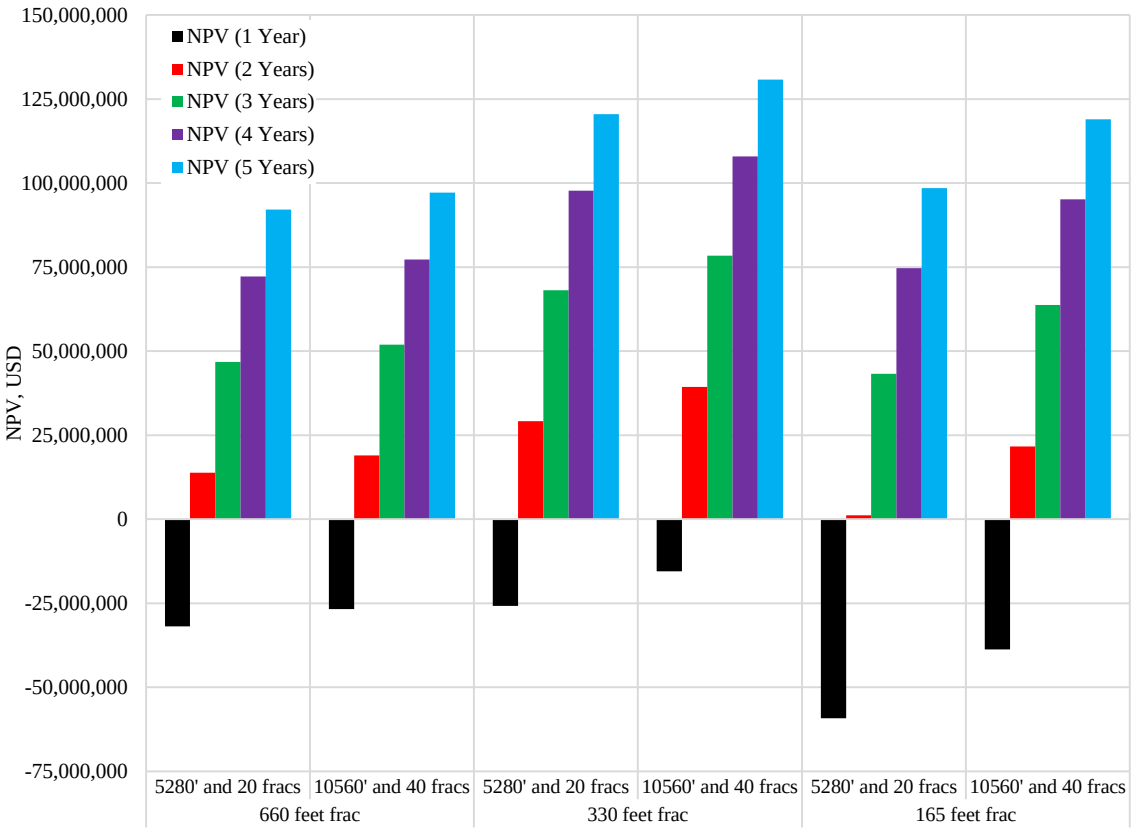

Fig. 7.13 – NPV in oil system for different single well acreage and long or short completion. Best performance achieved for 10,560 ft completion with 330 ft fractures.

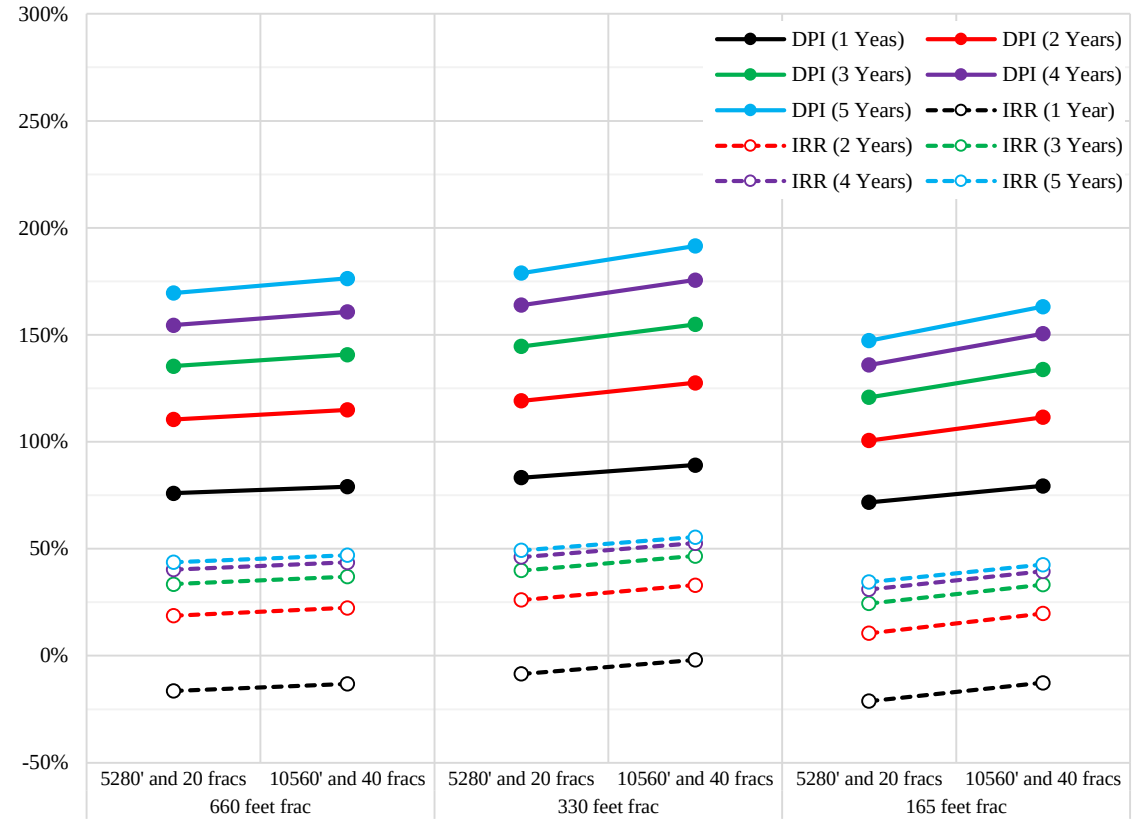

Fig. 7.14 – NPV and IRR in oil system for different single well acreage and long or short completion. Best performance achieved for 10,560 ft completion with 330 fractures.

7.4 Effect of Stress Dependent Transmissibilities

The decision to include stress dependent transmissibilities can significantly influence on the numerical model performance. By stress we understand the difference between initial reservoir pressure (overburden pressure) and actual pressure in the cell. Physically, by including stress dependency we agree that total fracture area is reducing with time due to pressure depletion of the reservoir. Such effect should result into increased liquid drop-out around stimulated area due to more rapid pressure drop. Ultimately, with very severe stress dependency, flow to the fracture area will be substituted by radial flow to the wellbore only. In this case, increased mobility of oil allow to produce higher volumes of liquid from gas condensate reservoirs. At the same time, gas production can be affected negatively. To quantify the possible effect of including stress dependencies we performed additional set of simulations in gas condensate system.

Figs. 7.15–7.16 show performance of base case scenario with and without stress dependent transmissibilities. Cumulative oil production is higher when including stress dependency by almost 11% to the case when dependency is not included. At the same time, cumulative gas production was lower by almost 14%. Gas production rate for stress dependent case was below stress independent case during all simulation time. Oil production rates are have no difference after approximately 2.5 years of production. Therefore, additional oil mobility resulted in restriction of gas flow to the wellbore.

Fig. 7.17 illustrate the difference in producing GOR and OGR for two both cases. Whitson and Sunjerga (2012) presented results without stress dependent transmissibilities showing that OGR trend increases over the time. Including of stress dependency yields higher initial OGR which decreases over the time. After 5 years both models approach almost the same values. Base case for both models yield almost the same NPV, DPI and IRR meaning that additionally produced oil balanced the cash flow from reduced gas production.

To observe the difference in sensitivity results when pressure transmissibilities are not included, we made additional run for this case with different initial reservoir pressures. NPV and DPI results are shown in **Fig. 7.18**. Excluding stress dependencies yielded monotonic economic effect from increased reservoir pressure. It is noticeable, that the biggest difference between results here and in Chapter 5 achieved for pressure of 12,500 and 14,500 psia. However, the results for lower pressures in both models show relatively the same economic performance. It can be explained that magnitude of transmissibility modification depends on the initial reservoir pressure and the higher the initial pressure, the stronger the negative effect on the transmissibilities. For reservoirs with high initial pressure it yields very negative result in both oil and gas production. With pressure lower than 10,000 psia the difference between two models is not very dramatic.

Figs. 7.19-7.20 confirm monotonic dependence of total production of oil and gas. Excluding stress dependency yielded higher cumulative oil and gas production by 25% and 60% respectively comparing with model with stress dependent transmissibilities (see Figs. 5.8–5.9). It clearly confirms the negative effect of fracture area reduction on total production, even if early-time OGR is higher in stress dependent model.

Fig. 7.21 indicate that models with pressures between 2,500 and 7,500 psia show stable producing OGR level during the five years period. Slight increase can be observed during the first two years due to involvement of the area beyond the fracture into drainage process. This corresponds with the results published by Whitson and Sunjerga (2012). However, higher initial reservoir pressure indicate rapid decline in producing OGR. Starting with about 90 STB/MMscf, it drop to 60 STB/MMscf after few years for both 12,500 and 14,500 psia models. This can be explained by rapid depletion of the area beyond the fracture tip due to relative high initial permeability of 500 nd. By changing reservoir permeability to 100 nd we can achieve stable OGR level within 5 years for a wider range of initial reservoir pressures (**Fig. 7.22)**. Oscillations, observed for high initial reservoir pressures can be avoided by finer gridding of simulation area.

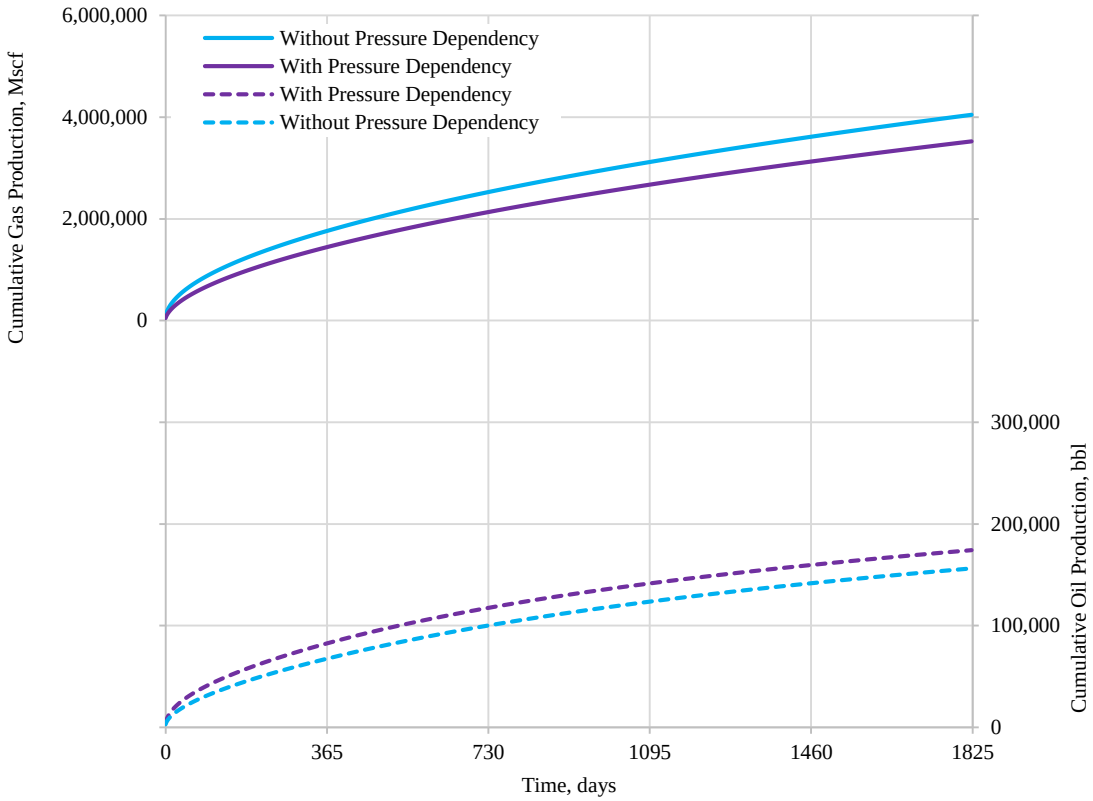

Fig. 7.15 – Cumulative oil and gas production for base case with and without stress dependent transmissibilities.

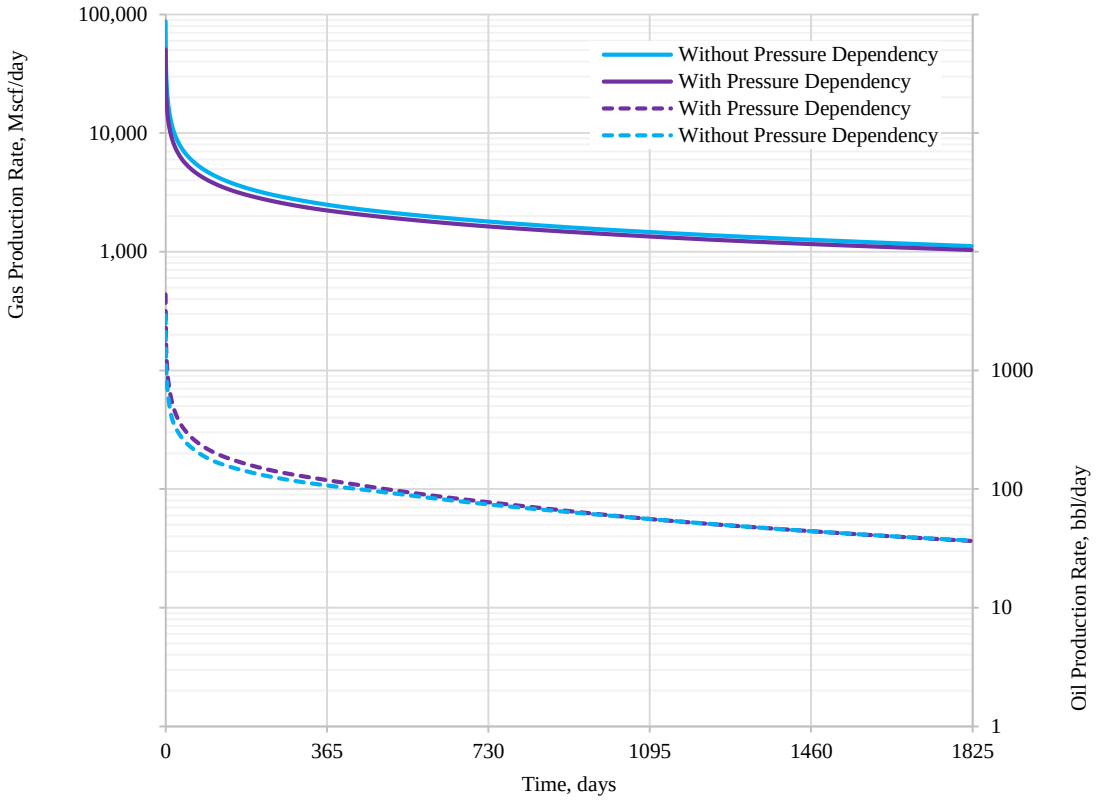

Fig. 7.16 – Oil and gas production rates system for base case with and without stress dependent transmissibilities. Oil production rates are identical after 2.5 years.

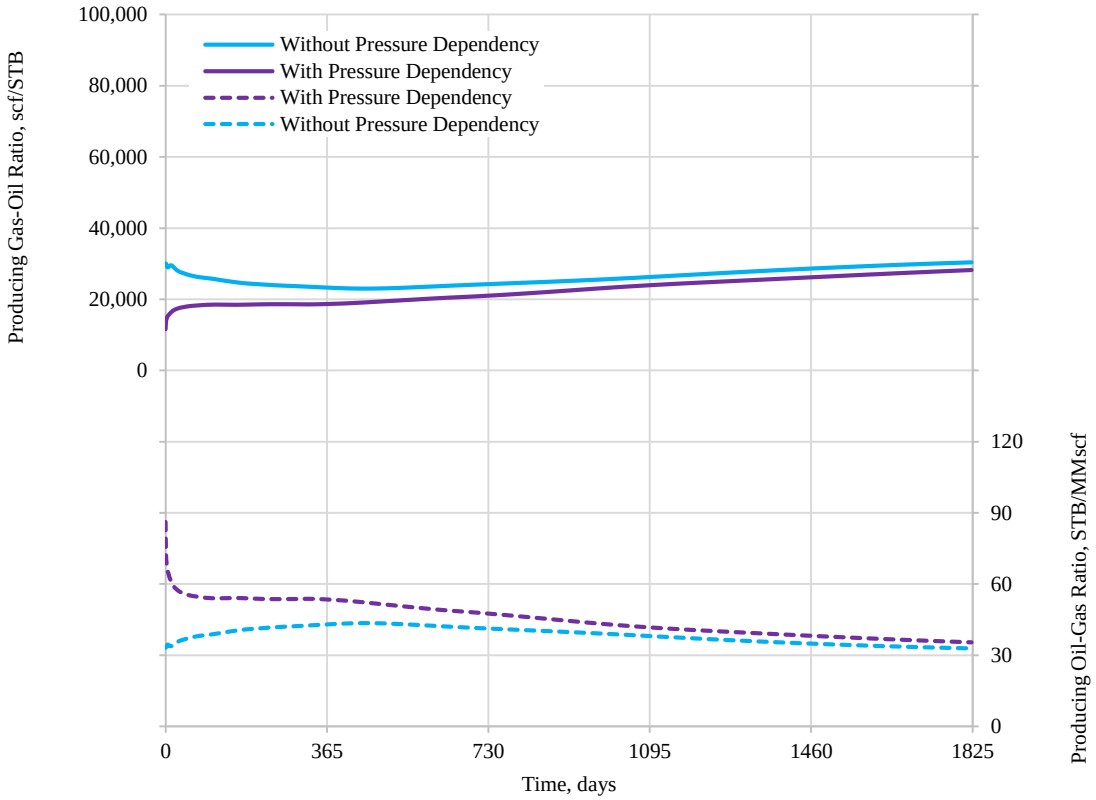

Fig. 7.17 – Producing GOR and OGR for base case with and without stress dependent transmissibilities. Initial difference in GOR and OGR is declining with the time.

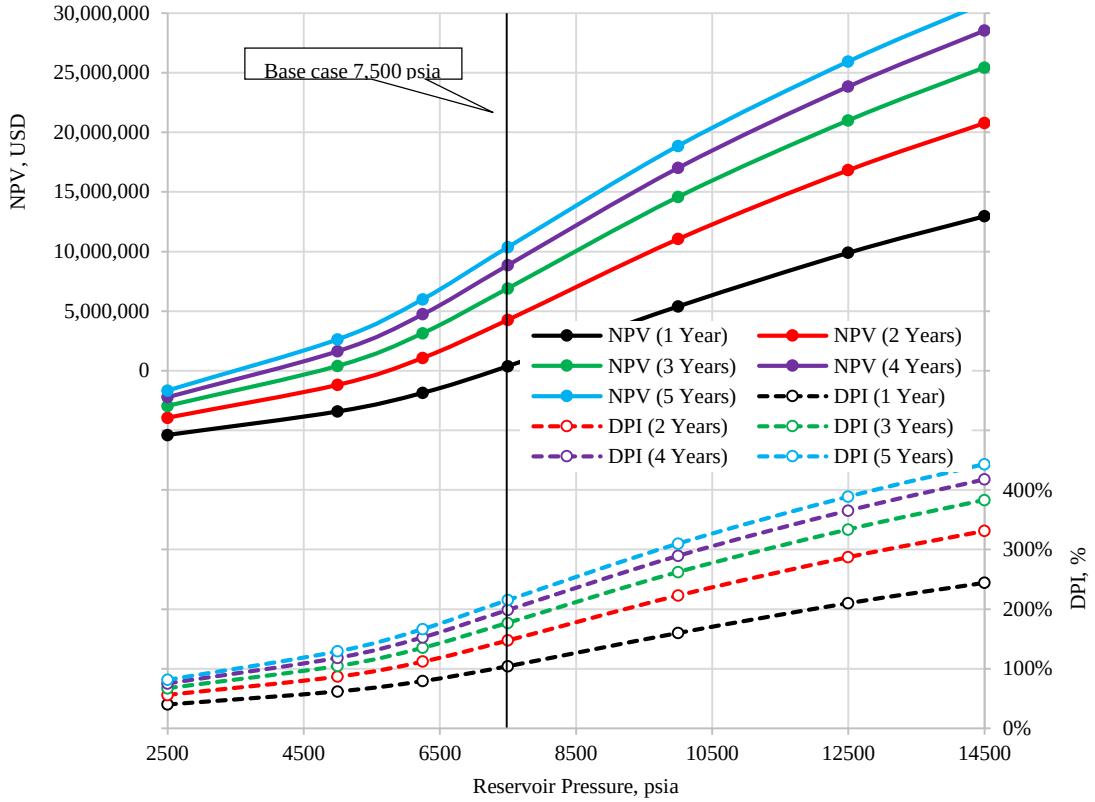

Fig. 7.18 – NPV and for base case without stress dependent transmissibilities. Results monotonically show advantage of higher initial reservoir pressure.

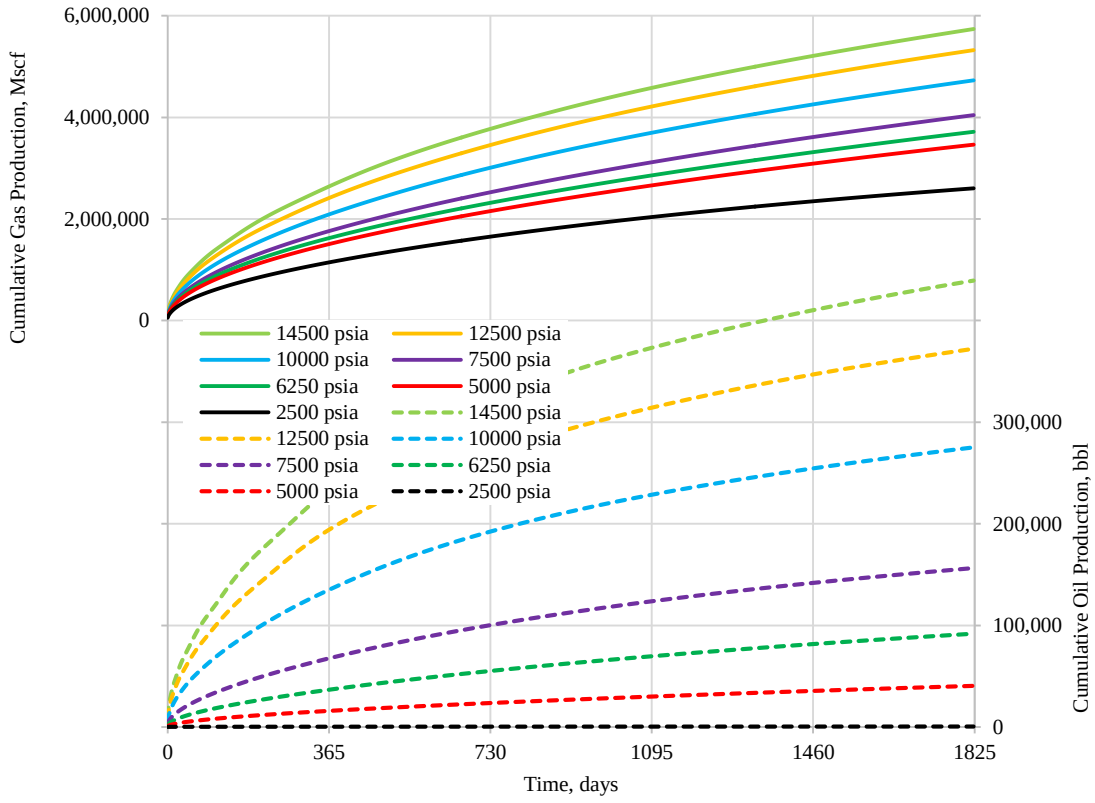

Fig. 7.19 – Cumulative oil and gas production for base case without stress dependent transmissibilities.

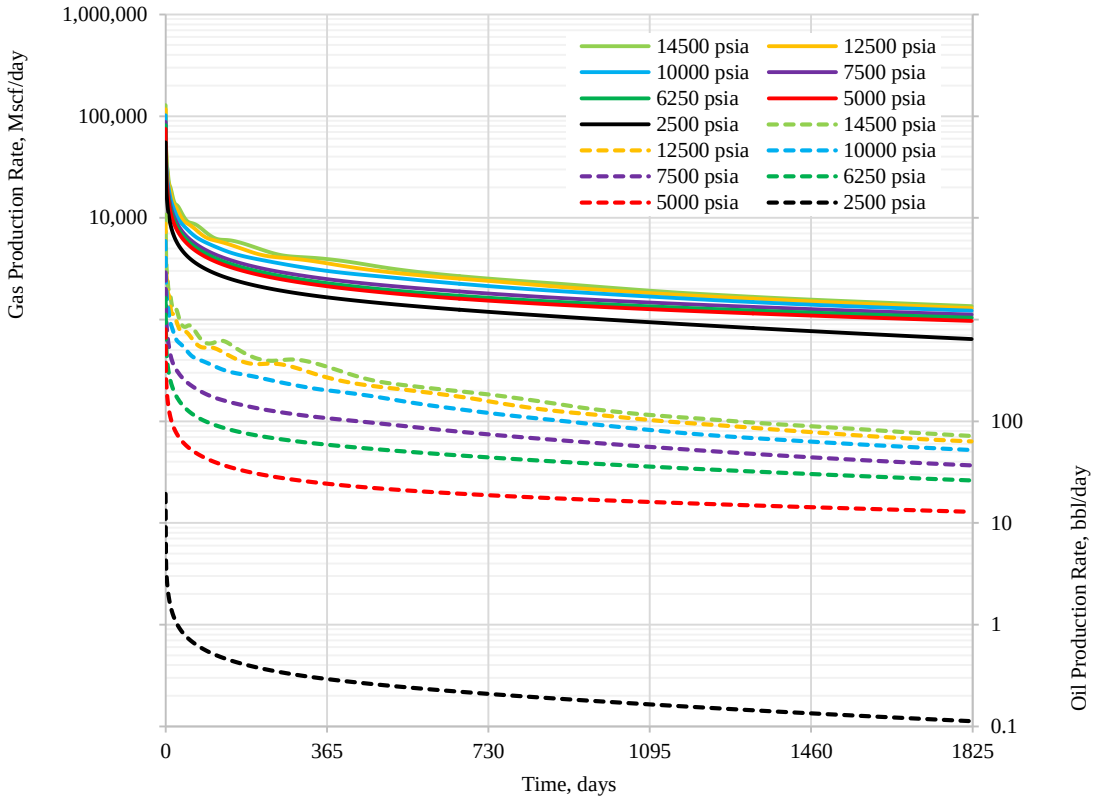

Fig. 7.20 – Oil and gas production rates for base case without stress dependent transmissibilities. Oscillations in 12,500 and 14,500 psia cases are due to numerical instability of the model and can be resolved by finer gridding.

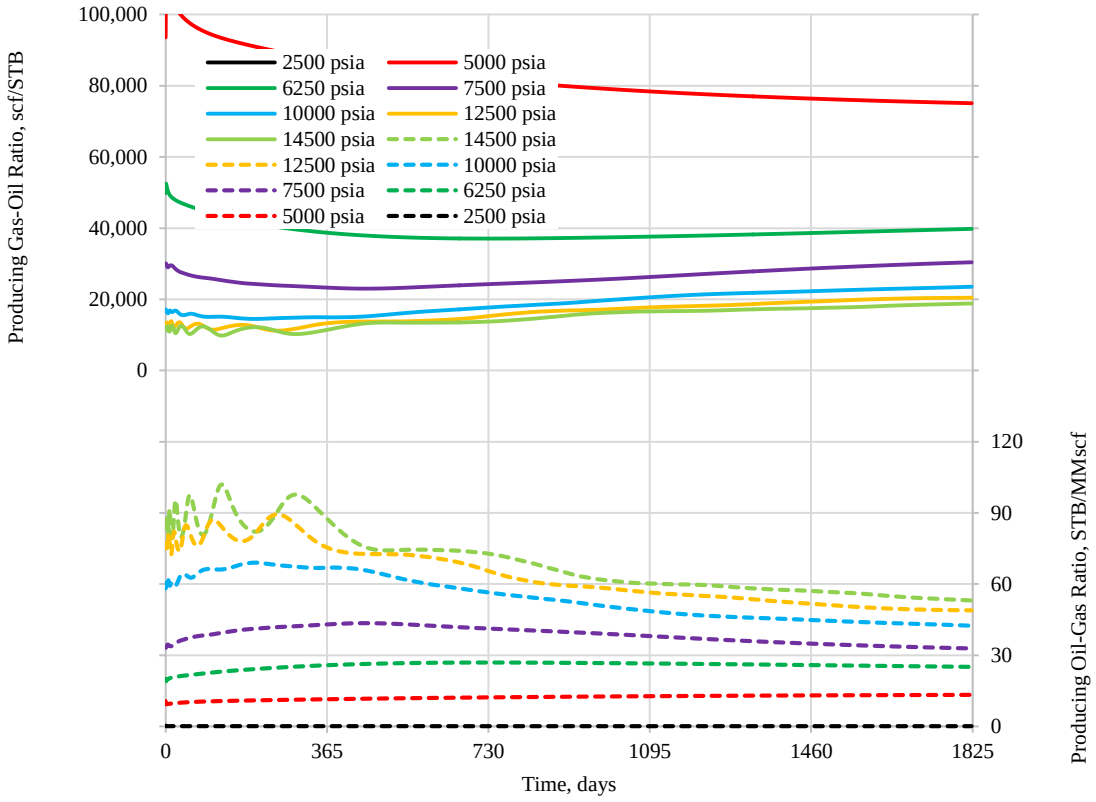

Fig. 7.21 – Producing GOR and OGR for base case without stress dependent transmissibilities. Decline in OGR for high pressures after 1 year is a result of accelerated depletion of the contributing area beyond fracture tip.

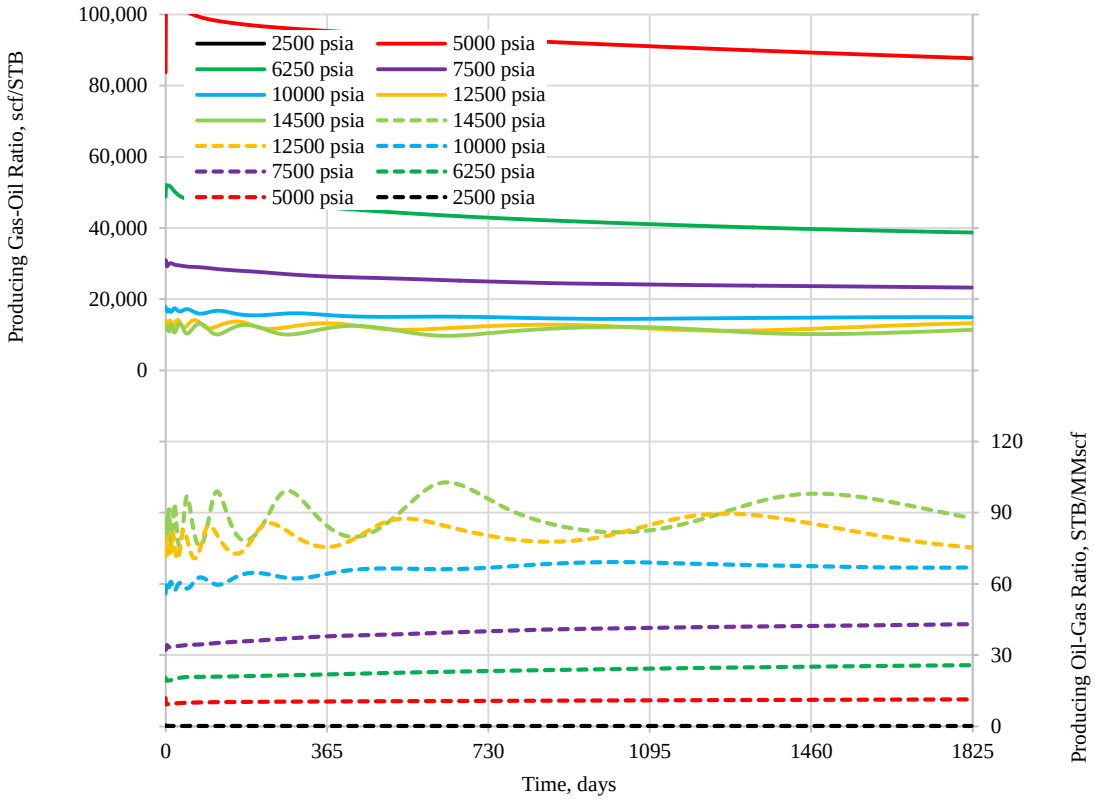

Fig. 7.22 – Producing GOR and OGR with 100 nd matrix permeability without stress dependent transmissibilities. For low permeability OGR slightly tipping up due to limited contribution from the area beyond the fracture. Oscillations are due to numerical instability and can be resolved by finer gridding.

THIS PAGE INTENTIONALLY LEFT BLANK

Chapter 8

Conclusions

The project achieved valuable results for economic assessment of shale development. Some results are not related to a specific reservoir or a well, but they can be used to help in evaluation of a company's specific projects. The following are the general conclusions which can be made based on the thesis:

1. Net present value should be supplemented by internal rate of return and discounted profitability index for more careful economic justification of a project. While net present value estimates the monetary profit from project implementation, discounted profitability index effectively shows the investments required to achieve a specific net present value and should be used by companies of any site. Internal rate of return helps to estimate the break-even cost of capital of the project and is important for small size companies with higher cost of capital investments.
2. Fluctuations of oil and gas prices call for additional attention to the economic planning horizon. With two significant oil price falls within the last 7 years, companies should optimize project economy in a 5–7 year scale rather than 20–30 year scale. This approach could also reduce payout time of the project and increase earlier cash flow for continuous drilling program.
3. The internal rate of return increment becomes insignificant after 3–4 years. Because of a rapid production decline within the first years and annual discounting effect, companies should not expect significant increase of internal rate of return after 4 years.
4. The sole use of net present value, discounted profitability index or internal rate of return in economic optimization can lead to a different optimal well completion and significantly different when optimizing total number of fractures or fracture half-length. Discounted profitability index tends to yield the highest investment efficiency in wells with lower capital expenditures while net present value and internal rate of return are the highest when early production is accelerated.
5. A longer well shows monotonically better economic performance compared with a shorter well when fracture spacing is kept constant if linear cost models are applied for horizontal length and a number of fractures. If the cost models are non-linear, the economic performance will be non-monotonic.

6. Including stress dependent transmissibilities only in the fracture can significantly influence the well performance. Fracture permeability approaches matrix permeability faster in a reservoir with higher initial pressure and a greater slope parameter *m*, due to higher stress in the fracture cells. The effect yields higher producing OGR at earlier time compared with the model without stress dependent permeabilities. However, from the models with stress dependency, cumulative oil and gas production can be lower by 25% and 60%, respectively.

The following conclusions are more specific and based on our model, described in Chapter 3. However, one can use them for economic assessment for other specific projects:

1. Matrix permeability has significant influence on the model performance and economics. Break-even permeabilities for dry gas, gas condensate and oil systems are 90, 120 and 130 nd respectively after 5 years of production. Longer production will not significantly affect break-even permeability values because of severe production decline and annual discounting effect.
2. Initial reservoir pressure has a non-monotonic effect on the reservoir performance and economics when including stress dependent permeabilities. Dry gas, gas condensate and oil systems indicated optimal initial pressures of around 7,500, 12,000 and 8,000 psia respectively. Higher initial pressure increases the in-situ fluid viscosity, causing additional pressure losses which overcome positive effect from increased initial fluid-in-place.
3. Break-even reservoir thickness varies between 90 and 110 ft for 5 years of production. Assuming that the fracture penetrates reservoir thickness completely, an additional 10 ft of the reservoir thickness increases NPV by 1 million USD in dry gas and gas condensate systems and by 0.7 million USD for oil system.
4. Fracture spacing affects the production behavior differently. Increased fracture spacing increases cumulative production in dry gas systems due to the boundary-dominated flow regime in the base case scenario. Meanwhile in an oil system, increased fracture spacing has no effect on total production due to the infinite-acting behavior of the reservoir.
5. Changing of bottomhole pressure in 500–3,500 psia range has little effect on economic performance of a gas condensate reservoir within the first year. Increased cash flow from additionally produced oil during this period overcomes the losses from decreased gas production. In 5 years, lower BHP yields better project economy.
6. The negative economic effect from low reservoir permeability cannot be balanced by increased fracture half-length while keeping productivity index of the well constant. The cost of maintaining constant PI in 103–1,125 nd reservoirs is significantly higher than economic outcome from increased oil and gas production.
7. Gas desorption in a dry gas model showed maximum increase of 8% in total gas production. Corresponding increments of net present values, discounted profitability index and internal rate of return are 18%, 12%, and 8.5% respectively. The desorption process is more sensitive to Langmuir volume than Langmuir pressure within our pressure range; difference in cumulative gas production was observed only after one year.

8. An increase in commodity prices by 30% will yield a positive economic effect until corresponding Capex increased by 60% for net present value, and 30% for discounted profitability index and internal rate of return. If oil and gas prices are 25% lower than the base case, the negative economic effect can be balanced through a 45% reduction in Capex for net present value and a 23% reduction for discounted profitability index and internal rate of return.
9. Well spacing sensitivity for a development area of 1×2 mi based on two short (5,280 ft) and one long (10,560 ft) completions indicated different required number of wells for optimal development. For all cases, the long completion option is more economically attractive than the short solution because cost models for different number of fractures and well horizontal length are linear. The economic optimum achieved with 16 long wells for the dry gas case, 8 long wells for gas condensate, and 16 long wells for the oil case per development area.

THIS PAGE INTENTIONALLY LEFT BLANK

Chapter 9

Recommendations and Further Work

It is recommended to select optimal shale well design using several economic metrics together. Net present value is a proven and well-known metric for economic assessment of a project, and can be reinforced by discounted profitability index and internal rate of return. Discounted profitability index seems to work more efficiently when coupled with net present value since it gives a scale of required investments to achieve a desired net present value. Internal rate of return does not change much after 4 years since the significant share of cash flow comes during the early production.

Companies should pay attention to improving cost models. Linear cost models for fracture treatment and horizontal section drilling give only a first order Capex estimation; however in a near-marginal project the completion design should be justified carefully. The cost model should be improved along with the actual cost data acquired from the previous project and should be reviewed periodically.

Further work could be connected with the current actual limitations of the model. At first, the introduction of non-linear cost increment for number of fracs and horizontal well lengths could have a significant effect on economic justification of some sensitivity cases. This can only be done if enough relevant drilling data with exact costs are available. Also, it is interesting to use other fracture models to assess reservoir performance. Fracture network model and dual porosity model may lead into different break-even values and magnitude of change in economic metrics for different sensitivities. Simulation of a whole well may provide a different result due to the superposition principle and faster pressure drawdown between fractures. Using heterogeneous models instead of homogeneous models and in-depth study on including stress dependent transmissibilities can help in better understanding of shale well performance. Finally, the economic performance analysis of a large number of wells changes with different oil and gas prices would be an interesting research for determining break-even points for major shale plays.

THIS PAGE INTENTIONALLY LEFT BLANK

Nomenclature

a	=	empirical constant of fracture treatment cost increase
$A_{drain.frac}$	=	fracture drainage area, acre
$A_{drain.well}$	=	well drainage area, acre
A_{frac}	=	total stimulated fracture area, ft^2
A_{well}	=	well spacing, acre
C_{compl}	=	variable cost of completion, USD
C_{fixed}	=	fixed and miscellaneous costs, USD
C_{frac}	=	stimulation cost of one fracture, USD
C_g	=	volume of adsorbed gas, scf/ton
$C_{m/d}$	=	mobilization/demobilization cost, USD
$C_{pump,}$	=	pumping cost, USD
C_{stim}	=	stimulation cost of fracture area, USD/ft^2
C_{tr}	=	total cost of treatment, USD
C_{well}	=	total well cost, USD
d_{horiz}	=	drilling cost of horizontal section, USD/ft
D_{horiz}	=	horizontal section drilling cost, USD
D_{total}	=	total drilling cost, USD
D_{vert}	=	vertical section drilling cost, USD
f_o	=	fraction of cash flow allocated to operational expenditures
f_r	=	fraction of cash flow allocated to royalties
f_t	=	fraction of cash flow allocated to taxes
h	=	reservoir thickness, ft
H	=	reservoir vertical depth, ft
i	=	discount rate, fraction
k	=	permeability, md or nd
k_{abs}	=	absolute permeability of the rock, md
k_f	=	current fracture permeability, md
k_{fi}	=	initial fracture permeability, md

k_i	=	effective permeability of a phase *i*, md
k_m	=	matrix permeability, md
k_{rg}	=	gas relative permeability as a function of gas saturation, fraction
k_{rgro}	=	end-point relative permeability of gas, fraction
k_{ri}	=	relative permeability of a phase *i*
k_{rocw}	=	end-point relative permeability of oil, fraction
k_{rog}	=	oil-gas relative permeability as a function of gas saturation, fraction
k_{row}	=	oil-water relative permeability as a function of water saturation, fraction
k_{rw}	=	water relative permeability as a function of water saturation, fraction
k_{rwro}	=	end-point relative permeability of water, fraction
L	=	distance between two fractures, ft
L_h	=	horizontal section length, ft
m	=	slope of stress dependent permeabilities
M_{pr}	=	mass of proppant, lbm
n_g	=	exponent for gas relative permeability curve
n_{og}	=	exponent for oil-gas relative permeability curve
n_{ow}	=	exponent for oil-water relative permeability curve
n_w	=	exponent for water relative permeability curve
N	=	number of the grid cells between two fractures
N_{frac}	=	total number of fractures created
p	=	reservoir pressure, psia
p_L	=	Langmuir pressure, psia
p_{ri}	=	initial reservoir pressure, psia
P_{av}	=	hydraulic power of pump, psi
P_{fl}	=	price of fracturing fluid, USD/gal
P_g	=	price of gas, USD/Mscf
P_{HC}	=	price of hydrocarbons, USD/bbl or USD/Mscf
P_o	=	price of oil, USD/bbl
P_{pr}	=	price of proppant, USD/lbm
P_{pump}	=	price of pumping, USD/psi
P_w	=	cost of water disposal, USD/bbl
P_{wf}	=	bottomhole pressure, psia
$Q_{g,t}$	=	cumulative gas production at year t, Mscf
$Q_{o,t}$	=	cumulative oil production at year t, bbl
$Q_{w,t}$	=	cumulative water production at year t, bbl
r	=	rate of return, fraction
r_i	=	the distance from the center of the fracture to the edge of cell, ft
R_s	=	solution gas, scf/STB
R_t	=	cash flow on time t, USD
S_g	=	gas saturation, fraction
S_{gc}	=	critical gas saturation, fraction

S_o	=	artificial oil saturation, fraction
S_{org}	=	residual oil saturation to gas, fraction
S_{orw}	=	residual oil saturation to water, fraction
S_w	=	water saturation, fraction
S_{wc}	=	connate water saturation, fraction
t	=	time, years
V_{HC}	=	volume of produced hydrocarbons within a year, bbl or Mscf
V_L	=	Langmuir volume, scf/ton
V_{tf}	=	volume of fracturing fluid, gal
w_f	=	fracture width, in
x_{extend}	=	simulation model extend in X-direction, ft
x_f	=	fracture new half-length, ft
x_{f0}	=	fracture initial half-length, ft
y_{extend}	=	simulation model extend in Y-direction, ft
ρ_s	=	bulk shale density, g/cm^3
φ	=	porosity, fraction

THIS PAGE INTENTIONALLY LEFT BLANK

References

Conference Papers and Journal Articles

Aghighi, M. A., Valencia, K. J. L., Chen, Z., Rahman, S. S. 2006. An Integrated Approach to the Design and Evaluation of Hydraulic Fracture Treatments in Tight Gas and Coalbed Methane Reservoirs. Presented at SPE Annual Technical Conference and Exhibition, San Antonio, Texas, 24-27 September. SPE-102880-MS. http://dx.doi.org/10.2118/102880-MS

Barree, R. D., Cox, S. A., Miskimins, J. L., Gilbert, J. V., Conway, M. W. 2015. Economic Optimization of Horizontal-Well Completions in Unconventional Reservoirs. *SPE Production & Optimization*. SPE-168612-PA. http://dx.doi.org/10.2118/168612-PA

Britt, L. K., Smith, M. B. 2009. Horizontal Well Completion, Stimulation Optimization, and Risk Mitigation. Presented at SPE Eastern Regional Meeting, Charleston, West Virginia, 23-25 September. SPE-125526-MS. http://dx.doi.org/10.2118/125526-MS

Gonzales, V. M., Callard, J. G. 2011. Optimizing Horizontal Stimulation Design Utilizing Reservoir Characterization from Decline Curve Analysis. Presented at SPE Production and Operations Symposium, Oklahoma City, Oklahoma, 27-29 March. SPE-142382-MS. http://dx.doi.org/10.2118/142382-MS

Juell, A. O., Whitson, C. H. 2013. Optimized Well Modeling of Liquid-Rich Shale Reservoirs. Presented at SPE Annual Technical Conference and Exhibition, New Orleans, Louisiana, 30 September - 2 October. SPE-166380-MS. http://dx.doi.org/10.2118/166380-MS

Jukes, R. H., McIntosh, C. J., Amorer, G. J., Economides, M. J. 2012. NPV-Based Design for Coal Seam Reservoirs. Presented at SPE Canadian Unconventional Resources Conference, Calgary, Alberta, 30 October - 1 November. SPE-161645-MS. http://dx.doi.org/10.2118/161645-MS

Lalehrokh, F., Bouma, J. 2014. Well Spacing Optimization in Eagle Ford. Presented at SPE/CSUR Unconventional Resources Conference - Canada, Calgary, Alberta, 30 September - 2 October. SPE-171640-MS. http://dx.doi.org/10.2118/171640-MS

Lei, G., Cheng, N., Whitson, C. H. 2014. Liquid-Rich Shale versus Conventional Depletion Performance. Presented at SPE/EAGE European Unconventional Conference and Exhibition, Vienna, 25-27 February. SPE-167788-MS. http://dx.doi.org/10.2118/167788-MS

Marongiu-Porcu, M., Ajao, O., Dalamarinis, P., Economides, M. J. 2013. On the Economic Optimization of the Fracturing of Coal Seam Reservoirs. Presented at SPE Asia Pacific Oil & Gas Conference and Exhibition, Jakarta, Indonesia, 22-24 October. SPE-165804-MS. http://dx.doi.org/10.2118/165804-MS

Marongiu-Porcu, M., Economides, M. J., Holditch, S. A. 2008. Economic and Physical Optimization of Hydraulic Fracturing. Presented at SPE International Symposium and Exhibition on Formation Damage Control, Lafayette, Louisiana, 13-15 February. SPE-111793-MS. http://dx.doi.org/10.2118/111793-MS

Marongiu-Porcu, M., Wang, X., Economides, M. J. 2009. Delineation of Application and Physical and Economic Optimization of Fractured Gas Wells. Presented at SPE Production and Operations Symposium, Oklahoma City, Oklahoma, 4-8 April. SPE-120114-MS. http://dx.doi.org/10.2118/120114-MS

Nobakht, M., Ambrose, R., Clarkson, C. R., Youngblood, J. E., Adams, R. 2013. Effect of Completion Heterogeneity in a Horizontal Well with Multiple Fractures on the Long-Term Forecast in Shale-Gas Reservoirs. Presented at Canadian Unconventional Resources & International Petroleum Conference, Calgary, Alberta, 19-21 October. SPE-149400-PA. http://dx.doi.org/10.2118/149400-PA

Pendleton, L. E. 1991. Horizontal Drilling Review. Presented at The Integration of Geology, Geophysics, Petrophysics, and Petroleum Engineering in Evaluating (Assessing) Horizontal Wells, Houston, Texas, 3-6 November. SPE-23535-MS. http://dx.doi.org/10.2118/23535-MS

Rueda, J. I., Zillun, R., Holditch, S. A. 1994. Using a Mixed Integer Linear Programming Technique to Optimize a Fracture Treatment Design. Presented at Eastern Regional Conference & Exhibition, Charleston, West Virginia, 8-10 November. SPE-29184-MS. http://dx.doi.org/10.2118/29184-MS

Veatch, R. W. 1986. Economics of Fracturing: Some Methods, Examples, and Case Studies. Presented at 61st Annual Technical Conference and Exhibition of the Society of Petroleum Engineers, New Orleans, Louisiana, 5-8 October. SPE-15509-MS. http://dx.doi.org/10.2118/15509-MS

Walls, J. D., Sinclair, S. W. 2011. Eagle Ford Shale Reservoir Properties from Digital Rock Physics. *First Break* **29** (6).

Whitson, C. H., Sunjerga, S. 2012. PVT in Liquid-Rich Shale Reservoirs. Presented at SPE Annual Technical Conference and Exhibition, San Antonio, Texas, 8-10 October. SPE-155499-MS. http://dx.doi.org/10.2118/155499-MS

Whitson, C. H., Torp, S. B. 1983. Evaluating Constant-Volume Depletion Data. *Journal of Petroleum Technology*. http://dx.doi.org/10.2118/10067-PA

Yu, W., Sepehrnoori, K. 2014. Sensitivity Study and History Matching and Economic Optimization for Marcellus Shale. Presented at Unconventional Resources Technology Conference, Denver, Colorado, 25-27 August. SPE-2014-1923491-MS. http://dx.doi.org/10.15530/urtec-2014-1923491

Books, Presentations and Thesis

Caputo, J. 2011. Shale Plays: Basic Geological and Engineering Concepts. Presented at AAPL's 57th annual meeting, Boston, Massachusetts, 8-11 June.

Jackson, J. A., Bates, R. L. 1997. *Glossary of Geology*, 4th edition, American Geological Institution.

Lei, G. 2012. Producing Gas-Oil Ratio Performance of Conventional and Unconventional Reservoirs. Master of Science Thesis, Norwegian University of Science and Technology (NTNU).

Online Resources

"A Primer for Understanding Canadian Shale Gas". 2009. National Energy Board, https://www.neb-one.gc.ca/nrg/sttstc/ntrlgs/rprt/archive/prmrndrstndngshlgs2009/prmrndrstndngshlgs2009-eng.html (accessed 20 March 2015).

"Adsorption Isotherm". 2015. Amrita Vishwa Vidyapeetham University, http://amrita.vlab.co.in/?sub=2&brch=190&sim=606&cnt=1 (accessed 26 March 2015).

"Bloomberg Professional Service". 2015. Bloomberg Finance L.P., http://www.bloomberg.com/professional

"Financial Dictionary". 2015. Investopedia, http://www.investopedia.com/dictionary/ (accessed 25 March 2015).

"Geologic Glossary". 2014. U.S. Geological Survey, http://geomaps.wr.usgs.gov/parks/misc/glossarys.html (accessed 25 March 2015).

"Hydraulic Fracturing 101". 2015. Halliburton Company, http://www.halliburton.com/public/projects/pubsdata/Hydraulic_Fracturing/fracturing_101.html (accessed 20 March 2015).

"International Energy Outlook 2013". 2014. U.S. Energy Information Administration, http://www.eia.gov/forecasts/archive/ieo13/ (accessed 21 April 2015)

"Langmuir Isotherm". 2014. IHS, http://www.fekete.com/SAN/WebHelp/FeketeHarmony/Harmony_WebHelp/Content/HTML_Files/Reference_Material/General_Concepts/Langmuir_Isotherm.htm (accessed 1 April 2015).

"New Well-Productivity Data Provide US Shale Potential Insights". 2014. Oil and Gas Journal, http://www.ogj.com/articles/print/volume-112/issue-11/drilling-production/new-well-productivity-data-provide-us-shale-potential-insights.html (accessed 25 March 2015).

"Oil Prices Fall Amid Record Inventories". 2015. The Wall Street Journal, http://www.wsj.com/articles/oil-prices-resume-their-fall-1426760586 (accessed 19 March 2015).

"Oilfield Glossary". 2015. Schlumberger Ltd., http://www.glossary.oilfield.slb.com/ (accessed 15 March 2015).

"Pipe-It Manual". 2015. Petrostreamz AS, http://www.petrostreamz.com/

"Quicksilver Resources Files Bankruptcy as Gas Price Drops". 2015. Bloomberg Business, http://www.bloomberg.com/news/articles/2015-03-17/quicksilver-resources-files-bankruptcy-as-gas-price-drops (accessed 17 March 2015).

"Rig Count". 2015. Baker Hughes Inc., http://www.bakerhughes.com/rigcount (accessed 5 March 2015).

"Sensor Reservoir Simulator Manual". 2011. Coats Engineering Inc., http://www.coatsengineering.com/

"SensorGrid Documentation". 2012. Petrostreamz AS, http://www.petrostreamz.com/

"Shale". 2015. Geology.com: Geoscience News and Information, http://geology.com/rocks/shale.shtml (accessed 13 March 2015).

"Shale Gas and Tight Oil are Commercially Produced in Just Four Countries". 2015. U.S. Energy Information Administration, http://www.eia.gov/todayinenergy/detail.cfm?id=19991 (accessed 21 April 2015)

"Shale Oil and Gas". 2015. Halliburton Company, http://www.halliburton.com/en-US/ps/solutions/unconventional-resources/shale.page (accessed 14 March 2015).

"Technically Recoverable Shale Oil and Shale Gas Resources: An Assessment of 137 Shale Formations in 41 Countries Outside the United States". 2013. U.S. Energy Information Administration, http://www.eia.gov/analysis/studies/worldshalegas/ (accessed 21 April 2015)

"The Dangerous Economics of Shale Oil". 2014. Peak Prosperity, http://www.peakprosperity.com/blog/90220/dangerous-economics-shale-oil (accessed 22 March 2015).

"The Process of Hydraulic Fracturing". 2015. U.S. Environmental Protection Agency, http://www2.epa.gov/hydraulicfracturing/process-hydraulic-fracturing (accessed 20 March 2015).

"Three Main Sources of Unconventional Gas". 2015. Total S.A., http://www.total.com/en/energies-expertise/oil-gas/exploration-production/strategic-sectors/unconventional-gas/presentation/three-main-sources-unconventional-gas (accessed 15 March 2015).

"Understanding Hydraulic Fracturing". 2015. Canadian Society for Unconventional Gas, http://www.csur.com/images/CSUG_publications/CSUG_HydraulicFrac_Brochure.pdf (accessed 17 March 2015).

"Well Count". 2015. Baker Hughes Inc., http://www.bakerhughes.com/wellcount (accessed 5 March 2015).

THIS PAGE INTENTIONALLY LEFT BLANK

Appendix A

Units Conversion

TABLE 6 – UNIT CONVERSION FACTORS		
To convert from	To	Multiply by
Feet (ft)	Meters (m)	0.3048
Miles (mi)	Meters (m)	1609.3
Inches (in)	Centimeters (cm)	2.54
Squared feet (ft^2)	Squared meters (m^2)	0.0923
Acres (acre)	Squared meters (m^2)	4046.8
US barrel (bbl)	Cubic meters (m^3)	0.1589
Cubic feet (ft^3)	Cubic meters (m^3)	0.0283
Pounds (lbm)	Kilograms (kg)	0.4536

THIS PAGE INTENTIONALLY LEFT BLANK

Appendix B

Fluid Composition and EOS

TABLE 7 – FLUID COMPOSITION FOR EOS			
Component	Mole Fracture	Component	Mole Fracture
H_2S	0.00000000	C_{12}	0.00973391
N_2	0.00167534	C_{13}	0.00764815
CO_2	0.02539132	C_{14}	0.00601851
C_1	0.63558247	C_{15}	0.00474393
C_2	0.08130903	C_{16}	0.00374585
C_3	0.04548081	C_{17}	0.00296320
I-C_4	0.01047610	C_{18}	0.00234856
N-C_4	0.01786676	C_{19}	0.00186508
I-C_5	0.00819902	C_{20}	0.00148411
N-C_5	0.00879218	C_{21}	0.00118336
C_6	0.01248101	C_{22}	0.00094551
C_7	0.03118978	C_{23}	0.00075701
C_8	0.02647679	C_{24}	0.00060735
C_9	0.02020222	C_{25}	0.00048827
C_{10}	0.01582676	C_{26+}	0.00211233
C_{11}	0.01240528	TOTAL	1.00000000

Critical saturation pressure p_{crit} = 4906.4 psia.
First separation stage at 150 psia and 100 °F.
Second separation stage at 14.7 psia and 60 °F

TABLE 8 – EOS MODEL AND BLACK OIL PVT											
	M	T_c R	P_c psia	Z_{crit}	Shift-f	ω	Parachor	Binary Interaction Parameters			
								N_2	CO_2	C_1	C_2
H_2S	34.082	672.12	1300.0	0.28292	0.10153	0.09000	80.100				
N_2	28.014	227.16	492.84	0.29178	-0.00090	0.03700	59.100	0.00			
CO_2	44.010	547.42	1069.5	0.27433	0.21749	0.22500	80.000	0.00	0.00		
C_1	16.043	343.01	667.03	0.28620	-0.00247	0.01100	71.000	0.08	0.02	0.12	
C_2	30.070	549.58	706.62	0.27924	0.05894	0.09900	111.00	0.07	0.06	0.12	0.00
C_3	44.097	665.69	616.12	0.27630	0.09075	0.15200	151.00	0.07	0.08	0.12	0.00
I-C_4	58.123	734.13	527.94	0.28199	0.10952	0.18600	188.80	0.06	0.08	0.12	0.00
N-C_4	58.123	765.22	550.56	0.27385	0.11028	0.20000	191.00	0.06	0.08	0.12	0.00
I-C_5	72.150	828.70	490.37	0.27231	0.09773	0.22900	227.40	0.06	0.08	0.12	0.00
N-C_5	72.150	845.46	488.78	0.26837	0.11947	0.25200	231.00	0.06	0.08	0.12	0.00
C_6	82.422	924.04	489.98	0.24891	0.13417	0.23825	232.81	0.05	0.08	0.12	0.00
C_7	96.053	990.58	454.18	0.26708	0.14355	0.27411	265.53	0.03	0.08	0.10	0.02586
C_8	108.89	1043.4	421.37	0.26505	0.15263	0.31051	296.33	0.03	0.08	0.10	0.02979
C_9	122.04	1093.5	388.54	0.26121	0.17011	0.35127	327.89	0.03	0.08	0.10	0.03393
C_{10}	134.96	1138.0	360.26	0.25783	0.18663	0.39131	358.9	0.03	0.08	0.10	0.03780
C_{11}	147.80	1178.2	335.58	0.25479	0.20229	0.43091	389.72	0.03	0.08	0.10	0.04145
C_{12}	160.55	1214.9	313.96	0.25202	0.21703	0.46995	420.31	0.03	0.08	0.10	0.04483
C_{13}	173.19	1248.7	294.94	0.24952	0.2308	0.50837	450.67	0.03	0.08	0.10	0.04801
C_{14}	185.74	1279.8	278.13	0.24726	0.24362	0.54615	480.77	0.03	0.08	0.10	0.05096
C_{15}	198.18	1308.7	263.19	0.24523	0.25551	0.58326	510.63	0.03	0.08	0.10	0.05371
C_{16}	210.51	1335.5	249.88	0.24342	0.26648	0.61969	540.22	0.03	0.08	0.10	0.05627
C_{17}	222.73	1360.6	237.95	0.24182	0.27659	0.65545	569.55	0.03	0.08	0.10	0.05864
C_{18}	234.83	1384.1	227.23	0.24043	0.28589	0.69052	598.60	0.03	0.08	0.10	0.06085
C_{19}	246.83	1406.2	217.56	0.23921	0.29442	0.72492	627.39	0.03	0.08	0.10	0.06290
C_{20}	258.71	1427.0	208.81	0.23817	0.30224	0.75865	655.91	0.03	0.08	0.10	0.06481
C_{21}	270.48	1446.7	200.85	0.23730	0.3094	0.79172	684.16	0.03	0.08	0.10	0.06659
C_{22}	282.14	1465.3	193.61	0.23658	0.31594	0.82413	712.14	0.03	0.08	0.10	0.06825
C_{23}	293.69	1483.0	186.98	0.23600	0.32191	0.8559	739.86	0.03	0.08	0.10	0.06980
C_{24}	305.13	1499.8	180.91	0.23556	0.32736	0.88704	767.32	0.03	0.08	0.10	0.07124
C_{25}	316.47	1515.8	175.33	0.23524	0.33233	0.91755	794.52	0.03	0.08	0.10	0.07260
C_{26+}	412.23	1631.4	140.76	0.23657	0.36046	1.16190	1024.3	0.03	0.08	0.10	0.08150

Omega-A = 0.42748, Omega-B = 0.08664

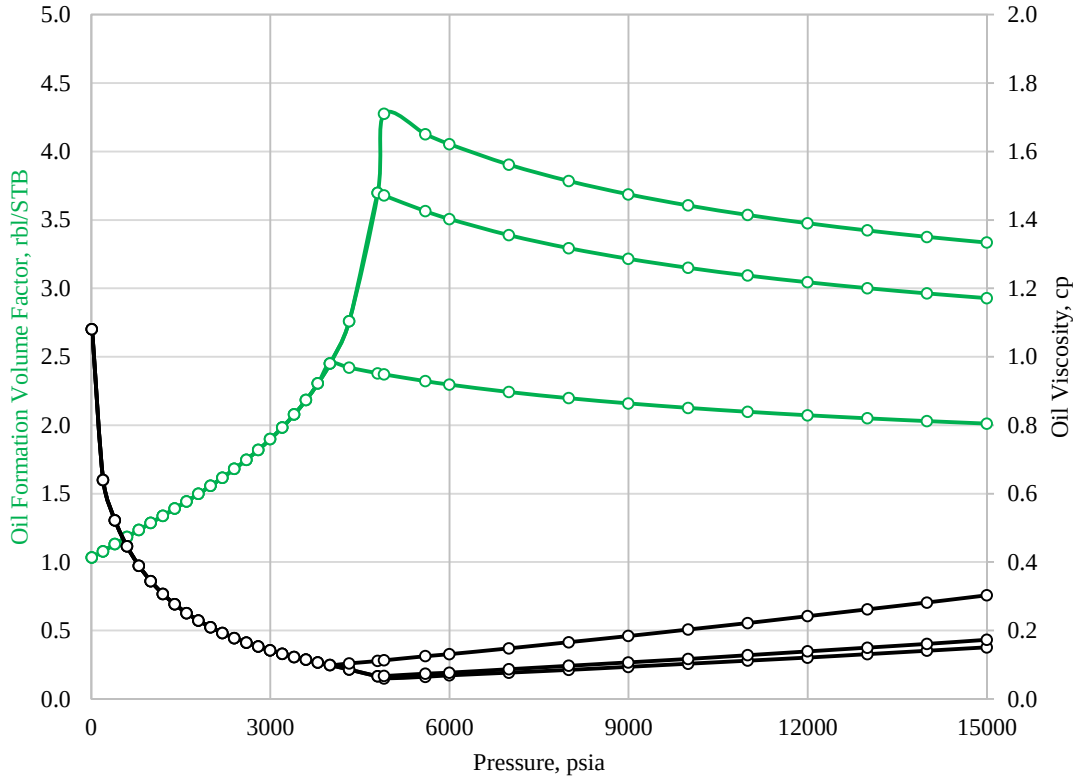

Fig. B.1 – Oil formation volume factor and viscosity.

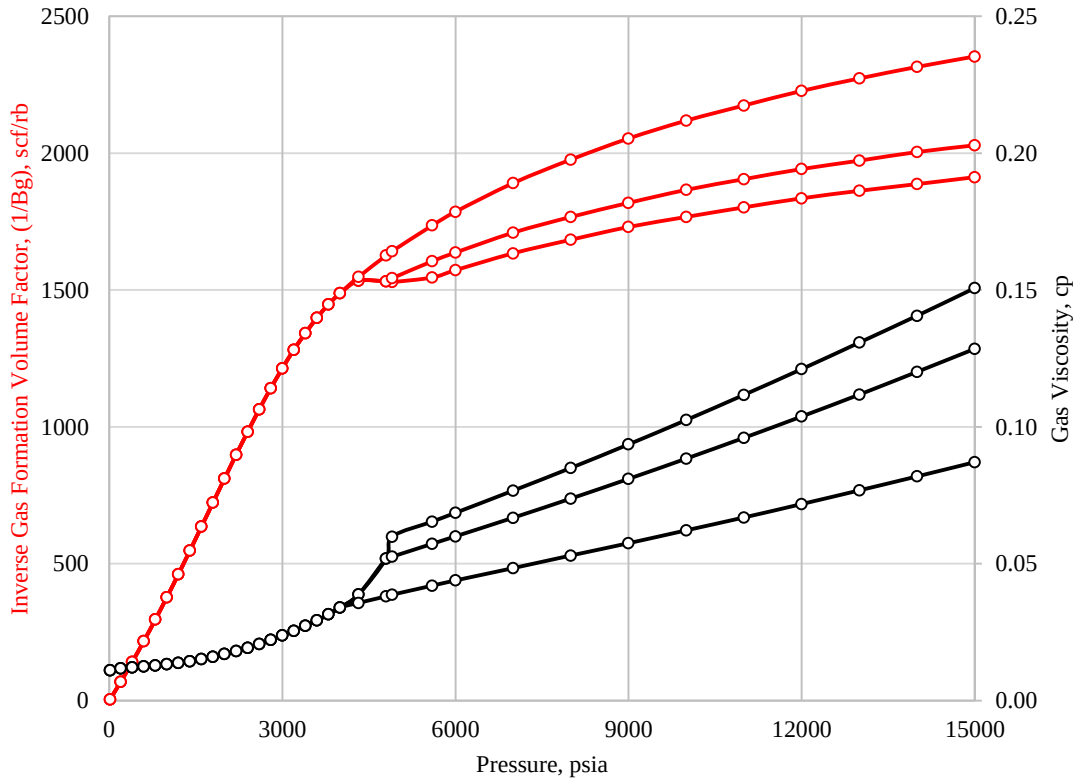

Fig. B.2 – Gas formation volume factor and viscosity

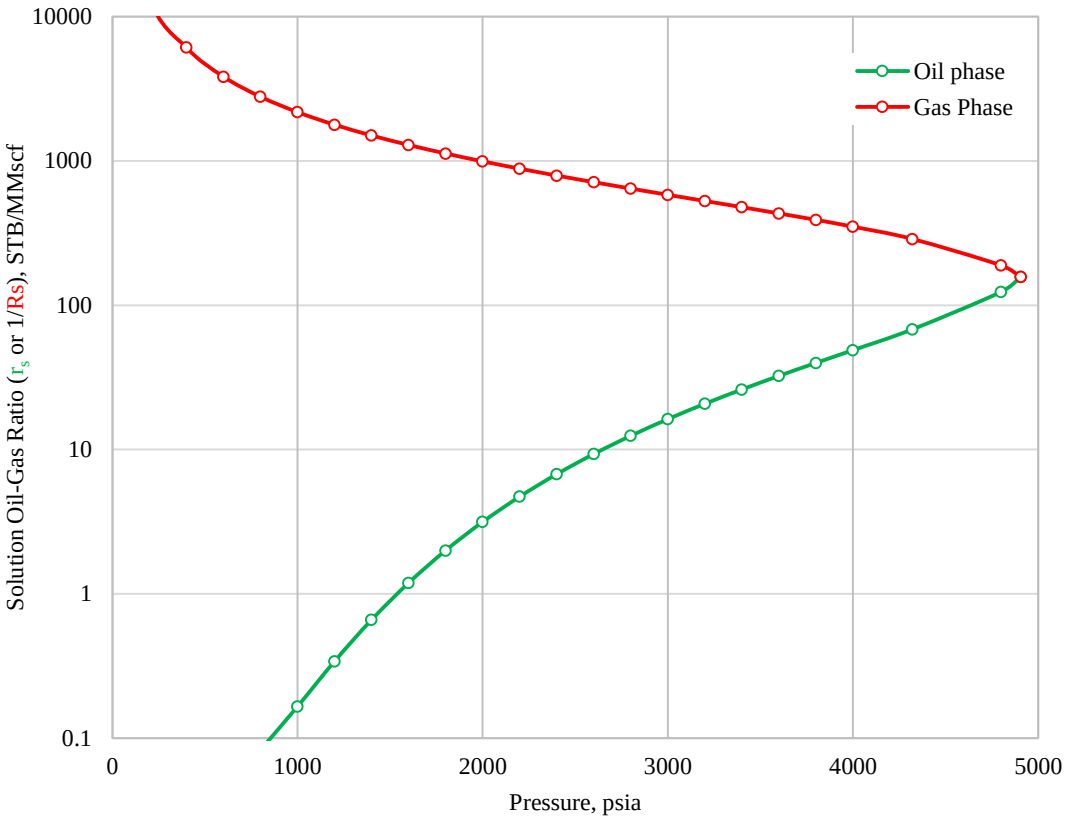

Fig. B.3 – Solution Gas-Oil (and Gas-Oil) Ratio for gas and oil phases.

Appendix C

SENSOR Input File Example

```
TITLE
    Economic Optimization of Shale Wells
    Kirill Karadzhov, NTNU
    Gas Condensate Well, Base Case
    Master's Thesis Project
    March 2015
ENDTITLE

GRID 39 20 1
PCMULT2 1. 0.
RUN
CPU
IMPLICIT


C    Bwi cw     denw  visw  cr      pref
MISC 1   3.0E-6 62.4  0.5   4.0E-6  6000

C ---------------------------------------------------------------------------
C Cell width along wellbore
C ---------------------------------------------------------------------------
DELX XVAR
45.6399 29.8596 19.5354 12.7809 8.36183 5.47066 3.57914 2.34163 1.53199 1.0023
0.655745 0.429017 0.280681 0.183634 0.120141 0.0786014 0.0514244 0.033644
0.0220114 0.0833 0.0220114 0.033644 0.0514244 0.0786014 0.120141 0.183634
0.280681 0.429017 0.655745 1.0023 1.53199 2.34163 3.57914 5.47066 8.36183
12.7809 19.5354 29.8596 45.6399

C ----------------------------------------------------------------------------
C Cell width away from wellbore
C ----------------------------------------------------------------------------
DELY YVAR
30 30 30 30 30 30 30 30 30 30 0.109107 0.252016 0.582109 1.34456 3.10567
7.17351 16.5694 38.2722 88.4013 204.19


C ---------------------------------------------------------------------------
C Porosity
C ---------------------------------------------------------------------------
POROS CON
0.07

MOD
20 20 1 10 1 1 = 0.0354606
```

```
C -------------------------------------------------------------------------
C Rocktype (for relperm curves)
C -------------------------------------------------------------------------
ROCKTYPE CON
1

MOD
20 20 1 10 1 1 = 2

C -------------------------------------------------------------------------
C Assigning TMODTABLES (for stress dependent perm)
C -------------------------------------------------------------------------
TMODTYPE CON
1

MOD
20 20 1 10 1 1 = 2

C -------------------------------------------------------------------------
C Permeability
C -------------------------------------------------------------------------
KX CON
0.0005

MOD
20 20 1 10 1 1 = 12004.8

KY EQUALS KX
KZ EQUALS KX

C -------------------------------------------------------------------------
C Depth
C -------------------------------------------------------------------------
DEPTH CON
8530

C -------------------------------------------------------------------------
C Thickness
C -------------------------------------------------------------------------
THICKNESS CON
200

C -------------------------------------------------------------------------
C Relperm
C -------------------------------------------------------------------------

KRANALYTICAL 1          ! For matrix
0.2 0.1 0.1 0.1         ! Swc Sorw Sorg Sgc
1 1 1                   ! krw(Sorw) krg(Swc) kro(Swc)
2 2 2 2                 ! nw now ng nog
-10 10 1. PCGO

KRANALYTICAL 2          ! For fractures
0.20 0.001 0.001 0.1    ! Swc Sorw Sorg Sgc
1 1 1                   ! krw(Sorw) krg(Swc) kro(Swc)
1 1 1 1
-10 10 1. PCGO          ! pcgo_frac

SWINIT CON
 0.4


C -------------------------------------------------------------------------
C Black-Oil Table
C -------------------------------------------------------------------------
BLACKOIL    1     34    35    SRK

PRESSURES
14.7
200
400
```

```
600
800
1000
1200
1400
1600
1800
2000
2200
2400
2600
2800
3000
3200
3400
3600
3800
4000
4400
4800
5200
5600
6000
7000
8000
9000
10000
11000
12000
13000
14000
15000

RESERVOIR FLUID
0.00000000
0.00167534
0.02539132
0.63558247
0.08130903
0.04548081
0.01047610
0.01786676
0.00819902
0.00879218
0.01248101
0.03118978
0.02647679
0.02020222
0.01582676
0.01240528
0.00973391
0.00764815
0.00601851
0.00474393
0.00374585
0.00296320
0.00234856
0.00186508
0.00148411
0.00118336
0.00094551
0.00075701
0.00060735
0.00048827
0.00211233

INJECTION GAS EQUILIBRIUM
```

```
SEPARATOR
150   100
14.70 60.0

ENDBLACKOIL

C ========================================================================
C Fluid Properties
C ========================================================================
PVTEOS SRK
135    ! Reservoir temperature (deg F)

CPT         MW          TC          PC          ZCRIT       SHIFT       AC
PCHOR       OMEGA       OMEGB
   H2S       34.082       672.12       1300        0.28292     0.10153     0.09
80.1        0.42748     0.08664
   N2        28.014       227.16       492.84      0.29178     -0.0009     0.037
59.1        0.42748     0.08664
   CO2       44.01        547.42       1069.5      0.27433     0.21749     0.225
80          0.42748     0.08664
   C1        16.043       343.01       667.03      0.2862      -0.00247    0.011
71          0.42748     0.08664
   C2        30.07        549.58       706.62      0.27924     0.05894     0.099
111         0.42748     0.08664
   C3        44.097       665.69       616.12      0.2763      0.09075     0.152
151         0.42748     0.08664
   I-C4      58.123       734.13       527.94      0.28199     0.10952     0.186
188.8       0.42748     0.08664
   N-C4      58.123       765.22       550.56      0.27385     0.11028     0.2
191         0.42748     0.08664
   I-C5      72.15        828.7        490.37      0.27231     0.09773     0.229
227.4       0.42748     0.08664
   N-C5      72.15        845.46       488.78      0.26837     0.11947     0.252
231         0.42748     0.08664
   C6        82.422       924.04       489.98      0.24891     0.13417
0.23825     232.81      0.42748     0.08664
   C7        96.053       990.58       454.18      0.26708     0.14355
0.27411     265.53      0.42748     0.08664
   C8        108.89       1043.4       421.37      0.26505     0.15263
0.31051     296.33      0.42748     0.08664
   C9        122.04       1093.5       388.54      0.26121     0.17011
0.35127     327.89      0.42748     0.08664
   C10       134.96       1138         360.26      0.25783     0.18663
0.39131     358.9       0.42748     0.08664
   C11       147.8        1178.2       335.58      0.25479     0.20229
0.43091     389.72      0.42748     0.08664
   C12       160.55       1214.9       313.96      0.25202     0.21703
0.46995     420.31      0.42748     0.08664
   C13       173.19       1248.7       294.94      0.24952     0.2308
0.50837     450.67      0.42748     0.08664
   C14       185.74       1279.8       278.13      0.24726     0.24362
0.54615     480.77      0.42748     0.08664
   C15       198.18       1308.7       263.19      0.24523     0.25551
0.58326     510.63      0.42748     0.08664
   C16       210.51       1335.5       249.88      0.24342     0.26648
0.61969     540.22      0.42748     0.08664
   C17       222.73       1360.6       237.95      0.24182     0.27659
0.65545     569.55      0.42748     0.08664
   C18       234.83       1384.1       227.23      0.24043     0.28589
0.69052     598.6       0.42748     0.08664
   C19       246.83       1406.2       217.56      0.23921     0.29442
0.72492     627.39      0.42748     0.08664
   C20       258.71       1427         208.81      0.23817     0.30224
0.75865     655.91      0.42748     0.08664
   C21       270.48       1446.7       200.85      0.2373      0.3094
0.79172     684.16      0.42748     0.08664
   C22       282.14       1465.3       193.61      0.23658     0.31594
0.82413     712.14      0.42748     0.08664
   C23       293.69       1483         186.98      0.236       0.32191
0.8559      739.86      0.42748     0.08664
```

```
   C24       305.13      1499.8      180.91      0.23556     0.32736
0.88704     767.32      0.42748     0.08664
   C25       316.47      1515.8      175.33      0.23524     0.33233
0.91755     794.52      0.42748     0.08664
   C26+      412.23      1631.4      140.76      0.23657     0.36046
1.1619      1024.3      0.42748     0.08664

BIN
0           0           0.08        0.07        0.07        0.06        0.06
0.06        0.06
0.05        0.03        0.03        0.03        0.03        0.03        0.03
0.03        0.03
0.03        0.03        0.03        0.03        0.03        0.03        0.03
0.03        0.03
0.03        0.03        0.03
0           0.02        0.06        0.08        0.08        0.08        0.08
0.08        0.08
0.08        0.08        0.08        0.08        0.08        0.08        0.08
0.08        0.08
0.08        0.08        0.08        0.08        0.08        0.08        0.08
0.08        0.08
0.08        0.08
0.12        0.12        0.12        0.12        0.12        0.12        0.12
0.12        0.1
0.1         0.1         0.1         0.1         0.1         0.1         0.1
0.1         0.1
0.1         0.1         0.1         0.1         0.1         0.1         0.1
0.1         0.1
0.1
0           0           0           0           0           0           0
0.02586     0.02979
0.03393     0.0378      0.04143     0.04483     0.04801     0.05096
0.05371     0.05627     0.05864
0.06085     0.0629      0.06481     0.06659     0.06825     0.0698
0.07124     0.0726      0.0815
0           0           0           0           0           0           0
0           0
0           0           0           0           0           0           0
0           0
0           0           0           0           0           0           0
0
0           0           0           0           0           0           0
0           0
0           0           0           0           0           0           0
0           0
0           0           0           0           0           0           0
0           0           0           0           0           0           0
0           0
0           0           0           0           0           0           0
0           0
0           0           0           0           0
0           0           0           0           0           0           0
0           0
0           0           0           0           0           0           0
0           0
0           0           0           0           0           0           0
0           0
0           0           0           0           0           0           0
0           0
0           0           0
0           0           0           0           0           0           0
0           0
0           0           0           0           0           0           0
0           0
0           0
```

```
0           0           0           0           0           0           0
0           0
0           0           0           0           0           0           0
0           0
0
0           0           0           0           0           0           0
0           0
0           0           0           0           0           0           0
0           0
0           0           0           0           0           0           0
0           0
0           0           0           0           0           0           0
0
0           0           0           0           0           0           0
0           0
0           0           0           0           0           0           0
0           0           0           0           0           0           0
0           0
0           0           0           0           0           0
0           0           0           0           0           0           0
0           0
0           0           0           0           0
0           0           0           0           0           0           0
0           0
0           0           0           0
0           0           0           0           0           0           0
0           0
0           0           0
0           0           0           0           0           0           0
0           0
0           0
0           0           0           0           0           0           0
0           0
0
0           0           0           0           0           0           0
0           0
0           0           0           0           0           0           0
0
0           0           0           0           0           0           0
0           0           0           0           0           0
0           0           0           0           0
0           0           0           0
0           0           0
0           0
0

C -------------------------------------------------------------------------
C Stress dependent trans.
C -------------------------------------------------------------------------
 C Model: k/ko=10^(-m*(stress/ref pres))
 C  Fro matrix
  TMODTABLE 1
  7500 0
 C stress TXMOD TYMOD TZMOD

  -8000.00000000000 1000000.00000000 1000000.00000000 1000000.00000000
  -7733.33333333333 1000000.00000000 1000000.00000000 1000000.00000000
  -7466.66666666667 1000000.00000000 1000000.00000000 1000000.00000000
  -7200.00000000000 1000000.00000000 1000000.00000000 1000000.00000000
  -6933.33333333334 1000000.00000000 1000000.00000000 1000000.00000000
  -6666.66666666667 1000000.00000000 1000000.00000000 1000000.00000000
  -6400.00000000000 1000000.00000000 1000000.00000000 1000000.00000000
  -6133.33333333334 1000000.00000000 1000000.00000000 1000000.00000000
  -5866.66666666667 1000000.00000000 1000000.00000000 1000000.00000000
  -5600.00000000001 1000000.00000000 1000000.00000000 1000000.00000000
  -5333.33333333334 1000000.00000000 1000000.00000000 1000000.00000000
  -5066.66666666667 1000000.00000000 1000000.00000000 1000000.00000000
  -4800.00000000001 1000000.00000000 1000000.00000000 1000000.00000000
  -4533.33333333334 464158.883361290 464158.883361290 464158.883361290
  -4266.66666666668 215443.469003194 215443.469003194 215443.469003194
  -4000.00000000001 100000.000000003 100000.000000003 100000.000000003
```

```
 -3733.33333333334 46415.8883361291 46415.8883361291 46415.8883361291
 -3466.66666666668 21544.3469003195 21544.3469003195 21544.3469003195
 -3200.00000000001 10000.0000000003 10000.0000000003 10000.0000000003
 -2933.33333333334 4641.58883361294 4641.58883361294 4641.58883361294
 -2666.66666666668 2154.43469003196 2154.43469003196 2154.43469003196
 -2400.00000000001 1000.00000000004 1000.00000000004 1000.00000000004
 -2133.33333333335 464.158883361296 464.158883361296 464.158883361296
 -1866.66666666668 215.443469003197 215.443469003197 215.443469003197
 -1600.00000000001 100.000000000004 100.000000000004 100.000000000004
 -1333.33333333335 46.4158883361298 46.4158883361298 46.4158883361298
 -1066.66666666668 21.5443469003198 21.5443469003198 21.5443469003198
 -800.000000000016 10.0000000000005 10.0000000000005 10.0000000000005
 -533.333333333349 4.64158883361299 4.64158883361299 4.64158883361299
 -266.666666666682 2.15443469003198 2.15443469003198 2.15443469003198
 -1.5461409930e-15 1.00000000000004 1.00000000000004 1.00000000000004
 374.9999999999850 1.00000000000000 1.00000000000000 1.00000000000000
 749.9999999999850 1.00000000000000 1.00000000000000 1.00000000000000
 1124.999999999980 1.00000000000000 1.00000000000000 1.00000000000000
 1499.999999999980 1.00000000000000 1.00000000000000 1.00000000000000
 1874.999999999980 1.00000000000000 1.00000000000000 1.00000000000000
 2249.999999999980 1.00000000000000 1.00000000000000 1.00000000000000
 2624.999999999980 1.00000000000000 1.00000000000000 1.00000000000000
 2999.999999999980 1.00000000000000 1.00000000000000 1.00000000000000
 3374.999999999980 1.00000000000000 1.00000000000000 1.00000000000000
 3749.999999999980 1.00000000000000 1.00000000000000 1.00000000000000
 4124.999999999980 1.00000000000000 1.00000000000000 1.00000000000000
 4499.999999999980 1.00000000000000 1.00000000000000 1.00000000000000
 4874.999999999980 1.00000000000000 1.00000000000000 1.00000000000000
 5249.999999999980 1.00000000000000 1.00000000000000 1.00000000000000
 5624.999999999980 1.00000000000000 1.00000000000000 1.00000000000000
 5999.999999999980 1.00000000000000 1.00000000000000 1.00000000000000
 6374.999999999980 1.00000000000000 1.00000000000000 1.00000000000000
 6749.999999999980 1.00000000000000 1.00000000000000 1.00000000000000
 7124.999999999980 1.00000000000000 1.00000000000000 1.00000000000000
 7499.999999999980 1.00000000000000 1.00000000000000 1.00000000000000


C  For fractures
 TMODTABLE 2
 7500 0
C stress TXMOD TYMOD TZMOD

 -8000.00000000000 1000000.00000000 1000000.00000000 1000000.00000000
 -7733.33333333333 1000000.00000000 1000000.00000000 1000000.00000000
 -7466.66666666667 1000000.00000000 1000000.00000000 1000000.00000000
 -7200.00000000000 1000000.00000000 1000000.00000000 1000000.00000000
 -6933.33333333334 1000000.00000000 1000000.00000000 1000000.00000000
 -6666.66666666667 1000000.00000000 1000000.00000000 1000000.00000000
 -6400.00000000000 1000000.00000000 1000000.00000000 1000000.00000000
 -6133.33333333334 1000000.00000000 1000000.00000000 1000000.00000000
 -5866.66666666667 1000000.00000000 1000000.00000000 1000000.00000000
 -5600.00000000001 1000000.00000000 1000000.00000000 1000000.00000000
 -5333.33333333334 1000000.00000000 1000000.00000000 1000000.00000000
 -5066.66666666667 1000000.00000000 1000000.00000000 1000000.00000000
 -4800.00000000001 1000000.00000000 1000000.00000000 1000000.00000000
 -4533.33333333334 464158.883361290 464158.883361290 464158.883361290
 -4266.66666666668 215443.469003194 215443.469003194 215443.469003194
 -4000.00000000001 100000.000000003 100000.000000003 100000.000000003
 -3733.33333333334 46415.8883361291 46415.8883361291 46415.8883361291
 -3466.66666666668 21544.3469003195 21544.3469003195 21544.3469003195
 -3200.00000000001 10000.0000000003 10000.0000000003 10000.0000000003
 -2933.33333333334 4641.58883361294 4641.58883361294 4641.58883361294
 -2666.66666666668 2154.43469003196 2154.43469003196 2154.43469003196
 -2400.00000000001 1000.00000000004 1000.00000000004 1000.00000000004
 -2133.33333333335 464.158883361296 464.158883361296 464.158883361296
 -1866.66666666668 215.443469003197 215.443469003197 215.443469003197
 -1600.00000000001 100.000000000004 100.000000000004 100.000000000004
 -1333.33333333335 46.4158883361298 46.4158883361298 46.4158883361298
 -1066.66666666668 21.5443469003198 21.5443469003198 21.5443469003198
 -800.000000000016 10.0000000000005 10.0000000000005 10.0000000000005
 -533.333333333349 4.64158883361299 4.64158883361299 4.64158883361299
```

```
  -266.666666666682 2.15443469003198 2.15443469003198 2.15443469003198
  -1.5461409930e-15 1.00000000000004 1.00000000000004 1.00000000000004
  374.9999999999850 0.64938163157622 0.64938163157622 0.64938163157622
  749.9999999999850 0.42169650342859 0.42169650342859 0.42169650342859
  1124.999999999980 0.27384196342644 0.27384196342644 0.27384196342644
  1499.999999999980 0.17782794100389 0.17782794100389 0.17782794100389
  1874.999999999980 0.11547819846894 0.11547819846894 0.11547819846894
  2249.999999999980 0.07498942093324 0.07498942093324 0.07498942093324
  2624.999999999980 0.04869675251658 0.04869675251658 0.04869675251658
  2999.999999999980 0.03162277660168 0.03162277660163 0.03162277660168
  3374.999999999980 0.02053525026457 0.02053525026457 0.02053525026457
  3749.999999999980 0.01333521432163 0.01333521432165 0.01333521432163
  4124.999999999980 0.00865964323360 0.00865964323360 0.00865964323360
  4499.999999999980 0.00562341325190 0.00562341325190 0.00562341325190
  4874.999999999980 0.00365174127254 0.00365174127254 0.00365174127254
  5249.999999999980 0.00237137370566 0.00237137370566 0.00237137370566
  5624.999999999980 0.00153992652605 0.00153992652605 0.00153992652605
  5999.999999999980 0.00100000000000 0.00100000000000 0.00100000000000
  6374.999999999980 0.00064938163157 0.00064938163157 0.00064938163157
  6749.999999999980 0.00042169650342 0.00042169650342 0.00042169650342
  7124.999999999980 0.00027384196342 0.00027384196342 0.00027384196342
  7499.999999999980 0.00017782794100 0.00017782794100 0.00017782794100

C -----------------------------------------------------------------------------
C Initialize
C -----------------------------------------------------------------------------
INITREG CON
1

INITIAL 1
DEPTH GOR
8630 8000
GOC 8630
PINIT 7500
ENDINIT

C ---------------------------------
C Trans. modification to fractures
C ---------------------------------
MODIFY TX 1.0
 19 19 10 10 1 1 * 1
 20 20 10 10 1 1 * 1

C ---------------------------------
C Define Wells
C ---------------------------------
WELL
        I  J  K  PI
 PROD   20 1  1  100

BHP
 PROD 1000

SKIP
THP
 PROD 100 -2
SKIPEND

WELLTYPE
 PROD MCF

PSM

MAPSFREQ 1
MAPSFILEFREQ 1
DTMAX 1
DT 0.000001
```

```
C ------------------------------------------------------------------------------
C Define rate schedules.
C ------------------------------------------------------------------------------

! Numbers automatically changed by Pipe-It:
WELL          PROD
INJ_PERIOD    0
INJ_RATE      0
SHUTIN_PERIOD 0
SYM_ELEMENTS  40
TEST_TIME     6

! User supplied data:
SCHEDULE
TIME   RATE          Q_TYPE PRESSURE      P_TYPE THP_TABLE
30     10000000      GAS    1000          BHP
60     10000000      GAS    1000          BHP
91     10000000      GAS    1000          BHP
182    10000000      GAS    1000          BHP
364    10000000      GAS    1000          BHP
729    10000000      GAS    1000          BHP
1459   10000000      GAS    1000          BHP
1824   10000000      GAS    1000          BHP
END

END
```